BST
BioScience Trends

IRCA
BSSA

IACMHR

www.biosciencetrends.com

BioScience Trends is one of a series of peer-reviewed journals of the International Research and Cooperation Association for Bio & Socio-Sciences Advancement (IRCA-BSSA) Group and is published bimonthly by the International Advancement Center for Medicine & Health Research Co., Ltd. (IACMHR Co., Ltd.) and supported by the IRCA-BSSA and Shandong University China-Japan Cooperation Center for Drug Discovery & Screening (SDU-DDSC).

BioScience Trends devotes to publishing the latest and most exciting advances in scientific research. Articles cover fields of life science such as biochemistry, molecular biology, clinical research, public health, medical care system, and social science in order to encourage cooperation and exchange among scientists and clinical researchers.

BioScience Trends publishes Original Articles, Brief Reports, Reviews, Policy Forum articles, Case Reports, News, and Letters on all aspects of the field of life science. All contributions should seek to promote international collaboration.

Editorial Board

BioScience Trends

Editorial and Head Office

Pearl City Koishikawa 603, 2-4-5 Kasuga, Bunkyo-ku,
Tokyo 112-0003, Japan

Tel: +81-3-5840-8764, Fax: +81-3-5840-8765
E-mail: office@biosciencetrends.com
URL: www.biosciencetrends.com

CONTENTS

Volume 11, Number 6, 2017

Review

Original Articles

CONTENTS   (*Continued*)

Brief Report

Communication

Letter

Guide for Authors

Copyright

Mini-Review

Direct-acting agents for hepatitis C virus before and after liver transplantation

Yasuhiko Sugawara*, Taizo Hibi

Departments of Transplantation/Pediatric Surgery and Gastroenterology and Hepatology, Postgraduate School of Life Science, Kumamoto University, Kumamoto, Japan.

Summary	Chronic hepatitis C virus (HCV) infection remains a widespread public health concern and many people are infected with HCV. HCV is one of the leading indications for liver transplantation. Direct-acting antiviral agents (DAAs) against HCV have changed the course of chronic HCV infection, however, making it a curable disease. DAA treatment may be initiated before or after liver transplantation. In the present review, we present the available data on DAA treatment of HCV in liver transplant recipients.

Keywords: Liver transplantation, living donor, hepatocellular carcinoma

1. Introduction

Chronic hepatitis C virus (HCV) infection is a serious public health concern worldwide and 130-150 million people are estimated to be infected with HCV (*1*). Chronic HCV infection remains the leading indication for liver transplantation. In the United States in 2011 (*2*), HCV-related cirrhosis was the most common indication for liver transplantation, accounting for approximately 28% to 40% of all liver transplantations.

HCV recurrence after transplantation is inevitable if HCV is not eradicated before transplantation (*3*). HCV reinfection causes significant damage to the liver graft, however, resulting in poor patient survival (*4*). Patients transplanted for HCV-related cirrhosis have a worse 5-year survival than those with other indications (*5*). One postoperative life -threatening condition is cholestatic hepatitis C, which occurs in approximately 5% of patients within the first year after transplantation (*6*).

Direct-acting antiviral agents (DAAs) have changed the outlook for HCV-infected patients. HCV recurrence and poorer graft survival have led to the use of DAA

agents in the liver transplantation setting (*7*). The present review discusses the clinical management of interferon-free regimens in patients with HCV in the liver transplantation setting.

2. Pre-transplant use

Treatment with DAAs substantially improves liver function in some patients with decompensated cirrhosis. Therefore, some patients on the waiting list can be delisted and avoid or postpone transplantation.

2.1. *Sofosbuvir-based therapy*

Sofosbuvir and simeprevir was well-tolerated, resulting in a sustained viral response for 12 weeks (SVR12) of 74% and 100% in patients with genotype 1a and 1b, respectively (*8*). In a multicenter study (*9*) with the same regimen in decompensated and compensated patients reported an SVR12 of 74% and 91%, respectively.

The SOLAR-I (*10*) and SOLAR II (*11*) studies disclosed that patients with advanced liver diseases and Child Pugh B or C cirrhosis who were waiting for liver transplantation treated with sofosbuvir, ledipasvir, and ribavirin had an SVR12 and SVR24 of 85-89% and 78-96%, respectively. In the ALLY-1 phase 3 study (*12*), 60 patients with cirrhosis and multiple genotypes (1, 2, 3, 4, and 6) were treated and an SVR12 was achieved in 92% of patients with Child-Pugh class A cirrhosis, 94% of patients with Child-Pugh class B, and 56% of

patients with Child-Pugh class C, respectively.

A UK study (*13*) reported an SVR12 from 60% to 92% in patients with decompensated cirrhosis with genotype 1 or 3 and a Child-Pugh score of more than 7 after administration of sofosbuvir with ledipasvir or daclastavir with or without ribavirin therapy. In another study (*14*), liver transplant candidates with hepatitis C cirrhosis underwent interferon-free therapy (sofosbuvir + ribavirin, sofosbuvir + daclastavir ± ribavirin, sofosbuvir + simeprevir ± ribavirin) and 88% of the patients with decompensated cirrhosis achieved an SVR12. Administration of new combination of sofosbuvir and velpatasvir for 12 weeks provided decompensated cirrhotic patients an SVR of 88% (*15*). In the ASTRAL-4 study (*16*), patients with decompensated cirrhosis and HCV genotypes 1, 2, 3, 4, and 6 underwent combined sofosbuvir and daclatasvir administration with or without ribavirin for 12 weeks or without ribavirin for 24 weeks and the SVR12 was 87%.

Donato *et al.* (*17*) reported that of 31 patients treated with sofosbuvir (400 mg/day) and ribavirin (600-1200 mg/day) for 24 to 48 weeks before liver transplantation, HCV was eradicated in 12 before liver transplantation.

2.2. *Gazaprevir and elbasvir*

The C-SALT study part A (*18*) revealed that gazaprevir and elbasvir in patients with Child Pugh class B decompensated cirrhosis yielded an SVR12 of 90%. There are no data on patients with Child Pugh class C decompensated cirrhosis. A European study (*19*) reported that 143 Child Pugh class B patients and 22 class C patients underwent sofosbuvir/daclastavir treatment with or without ribavirin for 24 weeks and achieved an SVR12 of 86% and 76%, respectively.

A recent study (*20*) analyzed the outcome of various DAAs for patients with HCV-related cirrhosis on the waiting list for transplantation. After treatment with DAAs for 6 months, HCV inactivation was achieved in 16% of the patients, but none of the patients were delisted. The model for end-stage liver disease scores improved by a median of 3.4 points and the Child-Turcotte-Pugh (CTP) scores improved by 2 points. Another study showed that 36% of the patients had a biologic response with regression to CTP class A after a 12 -week follow-up. In a study of subjects with hepatocellular carcinoma and well-compensated cirrhosis treated with sofosbuvir and ribavirin, 30 patients underwent transplantation and achieved an SVR12 (*21*). It is important to note, however, that no patients with decompensated cirrhosis were enrolled in that study.

2.3. *HCC recurrence*

A recent study (*22*) demonstrated higher rates of HCC

recurrence following HCV eradication by DAA agents. More recent prospective data , however, showed that the risk of HCC recurrence was comparable to that of the previous therapy with interferon.

2.4. *Benefit of pre-transplant use of DAA*

The benefits of pre-transplant use of DAA, however, remain uncertain. In cases of diseased donor liver transplantation, the improved MELD score after DAA therapy may lead to a loss of priority or even eligibility for liver transplantation. The 2016 EASL guidelines for HCV treatment advised postponing DAA therapy for patients with MELD scores ≥ 18. The use of costly DAAs in patients with a risk of progressive liver disease may be problematic. Furthermore, in cases with HCC, the risk of HCC recurrence may be increased after DAA therapy (*22,24*). Further prospective studies are needed to address several difficult questions in the pre-liver transplant cohort.

3. Treatment after transplantation

DAA is effective for the treatment of HCV in liver transplantation patients. Sofosbuvir and ribavirin were administered to 40 post-transplant patients for 24 weeks with recurrent HCV (all genotypes) and an SVR12 of 70% was achieved (*16*).

3.1. *Sofosbuvir and ledipasvir*

In the ALLY-1 study (*12*), daclastavir, sofosbuvir, and ribavirin were administered to patients. Of the study participants, 55% had advanced fibrosis or cirrhosis. A total of 53 patients with genotype 1a (58%), 1b (19%), and 3 (21%) were treated with daclatasvir (60 mg/day), sofosbuvir (400 mg/day), and ribavirin and achieved an SVR12 of 94%. Similarly, Letvitsky *et al.* (*25*) reported that 37 patients treated with sofosbuvir and ledipasvir achieved an SVR of 97%.

The SOLAR studies (*10,11*) recruited post-transplant patients with HCV infection (and also those with end-stage liver disease) having genotype 1 or 4. In the SOLAR 1 study (*10*), the cohort was post-transplant patients in the United States that were non-cirrhotic (*n* = 111) or cirrhotic having various extents of liver dysfunction (Child-Pugh class A, *n* = 51; Child Pugh class B, *n* = 52; and Child Pugh class C, *n* = 9). They received sofosbuvir and ledipasvir for 12 or 24 weeks and achieved an SVR12 of 96%, 98%, 86%, and 60%, respectively, after 12-week treatment, and of 96%, 98%, 88%, and 75%, respectively, after 24-week treatment.

In the SOLAR 2 study conducted in Europe, Canada, and New Zealand (*11*), the subjects also comprised non-cirrhotic (*n* = 89) or cirrhotic patients with various extents of liver dysfunction (Child Pugh class A, *n* = 58; Child Pugh class B, *n* = 40; and Child

Pugh class C, *n* = 7, but those with a Child Pugh score greater than 13 were excluded from the study. All the patients received sofosbuvir, ledipasvir, and ribavirin. The SVR12 when treated for 12 weeks was 93%, 100%, 95% and 50%, respectively, and the SVR12 when treated for 24 weeks was 100%, 96%, 100%, and 80%, respectively.

A report was published on a Japanese multicenter experience. A total of 53 patients who underwent liver transplantation for HCV (genotype 1b) cirrhosis were the subjects of the study. The regimen was sofosbuvir and ledipasvir without ribavirin for 24 weeks and the SVR12 was 98%. Saab *et al.* (*26*) reported the UCLA experience. The SVR12 was 85% after treatment with sofosbuvir and ledipasvir with or without ribavirin for 12 weeks, and 94% after treatment with sofosbuvir and ledipasvir without ribavirin for 12 weeks. Globke *et al.* (*27*) reported the Charite Campus Virchow experience in which the SVR12 was 100% in 51 patients.

3.2. *Sofosbuvir and simeprevir*

Sofosbuvir and simeprevir treatment has been evaluated in several studies, and demonstrates good tolerability and efficacy. The SVR12 in transplant patients was 88% (*28,29*).

In the HCV-TARGET study (*30*), 151 post-transplant patients infected with HCV genotype 1 were enrolled and received sofosbuvir and simeprevir with (*n* = 32) and without (*n* = 119) ribavirin for 12 (*n* = 136) or 24 weeks (*n* = 15). The SVR 12 was 88%. A similar study (*31*) reported an SVR12 of 90% in 123 transplant patients treated with sofosbuvir and simeprevir. In a similar study (*21*), 28 patients received a combination of sofosbuvir and simeprevir for 12 weeks and the SVR was 93%. Due to DAAs, graft survival for patients with HCV will improve compared with those undergoing transplantation for other indications for which recurrence may not be easily controlled.

The phase II SATURN study (*32*) demonstrated a 91% SVR12 in 35 post-transplant patients with HCV genotype 1. The regimen was a combination of simeprevir, daclatasvir, and ribavirin.

3.3. *Ombitasvir, paritaprevir-ritonavir, dasabuvir*

Some clinical trials have reported the effectiveness of combined treatment with ombitasvir, paritaprevir-ritonavir, dasabuvir, and ribavirin. In the CORAL I study, 34 post-liver transplant patients underwent this combination therapy for 24 weeks. In patients with genotype 1a and 1b, the SVR12 was 97% and 100%, respectively. The livers of the patients exhibited normal to mild fibrosis, however, and no cirrhotic patients were included in the study. Another study (*34*) revealed a 100% SVR12 in 9 post liver transplant patients on this regimen. In the AMBER-CEE study (*35*), the regimen

was ombitasvir, paritaprevir-ritonavir, and dasabuvir with or without ribavirin. A total of 35 patients (91% genotype 1b, 77% at fibrosis stage ≥ F2) underwent the regimen and the SVR12 was 100%.

4. Daclastavir-based regimens

In a Spanish multicenter study (*36*), 331 post-transplant patients underwent anti-HCV treatment consisting of daclastavir-sofosbuvir with or without ribavirin and daclastavir-simeprevir with or without ribavirin. Of note, 49% of the patients had advanced fibrosis (F4). The intention -to-treat SVR was 93%.

5. Fibrosing cholestatic hepatitis

Fibrosing cholestatic hepatitis (FCH) is a more severe form of HCC recurrence that occurs in less than 10% (*6*) of liver transplant recipients for HCV cirrhosis. FCH is characterized by a high viral load and divergent quasispecies (*37*). FCH results in progressive liver dysfunction and its prognosis is poor with more than 90% mortality (*38,39*). FCH can also occur after liver transplantation for hepatitis B cirrhosis and cytomegalovirus infection.

In the interferon era, the treatment response was poor, resulting in graft and patient loss. DAA is useful for FCH (*40,41*). In one study (*41*), sofosbuvir and ribavirin were administered to 10 FCH patients for 24 or 48 weeks and the SVR12 was 80%. Another study (*42*) showed that a 24-week treatment with simepredvir and sofosbuvir provided 80% SVR12. In the SOLAR 1 study (*10*), six patients with FCH underwent 12-or 24-week treatment with ledipasvir and sofosbuvir, which led to a significant decline in the total bilirubin level. A total of 23 patients with FCH received either sofosbuvir and daclatasvir (*n* = 15) or sofosbuvir and ribavirin (*n* = 8) for 24 weeks. At week 36, 22 patients (96%) had a complete clinical response (*14*). There was no death in the cohort. The CO23 ANRS CUPOT study (*40*) reported 23 patients with FCH treated with sofosbuvir-based regimens (sofosbuvir + ribavirin, pegylated interferon + sofosbuvir ± ribavirin, sofosbuvir + daclatasvir ± ribavirin). Clinical improvement was achieved after 24 weeks of therapy without the need for re-transplantation. A recent multicenter study (*43*) also reported an SVR12 of 94% (*n* = 117) and 98% (*n* = 45) after ledipasvir and sofosbuvir treatments, respectively, with and without ribavirin regimens.

6. Timing of DAA use

The optimal time to initiate DAA treatment remains to be clarified. Patients should be treated before HCV recurrence. In the ALLY1 trial (*12*), subjects were 4 months to 13 years post transplantation and in the SOLAR trials (*10,11*), subjects were more than

3 months post transplantation. Most centers initiate DAA therapy 6 months post transplantation (*3*). The feasibility of a preemptive approach should be evaluated.

7. Interactions between DAA and immunosuppressive drugs

Drug-to-drug interactions between most of recently devised new generation DAAs and immunosuppressive drugs is not a significant issue (*44*). The trough levels of immunosuppressive drugs, however, should be closely monitored. After a period of DAA use, the dose of tacrolimus should be increased to maintain a trough level because of improved function of the liver graft.

One exception is ritonavir in ombitasvir, paritaprevir-ritonavir, dasabuvir, and ribavirin therapy. Due to the inhibitory effect of ritonavir on CYP3A-4 to metabolize cyclosporine or tacrolimus, the trough level of the drugs increase (tacrolimus, 57-86 fold, cyclosporine, 4.3-5.8 fold) (*45*). Simeprevir is reported to increase the level of cyclosporine 6-fold (*46*). Grazoprevir and elbastavir have drug-to-drug interactions with tacrolimus, increasing the level to 143%, as well as with cyclosporine, increasing the level to 115% (*7*).

8. Future perspective

Due to the introduction of DAAs for HCV, the need for transplantation for chronic HCV will be reduced as a result of the improved liver function (*47*). A recent study showed that the proportion of HCV-infected patients on the waiting list for HCC and decompensated cirrhosis will decrease whereas the proportion of patients with non-alcoholic steatohepatitis on the waiting list will increase (*48*). Fibrosing cholestatic hepatitis as an indication for re-transplantation may be significantly reduced because of DAA treatment. It is unlikely that the total volume of deceased donor liver transplantation will decrease, however, because this is regulated by the number of the deceased donors (*47*).

9. Conclusions

The currently available DAAs achieve a satisfactory SVR12 in post-liver transplantation patients. Drugs with a maximum SVR12 and minimum interaction with immunosuppressive and adverse events would be ideal, and this goal is very nearly met by the current DAAs. Optimal timing of the DAA treatment is not yet established, but it may be appropriate to consider DAA treatment after the patients' condition and graft function become stable.

References

1. van Tilborg M, Maan R, van der Meer AJ, de Knegt RJ. Interferon-free antiviral therapy for chronic hepatitis C among patients in the liver transplant setting. Best Pract Res Clin Gastroenterol. 2017; 31:219-25.
2. Kim WR, Lake JR, Smith JM, Skeans MA, Schladt DP, Edwards EB, Harper AM, Wainright JL, Snyder JJ, Israni AK, Kasiske BL. OPTN/SRTR 2015 annual data report: Liver. Am J Transplant. 2017; 17(Suppl 1):174-251.
3. Jothimani D, Govil S, Rela M. Management of post liver transplantation recurrent hepatitis C infection with directly acting antiviral drugs: A review. Hepatol Int. 2016; 10:749-761.
4. Samuel D, Feray C. Recurrent hepatitis C after liver transplantation: Clinical and therapeutical issues. J Viral Hepat. 2000; 7:87-92.
5. Berenguer M, Lopez-Labrador FX, Wright TL. Hepatitis C and liver transplantation. J Hepatol. 2001; 35:666-678.
6. Narang TK, Ahrens W, Russo MW. Post-liver transplant cholestatic hepatitis C: A systematic review of clinical and pathological findings and application of consensus criteria. Liver Transpl. 2010; 16:1228-1235.
7. Bhamidimarri KR, Satapathy SK, Martin P. Hepatitis C virus and liver transplantation. Gastroenterol Hepatol (N Y). 2017; 13:214-220.
8. Modi AA, Nazario H, Trotter JF, Gautam M, Weinstein J, Mantry P, Barnes M, Habib A, McAfee J, Teachenor O, Tujague L, Gonzalez S. Safety and efficacy of simeprevir plus sofosbuvir with or without ribavirin in patients with decompensated genotype 1 hepatitis C cirrhosis. Liver Transpl. 2016; 22:281-286.
9. Saxena V, Nyberg L, Pauly M, Dasgupta A, Nyberg A, Piasecki B, Winston B, Redd J, Ready J, Terrault NA. Safety and efficacy of simeprevir/sofosbuvir in hepatitis C-infected patients with compensated and decompensated cirrhosis. Hepatology. 2015; 62:715-725.
10. Charlton M, Everson GT, Flamm SL, *et al*. Ledipasvir and sofosbuvir plus ribavirin for treatment of HCV infection in patients with advanced liver disease. Gastroenterology. 2015; 149:649-659.
11. Manns M, Samuel D, Gane EJ, *et al*. Ledipasvir and sofosbuvir plus ribavirin in patients with genotype 1 or 4 hepatitis C virus infection and advanced liver disease: A multicentre, open-label, randomised, phase 2 trial. The Lancet Infectious diseases. 2016; 16:685-697.
12. Poordad F, Schiff ER, Vierling JM, Landis C, Fontana RJ, Yang R, McPhee F, Hughes EA, Noviello S, Swenson ES. Daclatasvir with sofosbuvir and ribavirin for hepatitis C virus infection with advanced cirrhosis or post-liver transplantation recurrence. Hepatology. 2016; 63:1493-1505.
13. Foster GR, Coppola C, Derbala M, Ferenci P, Orlandini A, Reddy KR, Tallarico L, Shiffman ML, Ahlers S, Bakalos G, Hassanein T; GUARD-C Study Group. Impact of safety-related dose reductions or discontinuations on sustained virologic response in HCV-infected patients: Results from the GUARD-C Cohort. PLoS One. 2016; 11:e0151703.
14. Coilly A, Roche B, Duclos-Vallee JC, Samuel D. Optimum timing of treatment for hepatitis C infection relative to liver transplantation. The lancet Gastroenterology & hepatology. 2016; 1:165-172.
15. Coilly A, Roche B, Duclos-Vallee JC, Samuel D. News and challenges in the treatment of hepatitis C in liver transplantation. Liver Int. 2016; 36 (Suppl 1):34-42.
16. Charlton M, Gane E, Manns MP, *et al*. Sofosbuvir and ribavirin for treatment of compensated recurrent

hepatitis C virus infection after liver transplantation. Gastroenterology. 2015; 148:108-117.

17. Donato MF, Morelli C, Romagnoli R, Invernizzi F, Mazzarelli C, Iemmolo RM, Montalbano M6, Lenci I7, Bhoori S, Pieri G, Berardi S, Caraceni P, Martini S; ITACOPS-SOF Bridging Study Group. Prevention of hepatitis C recurrence by bridging sofosbuvir/ribavirin from pre- to post-liver transplant: A real-life strategy. Liver Int. 2017; 37:678-683.

18. A SPECIAL MEETING REVIEW EDITION: Advances in the Treatment of Hepatitis C Virus Infection From EASL 2015: The 50th Annual Meeting of the European Association for the Study of the Liver * April 22-26, 2015 * Vienna, AustriaSpecial Reporting on:* Daclatasvir, Sofosbuvir, and Ribavirin Combination for HCV Patients With Advanced Cirrhosis or Posttransplant Recurrence: Phase 3 ALLY-1 Study* Efficacy and Safety of Grazoprevir and Elbasvir in Hepatitis C Genotype 1-Infected Patients With Child-Pugh Class B Cirrhosis (C-SALT Part A)* Ledipasvir/Sofosbuvir With Ribavirin Is Safe and Efficacious in Decompensated and Post Liver Transplantation Patients With HCV Infection: Preliminary Results of the Prospective SOLAR 2 Trial* Retreatment of Patients Who Failed 8 or 12 Weeks of Ledipasvir/Sofosbuvir-Based Regimens With Ledipasvir/Sofosbuvir for 24 Weeks* Sofosbuvir + Peginterferon/Ribavirin for 12 Weeks Vs Sofosbuvir + Ribavirin for 16 or 24 Weeks in Genotype 3 HCV Infected Patients and Treatment-Experienced Cirrhotic Patients With Genotype 2 HCV: The BOSON Study* Safety and Efficacy of the Combination Daclatasvir-Sofosbuvir in HCV Genotype 1-Mono-Infected Patients From the French Observational Cohort ANRS CO22 HEPATHER* C-SWIFT: Grazoprevir/Elbasvir + Sofosbuvir in Cirrhotic and Noncirrhotic, Treatment-Naive Patients With Hepatitis C Virus Genotype 1 Infection for Durations of 4, 6 or 8 Weeks and Genotype 3 Infection for Durations of 8 or 12 WeeksPLUS Meeting Abstract Summaries With Expert Commentary by: Steven L. Flamm, MD Chief, Liver Transplantation ProgramProfessor of Medicine and SurgeryNorthwestern University Feinberg School of MedicineChicago, Illinois. Gastroenterol Hepatol (N Y). 2015; 11(6 Suppl 3):1-23.

19. Welzel TM, Petersen J, Herzer K, Ferenci P, Gschwantler M, Wedemeyer H, Berg T, Spengler U, Weiland O, van der Valk M, Rockstroh J, Peck-Radosavljevic M, Zhao Y, Jimenez-Exposito MJ, Zeuzem S. Daclatasvir plus sofosbuvir, with or without ribavirin, achieved high sustained virological response rates in patients with HCV infection and advanced liver disease in a real-world cohort. Gut. 2016; 65:1861-1870.

20. Belli LS, Berenguer M, Cortesi PA, et al. Delisting of liver transplant candidates with chronic hepatitis C after viral eradication: A European study. J Hepatol. 2016; 65:524-531.

21. Curry MP, Forns X, Chung RT, et al. Sofosbuvir and ribavirin prevent recurrence of HCV infection after liver transplantation: An open-label study. Gastroenterology. 2015; 148:100-7.e1.

22. Reig M, Marino Z, Perello C, Inarrairaegui M, Ribeiro A, Lens S, Díaz A, Vilana R, Darnell A, Varela M, Sangro B, Calleja JL, Forns X, Bruix J. Unexpected high rate of early tumor recurrence in patients with HCV-related HCC undergoing interferon-free therapy. J Hepatol. 2016; 65:719-726.

23. EASL Recommendations on treatment of hepatitis C 2016. J Hepatol. 2017; 66:153-194.

24. Conti F, Buonfiglioli F, Scuteri A, Crespi C, Bolondi L, Caraceni P, Foschi FG, Lenzi M, Mazzella G, Verucchi G, Andreone P, Brillanti S. Early occurrence and recurrence of hepatocellular carcinoma in HCV-related cirrhosis treated with direct-acting antivirals. J Hepatol. 2016; 65:727-733.

25. Levitsky J, Verna EC, O'Leary JG, Bzowej NH, Moonka DK, Hyland RH, Arterburn S, Dvory-Sobol H, Brainard DM, McHutchison JG, Terrault NA. Perioperative ledipasvir-sofosbuvir for HCV in liver-transplant recipients. N Engl J Med. 2016; 375:2106-2108.

26. Saab S, Rheem J, Jimenez MA, et al. Effectiveness of ledipasvir/sofosbuvir with/without ribavarin in liver transplant recipients with hepatitis C. J Clin Transl Hepatol. 2017; 5:101-108.

27. Globke B, Raschzok N, Teegen EM, Pratschke J, Schott E, Eurich D. Treatment of hepatitis C virus recurrence after transplantation with sofosbuvir/ledipasvir: The role of ribavirin. Transpl Infect Dis. 2017; doi: 10.1111/tid.12647.

28. Gutierrez JA, Carrion AF, Avalos D, O'Brien C, Martin P, Bhamidimarri KR, Peyton A. Sofosbuvir and simeprevir for treatment of hepatitis C virus infection in liver transplant recipients. Liver Transpl. 2015; 21:823-830.

29. Nguyen NH, Yee BE, Chang C, Jin M, Lutchman G, Lim JK, Nguyen MH. Tolerability and effectiveness of sofosbuvir and simeprevir in the post-transplant setting: Systematic review and meta-analysis. BMJ open gastroenterology. 2016; 3:e000066.

30. Brown RS, Jr., O'Leary JG, Reddy KR, et al. Interferon-free therapy for genotype 1 hepatitis C in liver transplant recipients: Real-world experience from the hepatitis C therapeutic registry and research network. Liver Transpl. 2016; 22:24-33.

31. Pungpapong S, Aqel B, Leise M, Werner KT, Murphy JL, Henry TM, Ryland K, Chervenak AE, Watt KD, Vargas HE, Keaveny AP. Multicenter experience using simeprevir and sofosbuvir with or without ribavirin to treat hepatitis C genotype 1 after liver transplant. Hepatology. 2015; 61:1880-1886.

32. Forns X, Didier S, Mutimer D, et al. Efficacy of telaprevir-based therapy in stable liver transplant patients with chronic genotype 1 hepatitis C. Ann Hepatol. 2016; 15:512-523.

33. Kwo PY, Mantry PS, Coakley E, et al. An interferon-free antiviral regimen for HCV after liver transplantation. N Engl J Med. 2014; 371:2375-2382.

34. Yu ML, Chen YL, Huang CF, Lin KH, Yeh ML, Huang CI, Hsieh MH, Lin ZY, Chen SC, Huang JF, Dai CY, Chuang WL. Paritaprevir/ritonavir/ombitasvir plus dasabuvir with ribavirin for treatment of recurrent chronic hepatitis C genotype 1 infection after liver transplantation: Real-world experience. J Formos Med Assoc. 2017; pii: S0929-6646(17)30292-9.

35. Tronina O, Durlik M, Wawrzynowicz-Syczewska M, et al. Real-world safety and efficacy of ombitasvir/paritaprevir/ritonavir/+dasabuvir±ribavirin (OBV/PTV/r/+DSV±RBV) therapy in recurrent hepatitis C virus (HCV) genotype 1 infection post-liver transplant: AMBER-CEE study. Ann Transplant. 2017; 22:199-207.

36. Salcedo M, Prieto M, Castells L, et al. Efficacy and safety of daclatasvir-based antiviral therapy in hepatitis C virus recurrence after liver transplantation. Role of cirrhosis and

genotype 3. A multicenter cohort study. Transpl Int. 2017; 30:1041-1050.

37. Satapathy SK, Sclair S, Fiel MI, Del Rio Martin J, Schiano T. Clinical characterization of patients developing histologically-proven fibrosing cholestatic hepatitis C post-liver transplantation. Hepatol Res. 2011; 41:328-339.

38. Verna EC, Abdelmessih R, Salomao MA, Lefkowitch J, Moreira RK, Brown RS, Jr. Cholestatic hepatitis C following liver transplantation: An outcome-based histological definition, clinical predictors, and prognosis. Liver Transpl. 2013; 19:78-88.

39. Antonini TM, Sebagh M, Roque-Afonso AM, Teicher E, Roche B, Sobesky R, Coilly A, Vaghefi P, Adam R, Vittecoq D, Castaing D, Samuel D, Duclos-Vallée JC. Fibrosing cholestatic hepatitis in HIV/HCV co-infected transplant patients-usefulness of early markers after liver transplantation. Am J Transplant. 2011; 11:1686-1695.

40. Leroy V, Dumortier J, Coilly A, *et al*. Efficacy of sofosbuvir and daclatasvir in patients with fibrosing cholestatic hepatitis C after liver transplantation. Clin Gastroenterol Hepatol. 2015; 13:1993-2001.e1-2.

41. Forns X, Charlton M, Denning J, *et al*. Sofosbuvir compassionate use program for patients with severe recurrent hepatitis C after liver transplantation. Hepatology. 2015; 61:1485-1494.

42. Issa D, Eghtesad B, Zein NN, Yerian L, Cruise M, Alkhouri N, Adams R, Hanouneh IA. Sofosbuvir and simeprevir for the treatment of recurrent hepatitis C with fibrosing cholestatic hepatitis after liver transplantation. Int J Organ Transplant Med. 2016; 7:38-45.

43. Kwok RM, Ahn J, Schiano TD, T, *et al*. Sofosbuvir plus ledispasvir for recurrent hepatitis C in liver transplant recipients. Liver Transpl. 2016; 22:1536-1543.

44. Bunchorntavakul C, Reddy KR. Management of hepatitis C before and after liver transplantation in the era of rapidly evolving therapeutic advances. J Clin Transl Hepatol. 2014; 2:124-133.

45. Hepatitis C guidance: AASLD-IDSA recommendations for testing, managing, and treating adults infected with hepatitis C virus. Hepatology. 2015; 62:932-954.

46. EASL Recommendations on treatment of hepatitis C 2015. J Hepatol. 2015; 63:199-236.

47. Durand F, Francoz C. The future of liver transplantation for viral hepatitis. Liver Int. 2017;37(Suppl 1):130-135.

48. Goldberg D, Ditah IC, Saeian K, Lalehzari M, Aronsohn A, Gorospe EC, Charlton M. Changes in the prevalence of hepatitis C virus infection, nonalcoholic steatohepatitis, and alcoholic liver disease among patients with cirrhosis or liver failure on the waitlist for liver transplantation. Gastroenterology. 2017; 152:1090-9.e1.

Review

Yin-yang regulating effects of cancer-associated genes, proteins, and cells: An ancient Chinese concept in vogue in modern cancer research

Shuyong Wei*

College of Animal Science, Southwest University, Chongqing, China.

Summary
Great achievements have been made in human cancer research, but most of this research is focused on conditions at the microscopic rather than the systemic level. Recent studies have increasingly cited the ancient Chinese theory of yin-yang in an effort to expand beyond the microscopic level. Various cancer-associated genes and proteins such as mitogen-activated protein kinase (MAPK), p38, p53, c-Myc, tumor necrosis factor (TNF)-α, NF-κB, Cyclin D1, and cyclin-dependent kinase (CDK) and cells such as T cells, B cells, macrophages, neutrophils, and fibroblasts have been reported to regulate various types of cancers in a yin-yang manner. These studies have brought the theory of yin-yang into vogue in cancer research worldwide.

Keywords: Yin-yang, cancer, gene, protein, cell

1. Introduction

As molecular biology and technology develop, cancer research has increasingly focused on conditions at the microscopic level. Therefore, gathering detailed information to fully depict an organism remains a major challenge (*1*). The theory of yin-yang originated from ancient Chinese philosophy and was incorporated into traditional Chinese medicine after Huangdi's Internal Classic. Yin-yang is increasingly cited by modern researchers in an effort to expand beyond the microscopic focus of cancer research and to view biological phenomena from a macroscopic level.

The theory of yin-yang was introduced to Western medical journals more than 60 years ago (*2*). The relationship between disease and yin-yang was first described in 1971 (*3*), and the hypothesis of yin-yang regulation of cell function based on cyclic adenosine monophosphate (cAMP) and cyclic guanosine monophosphate (cGMP) was first reported in 1975 (*4*). This ancient Chinese theory has been increasingly

cited by recent authors and it has been adopted by researchers around the world (*5-7*). Various genes, proteins, and cells are reported to have yin-yang effects by promoting, inhibiting, and eradicating cancer. These studies provide a more comprehensive and systematic understanding of this complicated disease (Figure 1).

2. Yin-yang effect of cancer-associated genes and proteins

The yin-yang relationship between proliferation and differentiation of cells plays a pivotal role in the development of cancer. A yin-yang balance has been highlighted as a feature of cells (*7,8*), and some yin-yang regulating genes and proteins associated with cancer have been found over the last 30 years. MAPK, p53, c-Myc, and CDK are particularly important, and Bcl-2/Bcl-X1, c-JUN, hepatocyte nuclear factor (HNF) 4a, and miR-145 are also included in these pathways (Figure 2).

2.1. *MAPKs*

The MAPK family includes p38, jun nuclear kinases (JNKs), and extracellular signal-regulated kinases (ERKs), and the family plays important roles in cellular proliferation, differentiation, and apoptosis (*9*). Ordinarily, JNKs and p38 MAPK, which share several
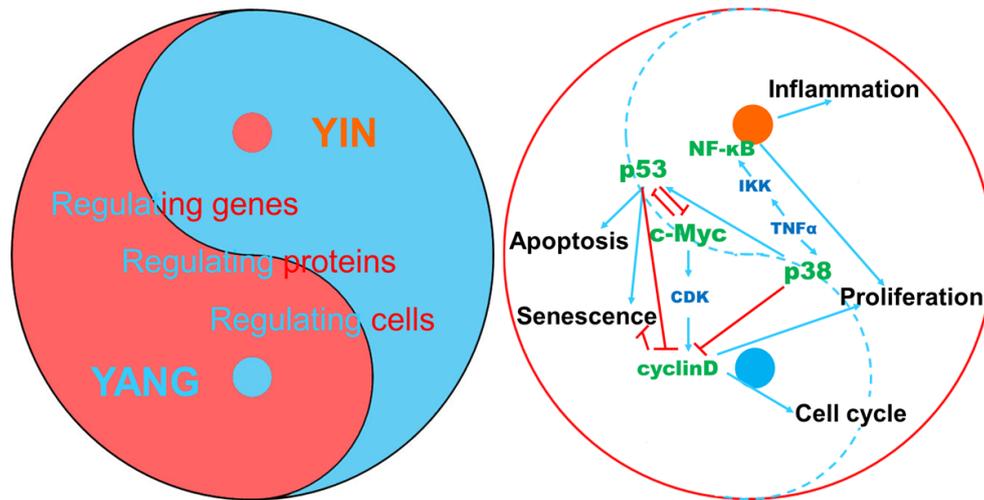
Figure 1. The yin-yang effects of cancer-associated genes and proteins. Yin represents the senescence and apoptosis of cancer cells; Yang represents cancer cells' life processes such as the cell cycle, proliferation, and suppression of senescence. Cancer-associated genes, proteins, and cells all have yin-yang effects on cancer development. The genes p38, p53, c-Myc, CDK, TNFα, and NF- κB play a particularly important role in cancer.
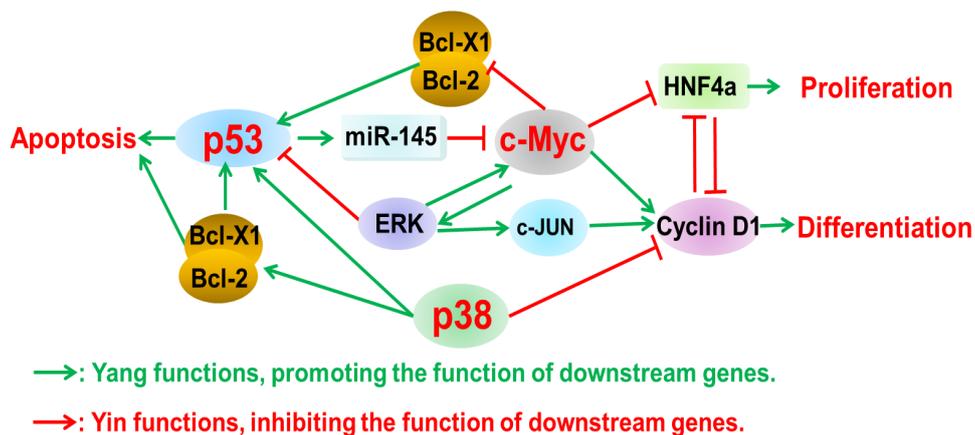
Figure 2. Effects of p38, c-Myc, p53, and Cyclin D1 on cancer cells. p38 MAPK can induce the apoptosis of cancer cells by activating p53 or Bcl-2/Bcl-X1, while p38 inhibits the differentiation of cells by inhibiting Cyclin D1. c-MYC and p53 can inhibit each other. c-MYC promotes cell differentiation by activating Cyclin D1 but it inhibits p53 activity through ERK or the Bcl-2/Bcl-X1 pathway and it inhibits cell proliferation through HNF4a. In contrast, p53 inhibits c-MYC by activating miR-145. ERK promotes Cyclin D1 and the differentiation of cells through the c-MYC and c-JUN pathways. HNF4a and Cyclin D1 can inhibit each other; the former regulates cell proliferation while the latter regulates cell differentiation.

upstream regulators such as MAPK kinase (MKK) 4, are considered to be cancer suppressors (*10*). However, the two stress-activated signaling pathways may promote cancer development. A study in p38MAPK knock-in mouse indicated that p38MAPK is a key component of human lung cancer, that it provides an early and pro-tumorigenic signal in the tissue microenvironment that is reprogrammed by p38MAPK-hyaluronan, and that it plays a critical role in driving lung tumorigenesis (*11*). A recent study on JNK1$^{-/-}$ mouse intestinal epithelial cells and Caco-2 cells reported that the interaction of JNK1 with the vitamin D receptor physically and functionally attenuates the calcitriol-mediated inhibition of cancer cell proliferation (*12*). In human vestibular schwannoma cells, JNK can enhance cell survival by suppressing

the accumulation of mitochondrial superoxides (*13*). Activated ERK1/2 kinases can up-regulate various transcription factors such as c-Myc, and subsequently promote cancer cell survival (*14*). However, another study has indicated that ERK can increase the transcription and stability of c-Jun and cyclinD1 and its receptor and that ERK can activate C kinase 1 (RACK1), enabling protein kinase C to enhance JNK activity (*15*). Furthermore, this signaling axis plays a central process in melanoma tumorigenesis.

2.2. p38 and p53

Both p38 and p53 are generally considered to be cancer suppressors, but they have both negative and

positive effects on cancer cells (*11,16-20*). p38 acts as a regulator in inflammation but as a suppressor in tumors. p38α, a prototypic p38 MAPK, was originally identified as an essential signaling kinase for the production of many inflammatory cytokines (*16*). p38 inactivation supports cell transformation *in vitro* and promotes experimental cancer development *in vivo*. By activating p53, phosphorylating Bcl2s, decreasing cyclin D expression, and inhibiting Cdc25 phosphatase, activated p38 mediates apoptosis induced by DNA damage (*17*). p38 is involved in oncogene-induced senescence, which is a mechanism of cancer suppression (*18*). p53 is considered to be a potent suppressor of tumorigenesis in mammals, and it is a multifunctional transcriptional regulator causing cells to stop growing or die when stressed or damaged (*19*). In organisms, the activity of p53 is optimally balanced, preventing the development of cancer as well as the premature occurrence of aging phenotypes. Tyner *et al*. reported that some tissues show delayed aging in p53$^{-/-}$ or p53$^{+/-}$ mice and that hyperactive p53 expression in mice induced substantial resistance to spontaneous tumorigenesis (*20*).

2.3. *c-Myc and p53*

c-Myc is important to the proliferation and growth of normal cells. The activated c-Myc oncogene contributes to the development of various human cancers, such as leukemia, lymphoma, and solid tumors. However, the deregulation of c-Myc also mediates intrinsic cancer suppression including apoptosis, cellular senescence, and DNA damage (*21*). The balance of p53 and c-Myc is important to cell proliferation, so Dai *et al*. (*22*) describe p53 as yin and c-Myc as yang. There is an inverse relationship between p53 and c-Myc in controlling cell growth and proliferation, and balanced regulation of the two genes is crucial to cells. A study revealed the networks of p53 and c-Myc regulation in cells (*23*). In brief, p53 induces miR-145 expression and subsequently suppresses c-Myc expression, and c-Myc can counterbalance the action of p53 action to a great degree.

2.4. *Cyclin D1 and CDK*

The proliferation and differentiation of cells, which are driven by cyclins and CDK, play a yin-yang role in cancer. Cyclin D1 is overexpressed in many tumors and can activate CDK4/6, and then phosphorylate and inactivate the tumor suppressor Rb. Rb suppresses tumor growth by inhibiting E2F, which is a transcription factor that regulates DNA synthesis. The action of Cyclin D1 on cell proliferation and differentiation is associated with HNF4α, c-Myc, CKip21, and p53 (*24,25*). HNF4α and cyclin D1 negatively regulate each other and are in turn regulated by other modulators, such as p53, c-Myc, and CKip21.

Cyclin D1 can inhibit the differentiation factor ChREBP in a CDK-independent fashion, decrease ChREBP gene transcription and protein function, and result in decreased expression of genes involved in differentiation (*24*).

2.5. *TNF-α and NF-κB*

An important prototypic pro-inflammatory cytokine, tumor necrosis factor alpha (TNF-α) binds to and activates its receptor TNFR. TNF-α is a key regulator of inflammation, cell survival, and cell apoptosis (*26,27*), and TNF-α has yin-yang effects on cancer. The combination of TNF and TNFR can activate downstream cell survival pathways through TNF receptor-associated factor (TRAF) and nuclear factor κB (NF-κB) and also caspase 8 and associated apoptotic pathways through fas-associated death domain (FADD) (*26*). TNFα acts as either a tumor-promoting or tumor-destructive factor (*28*). At a high dose, TNFα can selectively destroy tumor blood vessels and activate T cells that attack and eliminate cancer cells. However, a low dose of TNFα is found in several types of cancers and is important to the development of all stages of cancer (*26*). Activation of NF-κB is detected in various types of cancers (*29*). Signaling pathways mediated by Toll-like receptors (TLRs), TNFα, and interleukin (IL)-1β are involved in this activation (*30*). In some cancers, the essential activity of NF-κB is usually caused by genetic alterations in NF-κBs or their inhibitors IκBs. However, the deregulation of NF-κB activity is attributed to the regulation of the IKK/ NF-κB signal pathway (*31*). IKKβ-deleted mice have decreased expression of many genes including IL-1β, IL-6, TNFα, and COX-2, resulting in a significant reduction in tumor size and number (*32*).

3. Yin-yang effect of the tumor microenvironment and cells

3.1. *The tumor microenvironment and cancer*

Both tumor cells and neighboring normal cells play a role in establishing the tumor microenvironment. They serve as a passive medium for tumor cell growth and also as an arena for interaction of both microenvironmental components and tumor cells. Tumor cells can regulate gene expression in normal cells and vice versa, thereby influencing their phenotype (*33,34*). Specialized variants of hematopoietic and mesenchymal cells such as macrophages, granulocytes, and monocytes are recruited from the bone marrow or bloodstream during cancer development, and some of these cells can become tumor-associated cells. Such cells substantially contribute to the development of cancer.

Cancer-associated inflammation is a double-edged sword. By secreting cytokines and chemokines,

inflammatory cells can express both pro-tumorigenic (yang) and anti-tumorigenic (yin) effects on the proliferation, migration, and differentiation of many types of cancer cells based upon their level of expression in the tumor microenvironment (Figure 3). Pro-tumorigenic effects include releasing survival factors, growth factors, and promoting angiogenesis and lymphangiogenesis. Anti-tumorigenic effects include releasing NK cells, activating apoptosis, and reducing tumorigenicity. Various inflammation-associated cells, including T cells, B cells, macrophages, neutrophils, and fibroblasts, have yin-yang effects on cancer (Table 1).
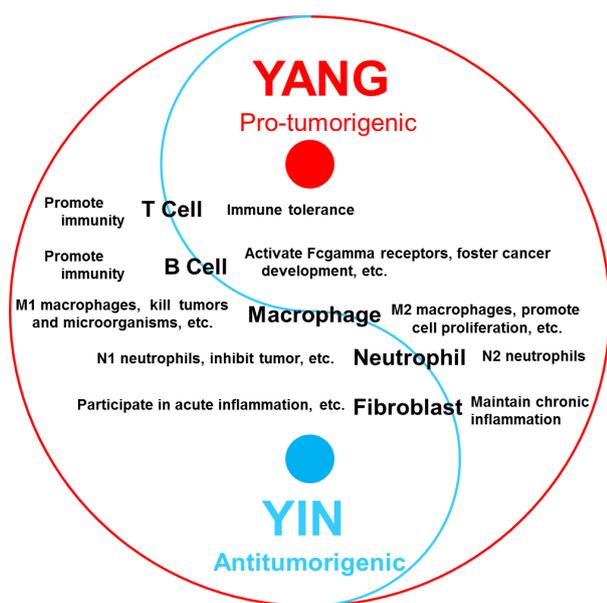
Figure 3. Yin-yang effects of tumor-associated cells. Yin represents antitumorigenic effects, including promoting immunity, killing microorganisms and tumors, and inhibiting tumor growth. Yang represents pro-tumorigenic effects, including immune tolerance, fostering cancer development, promoting cell proliferation, and maintaining chronic inflammation.

3.2. *T cells and B cells*

Tumor-related inflammation is an important component of the tumor microenvironment. Subpopulations of regulatory T cells (Tregs), which promote or inhibit the immune response, display yin-yang characteristics under certain conditions (*35*). The depletion of Tregs leads to the lack of suppression of immune cells, causing an excessive immune response and autoimmunity and promoting anti-tumor responses, while the expansion of Tregs can counteract autoimmunity and inhibit anti-tumor responses (*36*). As an example, inflammatory bowel disease can be induced by syngeneic CD4+CD45RB^{high} T cells but prevented by CD4+CD45RB^{low} T cells in mice (*37*). Furthermore, the costimulation of T cells also plays a crucial role in controlling immune function (as yang) and tolerance (as yin) (*38*). As the most prominent costimulatory receptors for T-cell activation, some proteins of the CD28 family seem to dampen T cell activation and regulate the induction of T cell tolerance (39).

B cells also play a role in inflammation and tumors. During carcinogenesis, B cells can produce antibodies, activate Fcgamma receptors (FcgammaRs) on resident and recruited myeloid cells, and foster cancer development (*40*). In transplanted B16 melanomas, B cells can drive M2-like polarization of macrophages and promote the growth of the melanoma by producing IL-10 (*41*). Mantovani *et al.* describes B cells as yin and macrophages as yang in the development of cancer (*42*).

3.3. *Macrophages*

Based on differences in activation and function, macrophages can be divided into classically activated macrophages such as M1 macrophages and alternatively activated macrophages such as M2 macrophages (*43,44*). These two types of macrophages regulate

Table 1. Yin-yang effects of inflammatory cells on cancer

Inflammatory cells	Effects on cancer		Ref.
	Yin (Antitumorigenic)	Yang (Pro-tumorigenic)	
T cells	Promote immunity	Immune tolerance	(*37-39*)
B cells	Promote immunity	Activate Fcgamma receptors, drive M2-like polarization of macrophages, and foster cancer development	(*41,42*)
Macrophages	M1 macrophages, kill microorganisms and tumors	M2 macrophages, promote cell proliferation, produce growth factors, active the arginase pathway and angiogenesis, and scavenge debris	(*45-47, 49-54*)
Neutrophils	N1 neutrophils, kill cells and inhibit tumor growth, regulate adaptive immune responses by interacting with dendritic cells	N2 neutrophils, secrete angiogenic factors and matrix-degrading enzymes, support metastatic phenotype acquisition, and suppress antitumor immunoreaction	(*56-63*)
Fibroblasts	Participate in acute inflammation, enable infiltrating immune cells to undergo apoptosis or exit the site through the lymphatic system	Maintain chronic inflammation	(*64-67*)

neoplastic progression and immune surveillance in a yin-yang manner (*45*). M1 macrophages are potent effector cells that kill microorganisms and tumors (*46-49*). However, M2 macrophages play roles in regulating inflammation and adaptive immunity (*50*), promoting cell proliferation by producing growth factors (*51*), activating the arginase pathway (52) and angiogenesis (*53*), and scavenging debris by expressing scavenger receptors (*54*).

3.4. *Neutrophils*

Neutrophils are short-lived white blood cells derived from bone marrow myeloid precursors, and these cells can promote or inhibit cancer under particular conditions. By polarizing to either the "N1" or "N2" phenotype, tumor-associated neutrophils can respectively inhibit or promote the development of lung cancer (*55*). The functions of tumor-associated neutrophils are described as antitumorigenic (N1 phenotype) and pro-tumorigenic (N2 phenotype), and which phenotype they express is defined by transforming growth factor (TGF)-β, an immunosuppressive cytokine that can affect tumor progression (*56*). Consistent with this "N1-N2" hypothesis, TGF-β can inhibit the activity and cytotoxicity of neutrophils *in vitro* (*57*). The pro-tumorigenic function of neutrophils may be associated with secretion of angiogenic factors and matrix-degrading enzymes (*58,59*), facilitation of the acquisition of a metastatic phenotype (*60*), and suppression of an antitumor immunoreaction (*61*). Nonetheless, neutrophils can kill tumor cells and inhibit tumor growth (*62*) as well as regulating adaptive immune responses by interacting with dendritic cells (*63*).

3.5. *Fibroblasts*

In the tumor microenvironment, cancer-associated fibroblasts (CAFs) play an important role in the maintenance of chronic inflammation (*64*). In the normal inflammatory process, stromal fibroblasts dictate the type and duration of leukocyte infiltrates, enabling the infiltrating immune cells to undergo apoptosis or exit the site through the lymphatic system (*65*). When these regulatory circuits are damaged, however, inflammation becomes persistent and chronic (*66*). CAFs can both directly and indirectly contribute to the inflammatory process in tumors. They do so directly by recruiting immune cells to respond to the cytokines and chemokines they secrete, and they do so indirectly by modifying the extracellular matrix to favor different immune cells (*67*).

4. Conclusion

In conclusion, modern biological science and cancer research has consistently focused on phenomena at the cellular and molecular level, such as gene suppression and activation, promotion and suppression of apoptosis, protein degradation and synthesis, counteraction of inflammation and inflammation, and tumor suppression and oncogenic processes. This means that the theoretical framework is becoming more complex but less unified. A macroscopic theory is needed to integrate key concepts or the framework will lack important components or falter. The theory of yin-yang provides a macroscopic view on biological phenomena. As Dutt *et al.* said (*68*), the concepts of yin-yang provided the intellectual framework for Chinese scientific thinking, especially in biology and medicine.

Acknowledgements

References

1. Zhu X. Seeing the yin and yang in cell biology. Mol Biol Cell. 2010; 21:3827-3838.
2. Fields A. Yin and Yang in ancient Chinese medicine. West J Surg Obstet Gynecol. 1951; 59: VIII; passim.
3. Shiang E, Li FP. The Yin-Yang (Cold-Hot) Theory of disease. JAMA. 1971; 217:1108.
4. Goldberg ND, Haddox MK, Nicol SE, Glass DB, Sanford CH, Kuehl FA Jr, Estensen R. Biologic regulation through opposing influences of cyclic GMP and cyclic AMP: The Yin Yang hypothesis. Adv Cyclic Nucleotide Res. 1975; 5:307-330.
5. Kiemlian Kwee J. Yin and Yang of polyphenols in cancer prevention: A short review. Anticancer Agents Med Chem. 2016; 16:832-840.
6. Campisi J. Cellular senescence and lung function during aging. Yin and Yang. Ann Am Thorac Soc. 2016; Supplement 5:S402-S406.
7. Carrega P, Campana S, Bonaccorsi I, Ferlazzo G. The Yin and Yang of innate lymphoid cells in cancer. Immunol Lett. 2016; 179:29-35.
8. Frances M, Sladek. The yin and yang of proliferation and differentiation: Cyclin D1 inhibits differentiation factors ChREBP and HNF4α. Cell Cycle. 2012; 11:3153-3158.
9. Weston CR, Davis RJ. The JNK signal transduction pathway. Curr Opin Cell Biol. 2007; 19:142-149.
10. Whitmarsh AJ, Davis RJ. Role of mitogen-activated protein kinase 4 in cancer. Oncogene. 2007; 26:3172-3184.
11. Brichkina A, Bertero T, Loh HM, Nguyen NT, Emelyanov A, Rigade S, Ilie M, Hofman P, Gaggioli C, Bulavin DV. p38MAPK builds a hyaluronan cancer niche to drive lung tumorigenesis. Genes Dev. 2016; 30:2623-2636.
12. Bi X, Shi Q, Zhang H Bao Y, Hu D, Pohl N, Fang W, Dong H, Xia X, Fan D, Yang W. c-Jun NH2-teminal kinase 1 interacts with vitamin D receptor

and affects vitamin D-mediated inhibition of cancer cell proliferation. J Steroid Biochem Mol Biol. 2016; 163:164-172.

13. Yue WY, Clark JJ, Fernando A, Domann F, Hansen MR. Contribution of persistent C-Jun N-terminal kinase activity to the survival of human vestibular schwannoma cells by suppression of accumulation of mitochondrial superoxides. Neuro Oncol. 2011; 13:961-973.

14. Steelman LS, Franklin RA, Abrams SL, Chappell W, Kempf CR, Bäsecke J, Stivala F, Donia M, Fagone P, Nicoletti F, Libra M, Ruvolo P, Ruvolo V, Evangelisti C, Martelli AM, McCubrey JA. Roles of the Ras/Raf/MEK/ ERK pathway in leukemia therapy. Leukemia. 2011; 25:1080-1094.

15. Lopez-Bergami P, Huang C, Goydos JS, Yip D, Bar-Eli M, Herlyn M, Smalley KS, Mahale A, Eroshkin A, Aaronson S, Ronai Z. Rewired ERK-JNK signaling pathways in melanoma. Cancer Cell. 2007; 11:447-460.

16. Yokota T, Wang Y. p38 MAP kinases in the heart. Gene. 2016; 575:369-376.

17. Rovida E, Sbarba PD. p38 and cancer: Yang gets Yin. Cancer Biol Ther. 2008; 7:1241-1242.

18. Bulavin DV, Demidov ON, Saito S, Kauraniemi P, Phillips C, Amundson SA, Ambrosino C, Sauter G, Nebreda AR, Anderson CW, Kallioniemi A, Fornace AJ Jr, Appella E. Amplification of PPM1D in human tumors abrogates p53 tumor-suppressor activity. Nat Genet. 2002; 31:210-215.

19. Campisi J. Cancer and aging: yin, yang, and p53. Sci Aging Knowledge Environ. 2002; 1:1.

20. Tyner SD, Venkatachalam S, Choi J, Jones S, Ghebranious N, Igelmann H, Lu X, Soron G, Cooper B, Brayton C, Park SH, Thompson T, Karsenty G, Bradley A, Donehower LA. p53 mutant mice that display early ageing-associated phenotypes. Nature. 2002; 415:45-53.

21. Larsson LG, Henriksson MA. The Yin and Yang functions of the Myc oncoprotein in cancer development and as targets for therapy. Exp Cell Re. 2010; 316:1429-1437.

22. Dai MS, Jin Y, Gallegos JR, Lu H. Balance of Yin and Yang: Ubiquitylation-mediated regulation of p53 and c-Myc. Neo-plasia. 2006; 8:630-664.

23. Sachdeva M, Mo YY. p53 and c-myc: How does the cell balance "yin" and "yang"? Cell Cycle. 2009; 8:1303.

24. Frances M, Sladek. The yin and yang of proliferation and differentiation: Cyclin D1 inhibits differentiation factors ChREBP and HNF4α. Cell Cycle. 2012; 11:3153-3158.

25. Hanse EA, Mashek DG, Becker JR, Solmonson AD, Mullany LK, Mashek MT, Towle HC, Chau AT, Albrecht JH. Cyclin D1 inhibits hepatic lipogenesis *via* repression of carbohydrate response element binding protein and hepatocyte nuclear factor 4α. Cell Cycle. 2012; 11:2681-2690.

26. Malleo G, Mazzon E, Siriwardena AK, Cuzzocrea S. TNF-alpha as a therapeutic target in acute pancreatitis--Lessons from experimental models. Scientific World Journal. 2007; 7:431-448.

27. Balkwill F. TNF-alpha in promotion and progression of cancer. Cancer Metastasis Rev. 2006; 25:409-416.

28. Szlosarek P, Charles KA, Balkwill FR. Tumour necrosis factor-alpha as a tumour promoter. Eur J Cancer. 2006; 42:745-750.

29. Yuan R, Xu H, Liu X, Tian Y, Li C, Chen X, Su S, Perelshtein I, Gedanken A, Lin X. Zinc-doped copper oxide nanocomposites inhibit the growth of human cancer cells through reactive oxygen species-mediated NF-κB activations. ACS Appl Mater Interfaces. 2016; 8:31806-31812.

30. Mantovani A, Allavena P, Sica A, Balkwill F. Cancer-related inflammation. Nature. 2008; 454:436–444.

31. Xiao G, Fu J. NF-κB and cancer: A paradigm of Yin-Yang. Am J Cancer Res. 2011; 1:192-221.

32. Greten FR, Eckmann L, Greten TF, Park JM, Li ZW, Egan LJ, Kagnoff MF, Karin M. IKKbeta links inflammation and tumorigenesis in a mouse model of colitis-associated cancer. Cell. 2004; 118:285-296.

33. Witz IP. Yin-yang activities and vicious cycles in the tumor microenvironment. Cancer Res. 2008; 68:9-13.

34. Mantovani A, Sica A, Allavena P, Garlanda C, Locati M. Tumor-associated macrophages and the related myeloid-derived suppressor cells as a paradigm of the diversity of macrophage activation. Hum Immunol. 2009; 70:325-330.

35. Singer BD, King LS, D'Alessio FR. Regulatory T cells as immunotherapy. Front Immunol. 2014; 5:46.

36. Galgani M, Di Giacomo A, Matarese G, La Cava A. The Yin and Yang of CD4+ regulatory T cells in autoimmunity and cancer. Curr Med Chem. 2009; 16:4626-4631.

37. De Winter H, Cheroutre H, Kronenberg M. Mucosal immunity and inflammation. II. The yin and yang of T cells in intestinal inflammation: Pathogenic and protective roles in a mouse colitis model. Am J Physiol. 1999; 276:1317-1321.

38. Nurieva RI, Liu X, Dong C. Yin-Yang of costimulation: Crucial controls of immune tolerance and function. Immunol Rev. 2009; 229:88-100.

39. Janeway CA Jr, Medzhitov R. Innate immune recognition. Annu Rev Immunol. 2002; 20:197-C216.

40. Zhang Z, Zhu Y, Wang Z, Zhang T, Wu P, Huang J. Yin-yang effect of tumor infiltrating B cells in breast cancer: From mechanism to immunotherapy. Cancer Lett. 2017; 393:1-7.

41. Wong SC, Puaux AL, Chittezhath M, Shalova I, Kajiji TS, Wang X, Abastado JP, Lam KP, Biswas SK. Macrophage polarization to a unique phenotype driven by B cells. Eur J Immunol. 2010; 40:2296-2307.

42. Mantovani A. B cells and macrophages in cancer: Yin and yang. Nat Med. 2011; 17:285-286.

43. Gordon S. Alternative activation of macrophages. Nat Rev Immunol. 2003; 3:23-35.

44. Mantovani A, Sica A, Locati M. Macrophage polarization comes of age. Immunity. 2005; 23:344-346.

45. Allavena P, Sica A, Garlanda C, Mantovani A. The Yin-Yang of tumor-associated macrophages in neoplastic progression and immune surveillance. Immunol Rev. 2008; 222:155-161.

46. Forssell J, Oberg A, Henriksson ML, Stenling R, Jung A, Palmqvist R. High macrophage infiltration along the tumor front correlates with improved survival in colon cancer. Clin Cancer Res. 2007; 13:1472-1479.

47. Galarneau H, Villeneuve J, Gowing G, Julien JP, Vallières L. Increased glioma growth in mice depleted of macrophages. Cancer Res. 2007; 67:8874-8881.

48. Ong SM, Tan YC, Beretta O, Jiang D, Yeap WH, Tai JJ, Wong WC, Yang H, Schwarz H, Lim KH, Koh PK, Ling KL, Wong SC. Macrophages in human colorectal cancer are pro-inflammatory and prime T cells towards an anti-tumour type-1 inflammatory response. Eur J Immunol. 2012; 42:89-100.

49. Sica A, Mantovani A. Macrophage plasticity and polarization: *In vivo* veritas. J Clin Invest. 2012; 122:787-795.

50. Helm O, Held-Feindt J, Grage-Griebenow E, Reiling N, Ungefroren H, Vogel I, Krüger U, Becker T, Ebsen M, Röcken C, Kabelitz D, Schäfer H, Sebens S. Tumor-associated macrophages exhibit pro- and anti-inflammatory properties by which they impact on pancreatic tumorigenesis. Int J Cancer. 2014. 135:843-861.

51. Zhang B, Zhang Y, Yao G, Gao J, Yang B, Zhao Y, Rao Z, Gao J. M2-polarized macrophages promote metastatic behavior of Lewis lung carcinoma cells by inducing vascular endothelial growth factor-C expression. Clinics (Sao Paulo). 2012; 67:901-906.

52. Grailer JJ, Haggadone MD, Sarma JV, Zetoune FS, Ward PA. Induction of M2 regulatory macrophages through the β2-adrenergic receptor with protection during endotoxemia and acute lung injury. J Innate Immun. 2014; 6:607-618.

53. Jetten N, Verbruggen S, Gijbels MJ, Post MJ, De Winther MP, Donners MM. Anti-inflammatory M2, but not pro-inflammatory M1 macrophages promote angiogenesis *in vivo*. Angiogenesis. 2014; 17:109-118.

54. Xu Y, Qian L, Zong G, Ma K, Zhu X, Zhang H, Li N, Yang Q, Bai H, Ben J, Li X, Xu Y, Chen Q. Class A scavenger receptor promotes cerebral ischemic injury by pivoting microglia/macrophage polarization. Neuroscience. 2012; 218:35-48.

55. Mantovani A. The yin-yang of tumor-associated neutrophils. Cancer Cell. 2009; 16:173-174.

56. Fridlender ZG, Sun J, Kim S, Kapoor V, Cheng G, Ling L, Worthen GS, Albelda SM. Polarization of tumor-associated neutrophil phenotype by TGF-beta: "N1" versus "N2" TAN. Cancer Cell. 2009; 16:183-194.

57. Bierie B, Moses HL. Tumour microenvironment: TGFbeta: The molecular Jekyll and Hyde of cancer. Nat Rev Cancer. 2006; 6:506-520.

58. Pekarek LA, Starr BA, Toledano AY, Schreiber H. Inhibition of tumor growth by elimination of granulocytes. J Exp Med. 1995; 181:435-440.

59. Shojaei F, Singh M, Thompson JD, Ferrara N. Role of Bv8 in neutrophil-dependent angiogenesis in a transgenic model of cancer progression. Proc Natl Acad Sci U S A. 2008; 105:2640-2645.

60. Tazawa H, Okada F, Kobayashi T, Tada M, Mori Y, Une Y, Sendo F, Kobayashi M, Hosokawa M. Infiltration of neutrophils is required for acquisition of metastatic phenotype of benign murine fibrosarcoma cells: implication of inflammation-associated carcinogenesis and tumor progression. Am J Pathol. 2003; 163:2221-2232.

61. Schmielau J, Finn OJ. Activated granulocytes and granulocyte-derived hydrogen peroxide are the underlying mechanism of suppression of t-cell function in advanced cancer patients. Cancer Res. 2001; 61:4756-4760.

62. Hicks AM, Riedlinger G, Willingham MC, Alexander-Miller MA, Von Kap-Herr C, Pettenati MJ, Sanders AM, Weir HM, Du W, Kim J, Simpson AJ, Old LJ, Cui Z. Transferable anticancer innate immunity in spontaneous regression/complete resistance mice. Proc Natl Acad Sci U S A. 2006; 103:7753-7758.

63. van Gisbergen KP, Geijtenbeek TB, van Kooyk Y. Close encounters of neutrophils and DCs. Trends Immunol. 2005; 26:626-631.

64. Raz Y, Erez N. An inflammatory vicious cycle: Fibroblasts and immune cell recruitment in cancer. Exp Cell Res. 2013; 319:1596-1603.

65. Filer A, Raza K, Salmon M, Buckley CD. The role of chemokines in leucocyte-stromal interactions in rheumatoid arthritis. Front Biosci. 2008; 13:2674-2685.

66. Parsonage G, Filer AD, Haworth O, Nash GB, Rainger GE, Salmon M, Buckley CD. A stromal address code defined by fibroblasts. Trends Immunol. 2005; 26:150-156.

67. Servais C, Erez N. From sentinel cells to inflammatory culprits: Cancer-associated fibroblasts in tumour-related inflammation. J Pathol. 2013; 229:198-207.

68. Dutt T, Toh CH. The Yin-Yang of thrombin and activated protein C. Br J Haematol. 2008; 140:505-515.

Original Article

The impact of population aging on medical expenses: A big data study based on the life table

Changying Wang[1,§], Fen Li[1,§], Linan Wang[1], Wentao Zhou[2], Bifan Zhu[1], Xiaoxi Zhang[1], Lingling Ding[3], Zhimin He[3], Peipei Song[4], Chunlin Jin[1,*]

[1] *Shanghai Health Development Research Center, Shanghai Medical Information Center, Shanghai, China;;*
[2] *JiangXi Province Center for Disease Control and Prevention, Jiangxi, China;*
[3] *Xiangya School of Public Health, Central South University, Hu'nan, China;*
[4] *Graduate School of Frontier Sciences, The University of Tokyo, Tokyo, Japan.*

Summary **This study shed light on the amount and structure of utilization and medical expenses on Shanghai permanent residents based on big data, simulated lifetime medical expenses through combining of expenses data and life table model, and explored the dynamic pattern of aging on medical expenditures. 5 years were taken as the class interval, the study collected and did the descriptive analysis on the medical services utilization and medical expenses information for all ages of Shanghai permanent residents in 2015, simulated lifetime medical expenses by using current life table and cross-section expenditure data. The results showed that in 2015, outpatient and emergency visits per capita in the elderly group (aged 60 and over) was 4.1 and 4.5 times higher than the childhood group (aged 1-14), and the youth and adult group (aged 15-59); hospitalization per capita in the elderly group was 3.0 and 3.5 times higher than the childhood group, and the youth and adult group. People survived in the 60-64 years group, their expected whole medical expenses (105,447 purchasing power parity Dollar) in the rest of their lives accounted for 75.6% of their lifetime. A similar study in Michigan, US showed that the expenses of the population aged 65 and over accounted for 1/2 of lifetime medical expenses, which is much lower than Shanghai. The medical expenses of the advanced elderly group (aged 80 and over) accounted for 38.8% of their lifetime expenses, including 38.2% in outpatient and emergency, and 39.5% in hospitalization, which was slightly higher than outpatient and emergency. There is room to economize in medical expenditures of the elderly people in Shanghai, especially controlling hospitalization expenses is the key to saving medical expenses of elderly people aged over 80 and over.**

Keywords: Population aging, life table, big data, lifetime medical expenses

1. Introduction

China had entered an aging society by the end of the last century. According to "2015 Statistical Bulletin of National Economy and Social Development", people aged 60 and over accounted for 16.1% (222.00 million)

of the total population, and people aged 65 and over accounted for 10.5% (183.86 million) of the total population in 2015 in China (*1*). Shanghai is one of the Chinese cities where population aging emerged earliest. It showed that people aged 60 and over accounted for 30.21% (4.36 million) of Shanghai's registered population in 2015 (*2*). As age increases, health status and medical demands change correspondingly, while along with social and economic development, income improvement and medical technology progresses, the impact of population aging on medical expenses has become an enormous challenge for the healthcare system.

Healthcare demands are considerable, and growing

with an aging population. Take Shanghai as an example, Xu (2005) found that the overall health status of elderly people was below average, 70-80% of elderly people aged 60 and over had chronic diseases, and the prevalence of the elderly was 4.2 times higher than the total (*3*).The direct consequence of high prevalence of chronic disease is mounting medical expenditures. Yan (2013) reported that the proportion of medical expenses for the elderly was 75.2% of total family medical expenses in 2006 (*4*), and Tao (2010) revealed the prevalence of chronic disease was 73.76%among the elderly in the Nanhui District of Shanghai in 2010 (*5*). A study in Hubei Province by Zhang (2015) showed similar results (*6*). Therefore, some studies took population aging as the factor driving increasing medical expenses. Huang (2012) indicated that the growth of the aging population was one of the factors leading to medical expenses soaring, especially the rising death rate in the population aged 65 and over (*7*). However, other studies found that increasing medical expenditures were affected by multiple factors, aging was one of these but not the most important one. Wang (2014) thought that aging would gently release the demands for medical services in the elderly population, but the income improving, medical insurance expanding and technology progressing would rapidly boost medical expenses (*8*). Ma (2015) realized that gender, age, marriage status and urban-rural disparities all had an appreciable impact on medical expenditure in elderly people (*9*). Yu (2011) conducted a study based on panel data from 20 provinces from 2002-2008, and found that population aging could only explain 3.9% of per capita increased medical expenses, and 5.7% of per capita increased medical expenses rates (*10*).

International research showed that the growth rate of medical expenses per capita in the elderly population was higher and increased faster than other age groups. An investigation by Cutler &Meara (1998) found that between 1953-1987, the average medical expense growth rate of people aged 65 and over was 8%, higher than the population aged 1-64 (4.7%) (*11*). Waldo &Lazenby (1984) (*12*), Buchner &Wasem (2006) (*13*) illustrated that population aging would aggravate the burden of medical expenses. The reason was that when age increased, health status got worse, which led to rising medical services demands and expenses. Reinhardt (2003) found that population aged 65 and over was 3 times more that population aged 34-44 (*14*). Lassman *et al.* (2014) drew the conclusion that medical expenses per capita in the elderly was 5 times more that the children group (*15*). Alemayehu (2004) adopted a lift table model, using cross sectional medical expenses and death data of every single individual enrolled, to construct a hypothetical current population longitudinal medical expenses data from birth to death. It was noted that from 65 and over, the expected medical expenses accounted for 1/2 of lifetime medical expenses, and

females were 1/4 higher than males (*16*).

From the comparison of domestic and oversea studies, it is notable that the domestic studies had the following weaknesses: First, in regard to the data source, majority of studies are sampling surveys, few are whole sample studies, and are not able to represent the whole population. Second, in terms of the methods, most are qualitative analysis, few are quantitative studies. The statistics measurements and modeling need to be explored, especially when there is a lack of mature method references for measuring lifetime medical expenses. Moreover, some attribution studies used general regression analysis, but general regression analysis, analysis of variance or analysis of covariance do not conform to the characteristics of medical services utilization and medical expenses, since medical expenses may be a non-normal distribution.

There is a greater need for the elderly population and medical expenses evidence to support elderly policies in China. With the development of health information technology, medical big data is gradually captured, therefore exploring information to serve policy making is optimal. In regard to methodology, the internationally recognized method has matured after nearly a half century of development. It is appropriate to use a life table to conduct the study on population aging and medical expenses, and to provide evidence references for policy making. This study shed light on the amount and structure of utilization and medical expenses in Shanghai permanent residents based on big data, constructed using hypothetical "lifetime" medical expenses through a combination of life table model and cross-sectional medical expenses data, and explored the dynamic pattern of aging on medical expenses. Shanghai permanent residents refers to residents who live in Shanghai for over 6 months, while Shanghai registered residents refers to residents registered with Shanghai Public Security Bureau. In 2015, Shanghai registered residents were 24.15 million, Shanghai permanent residents were 14.43 million (*2*).

2. Data and Methods

2.1. *Data*

Data of this study was collected from the entitlement of use of the Health Information Web of Shanghai Municipal Health and Family Planning Commission Information Center. Take 5 years as the class interval, gather the medical services utilization and medical expenses information for all ages of Shanghai permanent residents in 2015. Simulate lifetime medical expenses by using current life table and cross-section medical expenses data. In the life table, take age 0-1 as a separated group from the group aged 0-4, since the medical services utilization of infants is different from other children. The data was classified by outpatient

and emergency visits, and hospitalization. All medical institutions in Shanghai were covered, including hospitals, community health centers, maternal and child health hospitals, specialized disease prevention and control institutions, and outpatient departments. In this study, the elderly group was defined as population aged 60 and over, population aged 1-14, 15-59 was defined as the childhood group, and the youth and adult group, respectively. Shanghai total population of current life table data (5 years as the class interval) in 2015 was gathered by Shanghai Center for Disease Control and Prevention Center.

2.2. Descriptive analysis

Take 5 years as the class interval, describe the age and gender structure of Shanghai permanent residents, and the distributions in outpatient and emergency visits, hospitalization utilization and expenses per capita.

2.3. Life table model

Current life table and cross-sectional medical expenses data were used to construct hypothetical lifetime medical expenses. It was assumed that the technology, prices and other factors which would affect the healthcare service costs were kept constant, therefore the disease prevalence, incidence, development process and healthcare service costs did not change for ongoing time, and the age distribution of medical expenditures could present the hypothetical lifetime distribution of medical expenditures. The advantage of a life table model is that it eliminates the impact from confounding factors, including healthcare service prices, technology development, etc.

In the lifetime medical expenses model, the lifetime expenditure per capita at a given age a, projected from birth 0, the lifetime expected cost referred to the expenditure remaining after age a to death of the hypothetical life table person. Two kinds of lifetime expected costs at birth were estimated as follows:

(1) Lifetime expected cost at birth (LECB) Per capita LECB is the lifetime expected cost divided by the original cohort of 100,000 people. Lx is the person years lived by the cohort in the age interval x. Cx is per capita medical cost at the age interval x (x = 0-, 1-, 5-, 10-, .., 90-).

It could be drawn that per capita LECB at the age interval x:

$$LECB_a = \sum_{x=a}^{95} \left(\frac{c_x L_x}{l_0} \right)$$

The relative lifetime expected cost at the age interval x (RLECB):

$$RLECB_a = LECB_a / LECB_0 = \sum_{x=a}^{95} \left(\frac{c_x L_x}{l_0} \right) / \sum_{x=0}^{95} \left(\frac{c_x L_x}{l_0} \right)$$

(2) Lifetime expected cost for survivors (LECS) Per capita LECS is the lifetime expected cost divided by

the cohort of people who survived at the age interval x, since some people could die before this age interval x.

We could conduct that per capita LECS at the age interval x:

$$LECS_a = \sum_{x=a}^{95} \left(\frac{c_x L_x}{l_a} \right)$$

The relative lifetime expected cost for survivors at the age interval x (RLECB):

$$RLECS_a = LECS_a / LECS_0 = \sum_{x=a}^{95} \left(\frac{c_x L_x}{l_a} \right) / \sum_{x=0}^{95} \left(\frac{c_x L_x}{l_0} \right)$$

3. Results

3.1. Demographic characteristics

There were 24.15 million permanent residents in Shanghai in 2015. 2.17 million were the childhood group aged 0-14, which accounted for 9.00% of the total population; 17.27 million were the youth and adult group aged 15-59, which accounted for 71.50% of the total population; 4.71 million were the elderly group aged 60 and over, which accounted for 19.50% of the total population. Among the elderly group, taking 5 years as class interval, the group aged 90 and over had the least population, 0.11 million accounted for 0.43 of the total. Figure 1 shows the age and gender distribution in Shanghai population in 2015.

3.2. Medical services utilization and expenses

From outpatient and emergency visits point of view, the per capita visits in 2015 changed as the age went up, with multi peaks. The group aged 20-24 had the lowest per capita visits (0.81 times), which increased with rising age. After age 60, the per capita visits boosted remarkably, with per capita visits 1.6 times/month, and reached the highest value when at the group aged 80-84, with per capita visits 3.8 times/month, then slightly dropped. The per capita visits of the children, youth and adult and elderly group in 2015 were 6.0, 5.4 and 24.5 times, respectively. The number of the elderly group was 4.1 and 4.5 times higher than the children, youth and adult group.

Figure 2 represents the age and gender distribution in Shanghai per capita outpatient and emergency visits, and hospitalization in 2015, Figure 2A refers to outpatient and emergency visits, while Figure 2B refers to hospitalization. As per the figure, the per capita outpatient and emergency visits was slightly higher in the group aged 5-9, then decreased. After age 60, it was notable that the per capita outpatient and emergency visits increased fast, and kept dropping after age 80. The per capita hospitalization presented a rough "U" shape trend, with high values at the two ends and low in the middle. The per capita hospitalization of childhood, youth and adult and elderly groups in 2015 were 0.07, 0.06 and 0.21 times, respectively. The number of the
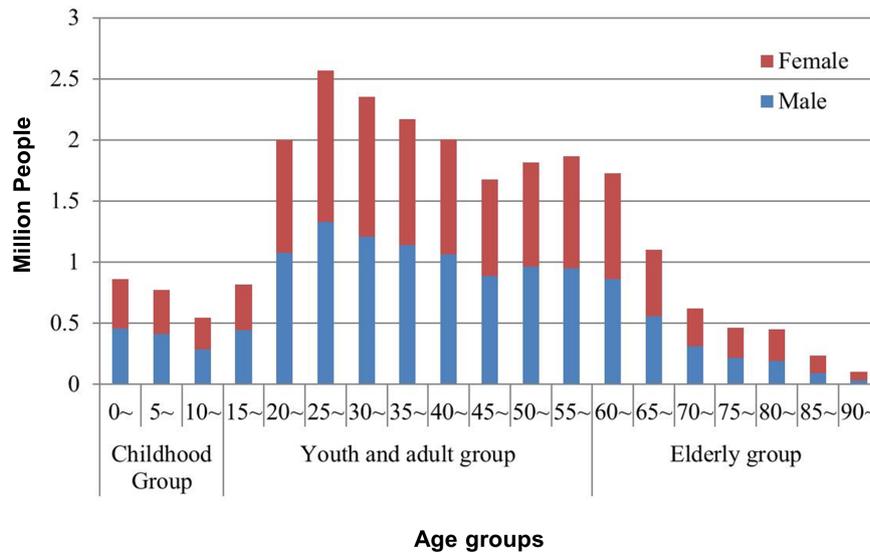
Figure 1. Shanghai population distribution by 5 year intervals and gender, in 2015 (Unit: Million people).
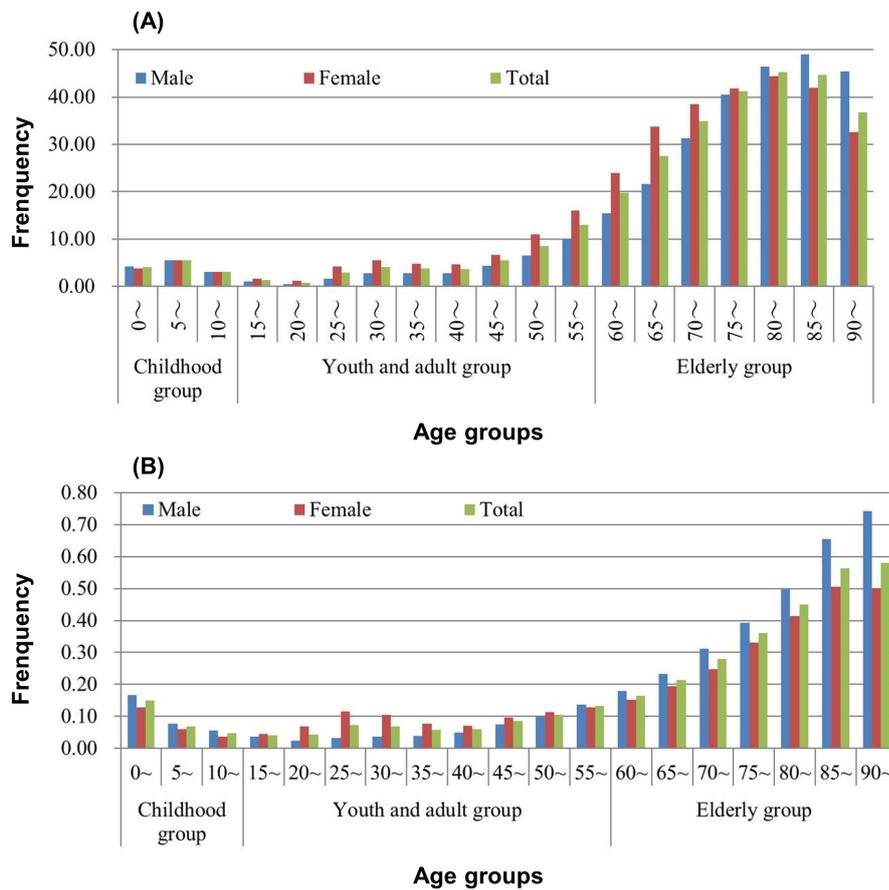
Figure 2. Shanghai per capita outpatient and emergency visits & hospitalization by 5 year intervals and gender in 2015 (Unit: Frequency). **(A),** Outpatient and emergency visits; **(B),** Hospitalization.

elderly group was 3.0 and 3.5 times higher than the children, youth and adult groups.

Figure 3 illustrates the age distribution pyramid of Shanghai permanent residents and medical expenses. It is notable that as age increases, the population shrinks, while the medical expense is distinctly increasing in general. Comparing with the permanent residents structure, the elderly population as 19.5% of total population, and accounted for 52.2% of total outpatient and emergency visits, and 45.3% discharged patients, which indicated that the elderly group consumes more medical resources. Moreover, the expenditure by age
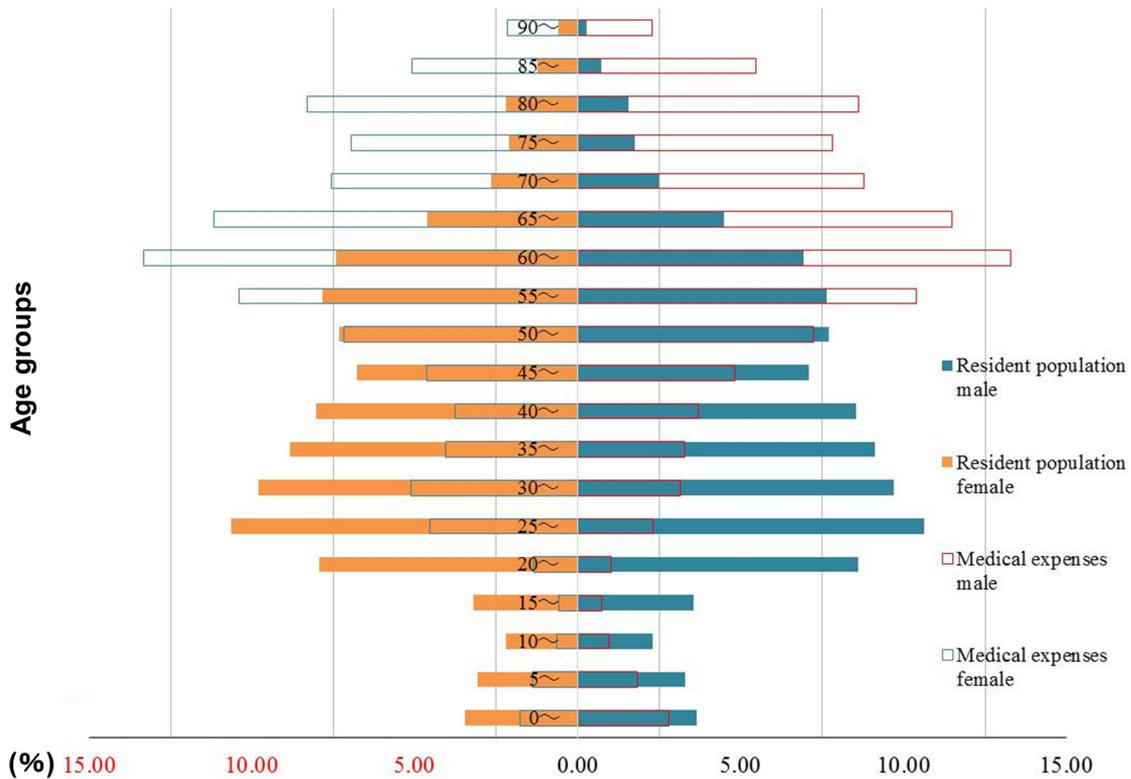
Figure 3. The age distribution pyramid of Shanghai permanent residents and medical expenses by 5 year intervals in 2015 (Unit: %).

distribution pattern had a similar tendency as services utilization by age, but a relatively higher concentration. The elderly population as 19.5% total population accounted for 63.2% of outpatient and emergency expenses, and 52.8% hospitalization expenses.

3.3. Permanent resident lifetime expected medical costs

3.3.1. Outpatient and emergency

In the life table lifetime outpatient and emergency expenses, the per capita expenses and per capita expenses of deaths were growing as age increased, in general. The tendency of per capita expenses was relatively smooth, while the tendency of per capita expenses of deaths showed a slight fluctuation. The group aged 0-1 had zero death expenses, this could be due to that most infant deaths happened in hospitalization, and in 2015 there were no infant deaths during outpatient and emergency visits.

From the results, it is worth noting that the per capita lifetime expected outpatient and emergency cost and the per capita lifetime expected outpatient and emergency cost of survivors declined as age was increasing, and the later slightly exceeded the former. It indicated that for the older group, there was less lifetime expected medical expenditure that an individual can consume. Table 1 presents the simulated results of lifetime expected outpatient and emergency costs. The per capita lifetime

expected outpatient and emergency cost from birth was 81,042 purchasing power parity (PPP) Dollar, when people survived to age 60, per capita lifetime expected outpatient and emergency cost of the group aged 60-64 was 62,776 PPP Dollar.

Figure 4A shows the age group distribution of per capita medical expenses and lifetime expected costs in outpatient and emergency, and Figure 4B shows the proportion of per capita lifetime expected cost of survivors in per capita lifetime expenses. In outpatient and emergency, as age increases, the per capita expenses of both overall population and deaths roughly increased, whilst the per capita expected cost of both overall population and the survivors declined, however the per capita outpatient and emergency expenses distinctly fell in the group aged 90 and over. The proportion of per capita lifetime expected cost of survivors in per capita lifetime expected cost in group aged 60-64 was 77.5%, illustrated that when people reached the age 60-64, one individual's expenses from now to death accounted for 77.5% of this person's whole lifetime outpatient and emergency expenses, which meant that almost eighty percent of outpatient and emergency expenditures was used in the elderly period after 60.

3.3.2. Hospitalization

From Table 2 we can draw the conclusion that compared with outpatient and emergency, the per capita

Table 1. Simulated results of lifetime expected outpatient and emergency cost

Age groups	Survivors	Deaths	Survivor person-years*	Survivor person years in total**	Per capita outpatient & emergency expenses (PPP Dollar***)	Per capita outpatient & emergency expenses of deaths (PPP Dollar)	Outpatient & emergency medical expenses in total (PPP Dollar)	Per capita lifetime expected outpatient& emergency cost (PPP Dollar)	Per capita lifetime expected outpatient& emergency cost of survivors (PPP Dollar)
0~	100,000	483	99,604	8,292,764	303	0	30,204,233	81,042	81,042
1~	99,517	185	397,699	8,193,160	303	620	120,599,540	80,740	81,130
5~	99,332	89	496,440	7,795,461	427	28	212,186,402	79,534	80,068
10~	99,243	98	495,974	7,299,021	262	43	129,752,788	77,412	78,002
15~	99,146	125	495,417	6,803,048	94	257	46,341,050	76,114	76,770
20~	99,021	100	494,854	6,307,630	57	290	28,301,234	75,651	76,399
25~	98,920	117	494,309	5,812,777	214	592	105,949,935	75,368	76,190
30~	98,803	158	493,621	5,318,468	325	512	160,656,994	74,308	75,208
35~	98,645	214	492,691	4,824,847	303	638	149,507,743	72,702	73,699
40~	98,431	340	491,303	4,332,156	296	804	145,219,772	71,207	72,339
45~	98,090	591	488,974	3,840,853	431	629	210,854,524	69,755	71,109
50~	97,499	1,003	484,989	3,351,879	674	565	326,795,392	67,646	69,375
55~	96,496	1,741	478,128	2,866,890	1,020	782	487,691,300	64,378	66,702
60~	94,755	2,468	467,605	2,388,762	1,477	737	690,570,762	59,501	62,776
65~	92,287	3,873	451,754	1,921,157	1,991	777	899,255,698	52,595	56,958
70~	88,414	6,623	425,515	1,469,403	2,495	778	1,061,707,239	43,603	49,258
75~	81,791	11,839	379,359	1,043,888	2,961	826	1,123,335,405	32,986	40,210
80~	69,952	17,472	306,079	664,530	3,365	920	1,029,998,095	21,753	30,867
85~	52,480	22,289	206,677	358,450	3,520	938	727,499,516	11,453	21,424
90~	30,191	30,191	151,773	151,773	2,752	867	417,753,490	4,178	13,837

* Survivor person-years refers to the person-years of people who are alive in this age group. ** Survivor person years in total refers to the total person-years of people who are alive in this age group to death. *** PPP Dollar to Chinese RMB currency in 2015 comes from Organisation for Economic Co-operation and Development database (*17*). PPP, purchasing power parity.
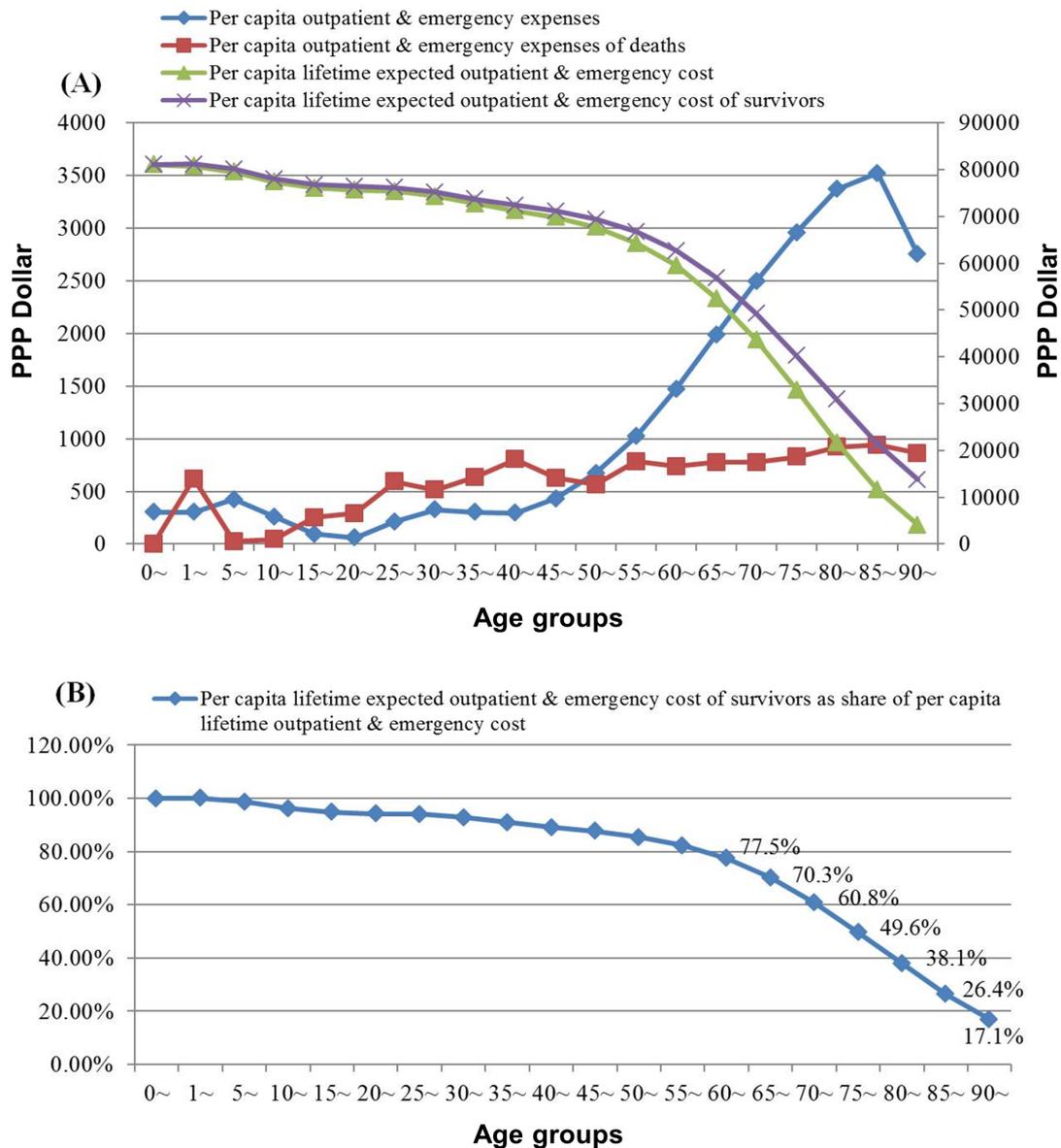
Figure 4.Per capita medical expenses and lifetime expected cost by age groups in outpatient and emergency(Unit: PPP Dollar) (A), and the proportion of per capita lifetime expected cost of survivors in per capita lifetime expenses in outpatient and emergency by 5 year intervals (Unit: %) (B). PPP, purchasing power parity.

hospitalization expenditure of deaths was higher, and not only far exceeded the per capita outpatient and emergency expenditure of deaths, but also exceeded per capita hospitalization expenditures. The per capita lifetime expected hospitalization cost from birth was 58,540 PPP Dollar, and accounted for 72.2% of the per capita lifetime expected outpatient and emergency cost from birth (81,042 PPP Dollar).The highest per capita expenditure of deaths appeared in the group aged 1-4, which was 45,095 PPP Dollar. It is noteworthy that, although the per capita hospitalization expenditure was increasing, the per capita hospitalization expenditure of deaths distinctly dropped with ascending age, and the relatively higher value emerged before the group aged 55-60, almost exceeding 20,000 PPP Dollar per capita.

Figure 5A refers to the age group distribution of

per capita medical expenses and lifetime expected cost by age groups in hospitalization, and Figure 5B presents the proportion of per capita lifetime expected cost of survivors in per capita lifetime expenses for hospitalization. As age increases, the change of per capita hospitalization expenses of deaths was sharper than that in outpatient and emergency expenses, with 3 peaks appearing at groups aged 1-4 (45,095 PPP Dollar), 25-29 (37,270 PPP Dollar), and 35-59 (28,958 PPP Dollar). Meanwhile, the per capita hospitalization expenses escalated mildly, and the per capita lifetime expected hospitalization cost of both overall population and the survivors dropped smoothly, and at group aged 90 and over, the per capita lifetime expected hospitalization cost of survivors edged up. The share of the per capita lifetime expected hospitalization

Table 2. Simulated results of lifetime expected hospitalization cost*

Age groups	Survivors	Deaths	Survivor person-years	Survivor person years in total	Per capita hospitalization expenses (PPP Dollar)	Per capita hospitalization expenses of deaths (PPP Dollar)	Hospitalization expenses in total (PPP Dollar)	Per capita lifetime expected hospitalization cost (PPP Dollar)	Per capita lifetime expected hospitalization cost of survivors (PPP Dollar)
0~	100,000	483	99,604	8,292,764	489	6,289	48,738,149	58,540	58,510
1~	99,517	185	397,699	8,193,160	489	45,095	194,601,807	58,053	58,251
5~	99,332	89	496,440	7,795,461	191	30,286	94,669,190	56,106	56,456
10~	99,243	98	495,974	7,299,021	177	29,470	87,824,948	55,160	55,551
15~	99,146	125	495,417	6,803,048	150	26,540	74,418,630	54,282	54,716
20~	99,021	100	494,854	6,307,630	124	25,782	61,321,289	53,537	54,041
25~	98,920	117	494,309	5,812,777	195	37,270	96,543,334	52,924	53,457
30~	98,803	158	493,621	5,318,468	211	23,759	104,243,782	51,959	52,550
35~	98,645	214	492,691	4,824,847	208	28,958	102,648,328	50,916	51,553
40~	98,431	340	491,303	4,332,156	264	19,963	129,660,882	49,890	50,616
45~	98,090	591	488,974	3,840,853	414	20,455	202,499,334	48,593	49,416
50~	97,499	1,003	484,989	3,351,879	520	20,056	252,114,726	46,568	47,556
55~	96,496	1,741	478,128	2,866,890	654	21,075	312,544,335	44,047	45,266
60~	94,755	2,468	467,605	2,388,762	837	19,807	391,411,163	40,922	42,671
65~	92,287	3,873	451,754	1,921,157	1,111	19,256	501,759,108	37,007	39,292
70~	88,414	6,623	425,515	1,469,403	1,438	17,840	612,064,070	31,990	34,845
75~	81,791	11,839	379,359	1,043,888	1,816	15,999	688,954,453	25,869	29,312
80~	69,952	17,472	306,079	664,530	2,266	14,962	693,578,081	18,980	23,395
85~	52,480	22,289	206,677	358,450	3,180	15,722	657,238,874	12,044	16,273
90~	30,191	30,191	151,773	151,773	3,605	15,947	547,154,403	5,472	18,123

* PPP Dollar to Chinese RMB currency in 2015 comes from Organisation for Economic Co-operation and Development database (17). PPP, purchasing power parity.
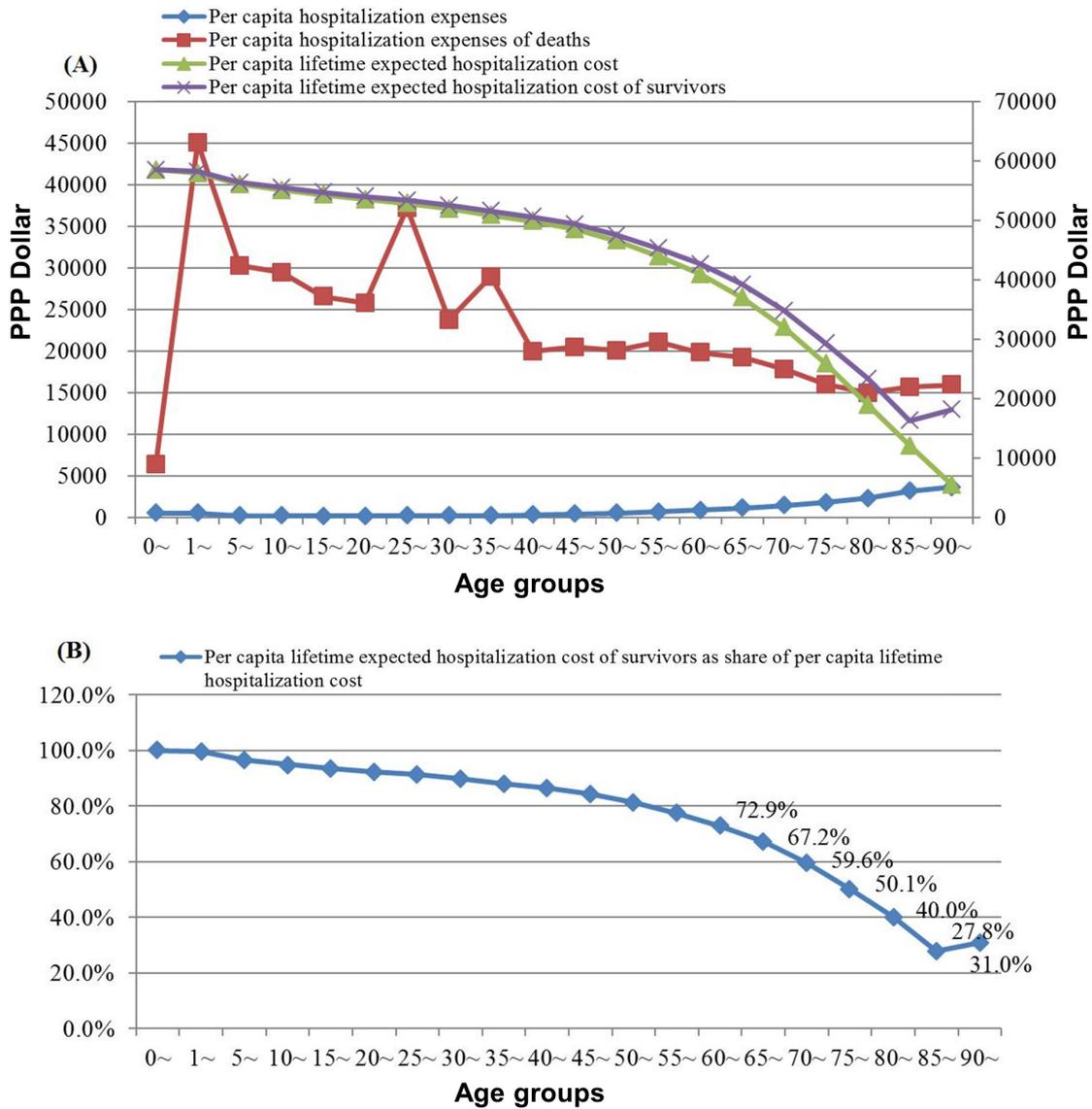
Figure 5. Per capita medical expenses and lifetime expected cost by age groups in hospitalization(Unit: PPP Dollar) (A), and the proportion of per capita lifetime expected cost of survivors in per capita lifetime expenses in hospitalization by 5 year intervals (Unit: %) (B). PPP, purchasing power parity.

cost of survivors in the per capital lifetime expected hospitalization cost was 72.9% in the group aged 60-64, which was 4.6 points lower than outpatient and emergency. It showed for people that lived to be in 60-64, the hospitalization expenses from now to death accounted for 72.9% of this individual's whole life hospitalization expenses. From groups aged 60-64 to 70-74, the proportions of hospitalization expenses from now to death in whole lifetime was below that of outpatient and emergency in the same age groups, whilst from age groups 75-79, to 90 and over, the proportions of hospitalization expenses from now to death in whole lifetime exceeded the proportions of outpatient and emergency in the same age groups. Generally, in the more advanced elderly group, the proportion of expenses in hospitalization tend to be higher than that in outpatient and emergency.

3.3.3. *Total medical expense*

Table 3 combines the outpatient and emergency, and hospitalization expenditures, and shows the results of simulated total lifetime expected cost. The per capita total medical expenses went up with increasing age, and was below the per capita total medical expenses of deaths. The per capita lifetime expected hospitalization cost from birth was 139,551 PPP Dollar, when people who survived to age 60, per capita lifetime expected cost of the group aged 60-64 was 105,447 PPP Dollar. However, since the hospitalization expenses were much higher than outpatient and emergency expenses, the per capita total medical expenses of deaths was mainly affected by per capita hospitalization expenses of deaths, presenting similar fluctuant features as hospitalization. After eliminating the deaths, the per capita total expected

Table 3. Simulated results of total lifetime expected cost*

Age groups	Survivors	Deaths	Survivor person-years	Survivor person years in total	Per capita total medical expenses (PPP Dollar)	Per capita total medical expenses of deaths (PPP Dollar)	Total medical expenses (PPP Dollar)	Per capita total lifetime expected cost (PPP Dollar)	Per capita total lifetime expected cost of survivors (PPP Dollar)
0~	100,000	483	99,604	8,292,764	793	6,289	78,942,383	139,582	139,551
1~	99,517	185	397,699	8,193,160	793	45,715	315,201,347	138,792	139,381
5~	99,332	89	496,440	7,795,461	618	30,314	306,855,592	135,640	136,525
10~	99,243	98	495,974	7,299,021	439	29,513	217,577,736	132,572	133,553
15~	99,146	125	495,417	6,803,048	244	26,797	120,759,680	130,396	131,485
20~	99,021	100	494,854	6,307,630	181	26,072	89,622,523	129,188	130,439
25~	98,920	117	494,309	5,812,777	410	37,862	202,493,269	128,292	129,647
30~	98,803	158	493,621	5,318,468	537	24,271	264,900,776	126,267	127,758
35~	98,645	214	492,691	4,824,847	512	29,595	252,156,071	123,618	125,251
40~	98,431	340	491,303	4,332,156	559	20,767	274,880,654	121,097	122,955
45~	98,090	591	488,974	3,840,853	845	21,084	413,353,859	118,348	120,525
50~	97,499	1,003	484,989	3,351,879	1,194	20,621	578,910,118	114,214	116,932
55~	96,496	1,741	478,128	2,866,890	1,674	21,857	800,235,635	108,425	111,968
60~	94,755	2,468	467,605	2,388,762	2,314	20,544	1,081,981,925	100,423	105,447
65~	92,287	3,873	451,754	1,921,157	3,101	20,032	1,401,014,805	89,603	96,251
70~	88,414	6,623	425,515	1,469,403	3,934	18,618	1,673,771,309	75,593	84,104
75~	81,791	11,839	379,359	1,043,888	4,777	16,825	1,812,289,858	58,855	69,522
80~	69,952	17,472	306,079	664,530	5,631	15,882	1,723,576,177	40,732	54,262
85~	52,480	22,289	206,677	358,450	6,700	16,660	1,384,738,390	23,496	37,697
90~	30,191	30,191	151,773	151,773	6,358	16,814	964,907,894	9,649	31,960

* PPP Dollar to Chinese RMB currency in 2015 comes from Organisation for Economic Co-operation and Development database (*17*). PPP, purchasing power parity.
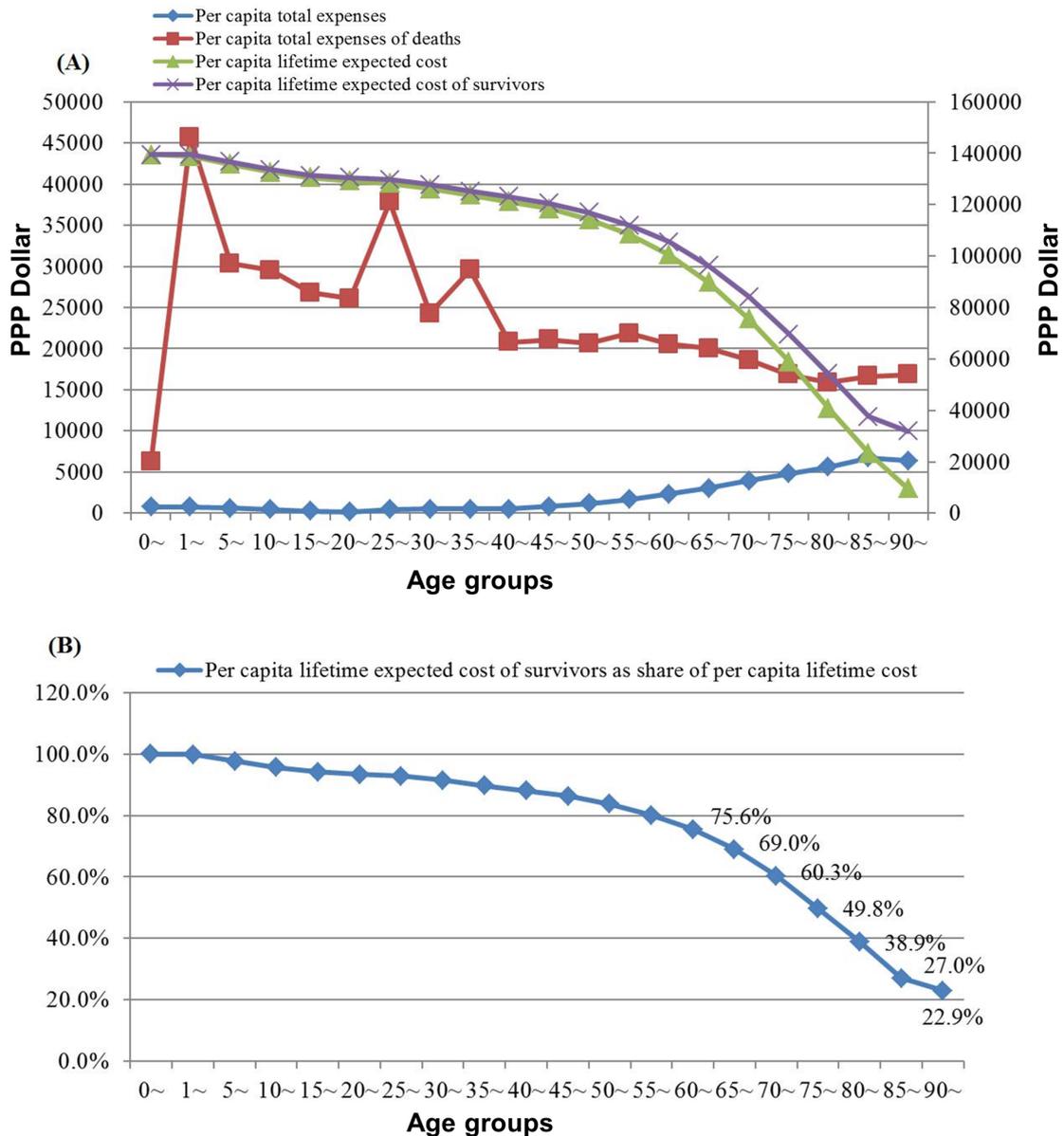
Figure 6. Per capita total medical expenses and total lifetime expected cost by age groups (Unit: PPP Dollar) (A), and the proportion of per capita total lifetime expected cost of survivors in per capita total lifetime expenses by 5 year intervals (Unit: %) (B).

cost of survivors wasa bit over the per capita total expected cost in the same age group.

Figure 6A is the age group distribution of per capita total medical expenses and total lifetime expected cost, and Figure 6B refers to the share of per capita total lifetime expected cost of survivors in per capita total lifetime expenses. The change of Figure 6A presented the approximated characteristics of Figure 5A, as age was trending up, the per capita total medical expenses of deaths increased, with 3 peaks appearing at groups aged 1-4 (45,715 PPP Dollar), 25-29 (37,862 PPP Dollar), and 35-59 (29,595 PPP Dollar). Meanwhile the per capita total expenses grew, and the per capita lifetime expected total cost of both overall population and the survivors fell. The proportions of per capita total lifetime expected

cost of survivors in per capita total medical expenses were 75.6% and 38.9%, in groups aged 60-64 and 80-84, respectively. The share of the group aged 90 and over reached 22.9%, which meant for people who live to 90, the total medical expenditure from now to death accounted for approximately twenty percent of their total lifetime medical expenditure.

4. Discussion

4.1. *Shanghai elderly people had higher shares of expected medical expenses in lifetime medical expenses*

According to the above results, the elderly population as 19.5% of the total population in Shanghai, not only

utilized a large portion of medical resources (52.2% of total outpatient and emergency visits, and 45.3% discharged patients), but also accounted for more than half of the medical expenses (63.2% of outpatient and emergency expenses, 52.8% hospitalization expenses). In addition, the expenses in elderly age accounted for a major portion (approximately eighty percent, Figure 6) of lifetime medical expenses, which indicated that the medical expenses are more concentrated in the aged phase, and reflected that the elderly population consumed a larger proportion of medical resources compared with other groups of the population. In comparison with other countries, it can be concluded that although the studies found similar results, the gap between elderly people and other age groups in medical expenses was less significant.

For example, the study by Alemayehu (2004) in Michigan (*16*), US showed that the expenses of population aged 65 and over accounted for 1/2 of lifetime medical expenses in this region. The analysis from Shanghai data revealed that in the group aged 60-64, the proportions of per capita expected cost in per capita lifetime cost in outpatient and emergency, and hospitalization accounted for 77.5% (Figure 4B) and 72.9% (Figure 5B), respectively. Excluding the confounding factors such as study times, it can still be concluded that the medical expenses in the elderly population of Shanghai far exceeded the corresponding rates of Michigan, US.

4.2. *The medical expenses of elderly aged 80 and over was expected to flow to hospitalization, while the expenses of elderly aged 60-79 was expected to flow to outpatient and emergency*

Our results illustrated that the proportion of per capita lifetime expected cost of survivors in per capita lifetime expenses of the advanced elderly (population aged 80 and over) accounted for 38.9% (Figure 6B) of their lifetime expenses, including 38.1% (Figure 4B) in outpatient and emergency, and 40.0% (Figure 5B) in hospitalization, which was slightly higher than in outpatient and emergency. Moreover, the three advanced age groups, aged 80-84, 85-89, and 90 and over, all have higher expected hospitalization costs in lifetime expenses (40.0%, 27.8%, 31.0%, respectively, Figure 5B), compared with expected outpatient and emergency costs in lifetime expenses (38.1%, 26.4%, 17.1%, respectively, Figure 4B), while the other elderly group aged from 60 to 79 represented the opposite. It is indicated that the expected medical cost in advanced elderly groups (aged 80 and over) was mainly concentrated in hospitalization, while the expected medical cost in the relatively younger elderly people (aged 60-79) largely flew to outpatient and emergency. This conclusion is also close to the actual situation in Shanghai.

There is room for saving medical expenses in the elderly people in Shanghai, especially in the hospitalization expenditure of the advanced elderly population. International experience suggested that elderly care and rehabilitation has a momentous function in replacing hospitalization, furthermore would bring benefits to the health of elderly people in the future (*15,16*).

Our study has some limitations: first of all, the hypothesis in this study is assuming that the technology, pricing and other factors are stable, and the prevalence, incidents, development process and costs of disease do not change with time. Therefore, the life table model cannot reflect the impact of health technology development, the outbreak of new disease, perishing of old disease, and inflation. Secondly, nursing care plays an important role in the lives of the elderly, however the nursing care expenditures were not included in this study. In Shanghai, currently most of nursing care expenses has been paid out-of-pocket, which applies difficulty for data collection of our full sample size study. Further research could investigate the role of nursing care in the age distribution of expenditures, as well as how these expenses play out over the lifetime with medical expenses.

5. Conclusion

The findings of our study extend the knowledge of age-specific medical expenses, and show a striking share of elderly people's medical resource utilization and expenses. Although the lifetime expenses studies have been well-documented, we have known little about it, for two reasons: first, most of the studies were conducted in developed countries, and may not be applied in developing counties; second, the vast majority of studies were based on sampling, which may bring selection bias. This study is an exploration of lifetime expenses simulation in a relatively more developed region of China, which has a large population base with rapidly aging people. Besides, our study covered all the emergency, outpatient, hospitalization and medical expenses data in Shanghai in 2015, which can fully represent the characteristics of medical spending concentration in the Shanghai population.

We found that the elderly population as 19.5% of total population in Shanghai, accounted for 63.2% of outpatient and emergency expenses (52.2% of total outpatient and emergency visits) and 52.8% of hospitalization expenses (45.3% discharged patients). When surviving to age 60, 75.6% of lifetime medical expenses were expected to be spent at age 60 and over (Figure 6B), with 77.5% in emergency and outpatient (Figure 4B), and 72.9% in hospitalization (Figure 5B). The groups aged 80 and over, have higher expected hospitalization costs in lifetime expenses (40.0% in ages 80-84, 27.8% in ages 85-89, and 31.0% in age 90

and over, Figure 5B) than outpatient and emergency cost in lifetime expenses (38.1% in ages 80-84, 26.4% in ages 85-89, and 17.1% in age 90 and over, Figure 4B). Among the advanced elderly (population aged 80 and over), their expected medical expenses were more concentrated in hospitalization. In addition, our results have implications for forecasting the expected medical expenses. We suggested addressing the elderly population for saving medical resources and expenses, especially in hospitalization expenditures of the advanced elderly population.

Acknowledgements

References

1. National Bureau of Statistics of the People's Republic of China. 2015 Statistical Bulletin of National Economy and Social Development. *http://www.stats.gov.cn/tjsj/zxfb/201602/t20160229_1323991.html* (Accessed August 29, 2017) (in Chinese)

2. Bureau of Statistics of Shanghai. 2016 Shanghai Statistic Yearbook. Beijing: China Statistics Press, 2017. (in Chinese)

3. Xu L. The challenge and its countermeasures from medical insurance fund owing to the trends of senility: Shanghai for instance. Inquiry Into Economic Issues. 2005; 12:50-60. (in Chinese)

4. Yan P, Li CX. Medical expenses burden and change in Chinese elderly people. Chinese Journal of Gerontology. 2013; 16:3935-3939. (in Chinese)

5. Tao H, Yao ZH, Ye S, Gao Y, Wu FJ, Zhu LH, Ye Y, Liu CJ, Feng XS. The health status and its impact factors in the elderly in Shanghai Nanhui. Chinese Journal Of Gerontology. 2010; 30:1412-1414. (in Chinese)

6. Zhang LJ, Chu ZQ, Gao XN, Chen YC. Analysis on the aging effect on the new rural cooperative medical system fund: Case study of a county in Hubei. Chinese Health Economics. 2015; 34:29-31. (in Chinese)

7. Huang TT. The impact of population aging on the growth of total health expenditure in China. Xiamen: Xiamen University, 2012. (in Chinese)

8. Wang CQ. Is aging the determinant of health expenditure growth or not? Population & Economics. 2014; 3:23-30. (in Chinese)

9. Ma AX, Xu YY. Determinants on aged population's health expenditures in China, Chinese Journal of Chinese Policy. 2015; 7:68-73. (in Chinese)

10. Yu YY. The impact of population aging to medical expenses – from the perspective of urban-rural disparity. World Economic Papers. 2011; 5:64-78. (in Chinese)

11. CulterDM, MearaE. The medical costs of the young and old: A forty-year perspective. Chicago: University of Chicago Press. 1998; 215-246.

12. Waldo DR, Lazenby HC. Demographic characteristics and health care use and expenditures by the aged in the United States: 1977-1984. Health Care Financing Review. 1984; 6:1-29.

13. Buchner F, Wasem J. "Steeping" health expenditure profiles. The Geneva Papers. 2006; 31:581-589.

14. Reinhardt U E. Does the aging of the population really drive the demand for health care? Health Affairs (Millwood). 2003; 22:27-39.

15. Lassman D, Hartman M, Washington B, Andrews K, Catlin A. US health spending trends by age and gender: Selected years 2002-10. Health Aff (Millwood). 2014; 33:815-822.

16. Alemayehu B, Warner KE. The lifetime distribution of health care costs. Health Serv Res. 2004; 39:627-642.

17. Organisation for Economic Co-operation and Development. Purchasing power parities. *https://data.oecd.org/conversion/purchasing-power-parities-ppp.htm* (Accessed August 23, 2017).

Effects of lifestyle advice provided by pharmacists on blood pressure: The COMmunity Pharmacists ASSist for Blood Pressure (COMPASS-BP) randomized trial

Hiroshi Okada[1,2,3,*], Mitsuko Onda[4], Masaki Shoji[5], Naoki Sakane[2], Yasushi Nakagawa[6], Takashi Sozu[7], Yui Kitajima[8], Ross T. Tsuyuki[3], Takeo Nakayama[1]

[1] *Department of Health Informatics, Kyoto University School of Public Health, Kyoto, Japan;*
[2] *Division of Preventive Medicine, Clinical Research, National Hospital Organization, Kyoto Medical Center, Kyoto, Japan;*
[3] *EPICORE Centre, Department of Medicine, Faculty of Medicine and Dentistry, University of Alberta, Edmonton, Alberta, Canada;*
[4] *Clinical Laboratory of Social and Administrative Pharmacy, Osaka University of Pharmaceutical Sciences, Osaka, Japan;*
[5] *Clinical Laboratory of Practical Pharmacy, Osaka University of Pharmaceutical Sciences, Osaka, Japan;*
[6] *Polon Company, Kobe, Japan;*
[7] *Department of Information and Computer Technology, Faculty of Engineering, Tokyo University of Science, Tokyo, Japan;*
[8] *Department of Management Science, Faculty of Engineering, Tokyo University of Science, Tokyo, Japan.*

Summary   The COMmunity Pharamcists ASSist for Blood Pressure (COMPASS-BP) study aimed to assess the effectiveness of lifestyle support programs administered in community pharmacies on hypertension control. This open-label, two-armed parallel group, cluster-randomized controlled trial included 73 pharmacies (clusters) in Japan randomized to a control or intervention group. Eligible hypertensive patients (*n* = 125), aged 20-75 years, received the intervention (*n* = 64) or the control treatment (*n* = 61), as dictated by their pharmacy randomization. Patients in the intervention group received brochures and healthy lifestyle advice from pharmacists using motivational interviewing methods during pharmacy visits over a 12-week period, with their usual pharmacy care. Conversely, the control group just received usual care. The main outcome measure was a change in morning systolic blood pressure (SBP) from baseline to week 12. The intervention group exhibited a decrease in morning SBP that was 6.0 mmHg greater than that of the control group (95% confidence interval [CI]: −11.0 to −0.9, *p* = 0.021). In a mixed-effect model for repeated measures analysis, the intergroup difference in morning SBP decrease was −4.5 mmHg (95% CI: −8.5 to −0.6, *p* = 0.024). Our findings indicate that implementation of a lifestyle advice program in pharmacies is feasible and may lead to reduced blood pressure.

Keywords: Community pharmacy, hypertension, home blood pressure measurement, patient education, mixed-effect model for repeated measures analysis

1. Introduction

One of the most common and important health problems faced by societies worldwide is hypertension. In particular, elevated morning systolic blood

pressure (SBP) has been identified as a risk factor for atherosclerotic disease (*1,2*), which is responsible for at least 45% and 51% of heart disease- and stroke-related deaths, respectively (*3*). Although these vascular diseases are major causes of death in Japan, only about 30% of men and 40% of women have controlled blood pressure (BP) (*4*). Home BP monitoring is preferred over hospital, clinic, or office BP measurements (*5,6*). Home BP monitors are sold in most community pharmacies in Japan. An estimated 77% of individuals with hypertension and 40% of individuals without hypertension use these devices (*7*).

Lifestyle plays an important role in the management

of hypertension. The provision of lifestyle advice was found effective in decreasing the recipient's weight, dietary sodium intake, and alcohol intake, while promoting physical activity, and resulted in better BP control (*8-11*). In Japan, the estimated average daily sodium intake is 10.6 g per day, which is more than twice the amount recommended by the World Health Organization (*3,7,9*). However, individuals with hypertension have very few opportunities to learn about healthy lifestyles from professionals in their communities.

Pharmacists are highly accessible healthcare professionals who can be a valuable social asset in the management of hypertension (*3*). Previous studies have shown that the administration of a care-based program to hypertensive patients at community pharmacies improved patients' BP control and outcomes (*12-14*). However, the consultations provided in previous studies were of relatively long durations (20-30 minutes), and require a more advanced scope of practice than is available in Japan currently. Previous studies also measured BP during clinic visits, rather than using the preferred strategy of home BP measurements. Therefore, our study was aimed to evaluate the effects of brief motivational lifestyle advice provided by pharmacists to hypertensive patients with the intent to improve home-monitored BP in a community setting (COMmunity Pharmacists ASSist for Blood Pressure [COMPASS-BP] Project).

2. Materials and Methods

2.1. *Trial design*

This study was a cluster randomized controlled trial. The clusters were community pharmacies. The pharmacies were randomly assigned to either the Intervention group or the Control group. Randomization was stratified by matched cluster sizes. Community pharmacies were recruited through direct requests to local pharmaceutical associations and chain pharmacies during explanatory meetings. Seventy-three pharmacies in 15 prefectures across Japan participated. Pharmacists and patients were not blinded to treatment allocation. The trial registration number is UMIN000014128 (May 31, 2014) (*https://upload.umin.ac.jp/cgi-open-bin/ctr_e/ctr_view. cgi?recptno=R000016452*)

2.2. *Participants*

Pharmacy eligibility criteria were as follows: *i*) more than 20 hypertensive patients visited the pharmacy each month; and *ii*) certified pharmacists delivered the training program according to the protocol. The protocol provided instructions on the correct method for home BP measurement through a brochure, as well as supportive communication and clinical practice guidelines regarding hypertension in Japan.

Patient eligibility criteria were as follows: *i*) hypertensive patients who visited pharmacies to obtain medication for more than three months; and *ii*) aged 20-75 years.

Patient exclusion criteria were as follows: *i*) serious complications, such as dialysis or chronic kidney disease; *ii*) dementia or mental illness; or *iii*) an otherwise determined lack of suitability for this lifestyle intervention study.

Data collection settings and locations: Study recruitment occurred during two periods: from September 2014 to March 2015 and from May 2015 to November 2015. Pharmacists recruited patients using standardized brochures and posters. Each pharmacy was asked to recruit three patients. Eligibility was verified using the most recent clinical BP data recorded in a BP diary within the previous three months and the medication history obtained from the pharmacy.

2.3. *Randomization*

Blocked randomization according to the pharmacy size (classified by the number of patients per day: small, 0-50 patients; middle, 51-100 patients; large, ≥ 101 patients) and type (chain or private pharmacy) was performed by the Center of Randomization at the Division of Prevention Medicine of Clinical Research Institute, National Hospital Organization Kyoto Medical Center, Japan.

2.4. *Blinding*

The participants and community pharmacists involved in this study could not be blinded because of the nature of the intervention. A statistician who was blinded to group allocation analysed the data.

2.5. *Intervention group*

2.5.1. *Pharmacist training*

Pharmacists who participated in this study completed a 4-hour training program on the methods for interviewing patients and providing information at community pharmacies. Candidate pharmacists were trained in the following three areas: *i*) The study purpose, *ii*) Correct home device methods for BP measurements, and *iii*) The provision of brief motivational advice to patients. The modified motivational interviewing, which was based on empowerment or coaching-style communication included three steps: *i*) using an open question, *ii*) setting each goal with patients, and *iii*) closing with encouragement. The program had the following five areas that could be selected by patients: *i*) reducing sodium intake, *ii*) including more vegetables in meals, *iii*) exercising, *iv*) losing weight, and *v*) reducing alcohol consumption.

2.5.2. *Patient training and registration*

Validated home BP monitors (HEN-7200; Omron Corporation, Kyoto, Japan) (*15*) and pedometers (HJ-205; Omron Corporation) were provided to all participants upon study entry at the pharmacy. The participants were instructed how to measure BP and count steps, then collected these data for two weeks before study randomization. The pharmacists checked these BP data for the initial two weeks; patients with less than two missing measurements were registered in the study (Figure 1).

Intervention group patients submitted their BP measurements and other personal data for evaluation and received advice about a healthy lifestyle from a certified pharmacist when they visited the pharmacy. The attending pharmacists were provided with 12 types of brochures, a BP diary, and a table listing food with high sodium content to support the five previously mentioned agenda items. The pharmacists gave the participants one of these tools and demonstrated its usage.

At the second visit (visit 1), a pharmacist and the Intervention group patient discussed goal setting and methods to induce lifestyle changes, according to the five agenda items. Pharmacists provided this information in a brochure, which was used by the patient when selecting the method. At every visit (visits 1-3), the pharmacist asked about the patient's lifestyle, goal accomplishments, and barriers to lifestyle changes. After reflecting on the previous visit, they discussed new goal setting during every visit. The pharmacists delivered a standardized intervention using a check list in the Case Report Form.

2.6. *Control Group*

Patients in the Control group were provided the same home BP monitor as the Intervention group and a basic explanation about their medication. The attending pharmacists checked and evaluated their BP and measurement methods without providing special consultations.

2.7. *Outcomes*

All participants were followed for 12 weeks. The main outcome was the change in morning home SBP, which was calculated as the difference between BP data from the pharmacy at baseline (visit 0) and the average home BP at 12 weeks (78-84 days). The secondary outcomes were medication changes, medication adherence (using the Modified Morisky Scale 8-item response option) (*16*), lifestyle changes (using the International Physical Activity Questionnaires) (*17,18*), changes in attitudes and knowledge about hypertension, and changes in home-monitored body mass index (BMI; weight in kg/squared height in m^2) between baseline (visit 0) and the last 12 weeks. Salt intake was determined using a validated seven-item questionnaire about the intake frequency of salty and processed foods, such as salty fish, pickles, and soups (*19*). Patients' quality of life was determined using the EuroQol questionnaire (*20*). The participants responded to the above-mentioned questionnaires at community pharmacies during their visit 0 (baseline) and visit 4 (12 weeks later). All participants wore a pedometer for more than 12 hours per day.

2.8. *Measurements*

Baseline BP was measured and recorded at the pharmacy upon study entry. In Japan, a patient diary is typically recommended to record home BP measurements and is
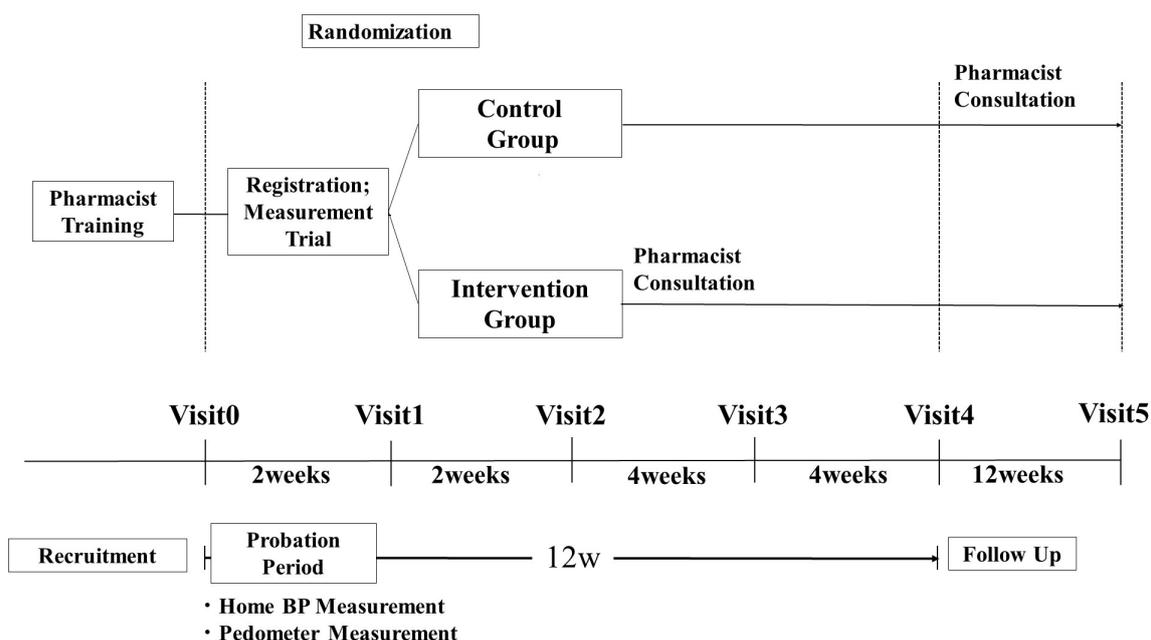

Figure 1. Study flow chart of COMPASS-BP.

used by hospitals and clinics to evaluate home BP data for hypertensive patients. Diaries were provided to all patients in the study to record BP and additional data, such as body weight and steps taken on each monitored date. The participants measured their BP twice daily (in the morning and at bedtime) by recording this information in their diary, thus enabling the sharing of these data with physicians and pharmacists. The participants' heights and weights were also checked. Medication data were collected from prescriptions. Study data were collected from all participants for 84 days. All conditions except the designated intervention were equal between the two groups.

Securing reliability of the data: During every visit to the pharmacy, patients were educated about appropriate BP measurement procedures based on the current clinical practice guidelines in Japan (*5*). The attending pharmacists recorded these data. Changes in patients' medications were checked and printed for inclusion in personal health records. At every visit, the attending pharmacist was required to check both the BP measurement method and any missing records.

2.9. *Sample size*

We assumed an SBP decrease of 5 mmHg, significance level of 5%, outcome variable standard deviation (SD) of 15, statistical power of 80%, and two-tailed significance test to calculate the required sample size in each group. Using an intra-class correlation of 0.1 and assuming three patients in each cluster, a minimum required sample size of 30 pharmacies per arm was determined, for 180 patients in both arms. To compensate for dropouts, the sample size was set to 33 pharmacies (99 patients) in both groups (total = 198). These calculations were conducted using sample size tables for clinical studies (*21*).

2.10. *Statistical analysis*

Continuous variables are presented as means and standard deviations (SD), whereas categorical variables are presented as numbers and percentages. The difference in the primary outcome between the groups was estimated with 95% confidence interval and compared using Student's *t*-tests. Furthermore, repeatedly measured home BP data were analysed using the mixed-effect model for repeated measures (MMRM) with the first-order autoregressive structure (AR[1]) (*22*), where the group, the measurement time, and the interaction of group and measurement time were included as the fixed effect and the baseline SBP as the covariate. Secondary outcome analysis between the two groups was performed using Student's *t*-test. All *p*-values were two-sided, with *p*-values < 0.05 considered as statistically significant. All data analyses were conducted using SAS statistical software version 9.4 (SAS Institute Inc., Cary, NC,

USA). The clustering effect was not considered because of the small cluster size (average 2 patients a pharmacy: 1-3 patients). All data are presented as means with SDs. The primary analyses used the last observation carried forward method to address missing data. For cases with missing data at baseline, we used the average BP from the first week.

2.11. *Ethics approval*

All related procedures in this study were approved by the Ethical Committee of Kyoto University School of Medicine (C1230). All patients provided written informed consent to participate in the study. The study protocol complied with the principles of the Declaration of Helsinki and written informed consent was obtained from participants prior to study recruitment. All data were analysed anonymously.

3. Results

Enrolment in the COMPASS-BP study began on September 1, 2014 with 55 pharmacies (112 patients) and on May 1, 2015 with another 18 pharmacies (13 patients). A total of 73 pharmacies were recruited for the study and were randomized. However, 17 pharmacies did not recruit any patients (7 pharmacies assigned to Intervention and 10 assigned to the Control). A total of 125 patients were recruited (64 in the Intervention and 61 in the Control). The cluster exclusion rate was 25.5% (25/98 pharmacies), and the allocated cluster rate was 76.7% (56/73 pharmacies). The final analysis included 30 pharmacies (64 patients) in the Intervention group and 26 pharmacies (61 patients) in the Control group (Figure 2). Although follow-up data were available for all participants, the baseline BPs for 44 of the 125 patients were not recorded; in these cases, the first week's BP was used as the baseline value.

Participants in the Intervention group were slightly younger (Intervention: 61.6 [9.9] years, Control: 66.6 [9.0]), had a lower incidence of diabetes (Intervention: 17.2%, Control: 24.6%), a higher incidence of hyperlipidaemia (Intervention: 37.5%, Control: 29.6%), and lower frequency of angiotensin receptor-II blocker/angiotensin-converting enzyme inhibitor use (Intervention: 65.6%, Control: 78.7%) (Table 1). Furthermore, the mean morning SBP and diastolic blood pressure (DBP) were slightly higher in the Intervention Group (Intervention: 135.2/81.6 [13.1/8.7] mmHg, Control: 131.8/76.6 [14.1/9.6]) (Table 2).

There were significant differences in the mean change in morning SBP and DBP between the two groups. The difference in change in SBP over the 12 weeks was −6.0 mmHg (Intervention: −1.1 mmHg, Control: +4.9 mmHg; 95% confidence interval [CI]: −11.0 to −0.9; *p* = 0.021; Table 2). The subsequent MMRM analysis yielded a slightly smaller but still significant estimated difference
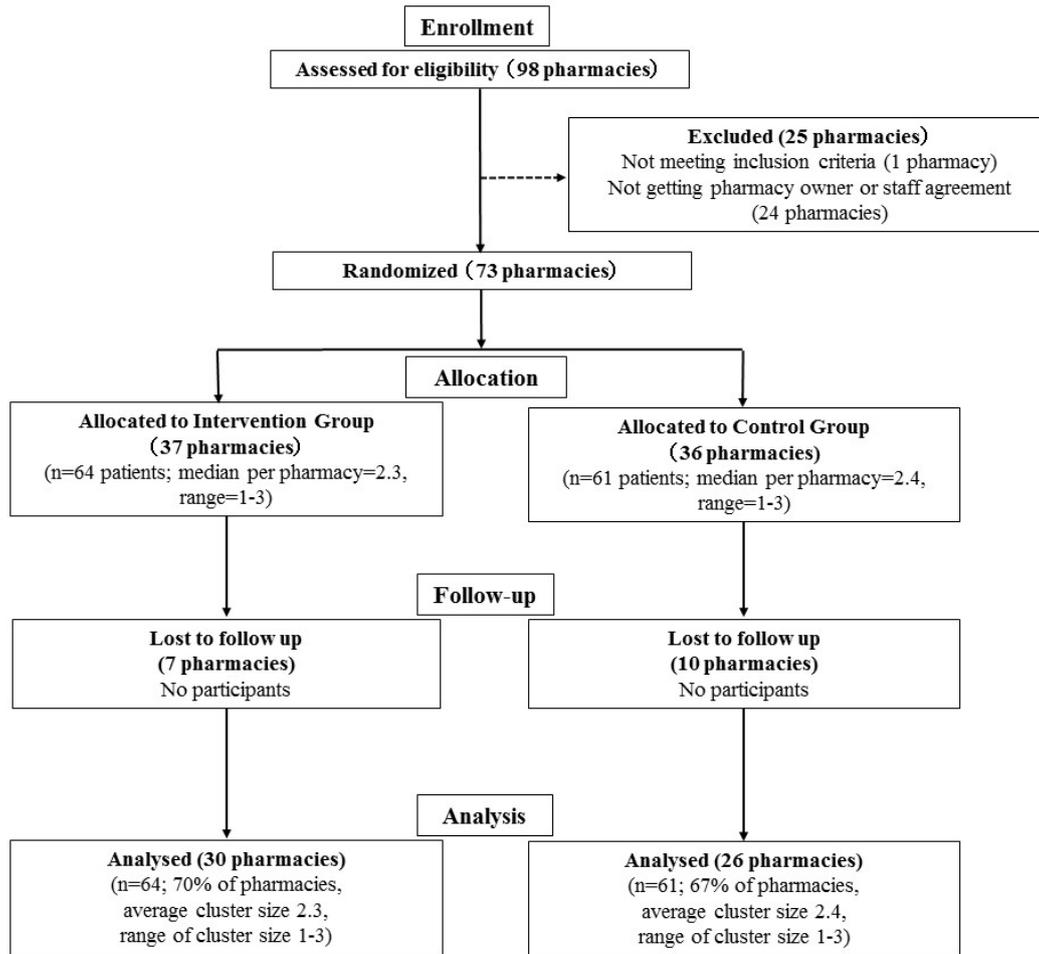
Figure 2. CONSORT flow chart of COMPASS-BP.

Table 1. Baseline characteristics of individuals and clusters

Variables	Intervention Group	Control Group
Cluster level		
No. of Pharmacies	37	36
Cluster type (%)[a]		
Small	23 (62.2)	25 (69.4)
Medium	7 (18.9)	6 (16.7)
Large	7 (18.9)	5 (13.9)
Individual level		
No. of patients	64	61
Age, years (SD)[*]	61.6 (9.9)	66.6 (9.0)
Gender, female (%)	40 (62.5)	35 (57.4)
Duration of Antihypertensive Medication		
Years, (%)[b]		
< 5	19/40 (47.5)	19/36 (52.8)
6-10	8 (20.0)	10 (27.8)
11-15	7 (17.5)	2 (5.6)
16-20	5 (12.5)	3 (8.3)
> 21	1 (2.5)	2 (5.6)
Comorbidities		
Diabetes (%)	11/64 (17.2)	15/61 (24.6)
Hyperlipidemia (%)	24/64 (37.5)	18/61 (29.6)
Medication (%)[c]		
ARB/ACE	42/64 (65.6)	48/61 (78.7)
CCB	39/64 (60.9)	45/61 (73.8)
Diuretic	11/64 (17.2)	6/61 (9.8)
α/β-Blocker	2/64 (3.1)	8/61 (13.1)
Renin inhibitor	0/64 (0.0)	1/61 (1.6)

[*]Age: $p = 0.004$. There were no significant differences expect for age in two groups. Missing data was not included in the analysis. [a]Pharmacies were classified by the number of patients seen per day. Small: 0-50, Middle: 51-100, Large: > 101. [b]Duration of medication use for hypertension was checked through patient self-reporting. [c]Categories of hypertensive medications taken by patients.

in the changes in morning SBP between the two groups (−4.5 mmHg; 95% CI: −8.5 to −0.6, *p* = 0.024; Table 3). DBP did not differ significantly between the two groups (−1.8 mmHg; 95% CI: 4.4 to 0.8, *p* = 0.169; Table 3).

According to International Physical Activity Questionnaires scores, the groups differed in terms of changes in physical activity. More Intervention patients were less physically active (266 to 243; Intervention: −23 [105]; Control: 119 [191]; *p* = 0.016; Table 4). No significant differences were observed for any other secondary endpoints, including quality of life, BMI, salt intake score, or knowledge about a healthy lifestyle.

4. Discussion

Lifestyle plays an important role in the management of hypertension. The COMPASS-BP trial was conducted to determine whether a brief, motivational interview-based intervention administered by pharmacists could improve BP. Our study demonstrated that the intervention was feasible and well accepted by pharmacists and patients. Notably, the attained SBP level was similar to those reported by previous studies (*13,14*). Although we did not observe large differences in BP, the results implied that the brief healthy lifestyle advice provided by pharmacists during daily practice had an effect on patients' BP control.

Motivational interviewing is a patient-centred strategy designed to elicit behaviour change by helping clients to explore and resolve ambivalence to change (*23*). Motivational interview-based interventions have been shown to enhance adherence and improve targeted diet-related outcomes (*24*). Self-monitoring involves the client keeping a record of thoughts, emotions, dietary behaviours, and health measurements, such as blood pressure. The patients can review this record for

Table 2. Reported BP at baseline and study completion

Items	Intervention Group (*n* = 64)		Control Group (*n* = 61)		*p*-Value		Difference (95% CI)	
	SBP	DBP	SBP	DBP	SBP	DBP	SBP	DBP
Baseline BP	135.2	81.6	131.8	76.6	0.166	0.003	3.4	5.0
mmHg (SD)	(13.1)	(8.7)	(14.1)	(9.6)			(-1.4 to 8.2)	(1.7 to 8.2)
12 Week BP	134.2	79.4	136.7	77.5	0.242	0.283	-2.5	1.9
mmHg (SD)	(10.4)	(10.1)	(13.8)	(8.8)			(-6.9 to 1.8)	(-1.6 to 5.3)
Difference	-1.1	-2.2	4.9	1.2	0.021	0.026	-6.0	-3.4
mmHg (SD)	(13.0)	(8.5)	(15.5)	(8.6)			(-11.0 to -0.9)	(-6.5 to -0.2)

BP, blood pressure.

Table 3. Mixed-effect model for repeated measures (MMRM) analysis of SBP and DBP

Dependent Variable (Intervention: *n* = 64, Control: *n* = 61)	Estimate difference	95% CI	*p*-Value
Morning SBP (mmHg) Ar(1)*	-4.5	-8.5 to -0.6	0.024
Morning DBP (mmHg) Ar(1)*	-1.8	-4.4 to 0.8	0.169

SBP: systolic blood pressure, DBP: diastolic blood pressure, Ar(1)*: auto regressive(1).

Table 4. Clinical and humanistic parameters of patients at baseline and study completion

Items	Intervention group (*n* = 64), Mean (SD)			Control group (*n* = 61), Mean (SD)			*p*-Value
	Baseline	After	Difference	Baseline	After	Difference	
Medication adherence[a]	13.3 (1.2)	13.6 (1.0)	0.3 (1.0)	13.6 (1.0)	13.7 (1.0)	0.1 (1.1)	0.398
WHO-5[b]	13.2 (4.4)	13.2 (4.2)	-0.1 (2.7)	12.9 (4.2)	13.6 (4.1)	-0.1 (3.1)	0.613
EQ-5D[c]	0.90 (0.14)	0.89 (0.14)	-0.01 (0.1)	0.92 (0.14)	0.88 (0.18)	0.00 (0.19)	0.797
BMI d	24.2 (3.3)	24.0 (2.5)	-0.1 (0.5)	24.3 (3.6)	24.4 (3.5)	0.0 (0.6)	0.768
Steps/day	6092 (3134)	5201 (3322)	-993 (2064)	5099 (2684)	4587 (2772)	-614 (1819)	0.502
IPAQ[e]	266 (228)	243 (225)	-23 (105)	245 (235)	385 (270)	119 (191)	0.016
Importance[f]	27.0 (3.4)	28.3 (4.1)	1.23 (3.1)	27.1 (4.2)	28.1 (2.6)	0.96 (2.7)	0.636
Confidence[g]	23.5 (4.1)	24.2 (4.0)	0.6 (3.0)	23.9 (4.5)	24.8 (3.8)	0.87 (3.0)	0.690
Salt-intake Score[h]	15.6 (3.3)	15.6 (3.8)	0.0 (2.6)	14.3 (2.5)	14.6 (3.3)	0.4 (2.5)	0.476
Knowledge[i]	5.6 (2.5)	6.5 (2.1)	0.9 (2.1)	5.6 (1.9)	6.6 (2.2)	1.0 (1.8)	0.768

[a]Medication adherence; a modified, 8-item. Morisky Medication Adherence Scale (MMAS). [b]WHO-5; the WHO-Five wellbeing index. [c]EQ-5D; standardized instrument for use as a measure of health outcome. [d]BMI; body mass index. [e]IPAQ; International Physical Activity Questionnaire. [f],[g]Importance/Confidence; Pharmacists' importance and confidence scores of diabetes care (out of 10). [h]Salt-intake Score; Intake frequency of the following foods, ranging from "everyday" to "not at all". 1) Salted fish, 2) Dried fish, 3) Processed fish meat, 4) Ham and sausage, 5) Pickles, 6) Noodles, 7) Miso soup. [i]Knowledge of healthy lifestyle choices, measured by 10 true or false questions.

triggers and patterns, which can then be used to assist with problem solving and goal setting (*25*). Although community pharmacists have previously conducted randomized controlled trials on lifestyle intervention that were based on motivational interviewing such as cognitive behavioural therapy, all of these trials were focused on improving medication adherence rather than mediating lifestyle changes (*26*). In our study, however, there was not a significant difference in adherence between the two groups. Thus, the change in BP in our study may reflect the effects of the pharmacists' support for patients.

Previous community pharmacy-based studies measured BP at pharmacies or clinics (*12-14*). In our study, we were able to analyse home BP measurement data collected during an 84-day period. The mixed-effect model repeated measure (MMRM) results suggest that the intergroup difference in SBP was significant, although the sample of data for analysis was small (125 patients). Therefore, a pharmacist-based intervention could likely promote improvements in BP.

We did not observe changes in physical activities, BMI, and lifestyle choices. The observed intergroup difference in BP might be attributable to the pharmacists' recommendations to the intervention participants regarding reduced sodium intake. Japanese people, especially those who are older, have high levels of sodium intake (> 10 g salt per day) (*5,7*). Because the participants in the current study were older and were likely to have high salt intake, they might have benefitted from the present intervention. However, a 24-hour urine collection analysis was needed to confirm this hypothesis, and this was not possible for this trial due to the practice setting.

It would be expected that the difference in BP observed in this study, about 6 mmHg, would be additive to other pharmacist interventions, for which there is substantial high quality evidence, such as recommending medication changes to the physician (*26*), or independent prescribing by pharmacists (*27*). As such, adding a brief motivational interview-based intervention could greatly enhance pharmacists' other clinical care.

Our study had some limitations of note. First, approximately one-quarter of the baseline data (*n* = 34) were missing. To address this, we used the average values from the first week of home readings, but these were likely lower than in-pharmacy measures, which may have decreased the differences between the two groups. Second, this was an open-label trial and all data were obtained from patients. Therefore, patients in both groups might have reported "desirable" data – an effect that might be greater in the Intervention group. Thirdly, though the difference between both arms was -6.0 mmHg, the change was mainly due to an increase in BP in the Control group (+4.9 mmHg) rather than a reduction in the Intervention group (-1.1 mmHg). This study was carried out from autumn to winter (112/125

patients from September to December) in Japan, where a 15°C drop in temperature occurs between September (23.2°C) and December (6.7°C) (*28*). A 1°C decrease in the mean outdoor temperature is associated with a rise of 0.41-0.43 mmHg in SBP in Japan (*29,30*). Thus, in this study, the pharmacists' intervention may have prevented the increase in BP caused by the drop in outdoor temperature, rather than having failed to cause an overall reduction in BP.

We attempted to reduce the risk of sampling bias by only including patients who adhered sufficiently to the strict status recording protocol during a 2-week run-in period. In other words, the present findings were based on what were likely already motivated patients. Another approach is needed to target less motivated patients in a real-world setting. However, most hypertensive patients in Japan have BP monitors in their homes. Accordingly, the results suggest that many of these patients could improve their BP through self-measures if they were educated and supported by pharmacists.

In conclusion, the COMPASS-BP study demonstrated that brief motivational advice given by community pharmacists could potentially improve the control of BP, particularly morning SBP measured at home, among hypertensive patients. Our findings indicate the benefits of implementing a pharmacist-provided lifestyle advice program for patients with chronic disease.

References

1. Kario K, Ishikawa J, Pickering TG, Hoshide S, Eguchi K, Morinari M, Hoshide Y, Kuroda T, Shimada K. Morning hypertension: The strongest independent risk factor for stroke in elderly hypertensive patients. Hypertens Res. 2006; 29:581-587.
2. Asayama K, Ohkubo T, Kikuya M, Obara T, Metoki H, Inoue R, Hara A, Hirose T, Hoshi H, Hashimoto J, Totsune K, Satoh H, Imai Y. Prediction of stroke by home "morning" versus "evening" blood pressure values: The Ohasama study. Hypertension. 2006; 48:737-743.
3. World Health Organization. A global brief on hypertension: Silent killer, global public health crisis. *http://apps.who.int/iris/bitstream/10665/79059/1/WHO_ DCO_WHD_2013.2_eng.pdf?ua=1* (accessed October 8, 2017)
4. Miura K, Nagai M, Ohkubo T. Epidemiology of

hypertension in Japan: Where are we now? Circ J. 2013; 77:2226-2231.

5. Shimamoto K, Ando K, Fujita T, *et al*. The Japanese Society of Hypertension Guidelines for the Management of Hypertension (JSH 2014). Hypertens Res. 2014; 37:253-390.

6. Cappuccio FP, Kerry SM, Forbes L, Donald A. Blood pressure control by home monitoring: Meta-analysis of randomised trials. BMJ. 2004; 329:145.

7. Japan Ministry of Health, Labour and Welfare. National Health and Nutrition Survey 2010. *http://www.mhlw.go.jp/ bunya/kenkou/eiyou/dl/h22-houkoku-09.pdf* (accessed October 8, 2017).

8. Neaton JD, Grimm RH Jr, Prineas RJ, *et al*. Treatment of Mild Hypertension Study. Final results. Treatment of Mild Hypertension Study Research Group. JAMA. 1993; 270:713-724.

9. Uechi K, Asakura K, Masayasu S, Sasaki S. Within-country variation of salt intake assessed *via* urinary excretion in Japan: A multilevel analysis in all 47 prefectures. Hypertens Res. 2017; 40:598-605.

10. Sacks FM, Svetkey LP, Vollmer WM, Appel LJ, Bray GA, Harsha D, Obarzanek E, Conlin PR, Miller ER 3rd, Simons-Morton DG, Karanja N, Lin PH; DASH-Sodium Collaborative Research Group. Effects on blood pressure of reduced dietary sodium and the Dietary Approaches to Stop Hypertension (DASH) diet. DASH-Sodium Collaborative Research Group. N Engl J Med. 2001; 344:3-10.

11. Dickinson HO, Mason JM, Nicolson DJ, Campbell F, Beyer FR, Cook JV, Williams B, Ford GA. Lifestyle interventions to reduce raised blood pressure: A systematic review of randomized controlled trials. J Hypertens. 2006; 24:215-233.

12. Aguiar PM, Balisa-Rocha BJ, Brito Gde C, da Silva WB, Machado M, Lyra DP Jr. Pharmaceutical care in hypertensive patients: A systematic literature review. Res Social Adm Pharm. 2012; 8:383-396.

13. Cheema E., Sutcliffe P, Singer DR. The impact of interventions by pharmacists in community pharmacies on control of hypertension: A systematic review and meta-analysis of randomized controlled trials. Br J Clin Pharmacol. 2014; 78:1238-1247.

14. Santschi V, Chiolero A, Colosimo AL, Platt RW, Taffé P, Burnier M, Burnand B, Paradis G. Improving blood pressure control through pharmacist interventions: A meta-analysis of randomized controlled trials. J Am Heart Assoc. 2014; 3:e000718.

15. Topouchian J, Agnoletti D, Blacher J, Youssef A, Ibanez I, Khabouth J, Khawaja S, Beaino L, Asmar R. Validation of four automatic devices for self-measurement of blood pressure according to the international protocol of the European Society of Hypertension. Vasc Health Risk Manag. 2011; 7:709-717.

16. Morisky DE, Ang A, Krousel-Wood M, Ward HJ. Predictive validity of a medication adherence measure in an outpatient setting. J Clin Hypertens. 2008; 10:348-354.

17. Murase N, Katsumura T, Ueda C, Inoue S, Shimomitsu T. Validity and reliability of Japanese version of International Physical Activity Questionnaire. Journal of Health and Welfare Statistics. 2002; 49:1-9. (in Japanese)

18. Craig CL, Marshall AL, Sjöström M, Bauman AE, Booth ML, Ainsworth BE, Pratt M, Ekelund U, Yngve A, Sallis JF, Oja P. International physical activity questionnaire: 12-country reliability and validity. Med Sci Sports Exerc. 2003; 35:1381-1395.

19. Arakawa K, Matsushita Y, Hrada J, Iwashita M. Obesity and diabetes. 2010; 9:870-872. (in Japanese)

20. Ikeda S, Shiroiwa T, Igarashi A, Noto S, Fukuda T, Saito S, Shimozuma K. Developing a Japanese version of the EQ-5D-5L value set. Journal of the National Institute of Public Health. 2015; 64:47-55. (in Japanese)

21. Machin D, Campbell MJ, Tan SB, Tan SH. Sample size tables for clinical studies, 3rd Edition. Wiley-Black well. 2008.

22. Mallinckrodt CH, Clark WS, David SR. Accounting for dropout bias using mixed-effects models. J Biopharm Stat. 2001; 11:9-21.

23. Miller WR, Rollnick S. Motivational interviewing: Preparing people for change 2nd edition. Guilford Press, New York, USA, 2002.

24. Spahn JM, Reeves RS, Keim KS, Laquatra I, Kellogg M, Jortberg B, Clark NA. State of the evidence regarding behavior change theories and strategies in nutrition counselling to facilitate health and food behavior change. J Am Diet Assoc. 2010; 110:879-891.

25. Hedegaard U, Hallas J, Ravn-Nielsen LV, Kjeldsen LJ. Process- and patient-reported outcomes of a multifaceted medication adherence intervention for hypertensive patients in secondary care. Res Social Adm Pharm. 2016; 12:302-318.

26. Santschi V, Rodondi N, Bugnon O, Burnier M. Impact of electronic monitoring of drug adherence on blood pressure control in primary care: A cluster 12-month randomised controlled study. Eur J Intern Med. 2008; 19:427-434.

27. Tsuyuki RT, Houle SK, Charrois TL, Kolber MR, Rosenthal MM, Lewanczuk R, Campbell NR, Cooney D, McAlister FA; RxACTION Investigators. Randomized trial of the effect of pharmacist prescribing on improving blood pressure in the community: The Alberta Clinical Trial in Optimizing Hypertension (RxACTION). Circulation. 2015; 132:93-100.

28. Japan Meteorological Agency. *http://www.jma.go.jp/jma/ indexe.html* (accessed October 8, 2017)

29. Kimura T, Senda S, Masugata H, Yamagami A, Okuyama H, Kohno T, Hirao T, Fukunaga M, Okada H, Goda F. Seasonal blood pressure variation and its relationship to environmental temperature in healthy elderly Japanese studied by home measurements. Clin Exp Hypertens. 2010; 32:8-12.

30. Iwabu A, Konishi K, Tokutake H, Yamane S, Ohnishi H, Tominaga Y, Kusachi S. Inverse correlation between seasonal changes in home blood pressure and atmospheric temperature in treated-hypertensive patients. Clin Exp Hypertens. 2010; 32:221-226.

Original Article

Shenqi detoxification granule combined with P311 inhibits epithelial-mesenchymal transition in renal fibrosis *via* TGF-β1-Smad-ILK pathway

Pingping Cai[1], Xiang Liu[2], Yuan Xu[1], Fanghua Qi[1], Guomin Si[1,*]

[1] *Department of Traditional Chinese Medicine, Shandong Provincial Hospital affiliated to Shandong University, Ji'nan, China;*
[2] *Department of Nephrology, Shandong Provincial Hospital affiliated to Shandong University, Ji'nan, China.*

Summary   **Shenqi detoxification granule (SDG), a traditional Chinese herbal formula, has been shown to have nephroprotective and anti-fibrotic activities in patients with chronic kidney disease (CKD). However, its mechanisms in renal fibrosis and the progression of CKD remain largely unknown. P311, a highly conserved 8-kDa intracellular protein, plays a key role in renal fibrosis by regulating epithelial-mesenchymal transition (EMT). Previously, we found P311 might be involved in the pathogenesis of renal fibrosis by inhibiting EMT *via* the TGF-β1-Smad-ILK pathway. We also found SDG combined with P311 could ameliorate renal fibrosis by regulating the expression of EMT markers. Here we further examined the effect and mechanism of SDG combined with P311 on TGF-β1-mediated EMT in a rat model of unilateral ureteral occlusion (UUO) renal fibrosis. After establishment of the UUO model successfully, the rats were gavaged with SDG daily and/or injected with recombinant adenovirus p311 (also called Ad-P311) through the tail vein each week for 4 weeks. Serum creatinine (Cr), blood urea nitrogen (BUN) and albumin (ALB) levels were tested to observe renal function, and hematoxylin eosin (HE) and Masson staining were performed to observe kidney histopathology. Furthermore, the expression of EMT markers (E-cadherin and α-smooth muscle actin (α-SMA)) and EMT-related molecules TGF-β1, pSmad2/3, Smad7 and ILK were observed using immunohistochemical staining and Western blot analysis. Treatment with SDG and P311 improved renal function and histopathological abnormalities, as well as reversing the changes of EMT markers and EMT-related molecules, which indicated SDG combined with P311 could attenuate renal fibrosis in UUO rats, and the underlying mechanism might involve TGF-β1-mediated EMT and the TGF-β1-Smad-ILK signaling pathway. Therefore, SDG might be a novel alternative therapy for treating renal fibrosis and delaying the progression of CKD. Furthermore, SDG combined with P311 might have a synergistic effect on attenuating renal fibrosis.**

Keywords: Shenqi detoxification granule (SDG), P311, renal fibrosis, epithelial-mesenchymal transition (EMT), TGF-β1-Smad-ILK pathway

1. Introduction

Chronic kidney disease (CKD) is an important public health problem and causes significant morbidity and mortality worldwide (*1*). Renal fibrosis is generally recognized as the most prominent feature and the common final manifestation of progressive CKD (*2*). To delay the progression of CKD, inhibition of renal fibrosis may be a key factor for developing new clinical treatment options. However, there are still few clinical treatment options, which can block the progression of CKD. Thus, many patients begin to seek out alternative therapies such as traditional Chinese medicine. Chinese herbal medicine has been used for thousands of years and has successfully treated a number of human diseases,

Address correspondence to:
Dr. Guomin Si, Department of Traditional Chinese Medicine, Shandong Provincial Hospital affiliated to Shandong University, No. 324, Jingwuweiqi Road, Ji'nan 250021, Shandong, China.
E-mail: sgm977@126.com

including some kidney diseases. Recently, several traditional Chinese medications with anti-inflammation, anti-oxidative, or immunomodulatory properties have attracted considerable interest as candidates for the development of novel CKD therapeutics (*3*).

Shenqi detoxification granule (SDG), a traditional Chinese herbal formula, has been used in the clinic for the treatment of CKD for many years (*4*). As shown in Table 1, SDG contains 12 herbs including Radix Astragali, Salvia miltiorrhiza, Angelica sinensis, and so on. According to the theoretical basis of traditional Chinese medicine, SDG possesses a function of tonifying the kidney, invigorating blood circulation and detoxifcation. In our previous basic and clinical studies, we found that SDG could decrease the levels of blood urea nitrogen (BUN), serum creatinine (Scr), and leptin, and increase the levels of albumin (ALB) (*5,6*). These findings indicated that SDG could effectively alleviate kidney injury and prevent the progress of CKD. Furthermore, the possible mechanism of SDG on inhibiting renal fibrosis might be involved in the transforming growth factor-β1 (TGF-β1)-Smad pathway in rats (*7*). However, the mechanisms of SDG in renal fibrosis and the progression of CKD remain largely unknown.

Renal fibrosis is characterized by the trans-differentiation of myofibroblasts and deposition of extracellular matrix (ECM) (*8*). During fibrosis, kidney resident cells such as fibroblasts, epithelial, endothelial or mesangial cells trans-differentiate into myofibroblasts that express and deposit excessive ECM proteins in the renal interstitial spaces, eventually leading to renal fibrosis and functional loss (*9*). Renal tubular epithelial-mesenchymal transition (EMT) is a critical step and key mechanism in the development of this condition, and about 30% of myofibroblasts are generated *via* EMT during kidney fibrosis (*10*). During the EMT process, tubular epithelial cells lose their adhesion molecules such as E-cadherin, and gain mesenchymal cell markers, such as alpha-smooth muscle actin (α-SMA), vimentin, fibronectin, and collagen I (*11*). TGF-β1 is a well-known pro-

fibrotic cytokine that plays an important role in renal fibrosis (*12*). It is a major inducer of EMT that has been shown to initiate and complete the whole EMT process (*13*). Emerging data indicate that TGF-β1 induces EMT in renal fibrosis primarily *via* the Smad signaling pathway (*14*). Upon TGF-β1 binding to its receptors, Serine/Threonine kinases are activated and induce phosphorylation of Smad2/Smad3, and then phosphorylated Smad2/3 partner with Smad4 and are translocated into the nucleus where they regulate the transcription of the target genes responsible for EMT. Integrin linked kinase (ILK) is an intracellular serine/threonine kinase involved in cell-matrix interactions (*15,16*). It is shown to be a key intracellular mediator that regulates TGF-β1-induced-EMT through the Smad signaling pathway in renal tubular epithelial cells. Since EMT is the key factor by which renal fibrosis develops, inhibiting the EMT program through the TGF-β1-Smad-ILK pathway is considered a potential mechanism for anti-fibrotic therapies.

P311, an 8-kD, 68-amino acid, intracellular polypeptide, is highly conserved across species and abundantly expressed in brain, smooth muscle, regeneration tissues, and malignant glioblastomas (*17*). It can bind to TGF-β latency associated protein and stimulate the translation of TGF-β. In addition, P311 has proved to be of importance in the process of myofibroblast differentiation and fibrosis with functions of promoting embryonic development, wound healing, as well as nerve and lung regeneration, and so on (*18-22*). In our previous studies, we found that P311 might be involved in the pathogenesis of renal fibrosis by inhibiting the EMT process *via* the TGF-β1-Smad-ILK pathway *in vitro* (*23*). P311 might be a novel target for control of renal fibrosis and the progression of CKD. We also found that SDG combined with P311 could ameliorate renal fibrosis and block the progression of CKD by regulating the expression of EMT-related protein α-SMA (*24*).

In the current study, we further examined the effect of SDG combined with P311 on TGF-β1-mediated EMT in a rat model of unilateral ureteral occlusion (UUO) renal

Table 1. Formulation of Shenqi detoxification granule (SDG)

Common name	Botanical name	Voucher specimen number	Part used	Weight (g)
Radix astragali	*Astragalus membranaceus* (Fisch.) Bge	10142	Root	60
Salvia miltiorrhiza	*Salvia miltiorrhiza* Bge.	10140	Rhizome	20
Angelica sinensis	*Angelica sinensis* (Oliv.) Diels	10136	Root	12
Rheum officinale	*Rheum officinale* Baill.	10137	Root and rhizome	10
Gordon euryale seed	*Euryale ferox* Salisb.	10156	Seed	15
Herba ecliptae	*Eclipta prostrata* L.	10152	Whole plant	15
Radix semiaquilegiae	*Semiaquilegia adoxoides* (DC.) Makino	10168	Root	15
Rhizoma imperatae	*Imperata cylindrica Beauv.* var. *major* (Nees) C. E. Hubb.	10126	Root	15
Processed radix aconiti lateralis	*Aconitum carmichaelii* Debx.	10172	Root	10
Herba epimedii	*Epimedium brevicornu* Maxim.	10176	Leaf	15
Cherokee rose fruit	*Rosa laevigata* Michx.	10146	Fruit	15
Hedyotis diffusa	*Hedyotis diffusa* Willd.	10124	Whole plant	15

fibrosis. After constructing a recombinant adenovirus p311 (also called Ad-P311) and transferring it into UUO rats, the preventing effect and possible mechanisms of SDG combined with P311 on TGF-β1-mediated EMT were explored.

2. Materials and Methods

2.1. *SDG preparation*

As shown in Table 1, SDG contained twelve ingredients including Radix Astragali, Salvia miltiorrhiza, Angelica sinensis, and so on. These ingredients were ordered from Shandong Hong-Ji-Tang pharmaceutical group corporation (Ji'nan, Shandong, China), and identified by Professor Bo Xu (Department of Pharmacy, Shandong Provincial Hospital affiliated to Shandong University, Ji'nan, Shandong, China). The voucher specimen numbers of these herbs are listed in Table 1, however, they have not been deposited into a publicly available herbarium. SDG was produced according to the method reported in our previous study (*4*). Briefly, these twelve ingredients were mixed in proportion, boiled with distilled water twice, and the resulting decoction was mixed and filtered using filter paper. Then, the filtered solution was collected and concentrated to a relative density. Finally, clear paste and excipient were mixed to make sugar-free granules, then dried, granulated, packed (10 g/bag), and labeled, which contained 20 g granules of 217 g crude drugs. Then the granules were made into 0.4 mg/mL liquid and kept at 4°C.

2.2. *Animals*

Sixty male Sprague-Dawley rats (8 weeks old, 200 ± 10 g) were bought from Shandong Experimental Animal Center (Ji'nan, Shandong, China), and were given free access to water and food throughout the experiments. All animals were housed in plastic cages with a room temperature of 22 ± 1°C and relative humidity of 50 ± 10% under a 12-h light/dark cycle. The rats were acclimatized for at least 1 week prior to the experiments. All animal experimental protocols were handled in accordance with the Code of Ethics of the World Medical Association. All experimental procedures were approved by the Institutional Animal Care and Use Committee of Shandong Provincial Hospital Affiliated to Shandong University (No. 2017-208).

2.3. *Establishment of UUO model*

UUO model was performed as described previously (*25*). Briefly, after induction of general anesthesia by intraperitoneal injection of 3% pentobarbital (Sigma, St. Louis, MO, USA) (1 mL/kg body wt), the abdominal cavity was exposed *via* midline incision and the left

ureter was ligated at 2 points with 4.0 silk (Niccho Kogyo Co., Ltd., Tokyo, Japan). Sham-operated rats had their ureters manipulated but not ligated and were used as controls.

2.4. *Experimental protocol*

The rats were randomly divided into six groups and given different treatments, each consisting of ten animals as follows: control group (or sham surgery group), UUO group, control + Ad-P311 group, UUO + Ad-P311 group, UUO + SDG group, and UUO + SDG + Ad-P311 group. Ad-P311 was constructed as described previously by the current authors and stored at -80°C for use (*23*). After establishment of the UUO model successfully, rats in the control group and UUO group were gavaged with 2 mL normal saline daily for 4 weeks and injected with 0.5 mL normal saline through tail vein each week for 4 weeks, while the rats in control + Ad-P311 group and UUO + Ad-P311 group were gavaged with 2 mL normal saline daily for 4 weeks and injected with 0.5 mL P311 adenovirus by tail vein each week for 4 weeks. In addition, the rats in UUO + SDG group were gavaged with 2 mL SDG daily for 4 weeks and injected with 0.5 mL normal saline through tail vein each week for 4 weeks, while the rats in UUO + SDG + Ad-P311 group were gavaged with 2 mL SDG daily for 4 weeks and injected with 0.5 mL P311 adenovirus by tail vein each week for 4 weeks.

After 4 weeks treatment, these rats were euthanized under ether and their blood and kidneys were harvested. To make the rats enter quickly into the state of anesthesia and reduce their pain and fear, inhaling ether was used as euthanasia method and this method was approved by the Institutional Animal Care and Use Committee of Shandong Provincial Hospital Affiliated to Shandong University. Serum Cr, BUN and ALB (BioVision, Inc., Milpitas, CA, USA) levels in the blood were tested using detection kits. Part of the kidney was fixed in 10% formalin solution and embedded in paraffin as 3 μm sections for hematoxylin and eosin (HE), Masson's trichrome and immunohistochemical staining. The other part of the kidney was stored at -80°C for Western blot analysis, which was performed as previously described to detect protein expression of E-cadherin, α-SMA, TGF-β1, phosphorylated Smad2/3 (pSmad2/3), Smad7 and ILK (Santa Cruz Biotechnology, Santa Cruz, CA, USA).

2.5. *Hematoxylin eosin (HE) staining and Masson staining*

To observe histological morphology changes of kidney tissue, HE staining and Masson staining were performed. First, kidney tissues were fixed with 10% neutral formaldehyde and dehydrated in graded ethanol. After permeation with xylene, they were embedded in paraffin.

Paraffin blocks were cut into 2 μm slices, mounted onto glass slides and stained using standard techniques of HE staining and Masson staining according to previous studies (*26*). Renal tubular injury index including inflammatory, cell infiltration, interstitial fibrosis, interstitial edema, cell vacuolar degeneration, tubular atrophy, and tubular expansion was measured to assess renal interstitial lesions. Ten different fields were selected to estimate the level of renal injury index with HE staining using a bio-image analysis system (Bio-Profile). Each parameter was evaluated and given a score from 0 to 4+, (0, no changes; 1+, changes affecting 5-25%; 2+, changes affecting 25-50%; 3+, changes affecting 50-75%; 4+, changes affecting 75-100%) (*28*). The severity of interstitial fibrosis was estimated by scanning 10 non-repeated fields in each sample with Masson staining. Blue-stained fibrotic areas were quantified by Image-Pro plus 6.0 software (Media Cybernetics, Rockville, MD, USA) (*27*). The results were expressed as the proportion of relative volume of scanned interstitium. All cases of HE and Masson staining were evaluated independently by two investigators and any discrepancy was resolved with a group discussion.

2.6. Immunohistochemical staining

To analyze the protein expression of α-SMA, pSmad2/3, and Smad7, immunohistochemistry staining assays were performed as described previously (*26*). First, paraffin sections were de-paraffinized, hydrated, and immersed in 0.3% hydrogen peroxide in methanol for 30 min to block the endogenous peroxidase activity. Second, the sections were incubated in primary antibodies (α-SMA, Smad2/3, and Smad7) overnight at 4°C, followed by incubation in anti-mouse secondary antibody for 1 h at room temperature. Third, visualization was carried out using a DAB horseradish peroxidase color development kit (Beyotime Institute of Biotechnology, Shanghai, China), and slides were counter stained in hematoxylin-1. Finally, ten random fields were examined per slice for expression of α-SMA, Smad2/3, and Smad7 using a Leica DM2500 optical microscope at a magnification of ×200. The mean optical density (MOD) was measured by Image-Pro Plus 6.0 image analysis software. All cases of immunohistochemical staining were evaluated independently by two investigators and any discrepancy was resolved with a group discussion.

2.7. Western blot analysis

Thirty micrograms of total cellular proteins were resolved by sodium dodecyl sulfate polyacrylamide gel electrophoresis (SDS PAGE) and transferred onto polyvinylidene fluoride (PVDF) transfer membranes for Western blot analysis (*28*). The results were quantified using Image J (National Institutes of Health,

Bethesda, MD, USA). The following antibodies were used: E-cadherin, α-SMA, TGF-β1, pSmad2/3, Smad7 and ILK (Santa Cruz Biotechnology, Santa Cruz, CA, USA).

2.8. Statistical analysis

Statistical analysis was performed using SPSS software, version 17.0 (SPSS Inc., USA). All experiments were performed in triplicate and the data were expressed as the mean ± standard deviation (SD). The statistical significance of differences were calculated using the *t*-test and one-way analysis of variance (ANOVA), and $p < 0.05$ was considered statistically significant.

3. Results

3.1. General condition of rats

After treatment for 4 weeks, rats in the control group and control + Ad-P311 group were still in good shape, glossy coat color and obesity, while rats in the UUO group, and SDG or Ad-P311 treatment groups had different degrees of anorexia, low spirits, matte coat color, and kidney enlargement, and even individual rats were dead from kidney failure. There were 8 deaths including 3 in the UUO group, 2 in UUO + SDG group, 2 in UUO + Ad-P311 group, and 1 in UUO + SDG + Ad-P311 group. In addition, there was a great change in body weight of rats after establishment of the UUO model and treatment with SDG or Ad-P311. As shown in Table 2, after 4 weeks of treatment, compared to control group, body weight in the UUO group ($p < 0.01$), UUO + SDG group ($p < 0.05$), UUO + Ad-P311 group ($p < 0.05$), and UUO + SDG + Ad-P311 ($p < 0.05$) group had different degrees of weight loss, while there was no significant difference in control group and control + Ad-P311 group ($p > 0.05$). Moreover, weight loss was reversed significantly by administration of SDG and Ad-P311 especially in the UUO + SDG + Ad-P311 group ($p < 0.01$) compared to that in UUO group.

3.2. Serum levels of Cr, BUN and ALB

After 4 weeks of treatment, serum levels of Cr, BUN and ALB were observed as shown in Table 3. Compared to control group, serum levels of Cr and BUN were increased significantly in the UUO group ($p < 0.01$), UUO + SDG group ($p < 0.05$), UUO + Ad-P311 group ($p < 0.05$), and UUO + SDG + Ad-P311 ($p < 0.05$) group, while there was no significant difference between control group and control + Ad-P311 group ($p > 0.05$). Moreover, serum levels of Cr and BUN were reversed significantly by administration of SDG and Ad-P311 especially in UUO + SDG + Ad-P311 group ($p < 0.01$) compared to that in UUO group. Compared to control group, serum levels of

Table 2. The body weight of rats in different groups at beginning and end of experiments

Group	Body weight at the beginning of experiment (g)	Body weight at the end of experiment (g)
Control group	199.60 ± 8.64	402.00 ± 14.65
Control + Ad-P311 group	$202.22 \pm 8.11^§$	$403.00 \pm 13.18^▲$
UUO group	$211.14 \pm 11.25^§$	$308.71 \pm 15.22^{**}$
UUO + SDG group	$201.88 \pm 6.20^§$	$356.38 \pm 7.03^{*\Delta}$
UUO + Ad-P311 group	$201.12 \pm 13.22^§$	$365.25 \pm 8.88^{*\Delta}$
UUO + SDG + Ad-P311 group	$205.33 \pm 8.54^§$	$379.00 \pm 9.34^{*\Delta\Delta}$

Note: Body weight at the beginning of experiment: $^§p > 0.05$ *vs.* Control group; Body weight at the end of experiment: $^▲p > 0.05$ *vs.* Control group, $^*p < 0.05$ *vs.* Control group, $^{**}p < 0.01$ *vs.* Control group, $^\Delta p < 0.05$ *vs.* UUO group, $^{\Delta\Delta}p < 0.01$ *vs.* UUO group.

Table 3. The serum levels of Cr, BUN and ALB of rats in different groups after 4 weeks of treatment

Group	Cr (μmol/L)	BUN (mmol/L)	ALB (g/L)
Control group	42.58 ± 2.95	6.33 ± 1.10	34.39 ± 1.66
Control + Ad-P311 group	$41.22 \pm 3.36^\Delta$	$7.03 \pm 0.90^\Delta$	$33.31 \pm 1.95^\Delta$
UUO group	$118.79 \pm 6.14^{▲▲}$	$32.64 \pm 4.02^▲$	$22.57 \pm 1.43^{▲▲}$
UUO + SDG group	$93.68 \pm 6.36^{▲*}$	$15.27 \pm 1.28^{▲*}$	$30.07 \pm 1.11^{▲*}$
UUO + Ad-P311 group	$76.23 \pm 4.45^{▲*}$	$12.37 \pm 1.33^{▲*}$	$25.13 \pm 0.97^{▲*}$
UUO + SDG + Ad-P311 group	$59.27 \pm 4.94^{▲**}$	$8.72 \pm 1.20^{▲**}$	$29.90 \pm 1.08^{▲*}$

Note: $^\Delta p > 0.05$ *vs.* Control group, $^▲p < 0.05$ *vs.* Control group, $^{▲▲}p < 0.01$ *vs.* Control group, $^*p < 0.05$ *vs.* UUO group, $^{**}p < 0.01$ *vs.*UUO group.

ALB were decreased significantly in UUO group ($p < 0.01$), UUO + SDG group ($p < 0.05$), UUO + Ad-P311 group ($p < 0.05$), and UUO + SDG + Ad-P311 ($p < 0.05$) group, while there was no significant difference between control group and control + Ad-P311 group ($p > 0.05$). Moreover, serum levels of ALB were reversed significantly by administration of SDG and Ad-P311 ($p < 0.05$) compared to that in UUO group.

3.3. *SDG combined with P311 attenuated UUO-induced fibrosis*

As shown in Figure 1A, HE staining demonstrated that there were no histological changes in kidneys of sham rats as shown in control group and control + Ad-P311 group, while kidneys developed remarkable pathological changes such as interstitial fibrosis, tubular expansion, atrophy and inflammatory cell invasion in UUO rats as shown in the UUO group. However, these histological lesions in the kidneys of UUO rats were attenuated by administration of SDG and Ad-P311 especially in UUO + SDG + Ad-P311 group compared to those in the UUO group. Consistent with pathological changes in experimental kidneys, UUO surgery resulted in about an 8-time increase of renal tubular injury index, but extent of damage was remarkably decreased from $83.20 \pm 2.80\%$ to $70.10 \pm 3.82\%$ by administration of SDG and Ad-P311 especially in the UUO + SDG + Ad-P311 group compared to that in UUO group ($p < 0.01$) (Figure 1B). As shown in Figure 2A, Masson staining showed that collagen deposition and fibrosis areas were significantly decreased by administration of SDG and Ad-P311 especially in the UUO + SDG + Ad-P311 group compared to those in the UUO group. Collagen accumulation had increased prominently about 3 fold in the interstitium of UUO kidneys, while administration
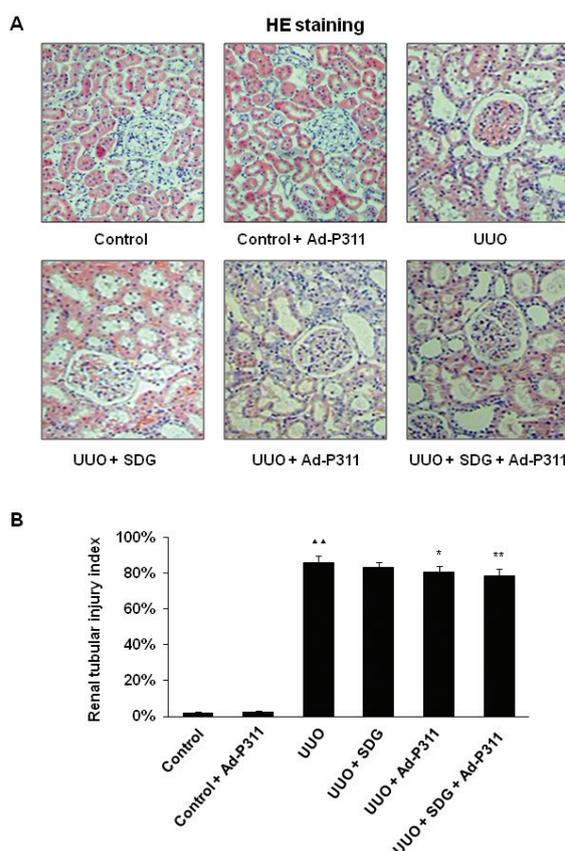
Figure 1. SDG combined with P311 attenuated UUO-induced pathological changes in the kidneys, which were detected by hematoxylin eosin (HE) staining. (A) HE staining (× 200); **(B)** The semi-quantitative accession of the renal tubular injury index in HE-stained sections of rat kidneys. $^{▲▲}p < 0.01$, compared to control group; $^*p < 0.05$, compared to UUO group; $^{**}p < 0.01$, compared to UUO group.

of SDG and Ad-P311 decreased the amount of collagen deposition from 2.94 ± 0.34 to 2.13 ± 0.30, compared to the UUO group ($p < 0.01$) (Figure 2B).
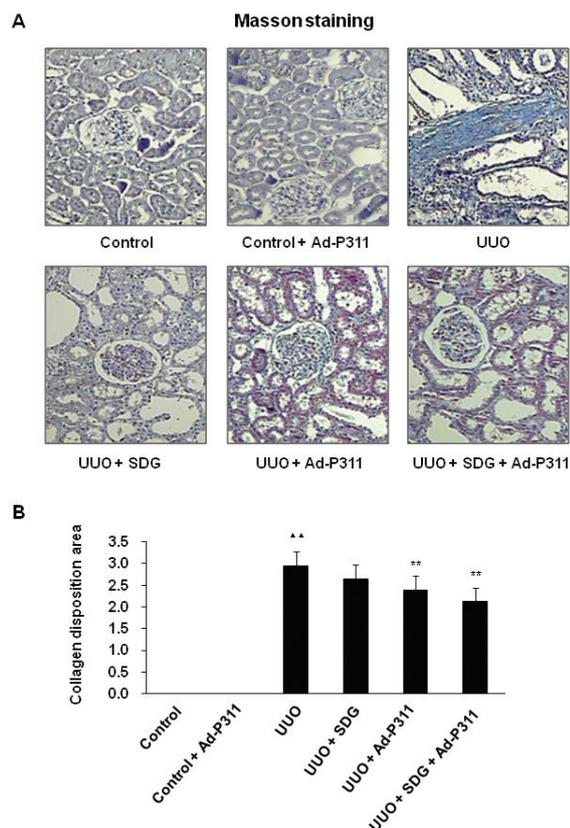
Figure 2. SDG combined with P311 attenuated UUO-induced pathological changes in the kidneys which were detected by Masson staining. (A) Masson staining (× 200); (B) The degree of interstitial collagen deposits in Masson-stained sections of rat kidneys. ▲▲*p* < < 0.01, compared to control group; **p* < 0.01, compared to UUO group.

Figure 3. SDG combined with P311 reversed the expression α-SMA, which was detected by immunohistochemical staining in UUO kidneys. (A) Representative photomicrograph illustrating α-SMA expression in UUO kidneys; (B) Graph showing the immunoreactive score of α-SMA in UUO kidneys by quantitative morphometric analysis. ▲▲*p* < 0.01, compared to control group; **p* < 0.05, compared to UUO group; ***p* < 0.01, compared to UUO group. Original magnifications, × 200.

3.4. *SDG combined with P311 reversed the expression α-SMA, pSmad2/3 and Smad7 detected by immuno-histochemical staining in UUO Kidneys*

Protein expression of mesenchymal marker α-SMA was investigated by immunohistochemical staining to explore the effect of SDG and Ad-P311 on EMT related markers in UUO Kidneys. As shown in Figures 3A and 3B, protein expression of α-SMA was increased significantly in UUO kidneys compared to that in the sham operated control kidneys (control group and control + Ad-P311 group) ($p < 0.01$), while there was no significant difference between control group and control + Ad-P311 group ($p > 0.05$). In contrast, the increased expression of α-SMA in UUO kidneys was reversed by the administration of SDG and Ad-P311 especially in the UUO + SDG + Ad-P311 group ($p < 0.01$) compared to UUO group.

Protein expression of Smad2/3 and Smad7 was also investigated by immunohistochemical staining to explore the possible mechanism of SDG and Ad-P311 on EMT of UUO Kidneys. As shown in Figures 4A and 4B, the protein expression of pSmad2/3 was dramatically

elevated in the UUO group compared with the sham groups (control group and control +Ad-P311 group) ($p < 0.01$), while there was no significant difference between control group and control + Ad-P311 group ($p > 0.05$). In contrast, SDG and Ad-P311 administration substantially ameliorated this elevation induced by UUO surgery. As shown in Figures 5A and 5B, protein expression of Smad7 was decreased significantly in UUO kidneys compared to that in the sham groups (control group and control + Ad-P311 group) ($p < 0.01$), while there was no significant difference between control group and control + Ad-P311 group ($p > 0.05$). In contrast, administration of SDG and Ad-P311 alleviated its decrease especially in UUO + SDG + Ad-P311 group ($p < 0.01$) compared to UUO group.

3.5. *SDG combined with P311 reversed the expression of EMT related proteins detected by Western blot analysis in UUO Kidneys*

To further explore the effect of SDG and Ad-P311 on EMT related markers in UUO Kidneys, expression of epithelial marker E-cadherin and mesenchymal marker
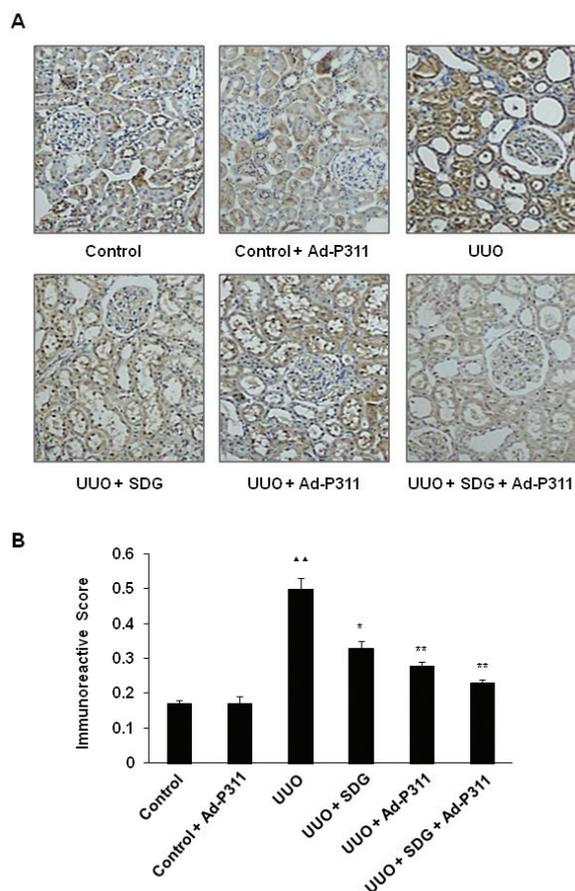
Figure 4. SDG combined with P311 reversed the expression pSmad2/3, which was detected by immunohistochemical staining in UUO kidneys. (A) Representative photomicrograph illustrating pSmad2/3 expression in UUO kidneys; **(B)** Graph showing the immunoreactive score of pSmad2/3 in UUO kidneys by quantitative morphometric analysis. ▲▲$p < 0.01$, compared to control group; *$p < 0.05$, compared to UUO group; **$p < 0.01$, compared to UUO group. Original magnifications, × 200.
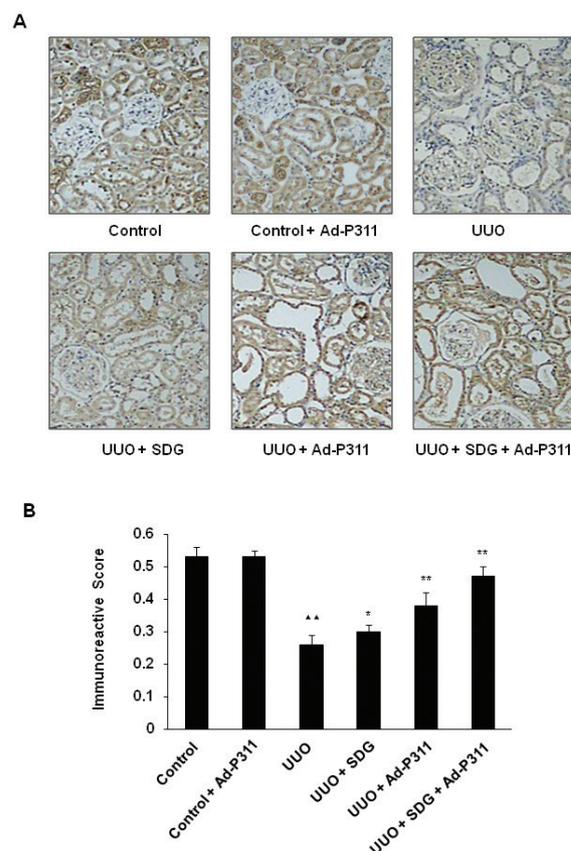
Figure 5. SDG combined with P311 reversed the expression of Smad7, which was detected by immunohistochemical staining in UUO kidneys. (A) Representative photomicrograph illustrating Smad7 expression in UUO kidneys; **(B)** Graph showing the immunoreactive score of Smad7 in UUO kidneys by quantitative morphometric analysis. ▲▲$p < 0.01$, compared to control group; *$p < 0.05$, compared to UUO group; **$p < 0.01$, compared to UUO group. Original magnifications, × 200.

α-SMA in UUO kidneys was examined by Western blot analysis. As shown in Figures 6A and 6B, the protein level of E-cadherin was decreased significantly in the UUO group compared with sham groups (control group and control +Ad-P311 group) ($p < 0.01$), while there was no significant difference between control group and control + Ad-P311 group ($p > 0.05$). However, administration of SDG and Ad-P311 alleviated its decrease. The protein expression of α-SMA was increased significantly in UUO kidneys compared to that in the sham operated control kidneys ($p < 0.01$), while there was no significant difference between control group and control + Ad-P311 group ($p > 0.05$). However, the increased expression of α-SMA in UUO kidneys was reversed by administration of SDG and Ad-P311 (Figures 6A and 6B).

To explore possible mechanism of SDG and Ad-P311 on EMT of UUO Kidneys, the protein expression of EMT related molecules TGF-β1, pSmad2/3, Smad7, and ILK were measured by Western blot analysis. As shown in Figures 7A and 7B, protein expression of TGF-β1,

pSmad2/3, and ILK was increased significantly in UUO kidneys compared to that in the sham operated control kidneys (control group and control +Ad-P311 group) ($p < 0.01$), while there was no significant difference between control group and control + Ad-P311 group ($p > 0.05$). However, administration of SDG and Ad-P311 alleviated all of the above changes significantly. Protein expression of Smad7 was decreased significantly in UUO kidneys compared to that in the sham operated control kidneys (control group and control +Ad-P311 group) ($p < 0.01$), while there was no significant difference between control group and control + Ad-P311 group (p > 0.05). However, the decreased expression of Smad7 in UUO kidneys was reversed by administration of SDG and Ad-P311 (Figures 7A and 7B).

4. Discussion

As a traditional Chinese herbal formula, SDG has been used clinically for treatment of CKD for many years (*4*). Radix Astragali and Salvia miltiorrhiza are the two
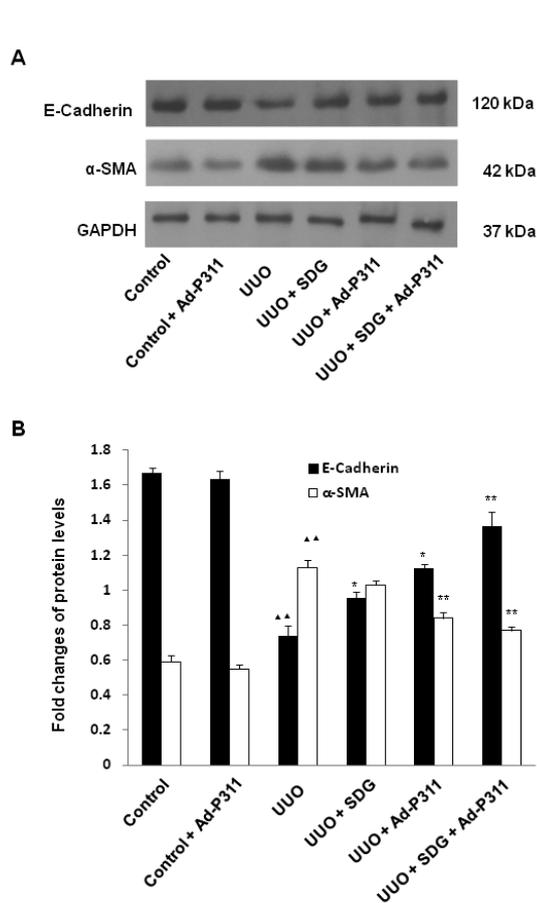
Figure 6. SDG combined with P311 reversed the expression of EMT markers (E-cadherin and α-SMA), which was detected by Western blot analysis in UUO Kidneys. (A) Expression of E-cadherin and α-SMA at the protein level in each group was determined with GAPDH used as an internal control. **(B)** The expression level of E-cadherin and α-SMA was quantitatively analyzed with Image J software. ▲▲$p <$ 0.01, compared to control group; *$p < 0.05$, compared to UUO group; **$p < 0.01$, compared to UUO group.

Figure 7. SDG combined with P311 reversed the expression of EMT related proteins TGF-β1, pSmad2/3, Smad7, and ILK, which was detected by Western blot analysis in UUO Kidneys. (A) Expression of TGF-β1, pSmad2/3, Smad7, and ILK at the protein level in each group was determined with β-actin used as an internal control. **(B)** The expression level of TGF-β1, pSmad2/3, Smad7, and ILK was quantitatively analyzed with Image J software. ▲▲$p < 0.01$, compared to control group; *$p < 0.05$, compared to UUO group; **$p < 0.01$, compared to UUO group.

principal ingredients of SDG, which play important roles in CKD treatment. A systematic review has shown that Radix Astragali used alone as a crude herb could offer some promising effects in reducing proteinuria and increasing hemoglobin and ALB in patients with CKD (*29*). Pharmacological studies have suggested that some formulas with Radix Astragali as a principal ingredient and some active compounds from Radix Astragali (*e.g.*, Astragaloside IV) are capable of ameliorating renal fibrosis *via* the TGF-β/Smad signaling pathway (*30,31*). In addition, Salvia miltiorrhiza and its active ingredients (*e.g.*, Tanshinone IIA) have proved to possess a protective effect on kidney injury by suppressing production of reactive oxygen species (ROS) (*32*) and regulating levels of TGF-β1 and collagen IV (*33*). Therefore, the inhibitory effect of Radix Astragali and Salvia miltiorrhiza on renal fibrosis might be one of the important mechanisms of SDG as an effective treatment for CKD.

Our previous studies indicated that SDG could

effectively reduce kidney damage and prevent progression of CKD with a possible mechanism involved in the TGF-β1-Smad pathway (*5-7*). We also found P311 might be involved in the pathogenesis of renal fibrosis by inhibiting the EMT process *via* the TGF-β1-Smad-ILK pathway *in vitro* (*23*). Moreover, SDG combined with P311 could ameliorate renal fibrosis and block progression of CKD by regulating expression of the EMT-related protein α-SMA (*24*). Here we further examined the effect and mechanism of SDG combined with P311 on TGF-β1-mediated EMT in a rat model of UUO renal fibrosis. We found that SDG combined with P311 could protect kidney function of UUO rats *via* improving Cr, BUN, and ALB serum levels. We also found that SDG combined with P311 could attenuate histological lesions including interstitial fibrosis, tubular expansion, and atrophy and inflammatory cell invasion in kidneys of UUO rats, and the underlying mechanism might involve EMT and the TGF-β1-Smad-ILK signaling pathway.

Renal fibrosis is an inevitable outcome of all kinds of progressive CKD. It is characterized by the trans-differentiation of myofibroblasts and excessive accumulation of ECM (*8*). Chronic inflammation is considered a major contributor to nephropathic changes, including renal fibrosis (*15*). During the process of renal fibrosis, inflammatory cells infiltrate and produce several molecules, such as growth factors, angiogenic factors, profibrotic cytokines, and proteinases. All of these factors can stimulate excessive accumulation of ECM through EMT, which results in renal fibrosis. Among these, profibrotic cytokine TGF-β1 is proposed to be a major regulator in inducing EMT and the generation of interstitial fibroblasts (*12,13*). It can induce the activation of fibroblasts to undergo a phenotypic transition to myofibroblasts with tubular epithelial cells losing their adhesion molecules (such as E-cadherin), and gaining mesenchymal cell markers (such as α-SMA) (*11*). In the current study, expression of TGF-β1 was increased significantly in UUO kidneys, but administration of SDG and Ad-P311 alleviated its increase. Moreover, α-SMA expression was increased significantly and E-cadherin expression was decreased significantly in UUO kidneys, while the changed expression of α-SMA and E-cadherin in UUO kidneys was reversed by the administration of SDG and Ad-P311. Therefore, consistent with previous reports, TGF-β1 is the most potent inducer capable of initiating and completing the entire EMT course. SDG combined with P311 could prevent TGF-β1-mediated EMT in UUO kidneys.

The TGF-β1/Smad signaling pathway plays a key role in initiating and completing the entire EMT course in fibrotic disease pathogenesis (*34*). Currently, eight different Smad proteins have been found in vertebrates. Smad protein, because it is the most important downstream signal transduction molecule of TGF-β1 in cells, transfers the TGF-β1 signal from cell surface to nucleus, which can regulate target gene transcription. After TGF-β1 binds to its receptor Tβ R II and recruits Tβ R I, the activated complex directly phosphorylates downstream receptor-regulated Smads (R-Smads, including Smad1, 2, 3, 5, and 8). Phosphorylated R-Smads (*e.g.*, Smad2/3), binds to the common partner Smad4 and forms the Smad complex that translocates into the nucleus to initiate gene transcription and regulate cell behavior. Another class of Smads is inhibitory Smads (I-Smads, including Smad6 and Smad7), which can competitively combine with TGF-β1 receptor, preventing phosphorylation of R-Smads (*35*). In renal fibrosis, Smad2/3 is reported as a key EMT regulatory molecule inducing EMT and collagen accumulation, while Smad7 is reported to have a renoprotective effect through blocking the profibrotic effect of TGF-β and inhibiting Smad2/3 activation (*11,36*). Here we found that pSmad2/3 expression was increased and Smad7 expression was decreased significantly in UUO kidneys, but administration of SDG and Ad-P311 alleviated all of

the above changes significantly. These results indicated that SDG combined with P311 not only regulates TGF-β1 but also the Smad signaling pathway. ILK is an intracellular serine/threonine protein kinase that interacts with the cytoplasmic domains of β-integrins and mediates integrin signaling in diverse types of cells (*11*). TGF-β1 mediated EMT has been suggested to be dependent on ILK function in a Smad-dependent manner during renal fibrosis (*15*). Here we found that ILK expression was increased significantly in UUO kidneys, however, administration of SDG and Ad-P311 significantly reversed the above changes. Taken together, these findings indicated that SDG combined with P311 attenuated TGF-β1-mediated EMT by regulating protein expression of pSmad2/3, Smad7 and ILK in UUO kidneys.

P311 is an intracytoplasmic protein that can bind to TGF-β latent associated protein and down-regulate expression of TGF-β1 and TGF-β2 (*17*). It has been shown to be of importance in the process of myofibroblast differentiation and fibrosis with functions of promoting embryonic development, wound healing, as well as nerve and lung regeneration, and so on (*18,20-22*). Pan *et al*. reported that P311 could block TGF-β1 signaling and cause an inhibition in collagen expression in myofibroblast transformation, suggesting that P311 might be involved in preventing fibrosis during wound repair (*18*). In our previous study, P311 could ameliorate renal fibrosis by blocking TGF-β1-mediated EMT *via* the TGF-β1-Smad-ILK pathway *in vitro* and UUO rats (*24*). However, Yao *et al*. found that P311 could promote renal fibrosis *via* TGFβ1/Smad signaling in the UUO model (*36*). This finding differs from our data. The relationship between P311 and TGF-β1 might be reasonable to explain this discrepancy, because infiltration of inflammatory cells is an early and characteristic feature of renal fibrosis (*37*). During renal fibrosis, at early stages of repair with abundant inflammatory cells, the antifibrogenic effect of P311 may be offset by TGF-β1 and exhibit a pro-fibrogenic effect, while at advanced stages of repair while inflammatory cells gradually disappeared, the antifibrogenic effect of P311 may increase over time and become maximal toward the end of the reparative process (*18*). Thus, here we found that SDG combined with P311 could ameliorate renal fibrosis by blocking the TGF-β1/Smad signaling pathway in UUO rats. Although SDG has the potential to be a cost-effective and safe treatment for renal fibrosis, further studies are needed to verify the active components of this herbal medicine.

5. Conclusions

In summary, our data present that SDG combined with P311 could attenuate renal fibrosis in UUO rats, and the underlying mechanism might involve TGF-β1-mediated EMT and the TGF-β1-Smad-ILK signaling pathway.

Therefore, SDG might be a novel alternative therapy for treatment of renal fibrosis and progression of CKD. Furthermore, SDG combined with P311 might have a synergistic effect on attenuating renal fibrosis. Taken together, these findings provide a new way for treatment of CKD.

Acknowledgements

References

1. Romagnani P, Remuzzi G, Glassock R, Levin A, Jager KJ, Tonelli M, Massy Z, Wanner C, Anders HJ. Chronic kidney disease. Nat Rev Dis Primers. 2017; 3:17088.
2. Liu Y. Cellular and molecular mechanisms of renal fibrosis. Nat Rev Nephrol. 2011; 7:684-696.
3. Zhong Y, Deng Y, Chen Y, Chuang PY, Cijiang He J. Therapeutic use of traditional Chinese herbal medications for chronic kidney diseases. Kidney Int. 2013; 84:1108-1118.
4. Peng M, Cai P, Ma H, Meng H, Xu Y, Zhang X, Si G. Chinese herbal medicine Shenqi Detoxification Granule inhibits fibrosis in adenine induced chronic renal failure rats. Afr J Tradit Complement Altern Med. 2013;11:194-204.
5. Li Y, Si GM, Zhang Y, Hu YS. Effect of the Shenqi Jiedu decoction on chronic renal failure: an experimental study. Journal of Shandong University (Health Science). 2007; 45:1015-1018. (in Chinese)
6. Zhang Y, Si GM, Xu DM, Li Y. Clinical observation of "Shenqi Jiedu Decoction" in treating chronic renal failure of turbidity and blood-stasis syndrome and its effects on peripheral blood adhesion molecule. Shanghai Journal of Traditional Chinese Medicine. 2008; 42:26-28. (in Chinese)
7. Li TT, Si GM, Chen FC. Effects of Shenqi Jiedu Decoction on expression of transforming growth factor-β1, smad2 and smad3 in renal tissues of rats with chronic renal failure induced by adenine. Zhong Xi Yi Jie He Xue Bao. 2010; 8:263-268. (in Chinese)
8. Qi W, Chen X, Poronnik P, Pollock CA. The renal cortical fibroblast in renal tubulointerstitial fibrosis. Int J Biochem Cell Biol. 2006; 38:1-5.
9. Kanasaki K, Taduri G, Koya D. Diabetic nephropathy: the role of inflammation in fibroblast activation and kidney fibrosis. Front Endocrinol (Lausanne). 2013; 4:7.
10. Iwano M, Plieth D, Danoff TM, Xue C, Okada H, Neilson EG. Evidence that fibroblasts derive from epithelium during tissue fibrosis. J Clin Invest. 2002; 110:341-350.
11. Liu Y. New insights into epithelial-mesenchymal transition in kidney fibrosis. J Am Soc Nephrol. 2010; 21:212-222.
12. Pohlers D, Brenmoehl J, Löffler I, Müller CK, Leipner C, Schultze-Mosgau S, Stallmach A, Kinne RW, Wolf G. TGF-beta and fibrosis in different organs - molecular pathway imprints. Biochim Biophys Acta. 2009; 1792:746-756.
13. Wang Q, Wang Y, Huang X, Liang W, Xiong Z, Xiong Z.
14. Integrin β4 in EMT: an implication of renal diseases. Int J Clin Exp Med. 2015; 8:6967-6976.
14. Jia L, Ma X, Gui B, Ge H, Wang L, Ou Y, Tian L, Chen Z, Duan Z, Han J, Fu R. Sorafenib ameliorates renal fibrosis through inhibition of TGF-β-induced epithelial-mesenchymal transition. PLoS One. 2015; 10:e0117757.
15. Kim MK, Maeng YI, Sung WJ, Oh HK, Park JB, Yoon GS, Cho CH, Park KK. The differential expression of TGF-β1, ILK and wnt signaling inducing epithelial to mesenchymal transition in human renal fibrogenesis: an immunohistochemical study. Int J Clin Exp Pathol. 2013; 6:1747-1758.
16. Li Y, Yang J, Dai C, Wu C, Liu Y. Role for integrin-linked kinase in mediating tubular epithelial to mesenchymal transition and renal interstitial fibrogenesis. J Clin Invest. 2003; 112:503-516.
17. Paliwal S, Shi J, Dhru U, Zhou Y, Schuger L. P311 binds to the latency associated protein and downregulates the expression of TGF-beta1 and TGF-beta2. Biochem Biophys Res Commun. 2004; 315:1104-1109.
18. Pan D, Zhe X, Jakkaraju S, Taylor GA, Schuger L. P311 induces a TGF-beta1-independent, nonfibrogenic myofibroblast phenotype. J Clin Invest. 2002; 110:1349-1358.
19. Mariani L, McDonough WS, Hoelzinger DB, Beaudry C, Kaczmarek E, Coons SW, Giese A, Moghaddam M, Seiler RW, Berens ME. Identification and validation of P311 as a glioblastoma invasion gene using laser capture microdissection. Cancer Res. 2001; 61:4190-4196.
20. Fujitani M, Yamagishi S, Che YH, Hata K, Kubo T, Ino H, Tohyama M, Yamashita T. P311 accelerates nerve regeneration of the axotomized facial nerve. J Neurochem. 2004; 91:737-744.
21. Zhao L, Leung JK, Yamamoto H, Goswami S, Kheradmand F, Vu TH. Identification of P311 as a potential gene regulating alveolar generation. Am J Respir Cell Mol Biol. 2006; 35:48-54.
22. Tan J, Peng X, Luo G, Ma B, Cao C, He W, Yuan S, Li S, Wilkins JA, Wu J. Investigating the role of P311 in the hypertrophic scar. PLoS One. 2010; 5:e9995.
23. Qi FH, Cai PP, Liu X, Peng M, Si GM. Adenovirus-mediated P311 inhibits TGF-β1-induced epithelialmesenchymal transition in NRK-52E cells *via* TGF-β1-Smad-ILK pathway. BioSci Trends. 2015; 9:299-306.
24. Gao R, Liu R, Si GM. Effect on the expression of α-SMA and α-SMA mRNA with Shenqi Jiedu Decoction combined with P311 in the Process of renal interstitial fibrosis. World Journal of Integrated Traditional and Western Medicine. 2016; 11:41-43. (in Chinese)
25. Baba I, Egi Y, Utsumi H, Kakimoto T, Suzuki K. Inhibitory effects of fasudil on renal interstitial fibrosis induced by unilateral ureteral obstruction. Mol Med Rep. 2015; 12:8010-8020.
26. Yin Y, Qi F, Song Z, Zhang B, Teng J. Ferulic acid combined with astragaloside IV protects against vascular endothelial dysfunction in diabetic rats. Biosci Trends. 2014; 8:217-226.
27. Liu QF, Ye JM, Deng ZY, Yu LX, Sun Q, Li SS. Ameliorating effect of Klotho on endoplasmic reticulum stress and renal fibrosis induced by unilateral ureteral obstruction. Iran J Kidney Dis. 2015; 9:291-297.
28. Lu H, Dong J, Zhang Y, Li C, Yu Q, Tang W. Pathological changes in primary cilia: a novel mechanism of graft cholangiopathy caused by prolonged cold preservation

in a rat model of orthotopic liver transplantation. Biosci Trends. 2014; 8:206-211.

29. Zhang HW, Lin ZX, Xu C, Leung C, Chan LS. Astragalus (a traditional Chinese medicine) for treating chronic kidney disease. Cochrane Database Syst Rev. 2014; 10:CD008369.

30. Zhao J, Wang L, Cao AL, Jiang MQ, Chen X, Wang Y, Wang YM, Wang H, Zhang XM, Peng W. HuangQi decoction ameliorates renal fibrosis *via* TGF-β/Smad signaling pathway *in vivo* and *in vitro*. Cell Physiol Biochem. 2016; 38:1761-1774.

31. Wang L, Chi YF, Yuan ZT, Zhou WC, Yin PH, Zhang XM, Peng W, Cai H. Astragaloside IV inhibits renal tubulointerstitial fibrosis by blocking TGF-β/Smad signaling pathway *in vivo* and *in vitro*. Exp Biol Med (Maywood). 2014; 239:1310-1324.

32. Lu X, Jin Y, Ma L, Du L. Danshen (Radix Salviae Miltiorrhizae) reverses renal injury induced by myocardial infarction. J Tradit Chin Med. 2015; 35:306-311.

33. Ahn YM, Kim SK, Lee SH, Ahn SY, Kang SW, Chung JH, Kim SD, Lee BC. Renoprotective effect of Tanshinone IIA, an active component of Salvia miltiorrhiza, on rats with chronic kidney disease. Phytother Res. 2010; 24:1886-1892.

34. O'Connor JW, Gomez EW. Biomechanics of TGFβ-induced epithelial-mesenchymal transition: implications for fibrosis and cancer. Clin Transl Med. 2014; 3:23.

35. Wang W, Koka V, Lan HY. Transforming growth factor-beta and Smad signalling in kidney diseases. Nephrology (Carlton). 2005; 10:48-56.

36. Yao Z, Yang S, He W, Li L, Xu R, Zhang X, Li H, Zhan R, Sun W, Tan J, Zhou J, Luo G, Wu J. P311 promotes renal fibrosis *via* TGFβ1/Smad signaling. Sci Rep. 2015; 5:17032.

37. Chen G, Chen H, Wang C, Peng Y, Sun L, Liu H, Liu F. Rapamycin ameliorates kidney fibrosis by inhibiting the activation of mTOR signaling in interstitial macrophages and myofibroblasts. PLoS One. 2012; 7:e33626.

Expression, purification, and biological characterization of *Anaplasma phagocytophilum* enolase

Xiaoge Gao[1],[§], Chen Zheng[2],[§], Xiangye Liu[2],*

[1] *Cancer Institute, Xuzhou Medical University, Xuzhou, Jiangsu Province, China;*
[2] *Jiangsu Key Laboratory of Immunity and Metabolism, Department of Pathogenic Biology and Immunology, Xuzhou Medical University, Xuzhou, Jiangsu Province, China;*

Summary   The obligate intracellular bacteria *Anaplasma phagocytophilum* is the etiological agent of human granulocytic anaplasmosis (HGA), an acute febrile tick-borne disease. *A. phagocytophilum* has a complex lifecycle within both vertebrate reservoirs and tick vectors, and employs a range of different molecules to infect and multiply within the host cells. Enolase is an essential glycolytic enzyme in intracellular glucose metabolism, but is also a multifunctional protein expressed on the pathogen surface, that binds to and promotes plasminogen conversion to plasmin. In this study, we generated recombinant ApEno protein (rApEno), and confirmed that rApEno retains its enzymatic activity. Furthermore, we demonstrated that rApEno binds to human plasminogen, and that this binding could be significantly reduced in the presence of lysine analogs (ε-aminocaproic acid). Additionally, rApEno promotes plasminogen to plasmin conversion in the presence of plasminogen activator. In conclusion, *A. phagocytophilum* enolase is a multifunctional protein which can catalyze the dehydration of 2-phospho-D-glycerate to phosphoenolpyruvate, and facilitate binding to host plasminogen.

Keywords: Anaplasma phagocytophilum, enolase, catalytic ability, plasminogen

1. Introduction

Human granulocytic anaplasmosis (HGA), caused by the obligate intracellular bacteria *Anaplasma phagocytophilum*, is an emerging tick-borne zoonosis in the United States, Europe, and Asia (*1*). *A. phagocytophilum* is primarily transmitted to humans *via* bites from infected ixodid ticks; however, transmission has also been reported to occur through blood transfusion and contact with infected mammal blood (*2*). After infection, the patient generally presents unexplained nonspecific symptoms such as fever, chills, headache, and myalgia, which may occur in the presence of abnormal laboratory features, which may include leukopenia, thrombocytopenia, and/or mildly elevated

liver enzymes (*3*).

   A. phagocytophilum is a significant tick-borne pathogen in terms of public health, and improving our understanding of its transmission methods is vital to enabling the development of appropriate control measures. *A. phagocytophilum*'s natural infectious cycle is dependent on the presence of infected vertebrate reservoir hosts and ixodid tick vectors (*4*). Within the vertebrate host, the bacteria colonizes neutrophils, but also infects other cells of myeloid and nonmyeloid origin. Of interest, it has also been reported to infect and multiply in several different ixodid tick tissues, including the midgut and salivary gland cells (*2*). Over recent decades, several molecules used by *A. phagocytophilum* to infect and multiply within vertebrate host cells have been well characterized (*4*). Moreover, a growing numbers of reports suggest that *A. phagocytophilum* can modulate tick gene and protein expression to facilitate bacterial acquisition and/or transmission in the tick vector (*5,6*). However, little information is available about the specific bacterial molecules playing key roles in tick gut and salivary gland infection.

   Enolase is a key cytoplasmic glycolytic enzyme

in intracellular glucose metabolism, and catalyzes the reversible dehydration of 2-phospho-D-glycerate (2-PGA) to phosphoenolpyruvate (PEP) in the penultimate step of glycolysis (*7*). In recent years, enolase has also been identified on the surface of a variety of eukaryotic cells, and there acts as a plasminogen receptor promoting conversion to plasmin when in the presence of plasminogen activator (*8*). Furthermore, it has been confirmed that surface-expressed enolase on vector-borne pathogens plays an essential role during pathogen invasion of vector gut by binding mammalian plasminogen (*9,10*).

In the present study, we characterized the protein structure of *A. phagocytophilum* enoalse (ApEno), and then generated recombinant ApEno (rApEno) *via* an *E. coli* expression system. Subsequently, we confirmed that rApEno catalyzes 2-PGA dehydration to PEP. Additionally, we demonstrated that rApEno binds to and promotes plasminogen conversion to the plasmin active form. Our results provide further evidence that these molecules likely contribute to *A. phagocytophilum*'s ability to infect tick vectors. However, further research is needed in order to fully elucidate ApEno's role during the bacterial infection process.

2. Materials and Methods

2.1. *Animals and ethics statements*

All mice were purchased from Beijing Vital River Laboratory Animal Technology Co., Ltd and maintained at the Xuzhou Medical University Animal Center. This study was carried out in strict agreement with the guidelines for the Care and Use of Laboratory Animals as defined by the Xuzhou Medical University Laboratory Animal Ethics Committee. All protocols involving mice were approved by the Xuzhou Medical University Laboratory Animal Ethics Committee (Permit Number: 201547).

2.2. *Reagents*

All reagents were purchased from Sigma-Aldrich, CO (St. Louis, USA) unless otherwise specified.

2.3. *ApEno characterization*

A. phagocytophilum str. HZ enolase amino acid sequences were obtained from the NCBI protein database (*11,12*). The enolase signature sequence and other domains were defined using ScanProsite online software (*http://prosite. expasy.org/scanprosite*), and MotifScan online software (*http://myhits.isb-sib.ch/cgi-bin/motif_scan*). Multiple protein sequences were aligned and analyzed using the MUSCLE multiple sequence alignment tool from the European Bioinformatics Institute (EMBL-EBI) (*http:// www.ebi.ac.uk/Tools/msa/clustalo*).

2.4. *ApEno cloning, recombinant expression, and purification*

The gene fragment encoding the entire ApEno coding sequence was synthesized by GENEWIZ® (GENEWIZ Suzhou, China). *Bam*HI and *Xho*I restriction sites were added to ApEno 5' and 3' ends, respectively, to facilitate cloning into the expression vector. ApEno was then cloned into the pGEX-4T-2 expression vector (TransGen Biotech, Beijing, China), and transformed into *Escherichia coli* BL21 Star (DE3) competent cells. Recombinant protein expression and purification were performed as previously described (*13*). In brief, *E. coli* cells were induced overnight with isopropyl-β-D-thiogalactopyranoside (IPTG), and then lysed with a sonicator. Following centrifugation, the supernatant was purified on a GSTrap 4B column. Finally, the purified protein was analyzed by sodium dodecyl sulfate-polyacrylamide gel electrophoresis (SDS-PAGE) followed by Coomassie brilliant blue staining.

2.5. *Mouse polyclonal antibody against rApEno*

Polyclonal antibodies against rApEno were generated as previously described (*13*). Briefly, 50 μg purified rApEno protein was mixed with MONTANIDE™ ISA 70 VG adjuvant (Seppic, Puteaux, France), and then subcutaneously injected into four- to six-week-old female Balb/c mice at two-weekly intervals. One week after the third immunization, mouse blood samples were isolated and centrifuged to obtain antibodies. Finally, antibody titer was measured using an indirect enzyme-linked immunosorbent assay (ELISA), and antibody specificity evaluated by western blot.

2.6. *rApEno enzymatic activity*

Purified rApEno enzymatic activity was determined by direct monitoring of absorbance enhancement at 240 nm using a Synergy HT spectrophotometer (Bio-Tek Instruments, Winooski, USA) as previously described (*14*). In brief, 1 mM 2-PGA was incubated with different concentrations of rApEno (2.5, 5, 10, and 20 ng/μL) in a 30°C preheated reaction buffer (100 mM HEPES buffer, 7.7 mM KCl, 10 mM MgSO$_4$, pH 7.0). The continuous assay was measured every 3 min for a period of 60 min.

In order to calculate the Michaelis-Menten constant (K_m) of rApEno, purified rApEno protein was incubated with differing 2-PGA concentrations (1, 1.5, 2, 4, 6, 8, and 10 mM) in reaction buffer. To analyze the effects of pH and temperature on rApEno activation, the assay was performed using a reaction buffer system at different pH values (3, 4, 5, 6, 7, 8, 9, 10, and 11) and temperature (4, 22, 30, 37, 50, 60, 70, and 80°C). Reactions were initiated by the addition of rApEno (1 μg/reaction) diluted in the corresponding buffer. GST protein was used as a negative control.

2.7. *Plasminogen binding analysis*

The analysis was performed in 96-well plates as previously described (*10*). In brief, each well was coated overnight at 4°C with 100 μL PBS containing 0.04 μg/μL human plasminogen. Non-specific binding sites were blocked with 2% BSA in PBS, then each well was incubated with 100 μL PBS containing 0.04 μg/μL rApEno for 2 h at 37°C. Following three washes with PBST (0.05% (V/V) Tween-20 in PBS), bound protein was detected using mouse anti-rApEno antibody and goat alkaline phosphatase (AP)-conjugated secondary antibodies. Finally, the wells were washed three times with PBST before the AP substrate was added and optical densities (OD) were read at 450 nm using a Bio-Tek plate reader. GST was used as a negative control. In addition, to analyze the role of lysine residues in plasminogen-enolase interactions, differing concentrations (0-100 mM) of lysine analog ε-aminocaproic acid (ε-ACA) were added together with rApEno to the plasminogen-coated plates.

2.8. *Plasminogen activation assay*

As previously described (*15*), 96-well plates were coated overnight with 4 μg rApEno or GST in 100 μL PBS at 4°C. Subsequently, plates were blocked and washed three times as above, and then 4 μg/well of human plasminogen was added and incubated for 2 h at 37°C. Wells were washed three times with PBST, and then 4 ng/well of human urokinase plasminogen activator (uPA) was added. Subsequently, 0.3 mM plasmin-specific substrate D-valyl-leucyl-lysine-p-nitroanilide dihydrochloride in PBS was added. Following overnight incubation at 37°C, absorbance was read at 405 nm using a Bio-Tek plate reader.

2.9. *Statistical analysis*

All data were collected from three independent experiments and presented as mean ± standard deviation (SD). Statistical comparisons of enzyme activity, plasminogen binding, and activation of rApEno were performed using one-way analysis of variance (ANOVA) and Tukey's multiple comparison tests. p values < 0.05 were considered to be significant and data analysis was performed with Prism 5.0 (GraphPad Software, Inc. USA).

3. Results

3.1. *Anaplasma phagocytophilum enolase*

An online search for *A. phagocytophilum* str. HZ proteomic sequences identified a protein (accession number: ABD44357) comprising 429 amino acids encoded by 1, 290 nucleotides. This protein was predicted to be a soluble 46.2 kDa polypeptide with a pI of 5.60, and presented an enolase signature motif spanning residues 338-351 ([338]VLIKPNQIGTLSET[351]). Following protein sequence analysis, eight conserved 2-PGA binding residues (Ala[47], His[161], Gln[169], Lys[341], His[369], Arg[370], Ser[371], and Lys[392]), two conserved dehydration residues (Glu[170] and Glu[211]), and four conserved Mg^{2+} binding amino acids (Ser[48], Asp[248], Glu[289], and Asp[316]), were identified. Moreover, [43]VPSGASVGKNEALELRDKDMNK[64] (loop1), [161]HADNGLDFQ[169] (loop2), and [254]FYDGKIYKFSGSSMS[268] (loop3) were predicted to form the catalytic loop. In addition, two predicted plasminogen-binding motifs were characterized at [254]FYDGKIY[260] and [262]FSGSSM[267] (Figure 1). The protein sequence also carried phosphorylation and
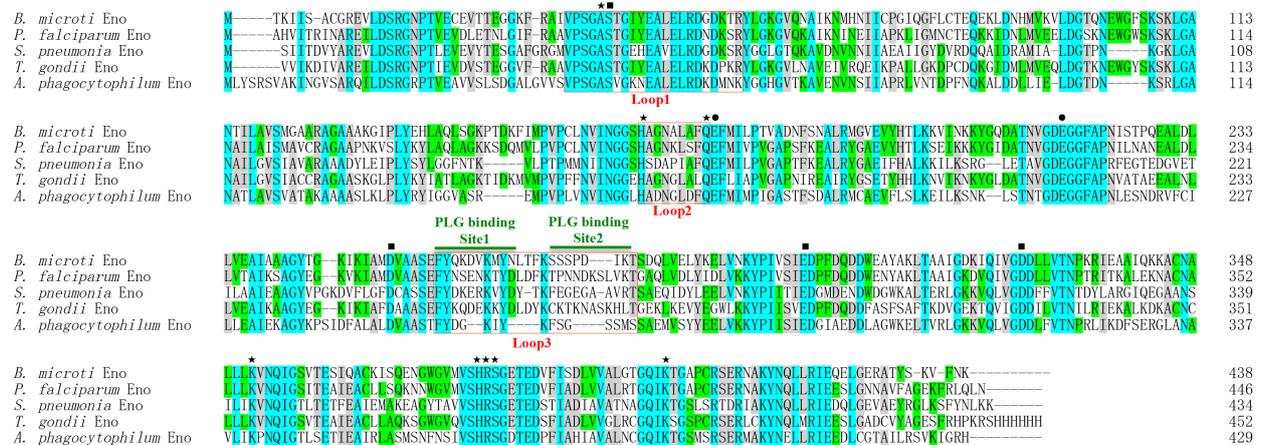
Figure 1. ApEno sequence characterization. Comparison of enolase amino acid sequences from *Babesia microti* (XP_012649799), *Plasmodium falciparum* (AAA18634), *Streptococcus pneumoniae* (AOG56016), *Toxoplasma gondii* (3OTR_A), and *Anaplasma phgocytophilum* (ABD44357), was performed with the MUSCLE multiple sequence alignment tool. Stars, circles, and rectangles were used to mark the residues interacting with 2-PGA, dehydration residues, and residues interacting with Mg^{2+} ions, respectively. Catalytic loops are marked with boxes, and plasminogen (PLG) binding sites are indicated with horizontal green lines.

N-glycosylation sites, but no trans-membrane domains, signal peptides, nor plant-like insertions.

3.2. rApEno expression, purification, and characterization

The synthesized full-length enolase coding sequence was cloned into the pGEX-4T-2 plasmid with an in-frame GST-tag as described above. rApEno expression was induced in *E. coli* and bacterial extracts were assessed by SDS-PAGE with Coomassie blue staining.
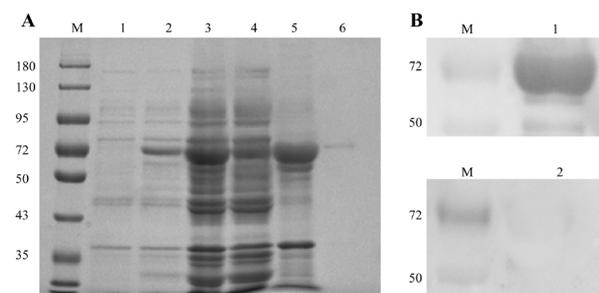
Figure 2. rApEno expression, purification, and characterization. (A) rApEno expression and purification were assessed by SDS-PAGE with Coomassie blue staining. M: Pre-stained protein ladder, Lane 1: Total cellular proteins of pGEX-4T-2 BL21 (DE3) cells, Lane 2: Total cellular proteins of non-induced pGEX-4T-2-ApEno BL21 (DE3) cells, Lane 3: Total cellular proteins of induced pGEX-4T-2-ApEno BL21 (DE3) cells, Lane 4: Supernatant of pGEX-4T-2-ApEno BL21 (DE3) cell lysate, Lane 5: Sediment of pGEX-4T-2-ApEno BL21 (DE3) cell lysate, Lane 6: GST-tagged purified recombinant ApEno protein. **(B)** Anti-rApEno serum specifically recognized purified recombinant ApEno. M: Pre-stained protein ladder, Lane 1: Purified GST-tagged rApEno proteins were immunoblotted with mouse polyclonal anti-rApEno serum. Lane 2: Purified GST-tagged rApEno proteins were immunoblotted with normal mouse serum.

A prominent band of approximately 72 kDa, GST-tagged rApEno, was observed in the induced cell lysate. Soluble GST-tagged rApEno protein was purified to homogeneity from bacterial lysates, producing a single band (Figure 2A). Anti-rApEno mouse serum, but not normal mouse serum, specifically recognized purified rApEno *via* western blot (Figure 2B).

3.3. rApEno enzymatic activity

The classical enzymatic activity of purified rApEno was evaluated by monitoring its ability to catalyze 2-PGA to PEP. Results showed that the catalytic activity of rApEno increased with increasing concentrations from 2.5 to 20 ng/μL (Figure 3A). The catalytic activity of rApEno also increased when 2-PGA concentration rose from 1.0 to 4.0 mM (Figure 3B). Moreover, the Michaelis constant (K_m) and maximum velocity (V_{max}) of rApEno was determined to be 6.053 mM and 21.87 μmol/L/min, respectively, by applying double-reciprocal Lineweaver-Burk plots (Figure 3C). This analysis also showed that the enzyme's optimal pH and temperature were 8.0 and 50°C, respectively (Figure 3D and 3E).

3.4. rApEno binds to human plasminogen and promotes its activation

ELISA binding assays were used to analyze the binding activity of rApEno to human plasminogen. The analysis showed that rApEno significantly binds to human plasminogen compared to the negative control ($p < 0.0001$) (Figure 4A). Interestingly, rApEno binding
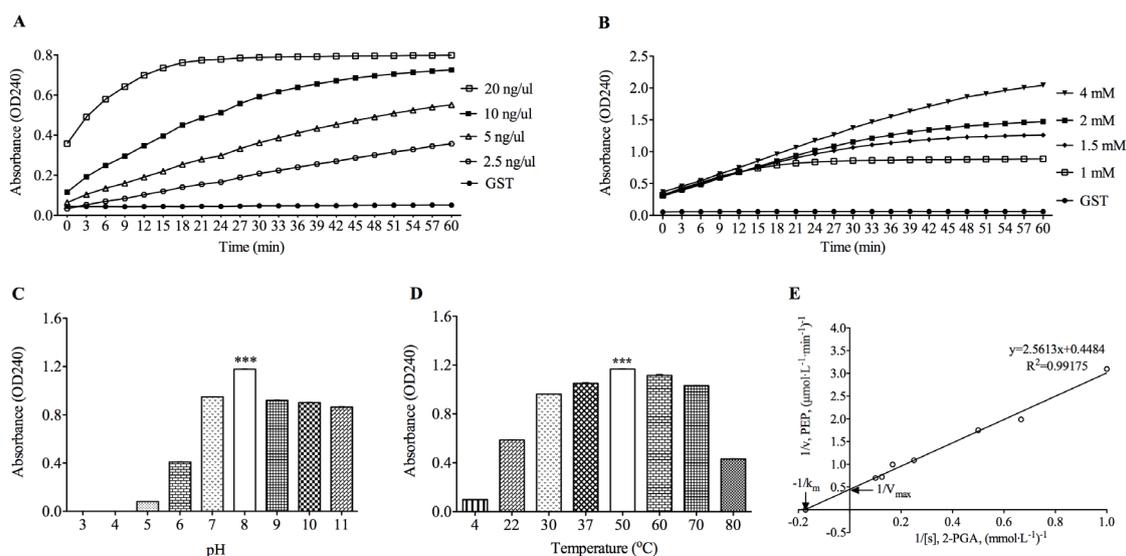
Figure 3. rApEno enzymatic activity and affecting factors. (A) Influence of different rApEno concentrations on enzymatic activity. **(B)** Influence of different 2-PGA concentrations on enzymatic activity. **(C)** rApEno K_m and V_{max} values were calculated with a double-reciprocal plot as 6.053 mM and 21.87 μmol/L/min, respectively. **(D)** rApEno activity in a buffer system spanning a pH range 3-11, enzymatic activity was maximal at pH 8.0. **(E)** rApEno activity in a buffer system covering a 4 - 80°C temperature range, enzymatic activity was maximal at 50°C. Relative activity of rApEno was measured by OD240 absorbance. All data shown represent the mean ± SD from three independent experiments. Significant differences as compared to other conditions are denoted by ***for $p < 0.0001$.
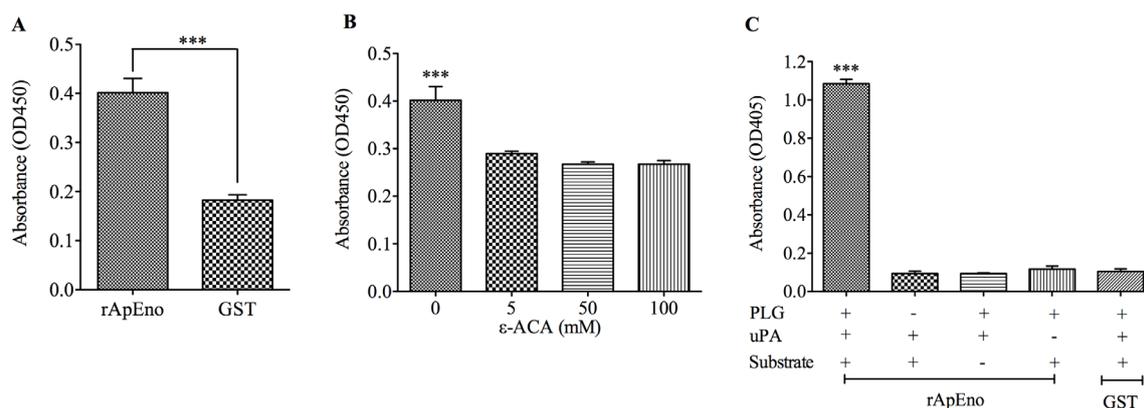
Figure 4. rApEno binds to human plasminogen and promotes its activation. (A) Relative rApEno binding activity to human plasminogen (PLG) was measured by absorbance at OD450, and GST served as a negative control for nonspecific binding. **(B)** rApEno binding activity was reduced in the presence of lysine analog (ε-ACA). **(C)** rApEno-coated 96-well plates were incubated with PLG, uPA, and/or a plasmin-specific chromogenic substrate, and GST served as a negative control. Proteolytic activity was monitored by absorbance at OD405. All data shown represent the mean ± SD from three independent experiments. Significant differences compared to other conditions are denoted by ***for $p < 0.0001$.

was significantly reduced with the addition of the lysine analog ε-ACA, which acts as an efficient binding competitor ($p < 0.0001$) (Figure 4B). As reported, enolase promotes plasminogen activation to plasmin. Our results confirmed that rApEno dramatically promoted plasmin activation in the presence of uPA, when compared to the GST negative control ($p < 0.0001$) (Figure 4C).

4. Discussion

Enolase is a multi-functional protein present in both prokaryotes and eukaryotes. As a cytoplasmic protein, enolase plays an important role in intracellular glucose metabolism; but as a surface expressed protein, it also plays a crucial role in several biological and pathophysiological processes: *e.g.* as a plasminogen receptor (*7*). In our study, we characterized a 46.2 kDa protein containing enolase signature motif residues, obtained from the gram-negative bacteria *A. phagocytophilum* str. HZ. In order to evaluate the potential catalytic and plasminogen-binding motif, enolase amino acid sequences from different hosts were aligned using MUSCLE multiple sequence alignment tools. As shown in Figure 1, ApEno possesses both 2-PGA binding residues and catalytic loops when compared to *Babesia microti* enolase and *Toxoplasma gondii* enolase (*13,16*). Furthermore, ApEno also possesses a conserved internal plasminogen-binding motif "FYDGKIYKFSGSSMS" located between amino acids 254 and 268, when compared to *Streptococcus pneumoniae* surface enolase (*17*). However, neither plant-like pentapeptide nor dipeptide insertions – which play crucial roles in k_{cat}/K_m and dissociation into monomers – were conserved in ApEno (*18,19*). Taken together, these results provide vital information for the further refinement of ApEno's function.

To biologically characterize ApEno, a synthesized ApEno gene was cloned and expressed in *E. coli* cells. SDS-PAGE showed that rApEno could be expressed in the supernatant, which aided the purification and study of its biological characteristics. Expression products were purified, and Balb/c mice were immunized to generate anti-rApEno serum. Western blots showed that anti-rApEno mouse serum specifically recognized purified rApEno, where normal mouse serum did not (Figure 2). This suggested that the anti-serum presented high specificity and could be used in subsequent experiments.

Although it has long been recognized as a cytosolic protein important in sugar metabolism, enolase also catalyzes the dehydration of 2-PGA to PEP in the penultimate step in glycolysis (*7*). Here, our results also showed that purified rApEno catalyzed the conversion of 2-PGA to PEP in reaction buffer with 10 mM Mg^{2+} at a wide range of pH values and temperatures. Interestingly, rApEno demonstrated the highest enzymatic activity at 50°C and pH 8.0 (Figure 3). Moreover, rApEno presented high K_m and V_{max} values during 2-PGA to PEP conversion, when compared to other infectious intracellular pathogens (*13,20*). This suggests that ApEno is highly adaptable to a changing surrounding environment. This may be due to the fact that the bacteria cannot use glucose as a carbon or energy source, but instead uses a partial glycolysis pathway which starts with fructose 1,6-biphosphate (*2*).

Many reports have demonstrated that enolase can also be expressed on the surface of organisms, and act as the plasminogen receptor (*10,13,21-23*). In order to characterize rApEno plasminogen binding, ELISA experiments were performed. The results showed that rApEno was also able to bind to human plasminogen, and that binding could be significantly reduced in the presence of lysine analogs (ε-ACA) (Figure 4A and

4B). These results confirmed that lysine analogs play an essential role in enolase-plasminogen interactions (*10,13,15*). The active form of plasminogen is plasmin, a serine protease, which can degrade cell extracellular matrix to assist pathogen infection of hosts (*24*). Furthermore, enolase can also promote plasminogen to plasmin conversion in the presence of tissue plasminogen activator (tPA) or urokinase plasminogen activator (uPA) (*13,15*). In the present study, we showed that rApEno dramatically enhanced plasmin activation in the presence of uPA (Figure 4C). It has been reported that *Plasmodium falciparum* enolase antibody was able to block merozoite invasion of red blood cells (*25*) suggesting that enolase could play an important role in the host cell invasion process. Herein, we hypothesized that *A. phagocytophilum* may utilize enolase to promote plasmin generation, which then degrades host cell membrane sections, enabling granulocyte invasion. However, further research is needed in order to confirm ApEno's role during the bacterial infection process of host cells. Enolase has also been identified as an important candidate antigen for vaccines against pathogen infection (*25-29*). Therefore, further research is also required to evaluate ApEno's potential as a candidate vaccine target to control anaplasmosis infection.

In conclusion, our results demonstrate that enolase from *A. phagocytophilum* possesses a highly conserved active site and plasminogen-binding domains. Recombinant ApEno catalyzes the reversible dehydration of 2-PGA to yield PEP. Furthermore, rApEno can bind to and promote the activation of plasminogen. In addition, we also confirmed that lysine residues play an important role in ApEno and plasminogen interaction. Our results provide new evidence that further supports the identification of molecules that likely contribute to successful *A. phagocytophilum* infection of tick vectors.

Acknowledgements

References

1. Stuen S, Granquist EG, Silaghi C. *Anaplasma phagocytophilum*--a widespread multi-host pathogen with highly adaptive strategies. Front Cell Infect Microbiol. 2013; 3:31.
2. Rikihisa Y. Mechanisms of obligatory intracellular infection with *Anaplasma phagocytophilum.* Clin Microbiol Rev. 2011; 24:469-489.
3. Sanchez E, Vannier E, Wormser GP, Hu LT. Diagnosis, treatment, and prevention of Lyme disease, human granulocytic anaplasmosis, and babesiosis: A review. JAMA. 2016; 315:1767-1777.
4. de la Fuente J, Estrada-Pena A, Cabezas-Cruz A, Kocan KM. *Anaplasma phagocytophilum* uses common strategies for infection of ticks and vertebrate hosts. Trends Microbiol. 2016; 24:173-180.
5. Hajdusek O, Sima R, Ayllon N, Jalovecka M, Perner J, de la Fuente J, Kopacek P. Interaction of the tick immune system with transmitted pathogens. Front Cell Infect Microbiol. 2013; 3:26.
6. Liu XY, Bonnet SI. Hard tick factors implicated in pathogen transmission. PLoS Negl Trop Dis. 2014; 8:e2566.
7. Diaz-Ramos A, Roig-Borrellas A, Garcia-Melero A, Lopez-Alemany R. Alpha-enolase, a multifunctional protein: Its role on pathophysiological situations. J Biomed Biotechnol. 2012; 2012:156795.
8. Ghosh AK, Jacobs-Lorena M. Surface-expressed enolases of Plasmodium and other pathogens. Mem Inst Oswaldo Cruz. 2011; 106 Suppl 1:85-90.
9. Ghosh AK, Coppens I, Gardsvoll H, Ploug M, Jacobs-Lorena M. Plasmodium ookinetes coopt mammalian plasminogen to invade the mosquito midgut. Proc Natl Acad Sci U S A. 2011; 108:17153-17158.
10. Nogueira SV, Smith AA, Qin JH, Pal U. A surface enolase participates in *Borrelia burgdorferi*-plasminogen interaction and contributes to pathogen survival within feeding ticks. Infect Immun. 2012; 80:82-90.
11. Dunning Hotopp JC, Lin M, Madupu R, *et al*. Comparative genomics of emerging human ehrlichiosis agents. PLoS Genet. 2006; 2:e21.
12. Lin M, Kikuchi T, Brewer HM, Norbeck AD, Rikihisa Y. Global proteomic analysis of two tick-borne emerging zoonotic agents: *Anaplasma phagocytophilum and ehrlichia chaffeensis*. Front Microbiol. 2011; 2:24.
13. Liu X, Zheng C, Gao X, Chen J, Zheng K. Complete molecular and immunoprotective characterization of *Babesia microti* enolase. Front Microbiol. 2017; 8:622.
14. Figueiredo BC, Da'dara AA, Oliveira SC, Skelly PJ. Schistosomes enhance plasminogen activation: The role of tegumental enolase. PLoS Pathog. 2015; 11:e1005335.
15. Floden AM, Watt JA, Brissette CA. *Borrelia burgdorferi* enolase is a surface-exposed plasminogen binding protein. PLoS One. 2011; 6:e27502.
16. Ruan J, Mouveaux T, Light SH, Minasov G, Anderson WF, Tomavo S, Ngo HM. The structure of bradyzoite-specific enolase from *Toxoplasma gondii* reveals insights into its dual cytoplasmic and nuclear functions. Acta Crystallogr D Biol Crystallogr. 2015; 71:417-426.
17. Bergmann S, Wild D, Diekmann O, Frank R, Bracht D, Chhatwal GS, Hammerschmidt S. Identification of a novel plasmin(ogen)-binding motif in surface displayed alpha-enolase of *Streptococcus pneumoniae*. Mol Microbiol. 2003; 49:411-423.
18. Dzierszinski F, Mortuaire M, Dendouga N, Popescu O, Tomavo S. Differential expression of two plant-like enolases with distinct enzymatic and antigenic properties during stage conversion of the protozoan parasite *Toxoplasma gondii*. J Mol Biol. 2001; 309:1017-1027.
19. Vora HK, Shaik FR, Pal-Bhowmick I, Mout R, Jarori GK. Effect of deletion of a plant like pentapeptide insert on kinetic, structural and immunological properties of enolase from *Plasmodium falciparum*. Arch Biochem Biophys. 2009; 485:128-138.
20. Bao S, Guo X, Yu S, Ding J, Tan L, Zhang F, Sun Y, Qiu X, Chen G, Ding C. *Mycoplasma synoviae* enolase is a plasminogen/fibronectin binding protein. BMC Vet Res.

2014; 10:223.

21. Lahteenmaki K, Kuusela P, Korhonen TK. Bacterial plasminogen activators and receptors. FEMS Microbiol Rev. 2001; 25:531-552.

22. Lee JH, Kang HK, Moon YH, Cho DL, Kim D, Choe JY, Honzatko R, Robyt JF. Cloning, expression and characterization of an extracellular enolase from *Leuconostoc mesenteroides*. FEMS Microbiol Lett. 2006; 259:240-248.

23. Mori Y, Yamaguchi M, Terao Y, Hamada S, Ooshima T, Kawabata S. alpha-Enolase of *Streptococcus pneumoniae* induces formation of neutrophil extracellular traps. J Biol Chem. 2012; 287:10472-10481.

24. Gonzalez-Miguel J, Siles-Lucas M, Kartashev V, Morchon R, Simon F. Plasmin in parasitic chronic infections: Friend or foe? Trends Parasitol. 2016; 32:325-335.

25. Pal-Bhowmick I, Mehta M, Coppens I, Sharma S, Jarori GK. Protective properties and surface localization of *Plasmodium falciparum* enolase. Infect Immun. 2007; 75:5500-5508.

26. Zhang S, Guo A, Zhu X, You Y, Hou J, Wang Q, Luo X, Cai X. Identification and functional characterization of alpha-enolase from *Taenia pisiformis* metacestode. Acta Trop. 2015; 144:31-40.

27. Membrebe JD, Yoon NK, Hong M, Lee J, Lee H, Park K, Seo SH, Yoon I, Yoo S, Kim YC, Ahn J. Protective efficacy of *Streptococcus iniae* derived enolase against Streptococcal infection in a zebrafish model. Vet Immunol Immunopathol. 2016; 170:25-29.

28. Mahana N, Abd-Allah HA, Salah M, Tallima H, El Ridi R. *Fasciola gigantica* enolase is a major component of worm tegumental fraction protective against sheep fasciolosis. Acta Trop. 2016; 158:189-196.

29. Zhang C, Gu Y, Tang J, Lu F, Cao Y, Zhou H, Zhu G, Cao J, Gao Q. Production of *Plasmodium vivax* enolase in *Escherichia coli* and its protective properties. Hum Vaccin Immunother. 2016;1-7.

Low-density lipoprotein receptor deficiency impaired mice osteoblastogenesis *in vitro*

Na Zhang[1,2,3,§], Yang Zhang[4,§], Jing Lin[1,2,3], Xuemin Qiu[1,2,3], Lanting Chen[1,2,3], Xinyao Pan[1,2,3], Youhui Lu[1,2,3], Jiali Zhang[1,2,3], Yan Wang[1,2,3], Dajin Li[1,2,3], Ling Wang[1,2,3,*]

[1] *Hospital & Institute of Obstetrics and Gynecology, Fudan University, Shanghai, China;*
[2] *The Academy of Integrative Medicine of Fudan University, Shanghai, China;*
[3] *Shanghai Key Laboratory of Female Reproductive Endocrine Related Diseases, Shanghai, China;*
[4] *First Affiliated Hospital, Heilongjiang University of Chinese Medicine, Harbin, China.*

Summary   Postmenopausal osteoporosis affected most elderly women with co-existence of lipid and bone metabolism disorders. However, the cellular and molecular mechanisms underlying the parallel progression and cross-talk of these systems remained unclear. In the present study, low-density lipoprotein receptor knockout (*LDLR-/-*) mice were chosen to elucidate the effect of LDLR in regulating the differentiation of osteoblasts, which were responsible for bone formation and modulation of osteoclastogenesis. Primary osteoblasts were isolated from the calvarium of newborn *LDLR-/-* or wild-type mice followed by osteoblastic differentiation culture *in vitro*. Alkaline phosphatase activity was significantly decreased in *LDLR-/-* osteoblasts compared to wild-type controls, combined with calcium deposit formation delay, implying impaired osteoblastogenesis *in vitro*. Consistent with these findings, the expression of *runt-related transcription factor 2* (*Runx2*) was decreased 3 days after differentiation in *LDLR-/-* osteoblasts compared to wild-type controls. Moreover, the expression of *Osterix* was decreased 7 days after differentiation in *LDLR-/-* osteoblasts compared to wild-type controls, later than Runx2. However, the osteoclastogenesis modulation role of osteoblasts was unaffected by the LDLR deficiency, evidenced by the same level of osteoprotegerin (OPG)/receptor activator of nuclear factor-κ B ligand (RANKL) axis between *LDLR-/-* and wild-type control osteoblasts. Our results provide a novel insight into the role of LDLR during osteoblastic differentiation and improve understanding of cross-talk between bone and lipid metabolisms.

Keywords: Postmenopausal osteoporosis, low-density lipoprotein receptor, osteoblast, osteoblastogenesis, alkaline phosphatase, runt-related transcription factor 2, Osterix

1. Introduction

Postmenopausal osteoporosis (PMO) affected most elderly women due to estrogen decline. Several epidemiological studies demonstrated the co-existence of lipid and bone metabolism disorders in postmenopausal females (*1-3*). Recent studies indicated a positive connection between cardiovascular disease and risk of osteoporosis, because high cholesterol levels and high low-density lipoprotein (LDL)-cholesterol levels had been described to correlate with low bone mineral density in PMO patients (*4-7*). Furthermore, the increased serum LDL-cholesterol level was indicated to be an index affecting the presence of prevalent non-vertebral fractures in postmenopausal females (*8*). Additionally, menopausal hormone therapy exerted benefit effects of reducing the risk of atherosclerosis (*9-11*). Therefore, hyperlipidemia may play an essential role in regulating osteoporosis progress.

Osteoporosis, a systemic metabolic skeletal disorder characterized by low bone mass and increased risk of fractures, is a consequence of bone turnover disruption caused by imbalance between osteoblast-mediated bone formation and osteoclast-mediated bone resorption. Pre-

osteoblasts were derived from pluripotent mesenchymal stem cells (MSCs), which were also the progenitors of adipocytes and chondrocytes (*12*). Osteoblastogenesis could be defined by four sequential stages: lineage commitment, proliferation, extracellular matrix (ECM) synthesis, and matrix mineralization (*13*). Runt-related transcription factor 2 (Runx2) was the master transcription regulator of osteoblast lineage commitment that inhibited MSCs from differentiating into the adipocytic lineages (*14*). Null mutation of *Runx2* in mice resulted in a cartilaginous skeleton with complete lack of osteoblasts (*15-17*). Runx2 regulated osteoblast-related molecules such as Osterix, type I collagen and alkaline phosphatase (ALP). Osterix was the second transcription factor for proliferative expansion of immature osteoblasts, and the expression of *Osterix* was absent in *Runx2* null mice but *Runx2* was expressed in *Osterix* null mice (*18,19*). Type I collagen was one of the major osteoblast-specific matrix proteins expressed by fully differentiated osteoblasts after complete mitosis, essential for both bone matrix synthesis and later mineralization (*20,21*). Moreover, osteoblasts took part in the regulation of osteoclastogenesis and bone resorption by producing receptor activator of nuclear factor-κ B ligand (RANKL), the ligand of RANK present in osteoclast precursor cells, and its decoy receptor osteoprotegerin (OPG) (*22*). Precise regulation of osteoblastogenesis and osteoclastogenesis was required for the maintenance of normal bone metabolism.

Several basic studies had established that oxidized-LDL inhibited osteoblastic differentiation and promoted adipocytic differentiation of MSCs *in vitro* (*23,24*). Moreover, oxidized-LDL increased *RANKL* expression and secretion in human osteoblast-like cells (*24-26*), indicating cross-talk between lipid and bone metabolism systems. LDL was transferred in particle form and internalized by binding to the receptor LDL receptor (LDLR) residing on the surface of liver cells (*27*). LDLR was the prototype member of the LDLR family that contained several key regulators involved in osteoblastic development. For example, human osteoblasts expressed low-density lipoprotein receptor-related protein (LRP) 1 with a capacity for osteocalcin carboxylation (*28*). LRP4, LRP5/6, and LRP8 were involved in the maintenance of bone (*29-36*). However, the role of LDLR in bone metabolism was unclear with controversial results in recent studies. LDLR deficient familial hypercholesterolemia patients showed normal bone mineral density at the femora neck (*37*). In an animal experiment, LDLR deficiency caused ectopic bone formation in an experimental osteoarthritis mouse model (*38*). Furthermore, Okayasu *et al.* showed that LDLR deficiency induced impaired pre-osteoclast fusion *in vitro* while increasing bone mass in LDLR deficient mice (*39*). However, decreased bone mass was detected in LDLR deficient mice with inhibition of osteoblastogenesis from bone marrow cells and

enhanced osteoclastogenesis *in vitro* (*40*), indicating that LDLR might regulate bone metabolism in a complex manner.

Previous work from our group showed that most of the LDLR family members were up-regulated during osteoblastic differentiation *in vitro*, except for LDLR, which was down-regulated in the late stages of pre-osteoblast mineralization culture, indicating a unique role of LDLR in osteoblastogenesis (*41*). The function of LDLR in regulating osteoblastic development and related mechanisms remained to be further explored. In the present study, we made use of LDLR deficient mice and pre-osteoblasts *in vitro* culture system to explore the effect of LDLR deficiency on this process.

2. Materials and Methods

2.1. *Mice*

LDLR knockout (*LDLR$^{-/-}$*) mouse strain (B6.129S7-Ldlrtm1Her/J) was purchased from Nanjing Biomedical Research Institute of Nanjing University (Nanjing, China), originally from the Jackson Laboratory. Data obtained from C57BL/6 wild-type (WT) mice purchased from the Laboratory Animal Facility of Chinese Academy of Science (Shanghai, China) were used as controls. After being habituated to housing conditions for 3 days, mice were mated (one male with two females per cage) under standard housing conditions at 24°C on a reversed 12-12 hour light-dark cycle. Standard rodent food and water were provided ad libitum at room temperature. Primary osteoblasts were isolated from the calvarium of newborn mice. Experimental animal housing and handling were conducted in accordance with guidelines for the care and use of laboratory animals at Fudan University, Shanghai, China and in conformity with the National Institutes of Health Guide for Care and Use of Laboratory Animals (Publication No. 85-23, revised 1985).

2.2. *Chemicals and reagents*

Serum and phenol red-free minimal essential medium (α-MEM) and fetal bovine serum (FBS) were purchased from Gibco-BRL (Gaithersburg, MD, USA). Dexamethasone, β-glycerophosphate disodium salt hydrate, ascorbic acid, and collagenase were obtained from Sigma-Aldrich Co (Saint Louis, MO, USA). Dispase was supplied by Hoffmann-La Roche Ltd (Basel, Schweiz). RNAiso Plus, PrimeScriptTM RT Master Mix (Perfect Real Time) Kit and SYBR Premix Ex Taq II (Tli RNaseH Plus) Kit were obtained from TaKaRa biotechnology (Otsu, Japan). 2×GC rich PCR MasterMix was purchased from Tiangen Biotech (Beijing) Co., Ltd (Beijing, China). BCIP/NBT Alkaline Phosphatase Color Development Kit, Alkaline Phosphatase Assay Kit and penicillin-streptomycin were obtained from the Beyotime

Institute of Biotechnology (Shanghai, China). Alizarin Staining kit was supplied by Genmed (Shanghai, China). All primers were synthesized by Shanghai Shenggong Company (Shanghai, China).

2.3. Genomic DNA isolation and genotyping

Genotypes of $LDLR^{-/-}$ mice were confirmed by polymerase chain reaction (PCR) analyses of genomic DNA. Generally, tissue samples were collected and incubated in 50mM NaOH at 95°C for 15 min. Then 1/10 of total volume 1M Tris HCl (PH = 8.0) was added and mixed well. After centrifugation at 12,000g for 15 min at room temperature, the supernatant was used for further PCR analyses with 2×GC rich PCR MasterMix. Touchdown PCR reaction was performed using the following conditions according to the protocol from the Jackson Laboratory website: 94°C for 2 min, followed by 10 cycles of 94°C for 20 sec, annealing temperature for 15 sec decreased 0.5°C every second cycle from 65°C, 68°C for 10 sec, then another 28 cycles of 94°C for 15 sec, 60°C for 15 sec, and 72°C for 10 sec, and finally an additional step of 72°C for 2 min before the end of the program. Primer mixture was made of 3 primers and the sequences are listed in Table 1. PCR product was electrophoresed on 1.5% low melting point agarose gel. The homozygote mutant showed a product of 179bp length with 351 bp for wild-type. The heterozygote mutant showed two separated bands of 179bp and 351bp length (Figure 1).

2.4. Primary osteoblasts isolation

Primary osteoblasts isolated from the calvarium of newborn mice were separated two days before the Osteogenic Induction Media treatment as described previously (41). Briefly, skull bones were extracted and digested in α-MEM medium with 0.1% collagenase and 0.2% dispase for 10 min at 94°C vortexed at 180 rpm, and the supernatant was discarded, then the digestion treatment was repeated 4 more times. Cells from the second to fifth digestion fraction were collected and resuspended in Growth Medium, which were supplemented with 10% serum, 10 units/mL penicillin and 10 μg/mL streptomycin in α-MEM medium without phenol red. 1×10^5 cells were sowed into each well of 6-well cell culture plates and 1×10^4 into 24-well cell culture plates. The isolated primary osteoblasts were cultured in an incubator at 37°C and 5% CO_2 for 2 days until 80% confluence.

2.5. Osteoblastic mineralization culture

Mineralization of osteoblasts is the process during which differentiated osteoblasts are induced to produce extracellular calcium deposits *in vitro*. In the osteoblastic mineralization culture system, primary

Table 1. Summary of oligonucleotide primers for $LDLR^{-/-}$ mice genotyping

Oligonucleotide	Sequence* (5'-3')
Common forward primer	TATGCATCCCCAGTCTTTGG
Wild-type reverse primer	CTACCCAACCAGCCCCTTAC
Mutant reverse primer	ATAGATTCGCCCTTGTGTCC

*The oligonucleotide sequences for genotyping were obtained from the Jackson Laboratory website: *https://www.jax.org/search?q=+002207*
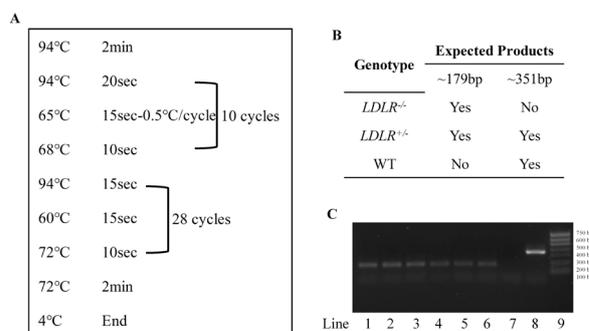
Figure 1. Schematic diagrams for the genotyping of the $LDLR^{-/-}$ mouse strain. Genomic DNA was isolated from the tissue samples and further analyzed by touchdown PCR reaction with primer mixture containing three primers. **(A)** The program cycle for touchdown PCR reaction. **(B)** Expected results for each mouse strain. **(C)** Gel image for the PCR products of $LDLR^{-/-}$ and wild-type (WT) mice, while ddH20 was served as the blank control. Line1-6: $LDLR^{-/-}$ mice with a product of ~179 bp, Line 7: ddH2O, Line 8: WT mice with a product of ~351 bp and Line 9: DNA marker. bp: base pair.

osteoblasts were treated with Osteogenic Induction Media containing 10% serum, 20 mM ascorbic acid, 1M β-glycerophosphate disodium salt hydrate, and 1 mM dexamethasone in phenol red-free α-MEM at 37°C and 5% CO_2, after reaching 80% confluence cultured in Growth Medium (42). Medium was refreshed once every two days. The differentiated osteoblasts were analyzed at specific time points in the following experiments.

2.6. RNA isolation and quantitative real-time PCR

Total RNA was isolated from primary osteoblasts in 6-well cell culture plates using the RNAiso Plus according to the manufacturer's instruction at specific time points after Osteogenic Induction Media treatment. Briefly, media was removed and 1 mL of RNAiso Plus was added into the well to lyse the cells. After homogenization by pipetting up and down, 0.2 mL chloroform per 1mL of RNAiso Plus was added to the mixture and mixed thoroughly. After incubation at room temperature for 15 min, the mixture was centrifuged for 15 min at 12,000 g at 4°C. The upper aqueous phase containing RNA was transferred to a clean tube carefully and precipitated by adding an equal volume 100% isopropanol. The RNA was concentrated by centrifugation at 12,000 g at 4°C for 10 min and washed with 75% ethanol. Then the RNA pellet was air-dried

Table 2. Summary of oligonucleotide primers for cDNA amplification

Oligonucleotide	Sequence (5'-3')
β-actin forward primer	CCTCTATGCCAACACAGT
β-actin reverse primer	AGCCACCAATCCACACAG
Col1a1 forward primer	TGACTGGAAGAGCGGAGAGTA
Col1a1 reverse primer	GACGGCTGAGTAGGGAACAC
OPG forward primer	CCTTGCCCTGACCACTCTTAT
OPG reverse primer	CGCCCTTCCTCACACTCAC
Osx forward primer	GCTCGTAGATTTCTATCCTC
Ostx reverse primer	CTTAGTGACTGCCTAACAGA
RANKL forward primer	CAAGATGGCTTCTATTACCTGT
RANKL reverse primer	TTGATGCTGGTTTTAACGAC
Runx2 forward primer	GACAGTCCCAACTTCCTGTG
Runx2 reverse primer	GCGGAGTAGTTCTCATCATTC

Col1a1: collagen type I alpha 1; OPG: osteoprotegerin; Osx: Osterix; RANKL: receptor activator of nuclear factor-κ B ligand; Runx2: runt-related transcription factor 2

for 5 min at room temperature and dissolved in RNase-free water. The reverse transcription reaction was conducted immediately after RNA isolation in a final volume of 10 μL containing 500 ng RNA sample, and 2 μL 5×PrimeScriptTM RT Master Mix (Perfect Real Time) according to the protocol from the reagent kit. Afterwards, quantitative real-time PCR was performed in a 20 μL mixture of 2 μL reverse transcription product, 10 μL 2×SYBR Premix Ex Taq II (Tli RNaseH Plus), 1.6 μL forward/reverse primer mixture for a final concentration of 0.4 μM and DNase free water up to the final volume. Reactions were performed using the following program: 95°C for 30 sec and cycles of 95°C for 5 sec and 60°C for 30 sec for 40 cycles, followed by a dissociation stage on Appliled BiosystemsInc 7900 HT (Waltham, MA, USA). Primers used are listed in Table 2. Gene expression was normalized to the level of house-keeping gene *β-actin* and analyzed using the standard $2^{-\Delta\Delta CT}$ method. All the experiments were repeated in triplicate.

2.7. *Alizarin Red S staining*

The deposited calcium deposits of differentiated primary osteoblasts were stained using Alizarin Red S according to the manufacturer's instructions as follows. After 7 days of Osteogenic Induction Media treatment in 24-well plates, cells were washed with 500 μL Cleaning Buffer and fixed with Fixation Buffer for 10 min at room temperature, then washed with Cleaning Buffer again. After fixation, 500 μL Alizarin Red S Staining Buffer was added to each well and the plate was incubated in the dark for 10 min at room temperature. The Staining Buffer was removed carefully when mineralized osteoblasts appeared bright orange-red while undifferentiated cells were slightly red or colorless. The plate was air-dried, and results were viewed by a HP scanner and recorded.

2.8. *ALP staining and activity analyses*

The ALP activity was greatly enhanced during osteoblastic differentiation *in vitro*. BCIP/NBT is the preferred staining substrate for ALP detection. After 7 days of Osteogenic Induction Media treatment in 24-well plates, cells were washed with 500 μL PBS and fixed with 4% paraformaldehyde for 20 min at room temperature, then washed with 500 μL PBS three times. The fixed cells were incubated in BCIP/NBT buffer mixed according to the protocol from the kit: 3 mL ALP Staining Buffer, 10 μL 300×BCIP Buffer and 20 μL 150×NBT Buffer for more than 30 min at room temperature avoiding light until the ALP positive differentiated osteoblasts appeared blue-violet. The reaction was stopped by adding excess deionized water. The results were visualized by a HP scanner and recorded. ALP activity in cell lysate was quantitated by using an Alkaline Phosphatase Assay kit according to the manufacturer's protocol. Absorbance was measured at 405 nm.

2.9. *Statistical analyses*

All values were presented as the mean ± SEM. Data differences were assessed by student's *t*-test with the aid of IBM SPSS software. A *p* value less than 0.05 was accepted as statistically significant. All experiments were repeated more than three times.

3. Results

3.1. *The LDLR deficiency inhibited the ALP activity in differentiated primary osteoblasts*

Data from our previous study showed that the expression of LDLR decreased during osteoblastic differentiation (*41*). To gain an insight into the role of LDLR in osteoblastic differentiation, we first examined the effect of LDLR deficiency on ALP activity of differentiated primary osteoblasts 7 days after Osteogenic Induction Media treatment. ALP staining showed that the ALP activity in *LDLR*$^{-/-}$ osteoblasts obviously decreased compared to osteoblasts from wild-type newborn mice (Figure 2A). The results demonstrated by ALP activity analyses showed that the ALP activity dramatically decreased in the *LDLR*$^{-/-}$ osteoblast cell lysate compared to wild-type controls (Figure 2B, *p* < 0.001), suggesting that LDLR might play a critical role in osteoblastic differentiation.

3.2. *The LDLR deficiency inhibited mineralization of differentiated primary osteoblasts*

To further test the effect of LDLR deficiency on mineralized matrix formation in osteoblasts, Alizarin Red S (ARS) staining was performed 7 days after Osteogenic Induction Media treatment. As shown in Figure 3A, calcium deposit formation labeled by ARS staining was impaired by LDLR deficiency. A marked difference in

A

WT   *LDLR$^{-/-}$*

B
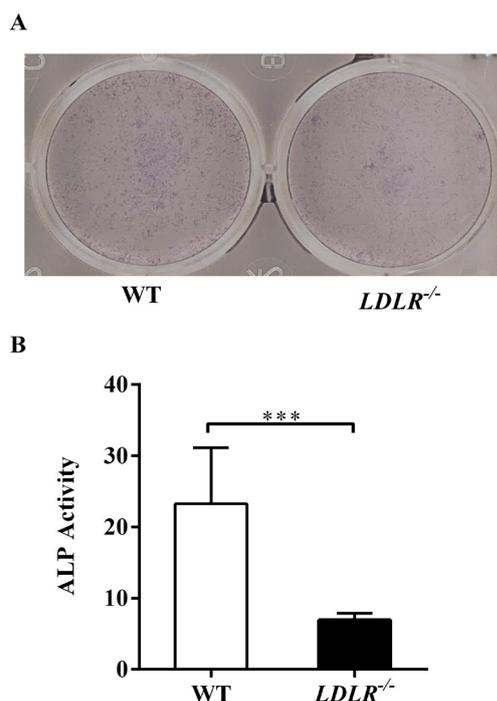
Figure 2. Impaired alkaline phosphatase (ALP) activity in the LDLR deficiency osteoblasts during differentiation *in vitro*. Primary osteoblasts from *LDLR$^{-/-}$* or wild-type (WT) mice were treated with Osteogenic Induction Media for 7 days, respectively. Then the ALP level and activity were examined. **(A)** ALP staining showed reduced osteoblastic differentiation in *LDLR$^{-/-}$* mice compared to WT controls. **(B)** ALP activity in the cell lysate significantly decreased in *LDLR$^{-/-}$* osteoblasts compared to WT controls. ***$p < 0.001$.

A

WT   *LDLR$^{-/-}$*

B
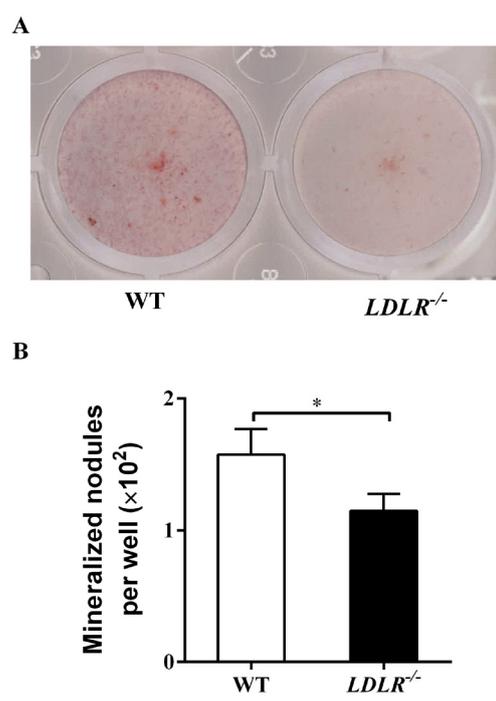
Figure 3. LDLR deficient osteoblasts showed delayed mineralization *in vitro*. After treatment with Osteogenic Induction Media for 7 days, the formation of calcium deposits was labeled using Alizarin Red S (ARS) staining of primary osteoblasts isolated from *LDLR$^{-/-}$* or wild-type (WT) mice, respectively. **(A)** ARS staining showed reduced calcium deposit formation in *LDLR$^{-/-}$* osteoblasts compared to WT controls. **(B)** Numbers of mineralized nodules per well were calculated from *LDLR$^{-/}$* or WT control osteoblasts. *$p < 0.05$.

mineralization level was also observed when comparing the number of mineralized nodules per well between the *LDLR$^{-/-}$* and wild-type groups (Figure 3B, $p < 0.05$), indicating that LDLR might be involved in the regulation of osteoblast mineralization.

3.3. *The LDLR deficiency decreased Runx2 and Osterix expression in differentiated primary osteoblasts*

All the results above showed a potential role of LDLR in regulating osteoblastic differentiation. Runx2 was the master transcription factor and regulated a series of osteoblast-related gene expressions. We therefore inspected the mRNA level of *Runx2*. In the wild-type group, *Runx2* expression was normal at day 3 of Osteogenic Induction Media treatment and dramatically increased at day 7 compared to day 0 (Figure 4A, $p = 0.333$, $p < 0.01$). In *LDLR$^{-/-}$* osteoblasts, *Runx2* expression decreased at day 3 of Osteogenic Induction Media treatment and increased at day 7 compared to day 0 (Figure 4A, $p < 0.05$, $p < 0.001$). When compared to the wild-type group, the *Runx2* mRNA level was slightly reduced in *LDLR$^{-/-}$* osteoblasts at day 0, was significantly impaired at day 3, and slightly reduced again at day 7 (Figure 4A, $p = 0.488$, $p < 0.05$, $p = 0.306$), indicating LDLR might regulate osteoblastic differentiation through the effect on *Runx2* expression in the early stages of differentiation *in vitro*.

Osterix was the second key factor in osteoblastic differentiation regulated down-stream of Runx2. In the wild-type group, *Osterix* expression increased at day 3 of osteoblastic differentiation and decreased at day 7 compared to day 0 (Figure 4B, $p < 0.001$, $p < 0.001$). In *LDLR$^{-/-}$* osteoblasts, the *Osterix* expression also significantly increased at day 3 and decreased at day 7 compared to day 0 of osteoblastic differentiation (Figure 4B, $p < 0.05$, $p < 0.01$). Compared to wild-type controls, *Osterix* expression was normal at day 3 of Osteogenic Induction Media treatment in the *LDLR$^{-/-}$* osteoblasts, but severely decreased at day 7 (Figure 4B, $p = 0.922$, $p < 0.01$), suggesting that the effect of LDLR deficiency on Osterix might be later than Runx2 or LDLR might regulate *Osterix* expression during osteoblastic differentiation through Runx2.

We also analyzed the expression level of functional factor Collagen-1 during osteoblastic differentiation *in vitro*. *Collagen-1* expression significantly increased at day 7 of osteoblastic differentiation compared to day 0 in both *LDLR$^{-/-}$* and wild-type groups (Figure 4C, $p < 0.001$, $p < 0.01$) and there was no significant difference at each time point between the two groups (Figure 4C, $p = 0.305$, $p = 0.243$, $p = 0.074$).
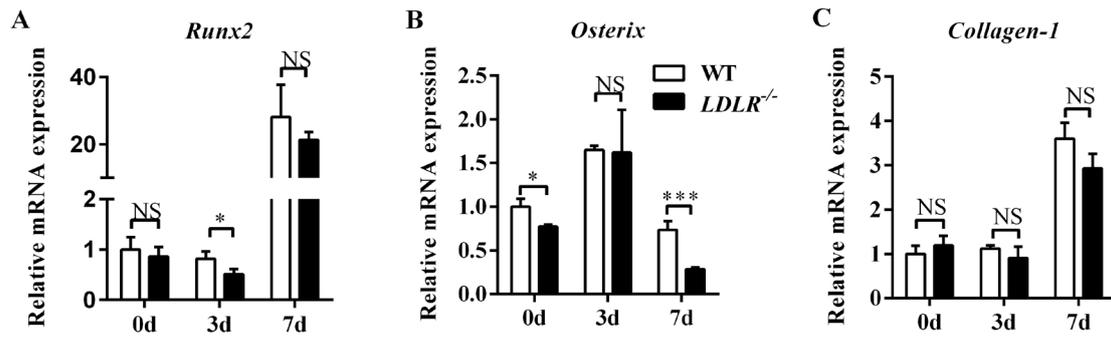
Figure 4. Relative mRNA expression levels of osteoblastic differentiation related factors. Primary osteoblasts from *LDLR*^{-/-} or wild-type (WT) mice were treated with Osteogenic Induction Media for 0 day (0d), 3 days (3d) and 7 days (7d), respectively. **(A)** *Runx2*, **(B)** *Osterix* and **(C)** *Collagen-1* mRNA levels relative to that in the WT osteoblasts at day 0 of differentiation. NS, no significant difference between these groups ($P > 0.05$). *$p < 0.05$, ***$p < 0.001$.
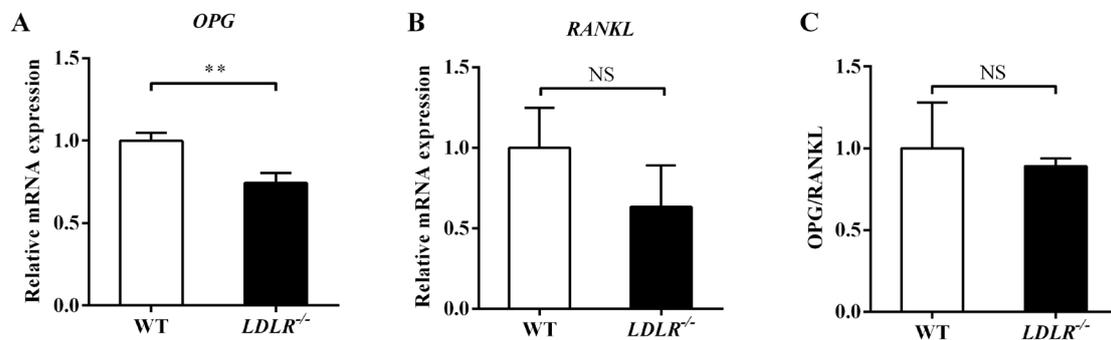
Figure 5. The OPG/RANKL level remained unaffected in LDLR deficient primary osteoblasts. Primary osteoblasts from *LDLR*^{-/-} or wild-type (WT) mice were cultured in the Growth Medium until reaching 80% confluence, respectively. **(A)** *OPG* and **(B)** *RANKL* mRNA levels relative to that in the WT osteoblasts. **(C)** The ratio of *OPG/RANKL* mRNA levels relative to that in the WT osteoblasts. NS, no significant difference between these groups ($P > 0.05$). **$p < 0.01$.

3.4. The OPG/RANKL level in osteoblast was not affected by LDLR deficiency

Besides the bone formation role, osteoblasts could regulate osteoclastogenesis by expressing OPG and RANKL. We isolated primary osteoblasts to examine the effect of LDLR deficiency on this process. Although the expression of OPG significantly decreased in *LDLR*^{-/-} osteoblasts compared to wild-type controls (Figure 5A, $p < 0.01$), the expression of RANKL was similar between the two groups (Figure 5B, $p = 0.149$). Actually, the ratio of OPG/RANKL slightly decreased in *LDLR*^{-/-} osteoblasts compared to wild-type controls with no significance (Figure 5C, $p = 0.636$), suggesting that the deficiency of LDLR might have no influence on the modulation role of osteoblasts to osteoclastogenesis.

4. Discussion

Several members of the LDLR family had been shown to take part in the regulation of osteoblastogenesis. Loss-of-function mutation in LRP5 was associated with decreased bone mass in osteoporosis-pseudoglioma syndrome (OPPG; MIM259770) patients (*30*), while

gain-of-function was associated with increased bone mass in other healthy patients (*43,44*). Moreover, mutation in LRP4 had been identified with high-bone-mass disorders in patients with sclerosteosis or van Buchem diseases (*33,45,46*). Our previous study showed that most of the LDLR family members increased during osteoblastic differentiation *in vitro*, such as LRP4/5/6, but the expression of LDLR decreased 25 days after differentiation *in vitro*, indicating LDLR might function in a unique way during osteoblastogenesis. To explore the effect of LDLR on osteoblastic development and function, we used a LDLR deficient mouse model and isolated pre-osteoblasts from calvarium of newborn mice. Our results showed that ALP activity of differentiated primary osteoblasts dramatically decreased in the *LDLR*^{-/-} group compared to wild-type controls. The mineralization level was also impaired in the *LDLR*^{-/-} group. By analyzing the expression of key transcriptional factors during osteoblastic differentiation, we confirmed that the expression of *Runx2* decreased, followed by impaired expression of *Osterix*, the direct factor regulated downstream of Runx2, in the *LDLR*^{-/-} group compared to wild-type controls. Our current study indicated that

LDLR might affect the differentiation and function of osteoblasts.

Osteoblasts originate from MSCs, which are also progenitors of adipocytes and chondrocytes. The Wnt signaling pathway played an essential role during development of osteoblasts. Activation of the Wnt signaling pathway promoted osteoblastic differentiation and inhibited expression of *peroxisome proliferator-activated receptor*-(*PPAR*-)γ. PPAR-γ was commonly considered as the key regulator of adipogenesis, and absence of PPAR-γ caused adipogenesis depletion. LRP5/LRP6 affected osteoblastogenesis by inducing the Wnt signal as co-receptor in the dual receptor complex with frizzled (FZD) (*32*). LRP4, the third member of the LRP5 and LRP6 subfamily of LDLRs, inhibited the Wnt signaling pathway by facilitating sclerostin action, the antagonist of Wnt signaling pathway (*29,36*). Dimerization of LRP6 through its LDLR domain induced canonical Wnt pathway activation (*47*). LDLR may induce the Wnt signal through the LDLR domain as well. Moreover, LRP6 could regulate LDLR-mediated LDL uptake (*48*). Is it possible that LDLR could affect the LRP6-mediated Wnt signaling pathway activation in turn? More experiments should be conducted to explore the Wnt signaling pathway activity and PPAR-γ level in the LDLR deficient osteoblasts *in vitro* and *in vivo*. The potential that LDLR deficiency might promote development of adipocytes should be further explored.

There had been controversial results in recent studies regarding the role of LDLR in bone metabolism. Okayasu *et al.* cultured bone marrow cells from *LDLR^-/-^* mice and detected reduced osteoclast formation from bone marrow cells *in vitro* with increased bone mass in these mice compared with wild-type controls. These authors attributed the reduction in osteoclast formation to a defect in cell-cell fusion of preosteoclasts. Furthermore, these authors demonstrated that the *LDLR^-/-^* derived preosteoclasts contained less osteoclast fusion regulator molecules such as Atp6v0d2 and DC-STAMP in the plasma membrane than those from wild-type preosteoclasts (*39*). However, Chen and colleagues detected decreased bone mass in the *LDLR^-/-^* mice, which was associated with decreased *Runx2* and *Collangen-1* expression during osteoblastogenesis and increased TRAP levels during osteoclastogenesis from bone marrow cells *in vitro*, implying that the decreased bone mass in *LDLR^-/-^* mice was associated with decreased osteoblastic function and increased osteoclastic function in these mice (*40*). In the present study, we isolated pre-osteoblasts from the calvarium of newborn *LDLR^-/-^* mice and detected ALP activity, calcium deposit formation, and osteoblastogenesis related factor expression 0, 3, and 7 days after differentiation. The activity of ALP decreased in *LDLR^-/-^* osteoblasts 7 days after differentiation compared to wild-type controls, combined with impaired calcium deposit formation that indicated inhibited

mineralization of differentiated osteoblasts. Consistent with impaired osteoblastogenesis, the expression of *Runx2* decreased 3 days after differentiation of *LDLR^-/-^* osteoblasts compared to wild-type controls, followed by decreased *Osterix* expression 7 days after differentiation, implying that LDLR might regulate *Osterix* expression during osteoblastic differentiation through Runx2. However, the modulation role of osteoblasts on osteoclastogenesis was not affected by LDLR deficiency, evidenced by the same level of the OPG/RANKL ratio between *LDLR^-/-^* and wild-type control osteoblasts. The bone mass and bone microarchitecture of *LDLR^-/-^* and wild-type mice *in vivo* should be analyzed in further studies.

The specific function of LDLR was to remove LDL-cholesterol particles from the circulation (*49,50*). Once entering endosomes, the LDL-LDLR complex dissociated due to the local low PH and the receptor was recycled to the plasma membrane for clearance of more cholesterol and cholesterol ester-containing LDL particles from the circulation. Then LDL was transported to lysosomes and degraded (*51*), Moreover, the degradation of LDLR was mediated by binding to proprotein convertase subtilisin/kexin type 9 (PCSK9). Interestingly, 17α-ethinyl estradiol treatment increased the binding of LDL to liver cell membranes *in vitro*. Moreover, the removal rate of rat and human LDL from blood plasma increased in estrogen-treated rats (*52,53*). Additionally, 17α-ethinyl estradiol at a pharmacologic dose increased LDLR number and mRNA level in livers of rabbits (*54*). In pituitary GH3 somatolactotropes, LDLR expression level and LDL uptake were up-regulated by estrogen treatment (*55*). Furthermore, the absence of PCSK9-triggered LDLR degradation led to a sex- and tissue-dependent subcellular distribution of LDLR that depends on estrogens (*56*). All the results indicated that LDLR may contribute to estrogen-mediated bone metabolism. Further studies are required to explore the effect of LDLR deficiency on ovariectomy-induced bone loss and its corresponding bone metabolism changes.

In conclusion, osteoblastic differentiation was disrupted by LDLR deficiency *in vitro*. Alkaline phosphatase activity significantly decreased in *LDLR^-/-^* osteoblasts *in vitro* compared to wild-type controls, combined with calcium deposit formation delay. LDLR deficiency reduced the expression of *Runx2* in early stages and down-regulated *Osterix* in later stages during osteoblastic development *in vitro*, but the OPG/RANKL level remained unaffected in *LDLR^-/-^* osteoblasts compared with wild-type controls *in vitro*.

Acknowledgements

References

1. Banks LM, Lees B, MacSweeney JE, Stevenson JC. Effect of degenerative spinal and aortic calcification on bone density measurements in post-menopausal women: links between osteoporosis and cardiovascular disease? Eur J Clin Invest. 1994; 24:813-817.

2. Li S, Guo H, Liu Y, Wu F, Zhang H, Zhang Z, Xie Z, Sheng Z, Liao E. Relationships of serum lipid profiles and bone mineral density in postmenopausal Chinese women. Clin Endocrinol (Oxf). 2015; 82:53-58.

3. von der Recke P, Hansen MA, Hassager C. The association between low bone mass at the menopause and cardiovascular mortality. Am J Med. 1999; 106:273-278.

4. Bijelic R, Balaban J, Milicevic S. Correlation of the lipid profile, BMI and bone mineral density in postmenopausal women. Mater Sociomed. 2016; 28:412-415.

5. Cui LH, Shin MH, Chung EK, Lee YH, Kweon SS, Park KS, Choi JS. Association between bone mineral densities and serum lipid profiles of pre- and post-menopausal rural women in South Korea. Osteoporos Int. 2005; 16:1975-1981.

6. Figueiredo CP, Rajamannan NM, Lopes JB, Caparbo VF, Takayama L, Kuroishi ME, Oliveira IS, Menezes PR, Scazufca M, Bonfa E, Pereira RM. Serum phosphate and hip bone mineral density as additional factors for high vascular calcification scores in a community-dwelling: the Sao Paulo Ageing & Health Study (SPAH). Bone. 2013; 52:354-359.

7. Hofbauer LC, Brueck CC, Shanahan CM, Schoppet M, Dobnig H. Vascular calcification and osteoporosis--from clinical observation towards molecular understanding. Osteoporos Int. 2007; 18:251-259.

8. Yamauchi M, Yamaguchi T, Nawata K, Tanaka K, Takaoka S, Sugimoto T. Increased low-density lipoprotein cholesterol level is associated with non-vertebral fractures in postmenopausal women. Endocrine. 2015; 48:279-286.

9. Barrett-Connor E, Bush TL. Estrogen and coronary heart disease in women. JAMA. 1991; 265:1861-1867.

10. Stampfer MJ, Colditz GA. Estrogen replacement therapy and coronary heart disease: a quantitative assessment of the epidemiologic evidence. Prev Med. 1991; 20:47-63.

11. Terauchi M, Honjo H, Mizunuma H, Aso T. Effects of oral estradiol and levonorgestrel on cardiovascular risk markers in postmenopausal women. Arch Gynecol Obstet. 2012; 285:1647-1656.

12. Chamberlain G, Fox J, Ashton B, Middleton J. Concise review: mesenchymal stem cells: their phenotype, differentiation capacity, immunological features, and potential for homing. Stem Cells. 2007; 25:2739-2749.

13. Titorencu I, Pruna V, Jinga VV, Simionescu M. Osteoblast ontogeny and implications for bone pathology: an overview. Cell Tissue Res. 2014; 355:23-33.

14. Komori T. Regulation of osteoblast differentiation by transcription factors. J Cell Biochem. 2006; 99:1233-1239.

15. Ducy P, Zhang R, Geoffroy V, Ridall AL, Karsenty G. Osf2/Cbfa1: a transcriptional activator of osteoblast differentiation. Cell. 1997; 89:747-754.

16. Komori T, Yagi H, Nomura S, et al. Targeted disruption of Cbfa1 results in a complete lack of bone formation owing to maturational arrest of osteoblasts. Cell. 1997; 89:755-764.

17. Otto F, Thornell AP, Crompton T, Denzel A, Gilmour KC, Rosewell IR, Stamp GW, Beddington RS, Mundlos S, Olsen BR, Selby PB, Owen MJ. Cbfa1, a candidate gene for cleidocranial dysplasia syndrome, is essential for osteoblast differentiation and bone development. Cell. 1997; 89:765-771.

18. Nakashima K, Zhou X, Kunkel G, Zhang Z, Deng JM, Behringer RR, de Crombrugghe B. The novel zinc finger-containing transcription factor osterix is required for osteoblast differentiation and bone formation. Cell. 2002; 108:17-29.

19. Zhang C. Transcriptional regulation of bone formation by the osteoblast-specific transcription factor Osx. J Orthop Surg Res. 2010; 5:37.

20. Murshed M, Harmey D, Millan JL, McKee MD, Karsenty G. Unique coexpression in osteoblasts of broadly expressed genes accounts for the spatial restriction of ECM mineralization to bone. Genes Dev. 2005; 19:1093-1104.

21. Zhang C, Cho K, Huang Y, Lyons JP, Zhou X, Sinha K, McCrea PD, de Crombrugghe B. Inhibition of Wnt signaling by the osteoblast-specific transcription factor Osterix. Proc Natl Acad Sci U S A. 2008; 105:6936-6941.

22. Boyle WJ, Simonet WS, Lacey DL. Osteoclast differentiation and activation. Nature. 2003; 423:337-342.

23. Diascro DD, Jr., Vogel RL, Johnson TE, Witherup KM, Pitzenberger SM, Rutledge SJ, Prescott DJ, Rodan GA, Schmidt A. High fatty acid content in rabbit serum is responsible for the differentiation of osteoblasts into adipocyte-like cells. J Bone Miner Res. 1998; 13:96-106.

24. Parhami F, Morrow AD, Balucan J, Leitinger N, Watson AD, Tintut Y, Berliner JA, Demer LL. Lipid oxidation products have opposite effects on calcifying vascular cell and bone cell differentiation. A possible explanation for the paradox of arterial calcification in osteoporotic patients. Arterioscler Thromb Vasc Biol. 1997; 17:680-687.

25. Maziere C, Salle V, Gomila C, Maziere JC. Oxidized low density lipoprotein enhanced RANKL expression in human osteoblast-like cells. Involvement of ERK, NFkappaB and NFAT. Biochim Biophys Acta. 2013; 1832:1756-1764.

26. Parhami F, Jackson SM, Tintut Y, Le V, Balucan JP, Territo M, Demer LL. Atherogenic diet and minimally oxidized low density lipoprotein inhibit osteogenic and promote adipogenic differentiation of marrow stromal cells. J Bone Miner Res. 1999; 14:2067-2078.

27. Lagace TA. PCSK9 and LDLR degradation: regulatory mechanisms in circulation and in cells. Curr Opin Lipidol. 2014; 25:387-393.

28. Niemeier A, Kassem M, Toedter K, Wendt D, Ruether W, Beisiegel U, Heeren J. Expression of LRP1 by human osteoblasts: a mechanism for the delivery of lipoproteins and vitamin K1 to bone. J Bone Miner Res. 2005; 20:283-

293.

29. Chang MK, Kramer I, Huber T, Kinzel B, Guth-Gundel S, Leupin O, Kneissel M. Disruption of Lrp4 function by genetic deletion or pharmacological blockade increases bone mass and serum sclerostin levels. Proc Natl Acad Sci U S A. 2014; 111:E5187-5195.

30. Gong Y, Slee RB, Fukai N, et al. LDL receptor-related protein 5 (LRP5) affects bone accrual and eye development. Cell. 2001; 107:513-523.

31. Joiner DM, Less KD, Van Wieren EM, Hess D, Williams BO. Heterozygosity for an inactivating mutation in low-density lipoprotein-related receptor 6 (Lrp6) increases osteoarthritis severity in mice after ligament and meniscus injury. Osteoarthritis Cartilage. 2013; 21:1576-1585.

32. Lara-Castillo N, Johnson ML. LRP receptor family member associated bone disease. Rev Endocr Metab Disord. 2015; 16:141-148.

33. Leupin O, Piters E, Halleux C, et al. Bone overgrowth-associated mutations in the LRP4 gene impair sclerostin facilitator function. J Biol Chem. 2011; 286:19489-19500.

34. Tamai K, Semenov M, Kato Y, Spokony R, Liu C, Katsuyama Y, Hess F, Saint-Jeannet JP, He X. LDL-receptor-related proteins in Wnt signal transduction. Nature. 2000; 407:530-535.

35. Xiong L, Jung JU, Guo HH, Pan JX, Sun XD, Mei L, Xiong WC. Osteoblastic Lrp4 promotes osteoclastogenesis by regulating ATP release and adenosine-A2AR signaling. J Cell Biol. 2017; 216:761-778.

36. Xiong L, Jung JU, Wu H, Xia WF, Pan JX, Shen C, Mei L, Xiong WC. Lrp4 in osteoblasts suppresses bone formation and promotes osteoclastogenesis and bone resorption. Proc Natl Acad Sci U S A. 2015; 112:3487-3492.

37. Awan Z, Alwaili K, Alshahrani A, Langsetmo L, Goltzman D, Genest J. Calcium homeostasis and skeletal integrity in individuals with familial hypercholesterolemia and aortic calcification. Clin Chem. 2010; 56:1599-1607.

38. de Munter W, Blom AB, Helsen MM, Walgreen B, van der Kraan PM, Joosten LA, van den Berg WB, van Lent PL. Cholesterol accumulation caused by low density lipoprotein receptor deficiency or a cholesterol-rich diet results in ectopic bone formation during experimental osteoarthritis. Arthritis Res Ther. 2013; 15:R178.

39. Okayasu M, Nakayachi M, Hayashida C, Ito J, Kaneda T, Masuhara M, Suda N, Sato T, Hakeda Y. Low-density lipoprotein receptor deficiency causes impaired osteoclastogenesis and increased bone mass in mice because of defect in osteoclastic cell-cell fusion. J Biol Chem. 2012; 287:19229-19241.

40. Chen X, Wang C, Zhang K, Xie Y, Ji X, Huang H, Yu X. Reduced femoral bone mass in both diet-induced and genetic hyperlipidemia mice. Bone. 2016; 93:104-112.

41. Gui Y, Duan Z, Qiu X, Tang W, Gober HJ, Li D, Wang L. Multifarious effects of 17-β-estradiol on apolipoprotein E receptors gene expression during osteoblast differentiation *in vitro*. Biosci Trends. 2016; 10:54-66.

42. Qiu X, Jin X, Shao Z, Zhao X. 17β-estradiol induces the proliferation of hematopoietic stem cells by promoting the osteogenic differentiation of mesenchymal stem cells. Tohoku J Exp Med. 2014; 233:141-148.

43. Boyden LM, Mao J, Belsky J, Mitzner L, Farhi A, Mitnick MA, Wu D, Insogna K, Lifton RP. High bone density due to a mutation in LDL-receptor-related protein 5. N Engl J Med. 2002; 346:1513-1521.

44. Little RD, Carulli JP, Del Mastro RG, et al. A mutation in the LDL receptor-related protein 5 gene results in the autosomal dominant high-bone-mass trait. Am J Hum Genet. 2002; 70:11-19.

45. Choi HY, Dieckmann M, Herz J, Niemeier A. Lrp4, a novel receptor for Dickkopf 1 and sclerostin, is expressed by osteoblasts and regulates bone growth and turnover *in vivo*. PLoS One. 2009; 4:e7930.

46. Loots GG, Kneissel M, Keller H, Baptist M, Chang J, Collette NM, Ovcharenko D, Plajzer-Frick I, Rubin EM. Genomic deletion of a long-range bone enhancer misregulates sclerostin in Van Buchem disease. Genome Res. 2005; 15:928-935.

47. Chen J, Yan H, Ren DN, Yin Y, Li Z, He Q, Wo D, Ho MS, Chen Y, Liu Z, Yang J, Liu S, Zhu W. LRP6 dimerization through its LDLR domain is required for robust canonical Wnt pathway activation. Cell Signal. 2014; 26:1068-1074.

48. Ye ZJ, Go GW, Singh R, Liu W, Keramati AR, Mani A. LRP6 protein regulates low density lipoprotein (LDL) receptor-mediated LDL uptake. J Biol Chem. 2012; 287:1335-1344.

49. Brown MS, Goldstein JL. A receptor-mediated pathway for cholesterol homeostasis. Science. 1986; 232:34-47.

50. Herz J. Deconstructing the LDL receptor--a rhapsody in pieces. Nat Struct Biol. 2001; 8:476-478.

51. Rao KN. The significance of the cholesterol biosynthetic pathway in cell growth and carcinogenesis (review). Anticancer Res. 1995; 15:309-314.

52. Chao YS, Windler EE, Chen GC, Havel RJ. Hepatic catabolism of rat and human lipoproteins in rats treated with 17 alpha-ethinyl estradiol. J Biol Chem. 1979; 254:11360-11366.

53. Kovanen PT, Brown MS, Goldstein JL. Increased binding of low density lipoprotein to liver membranes from rats treated with 17 alpha-ethinyl estradiol. J Biol Chem. 1979; 254:11367-11373.

54. Ma PT, Yamamoto T, Goldstein JL, Brown MS. Increased mRNA for low density lipoprotein receptor in livers of rabbits treated with 17 alpha-ethinyl estradiol. Proc Natl Acad Sci U S A. 1986; 83:792-796.

55. Smith PM, Cowan A, White BA. The low-density lipoprotein receptor is regulated by estrogen and forms a functional complex with the estrogen-regulated protein ezrin in pituitary GH3 somatolactotropes. Endocrinology. 2004; 145:3075-3083.

56. Roubtsova A, Chamberland A, Marcinkiewicz J, Essalmani R, Fazel A, Bergeron JJ, Seidah NG, Prat A. PCSK9 deficiency unmasks a sex- and tissue-specific subcellular distribution of the LDL and VLDL receptors in mice. J Lipid Res. 2015; 56:2133-2142.

Original Article

Does pneumoperitoneum affect perfusion index and pleth variability index in patients receiving combined epidural and general anesthesia?

Zen'ichiro Wajima[1,*], Toshiya Shiga[2], Kazuyuki Imanaga[3]

[1] *Department of Anesthesiology, Tokyo Medical University Hachioji Medical Center, Tokyo, Japan;*
[2] *Department of Anesthesiology and Intensive Care Medicine, International University of Health and Welfare, School of Medicine, Chiba, Japan;*
[3] *Department of Anesthesia, Shonan Kamakura General Hospital, Kanagawa, Japan.*

Summary	Plethysmographic variability index (PVI) is a dynamic index used for the purpose of fluid responsiveness in patients, and the effect of pneumoperitoneum on PVI is still unclear. We therefore attempted to determine whether PVI and perfusion index (PI) change before/after pneumoperitoneum in patients receiving combined epidural and general anesthesia, which is a common anesthesia method with intravenous remifentanil. Twenty patients underwent laparoscopic cholecystectomy or colectomy. Immediately before pneumoperitoneum, variables were measured at baseline I and were then measured every min for 5 min after pneumoperitoneum start. Immediately before pneumoperitoneum release, variables were measured at baseline II and were measured every min for 5 min after pneumoperitoneum release. Compared with baseline I values, after pneumoperitoneum start, significant increases occurred in stroke volume variation (SVV) at 1–5 min, and significant decreases occurred in PI at 1–5 min. PVI did not change. Compared with baseline II values, after pneumoperitoneum release, significant increases occurred in PI at 1–5 min, and significant decreases occurred in PVI at 4–5 min and SVV at 1–5 min. In patients receiving combined epidural and general anesthesia, we newly found that PI decreased but PVI remained unchanged with a sufficient dose of remifentanil and epidural anesthesia that can block noxious stimuli and also most sympathetic activity. Furthermore, we reconfirmed that PI increased and PVI decreased upon release of pneumoperitoneum. PI and PVI values must be estimated cautiously during and after pneumoperitoneum.

Keywords: Pneumoperitoneum, perfusion Index, pleth variability index, stroke volume variation, combined epidural and general anesthesia, remifentanil

1. Introduction

Dynamic indices such as stroke volume variation (SVV), pulse pressure variation, and systolic pressure variation have consistently been shown to be more accurate than static indicators such as central venous pressure (CVP) and pulmonary capillary wedge pressure for predicting fluid responsiveness in mechanically ventilated patients under general anesthesia (*1-4*). The accurate assessment of intravascular fluid status and measurement of fluid responsiveness have become increasingly important in peri-operative medicine and critical care (*4*). As a result, these dynamic indices are increasingly used to guide fluid therapy (*5*).

We recently reported that pneumoperitoneum increased SVV, and furthermore, upon release of the pneumoperitoneum, SVV decreased significantly (*6*). We have asserted that SVV values must be estimated cautiously during pneumoperitoneum (*6*). Pleth variability index (PVI) is another dynamic index, and many studies concluded that it is useful for the assessment of fluid responsiveness in patients (*2,7-9*) although one study concluded that PVI seems inaccurate to predict fluid responsiveness after conventional

cardiac surgery with cardiopulmonary bypass (*10*). However, in reference to the studies of Høiseth *et al.* (*11*) and Liu *et al.* (*3*), we believe that the effect of pneumoperitoneum on PVI is still unclear. In our recent study, however, we found that pneumoperitoneum increased SVV (*6*), and this result was very similar to that of several earlier studies (*12-15*). Høiseth *et al.* (*11*) showed that SVV did not change as pneumoperitoneum was established, whereas PVI increased in their study, and furthermore, in a recent study describing the effect of pneumoperitoneum on PVI, the baseline was 5 min after endotracheal intubation (*3*), and we believe that this methodology is questionable for this kind of this study. We therefore attempted to determine whether PVI, which is based on the respiratory variations in the perfusion index (PI) (*16*), and PI change both before and after pneumoperitoneum in patients receiving combined epidural and general anesthesia with intravenous remifentanil.

2. Materials and Methods

2.1. *Subjects*

We conducted this prospective study at International University of Health and Welfare Shioya Hospital, Japan. The study protocol was approved by the ethics committee of the International University of Health and Welfare Hospital (protocol number 13-B-31, 2013-12-25), and we registered this study in the "UMIN Clinical Trial Registry" (ID: UMIN000012863). We obtained written informed consent from each patient. Patients were eligible for inclusion in this study if they were to undergo laparoscopic gastrointestinal surgery (cholecystectomy and colectomy). All patients were classified as ASA physical status 1 and 2, and none had known diabetes mellitus; hypertension; cardiovascular (including non-sinus rhythm and 2° or 3° A-V block), pulmonary, endocrinologic, neurologic, or autonomic diseases; or diseases that affect intravascular fluid volume or balance, such as gastrointestinal obstructive or inflammatory diseases. All patients underwent preoperative fast for at least 8 hours, and no premedication was given to any of the patients.

2.2. *Anesthesia and monitors*

An epidural catheter was placed in one intervertebral space ranging from Th8-9 to Th11-12, at a distance of 4 cm inside the space cephaladly, before induction of general anesthesia. The epidural space was identified by the loss-of-resistance technique using physiological saline (*17,18*). Anesthesia consisted of 1% lidocaine epidural anesthesia, and the analgesia level was determined by a pinprick 15 min after lidocaine administration.

After establishing an analgesic level from T4 to L1, induction of general anesthesia was performed with propofol (initial effect-site concentration = 4 μg/mL) administered by a plasma target-controlled infusion method) and 1 μg/kg remifentanil intravenously (IV) in total, and rocuronium 0.6 mg/kg IV. After induction of anesthesia, a 23-gauge catheter was inserted in the left or right radial artery for direct arterial pressure monitoring, and the patients' lungs were mechanically ventilated by means of a semi-closed circle system at a fresh gas flow of 6 L/min (O_2, 2 L/min and air, 4 L/min). Controlled ventilation was set at 10 breaths/min, with a tidal volume of 8 mL/kg and an inspiratory:expiratory ratio of 1:2. Anesthesia during surgery was maintained with propofol (effect-site concentration ≥ 3 μg/mL), epidural anesthesia with 0.375% ropivacaine, and remifentanil at a rate of 0-0.5 μg/kg/min, and rocuronium. We achieved a target BIS between 40 and 60 and stable circulatory variables during surgery. After surgical skin preparation, the abdomen was insufflated with CO_2 to create and maintain a pneumoperitoneum at 10 mmHg.

Systolic arterial pressure (SAP), diastolic arterial pressure (DAP), heart rate (HR), cardiac output (CO), and SVV, stroke volume index (SVI), systemic vascular resistance (SVR), and pressure of end-tidal CO_2 ($P_{ET}CO_2$) were continuously monitored with a standard monitor (S/5 Anesthesia Monitor, GE Healthcare, Helsinki, Finland) and the FloTrac/Vigileo™ system (software version 03.06) (Edwards Lifesciences, Irvine, CA, USA). PVI and PI were also continuously monitored with Radical 7 (software version 7.9.1.0) (Masimo Corporation, Irvine, CA, USA).

We did not insert a central venous catheter into the patients to directly measure central venous pressure (CVP). Rather, we obtained the data for SVR using a fixed CVP equal to 0 mmHg by inputting the pressure into the FloTrac/Vigileo™ system (*19*).

2.3. *Study design*

Immediately before pneumoperitoneum, baseline registrations of the variables were obtained (baseline I), and these variables were measured every min for 5 min after pneumoperitoneum started. Immediately before pneumoperitoneum was released, registrations of the variables were obtained again (baseline II), and these variables were also obtained every min for 5 min after release of pneumoperitoneum. The position of the patient during measurements was kept horizontal. CO, SVV, SVI, and SVR were recorded 20 sec after SAP, DAP, HR, and $P_{ET}CO_2$ were recorded because the Vigileo™ samples the pressure waveform at 100 Hz over 20 sec to capture 2,000 data points for analysis, and parameter calculations are provided at the end of every 20-sec timeframe (*20,21*).

For laparoscopic cholecystectomy, before general anesthesia/epidural block induction, crystalloid at a volume of at least 10 mL/kg was infused followed by

an additional 10-15 mL/kg during the laparoscopic procedure (*22*). For laparoscopic colectomy, before general anesthesia/epidural block induction, colloid (6% hydroxyethyl starch [HES] 70/0.55/4–Saline HES; Fresenius Kabi Japan, Tokyo, Japan) was infused at 5 mL/kg followed intraoperatively by 3 mL/kg/hour of crystalloid plus 3 mL/kg/hour of colloid (6% HES 70/0.55/4), and measured blood loss was compensated with an equal volume of colloid (6% HES 70/0.55/4) until a predetermined critical hemoglobin level for blood transfusion was reached (*22*). Vasopressors were administered as needed.

We used the almost the same methodology that was used in our previous study (*6*).

2.4. *Statistical analyses*

Sample size was estimated from preliminary data obtained from 8 patients, and an assumption was made that a 3-point change in PVI between the baseline II value and that at 5 min after stopping pneumoperitoneum would be clinically relevant. Power analysis suggested that a minimum of 16 patients would be needed for a $\beta = 0.1$ and $\alpha = 0.05$. To compensate for potential dropouts, we enrolled 20 patients in this study. This analysis was performed using GraphPad StatMate 2.00 (GraphPad Software, Inc., La Jolla, CA, USA).

Values are expressed as means ± standard deviation (SD). Comparisons of SAP, MAP, DAP, HR, SVV, CO, SVI, $P_{ET}CO_2$, SVR, and airway pressure changes were performed with paired Student t-tests with Bonferroni's correction to determine whether there were significant differences between baseline values and the parameter values during pneumoperitoneum or after release of pneumoperitoneum. A *P* value of < 0.05 was required to reject the null hypothesis. All analyses were performed with GraphPad Prism 5.04 (GraphPad Software, Inc.).

3. Results

The 20 patients completing the study had an average (mean ± SD) age of 57 ± 15 years, body weight of 64 ± 18 kg, height of 162 ± 10 cm, and body surface area of 1.67 ± 0.24 m^2. The male:female ratio was 13:7, and the cholecystectomy:colectomy ratio was also 13:7. No patients received blood transfusion during surgery.

After pneumoperitoneum started, there were significant increases in heart rate (HR) at the 3- to 5-min time points (Figure 1), SVV at the 1- to 5-min time points, and SVR at the 2- to 5-min time points compared with baseline I values (Figure 2). There were significant decreases in $P_{ET}CO_2$ at the 1- to 2-min time points (Figure 1), PI at the 1- to 5-min time points, and SVI at the 1- to 3-min time points compared with baseline I values (Figure 2). Other values including PVI were unchanged (Figures 1, 2).

After release of pneumoperitoneum, there were significant increases in $P_{ET}CO_2$ at the 1-min time point (Figure 3), PI at the 1- to 5-min time points, and SVI at the 1-min time points compared with baseline II
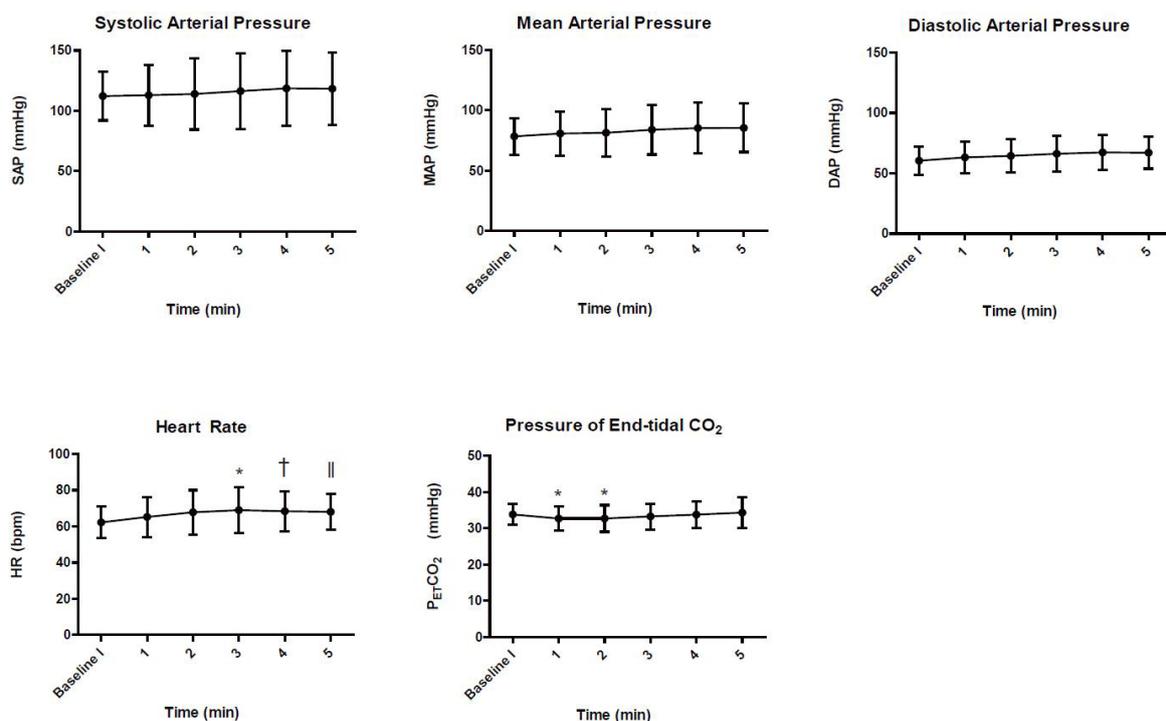
Figure 1. Sequential changes in systolic arterial pressure, mean arterial pressure, diastolic arterial pressure, heart rate, and pressure of end-tidal CO$_2$ at baseline I and after pneumoperitoneum. Data are expressed as mean ± standard deviation. *$P < 0.05$ *vs* baseline I; †$P < 0.01$ *vs* baseline I; ‖$P < 0.0005$ *vs* baseline I.
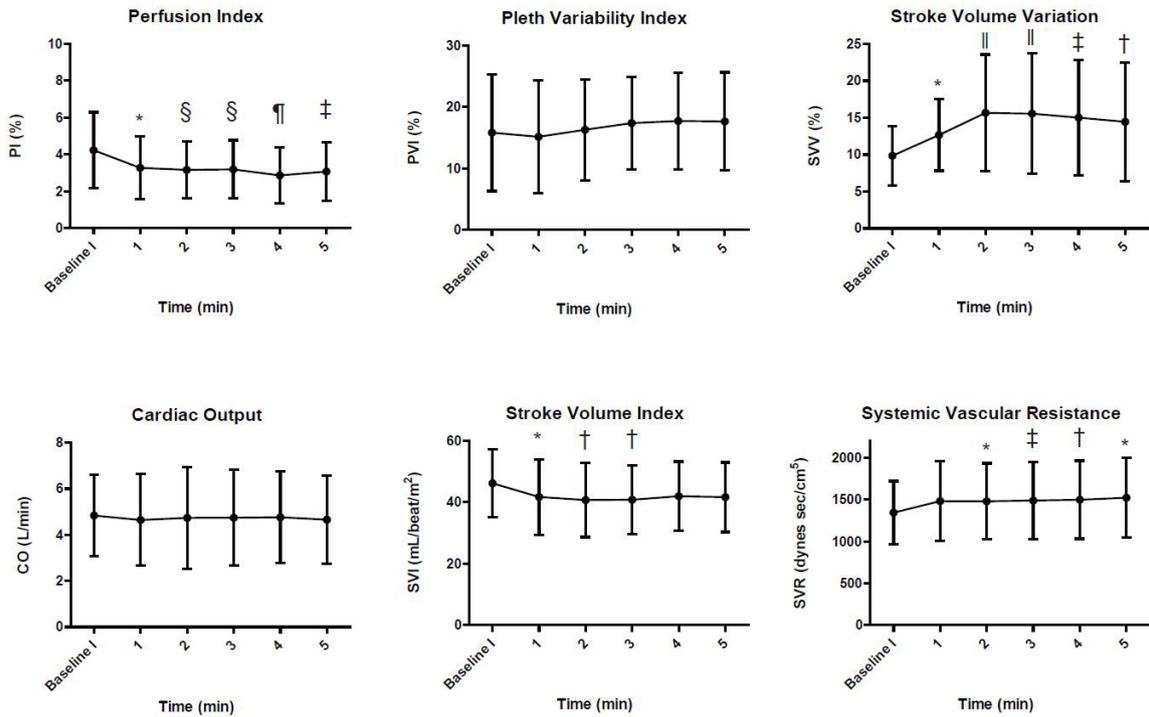
Figure 2. Sequential changes in perfusion index, pleth variability index, stroke volume variation, cardiac output, stroke volume index, and systemic vascular resistance at baseline I and after pneumoperitoneum. Data are expressed as mean ± standard deviation. $^*P < 0.05$ *vs* baseline I; $^†P < 0.01$ *vs* baseline I; $^‡P < 0.005$ *vs* baseline I; $^§P < 0.001$ *vs* baseline I; $^\|P < 0.0005$ *vs* baseline I; $^¶P < 0.0001$ *vs* baseline I.
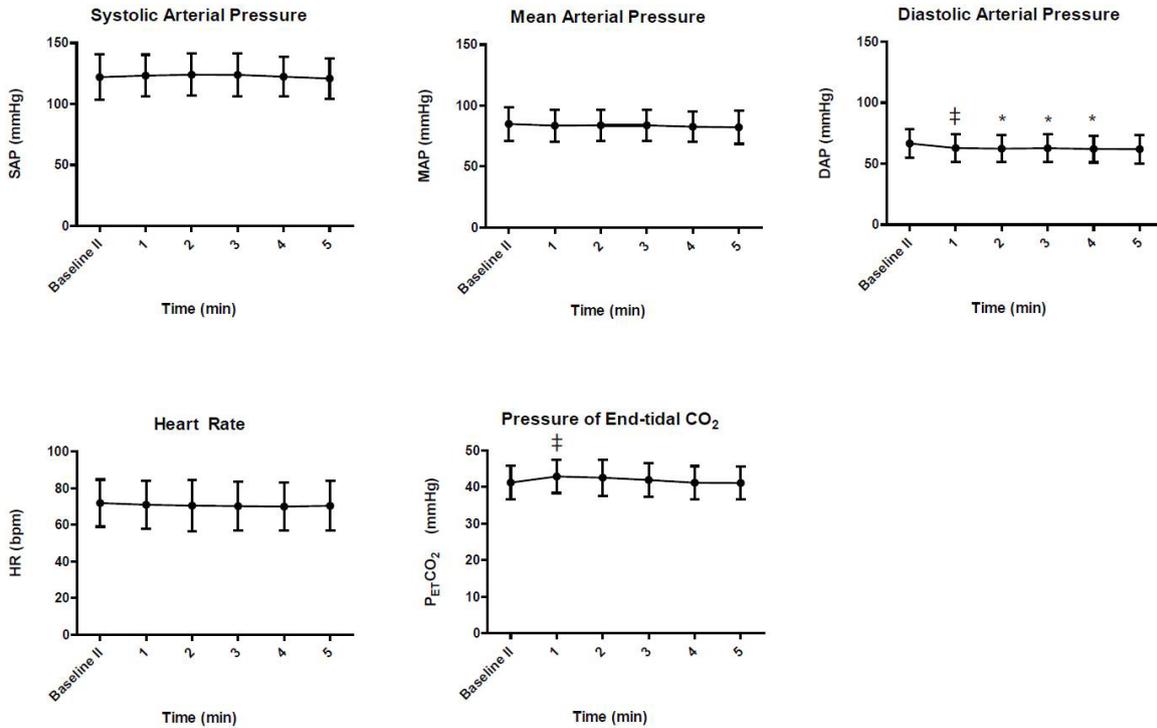
Figure 3. Sequential changes in systolic arterial pressure, mean arterial pressure, diastolic arterial pressure, heart rate, and pressure of end-tidal CO_2 at baseline II and after stopping pneumoperitoneum. Data are expressed as mean ± standard deviation. $^*P < 0.05$ *vs* baseline II; $^‡P < 0.005$ *vs* baseline II.
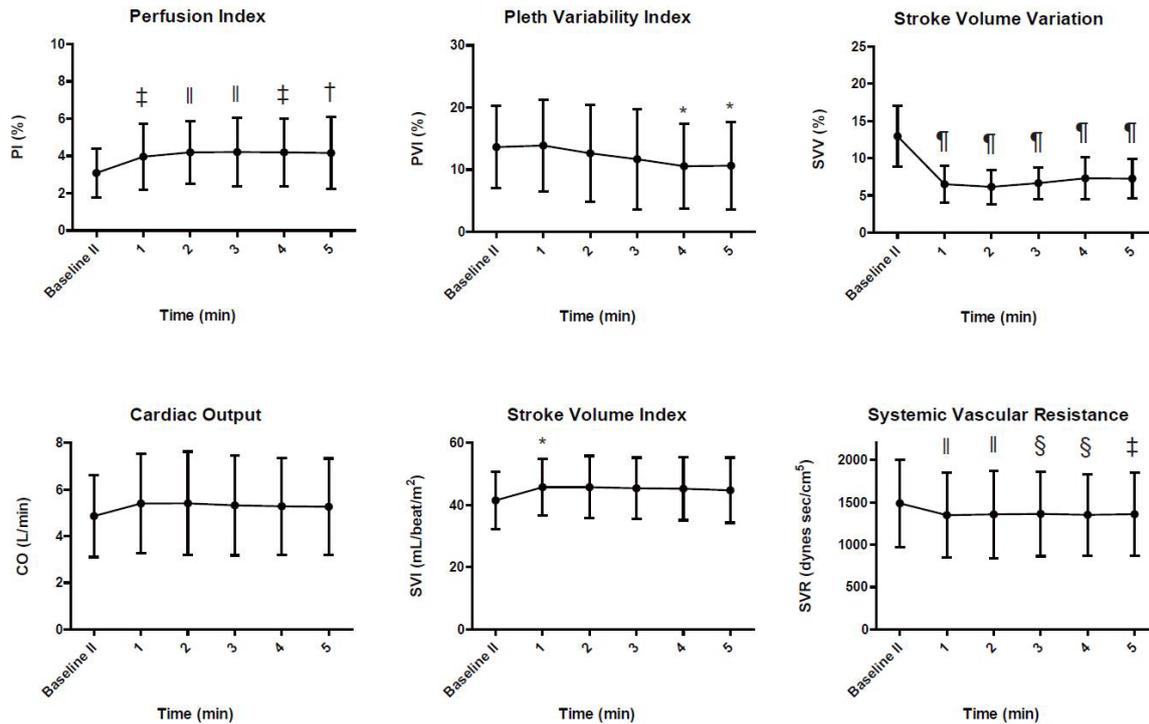
Figure 4. Sequential changes in perfusion index, pleth variability index, stroke volume variation, cardiac output, stroke volume index, and systemic vascular resistance at baseline II and after stopping pneumoperitoneum. Data are expressed as mean ± standard deviation. $^*P < 0.05$ *vs* baseline II; $^{\dagger}P < 0.01$ *vs* baseline II; $^{\ddagger}P < 0.005$ *vs* baseline II; $^{\S}P < 0.001$ *vs* baseline II; $^{\parallel}P < 0.0005$ *vs* baseline II; $^{\P}P < 0.0001$ *vs* baseline II.
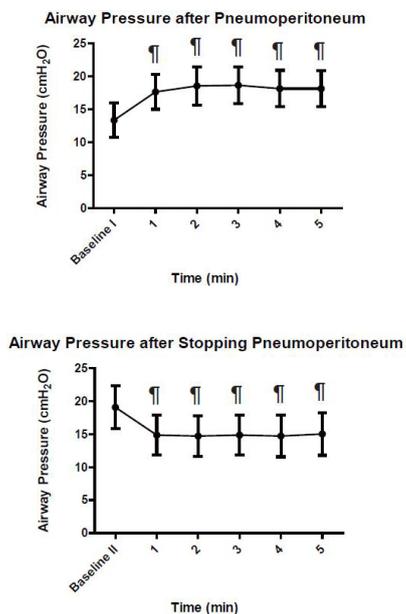
Figure 5. Sequential changes in airway pressure after pneumoperitoneum start and after stopping pneumoperitoneum. Data are expressed as mean ± standard deviation. $^{\P}P < 0.0001$ *vs* baseline I and baseline II.

(Figure 4). There were significant decreases in DAP at the 1- to 4-min time points (Figure 3), PVI at the 4- to 5-min time points, SVV at the 1- to 5-min time points, and SVR at the 1- to 5-min time points compared with baseline II (Figure 4). SAP, MAP, HR, and CO were unchanged (Figures 3, 4). Airway pressures during measurements are shown in Figure 5.

4. Discussion

In this study, pneumoperitoneum decreased PI, did not change PVI, and increased SVV, whereas upon release of pneumoperitoneum, PI increased and both PVI and SVV decreased significantly in patients receiving combined epidural and general anesthesia, which is a common anesthesia method, with intravenous remifentanil, a very potent opioid. Liu *et al.* (*3*) recently showed that both PVI and SVV increased and PI decreased significantly after pneumoperitoneum, and these values returned to the baseline level after release of pneumoperitoneum. However, they defined baseline as the values measured 5 min after endotracheal intubation, and we believe that this methodology is questionable for this kind of study because the values at 5 min after endotracheal intubation are considered to be unstable in terms of hemodynamics. Høiseth *et al.* (*11*) found that as pneumoperitoneum was established, PVI increased, PI decreased significantly, and SVV was unchanged. This reported lack of increase in SVV is questionable because in all reported animal studies (*12-15*), SVV increased after elevation of intra-abdominal pressure and/or pneumoperitoneum. We recently found that pneumoperitoneum increased SVV in humans (*6*), and furthermore, many animal studies showed that other

dynamic indices such as systolic pressure variation and pulse pressure variation (*23,24*) also increased during intra-abdominal hypertension (*12-15,25-27*). Therefore, the results of Liu *et al.* (*3*) and Høiseth *et al.* (*11*) might be questionable, including the change in PVI and PI values.

Our results relating to PVI and SVV after pneumoperitoneum were different than those of Høiseth *et al.* (*11*) and Liu *et al.* (*3*), and the reason for the discrepancy is unclear. However, we suppose this relates to differences in study design. For example, the anesthesia methods were quite different: we gave our patients combined epidural and general anesthesia using propofol, remifentanil, rocuronium, and epidural 0.375% ropivacaine as local anesthetics. In contrast, Høiseth *et al.* (*11*) inserted an epidural catheter in 9 of 20 patients but maintained just general anesthesia using desflurane and fentanyl, and Liu *et al.* (*3*) induced general anesthesia with midazolam, propofol, fentanyl, and rocuronium, and maintained general anesthesia with propofol, cisatracurium and a bolus of fentanyl as supplement. Furthermore, tidal volume, which is one of the deciding factors that can change dynamic indices values (*28-30*), was different with Høiseth *et al.* (*11*) (Liu *et al.* (*3*) never referred to tidal volume), and Høiseth *et al.* (*11*) applied positive end expiratory pressure of 5 cm H_2O, whereas we used zero end expiratory pressure. The patient characteristics were also not similar: the height and weight of the Høiseth *et al.* (*11*) patients were much higher than those of our patients. Moreover, the baseline SVV value in their study was 9%, and it increased non-significantly to 10% during the pneumoperitoneum. We also believe that it is questionable that the SVV value did not increase significantly during pneumoperitoneum because the SV in their study decreased by 20 % during pneumoperitoneum compared to the baseline value; SVV is defined as SVV (%) = $100 \times$ (SVmax – SVmin) / [(SVmax + SVmin) / 2], where SV = stroke volume and maximal and minimal values for SV are determined as SVmax and SVmin, respectively, over a single respiratory cycle of paced breathing (*19,20,31*).

Although the PVI did not change after pneumoperitoneum in our study, Høiseth *et al.* (*11*) found that PVI increased when pneumoperitoneum was established and explained the mechanisms of this result as follows: "This result may be caused by sympathetic activity (*32*) induced by surgery or possibly release of norepinephrine induced by pneumoperitoneum per se (*33*). The finger photoplethysmographic waveform is affected by vasoconstriction induced by cold pressor test, stimulating sympathetic stimulation (*34*). Both inflation of CO_2 and surgical stimulation may contribute to the changes observed in the photoplethysmographic variables. The same mechanisms probably explain the reduction in PI. These findings are supported by a study on PVI and PI during skin incision, in which

PVI increases and PI decreases with incision (*16*)." Høiseth *et al.* (*11*) did not use remifentanil (although we administered it properly and also gave epidural anesthesia, which can block sympathetic activity in fingertip (*35*)), and MAP and cardiac index increased significantly after pneumoperitoneum, whereas in our study, SAP, MAP, DAP, and CO were unchanged probably because we administered remifentanil properly, and epidural anesthesia as a noxious stimuli and also most sympathetic activity was blocked. Therefore, we believe that this is also one of the most probable reasons the PVI did not change significantly after the start of pneumoperitoneum in the present study. Furthermore, the mechanism of PI increase and PVI decrease after release of pneumoperitoneum in the present study owes to the decrease of sympathetic activity induced by the pneumoperitoneum (*11,32-34*).

There are several limitations associated with our study. We measured PI, PVI, and SVV values during the 5-min period immediately after the start and end of pneumoperitoneum, and we did not record these values during the time of pneumoperitoneum. However, we can surmise the values of PI, PVI, and SVV during surgery from the values of baseline II. Although Høiseth *et al.* (*11*) showed that SVV predicted fluid responsiveness relatively poor during ongoing laparoscopic surgery, we believe that reevaluation is needed. Furthermore, we did not insert central venous catheters into the patients to directly measure CVP, but we obtained the data for SVR using a fixed CVP (= 0 mmHg) by inputting the pressure into the FloTrac/Vigileo™ system as described above (*19*). Donati *et al.* (*36*) reported that after induction of pneumoperitoneum (endoabdominal pressure = 11-15 mmHg; patient in head-down position), CVP increased by 3.7 mmHg, and we thought this value would be negligible when the SVR was calculated by the FloTrac/ Vigileo™ system because our endoabdominal pressure was 10 mmHg, and also the position of the patients during measurements was kept horizontal.

In conclusion, although some studies showed that pneumoperitoneum decreases PI and increases PVI under general anesthesia, in this study, in patients receiving combined epidural and general anesthesia, PI decreased but PVI remained unchanged using a sufficient dose of remifentanil and epidural anesthesia that can block noxious stimuli and also most sympathetic activity. This is newly found information. Because we believe that blockade of noxious stimuli can change these values as Takeyama *et al.* (*16*) insisted, further studies are needed, *e.g.*, those in which the dose of remifentanil is changed. Furthermore, we could reconfirm that PI increased and PVI decreased upon release of the pneumoperitoneum. Because PVI based on a plethysmographic waveform can be affected by several factors, PI and PVI may be more fragile than SVV, and therefore, PI and PVI values must be estimated cautiously during and after pneumoperitoneum.

References

1. Michard F. Changes in arterial pressure during mechanical ventilation. Anesthesiology. 2005; 103:419-428.
2. Cannesson M, Desebbe O, Rosamel P, Delannoy B, Robin J, Bastien O, Lehot JJ. Pleth variability index to monitor the respiratory variations in the pulse oximeter plethysmographic waveform amplitude and predict fluid responsiveness in the operating theatre. Br J Anaesth. 2008; 101:200-206.
3. Liu F, Zhu S, Ji Q, Li W, Liu J. The impact of intra-abdominal pressure on the stroke volume variation and plethysmographic variability index in patients undergoing laparoscopic cholecystectomy. Biosci Trends. 2015; 9:129-133.
4. Ansari BM, Zochios V, Falter F, Klein AA. Physiological controversies and methods used to determine fluid responsiveness: A qualitative systematic review. Anaesthesia. 2016; 71:94-105.
5. Benes J, Giglio M, Brienza N, Michard F. The effects of goal-directed fluid therapy based on dynamic parameters on post-surgical outcome: A meta-analysis of randomized controlled trials. Crit Care. 2014; 18:584.
6. Wajima Z, Shiga T, Imanaga K. Pneumoperitoneum affects stroke volume variation in humans. J Anesth. 2015; 29:508-514.
7. Zimmermann M, Feibicke T, Keyl C, Prasser C, Moritz S, Graf BM, Wiesenack C. Accuracy of stroke volume variation compared with pleth variability index to predict fluid responsiveness in mechanically ventilated patients undergoing major surgery. Eur J Anaesthesiol. 2010; 27:555-561.
8. Desgranges FP, Desebbe O, Ghazouani A, Gilbert K, Keller G, Chiari P, Robin J, Bastien O, Lehot JJ, Cannesson M. Influence of the site of measurement on the ability of plethysmographic variability index to predict fluid responsiveness. Br J Anaesth. 2011; 107:329-335.
9. Broch O, Bein B, Gruenewald M, Hocker J, Schottler J, Meybohm P, Steinfath M, Renner J. Accuracy of the pleth variability index to predict fluid responsiveness depends on the perfusion index. Acta Anaesthesiol Scand. 2011; 55:686-693.
10. Fischer MO, Pelissier A, Bohadana D, Gerard JL, Hanouz JL, Fellahi JL. Prediction of responsiveness to an intravenous fluid challenge in patients after cardiac surgery with cardiopulmonary bypass: A comparison between arterial pulse pressure variation and digital plethysmographic variability index. J Cardiothorac Vasc Anesth. 2013; 27:1087-1093.
11. Høiseth LØ, Hoff IE, Myre K, Landsverk SA, Kirkebøen KA. Dynamic variables of fluid responsiveness during pneumoperitoneum and laparoscopic surgery. Acta Anaesthesiol Scand. 2012; 56:777-786.
12. Duperret S, Lhuillier F, Piriou V, Vivier E, Metton O, Branche P, Annat G, Bendjelid K, Viale JP. Increased intra-abdominal pressure affects respiratory variations in arterial pressure in normovolaemic and hypovolaemic mechanically ventilated healthy pigs. Intensive Care Med. 2007; 33:163-171.
13. Valenza F, Chevallard G, Porro GA, Gattinoni L. Static and dynamic components of esophageal and central venous pressure during intra-abdominal hypertension. Crit Care Med. 2007; 35:1575-1581.
14. Renner J, Gruenewald M, Quaden R, Hanss R, Meybohm P, Steinfath M, Scholz J, Bein B. Influence of increased intra-abdominal pressure on fluid responsiveness predicted by pulse pressure variation and stroke volume variation in a porcine model. Crit Care Med. 2009; 37:650-658.
15. Jacques D, Bendjelid K, Duperret S, Colling J, Piriou V, Viale JP. Pulse pressure variation and stroke volume variation during increased intra-abdominal pressure: An experimental study. Crit Care. 2011; 15:R33.
16. Takeyama M, Matsunaga A, Kakihana Y, Masuda M, Kuniyoshi T, Kanmura Y. Impact of skin incision on the pleth variability index. J Clin Monit Comput. 2011; 25:215-221.
17. Wajima Z, Shitara T, Ishikawa G, Kaneko K, Inoue T, Ogawa R. Analgesia after upper abdominal surgery using extradural administration of a fixed dose of buprenorphine in combination with lignocaine given at two infusion rates: A comparative study. Acta Anaesthesiol Scand. 1997; 41:1061-1065.
18. Wajima Z, Shitara T, Ishikawa G, Inoue T, Ogawa R. Analgesia after upper abdominal surgery with extradural buprenorphine with lidocaine. Can J Anaesth. 1998; 45:28-33.
19. Wajima Z, Shiga T, Imanaga K, Inoue T. Does intravenous landiolol, a β_1-adrenergic blocker, affect stroke volume variation? J Anesth. 2013; 27:890-894.
20. Wajima Z, Shiga T, Imanga K, Inoue T. Assessment of the effect of rapid crystalloid infusion on stroke volume variation and pleth variability index after a preoperative fast. J Clin Monit Comput. 2010; 24:385-389.
21. Biais M, Vidil L, Sarrabay P, Cottenceau V, Revel P, Sztark F. Changes in stroke volume induced by passive leg raising in spontaneously breathing patients: Comparison between echocardiography and Vigileo/FloTrac device. Crit Care. 2009; 13:R195.
22. Haljamäe H. Rules of thumb. In: Clinical fluid therapy in the perioperative setting (Hahn RG, ed.) Cambridge University Press, Cambridge, UK, 2011; pp. 18-28.
23. Marik PE, Cavallazzi R, Vasu T, Hirani A. Dynamic changes in arterial waveform derived variables and fluid responsiveness in mechanically ventilated patients: A systematic review of the literature. Crit Care Med. 2009; 37:2642-2647.
24. Zhang Z, Lu B, Sheng X, Jin N. Accuracy of stroke volume variation in predicting fluid responsiveness: A systematic review and meta-analysis. J Anesth. 2011; 25:904-916.
25. Tournadre JP, Allaouchiche B, Cayrel V, Mathon L, Chassard D. Estimation of cardiac preload changes by systolic pressure variation in pigs undergoing pneumoperitoneum. Acta Anaesthesiol Scand. 2000; 44:231-235.
26. Bliacheriene F, Machado SB, Fonseca EB, Otsuke D, Auler JO, Jr., Michard F. Pulse pressure variation as a tool to detect hypovolaemia during pneumoperitoneum. Acta Anaesthesiol Scand. 2007; 51:1268-1272.
27. Malbrain ML, de Laet I. Functional hemodynamics and increased intra-abdominal pressure: Same thresholds for different conditions ...? Crit Care Med. 2009; 37:781-783.
28. Biais M, Nouette-Gaulain K, Cottenceau V, Revel P, Sztark F. Uncalibrated pulse contour-derived stroke volume variation predicts fluid responsiveness in mechanically ventilated patients undergoing liver transplantation. Br J Anaesth. 2008; 101:761-768.
29. De Backer D, Heenen S, Piagnerelli M, Koch M, Vincent J-L. Pulse pressure variations to predict fluid responsiveness: Influence of tidal volume. Intensive Care

Med. 2005; 31:517-523.
30. Reuter DA, Bayerlein J, Goepfert MS, Weis FC, Kilger E, Lamm P, Goetz AE. Influence of tidal volume on left ventricular stroke volume variation measured by pulse contour analysis in mechanically ventilated patients. Intensive Care Med. 2003; 29:476-480.
31. Wajima Z, Shiga T, Imanaga K, Inoue T. Do induced hypertension and hypotension affect stroke volume variation in man? J Clin Anesth. 2012; 24:207-211.
32. Landsverk SA, Høiseth LO, Kvandal P, Hisdal J, Skare O, Kirkeboen KA. Poor agreement between respiratory variations in pulse oximetry photoplethysmographic waveform amplitude and pulse pressure in intensive care unit patients. Anesthesiology. 2008; 109:849-855.
33. Myre K, Rostrup M, Buanes T, Stokland O. Plasma catecholamines and haemodynamic changes during pneumoperitoneum. Acta Anaesthesiol Scand. 1998; 42:343-347.
34. Awad AA, Ghobashy MA, Ouda W, Stout RG, Silverman DG, Shelley KH. Different responses of ear and finger pulse oximeter wave form to cold pressor test. Anesth Analg. 2001; 92:1483-1486.
35. Veering BT, Cousins MJ. Epidural neural blockade. In: Cousins & Bridenbaugh's neural blockade in clinical anesthesia and pain medicine (Cousins MJ, Carr DB, Horlocker TT, Bridenbaugh PO, eds.). Lippincott Williams & Wilkin's, a Wolter Kluwer business, Philadelphia, PA, 2009; pp. 241-295.
36. Donati A, Munch C, Marini B, Orsetti G, Coltrinari R, Pietropaoli P. Transesophageal Doppler ultrasonography evaluation of hemodynamic changes during videolaparoscopic cholecystectomy. Minerva Anestesiol. 2002; 68:549-554.

Evaluation of insulin resistance improvement after laparoscopic sleeve gastrectomy or gastric bypass surgery with HOMA-IR

Yubing Zhu[§], Zhipeng Sun[§], Yanmin Du, Guangzhong Xu, Ke Gong, Bin Zhu, Nengwei Zhang[*]

Diabetes Surgery Centre, General Surgery Department, Peking University Ninth School of Clinical Medicine (Beijing Shijitan Hospital, Capital Medical University), Beijing, China.

Summary   **Our purpose was to explore the remission of insulin resistance after bariatric surgery to discover the mechanism of diabetes remission excluding dietary factors. A retrospective case control study was conducted on patients with type 2 diabetes, who underwent laparoscopic sleeve gastrectomy (LSG) or laparoscopic gastric bypass surgery (LGB) in Beijing Shijitan Hospital from April 1, 2012 to April 1, 2013. The laboratory and anthropometric data was analyzed pre-surgery and during a 2-year follow-up. HOMA-IR was calculated and evaluated. The two surgical procedures were compared. No significant difference in complete remission rate was observed between the two groups (LGB group: 62.1%, LSG group: 60.0%, p = 0.892). HOMA-IR was reduced to a stable level at the 3rd month after surgery. The cut-off value of HOMA-IR was 2.38 (sensitivity: 0.938, specificity: 0.75) and 2.33 (sensitivity: 0.941, specificity: 0.778) respectively for complete remission after LSG or LGB surgery. Insulin resistance was improved while GLP-1 and Ghrelin was changed significantly in patients with type 2 diabetes prior to weight loss either in the LSG or LGB group. HOMA-IR decreased to less than the cut-off value at the 3rd month and was closely related to complete remission. The mechanism of bariatric surgery was not due just to simply dietary factors or body weight loss but also the remission of insulin resistance.**

Keywords: Laparoscopic sleeve gastrectomy (LSG), laparoscopic gastric bypass (LGB), type 2 diabetes, homeostasis model of insulin resistance index (HOMA-IR)

1. Introduction

Currently, the procedures for treatment of diabetic mellitus with bariatric surgery mainly consists of 3 categories: surgeries for intake restriction, surgeries for poor absorption and surgeries with both effects. The intake restriction surgeries mainly include laparoscopic adjustable gastric banding and laparoscopic sleeve gastrectomy (LSG); the surgeries causing poor absorption mainly includes the laparoscopic biliopancreatic diversion; and the third classification have both the restriction and mal-absorption effects, including laparoscopic gastric bypass (LGB) (*1*).

In the general view of most people, the reasons for the therapeutic effects concerning diabetes by the three kinds of surgeries were due to the intake reduction or mal-absorption, not improvement of insulin resistance or islet function (*2*). Although some animal experiments showed that insulin resistance may be relieved after gastrointestinal bypass surgery (*3*). However, there was still no clinical study about evaluation of insulin resistance improvement after bariatric surgery.

In clinical practice, the common homeostasis model of insulin resistance index (HOMA-IR) was used to evaluate insulin resistance and functions of islet β cells. The results are significantly associated with the "gold standard", the glucose clamp results (*4*). The standard of insulin resistance index (HOMA-IR) was different in every race, every country (*5-14*). The cut-off values of HOMA-IR in a specific population should be defined, so that, we could know whether someone's HOMA-IR was normal or not (*7,15*). But, until now there wasn't any definite cut-off value of HOMA-IR for the adult Chinese population (Table 1).

[§]These authors contributed equally to this work.
[*]*Address correspondence to:*
Dr. Nengwei Zhang, Vice president of Chinese Society for Metabolic & Bariatric Surgery (CSMBS). Peking University Ninth School of Clinical Medicine (Beijing Shijitan Hospital, Capital Medical University). Tieyilu 10, Yangfangdian, Haidian District, Beijing 10038, China.
E-mail: zhangnw1@sohu.com

Table 1. Main cut-off values of HOMA-IR in recent literatures

Location and time	Sample size	Population characteristics	Threshold value	Criteria
Sweden, 2000 (*5*)	*n* = 4,816	Health population	2.0	75th percentile
France, 2002 (*6*)	*n* = 1,153	Age: 35 - 64; Health population	3.8	75th percentile
Caucasus, 2006 (*8*)	*n* = 1,156	Rural population; Non-diabetic	2.29	75th percentile
Brazil, 2006 (*7*)	*n* = 1,317	Age: 40 ± 12; BMI: 34 ± 10 kg/m^2	2.77	90th percentile
U.S., 2008 (*9*)	*n* = 2,804	Age ≥ 20; normal BMI and fasting glucose	2.73	66th percentile
Iran, 2010 (*10*)	*n* = 3,071	Adult individuals; age: 25 - 64	3.875	ROC curve
Iran, 2011 (*11*)	*n* = 1,036	Women individuals selected from among reproductive aged	2.63	95th percentile
Japan, 2012 (*12*)	*n* = 6,868	Non-diabetic subjects	1.7	ROC
China, 2013 (*13*)	*n* = 3,203	Age: 6 - 18 (children and teenagers)	3.0	95th percentile
Portugal, 2014 (*14*)	*n* = 1,784	Non-diabetic individuals in a cardiology ward; BMI < 25 Kg/m^2; FPG < 100 mg/dL	2.33	90th percentile

The main purpose of this article was to analyze the remission effect of insulin resistance after LGB or LSG procedures through specific HOMA-IR cut-off values, to illustrate the curative mechanism of bariatric surgery excluding dietary factors.

2. Materials and Methods

The study was performed in accordance with the Declaration of Helsinki of the World Medical Association and was approved by the Beijing Shijitan Hospital, Capital Medical University. All patients signed an informed consent form for this investigation.

2.1. Subjects

The study included 67 patients with type 2 diabetes who underwent bariatric surgery in Diabetes Surgery Centre, Beijing Shijitan Hospital from April 1, 2012 to April 1, 2013. Patients who underwent laparoscopic sleeve gastrectomy were included in the LSG group (*n* = 35), while patients who underwent laparoscopic Roux-en-Y gastric bypass surgery were included in the LGB group (*n* = 32).

The criteria for the diagnosis of type 2 diabetes (T2DM) was in accordance with American Diabetes Association (ADA 2013) criteria (*16*).

2.1.1. Inclusion Criteria

Surgical indications were based on recommended criteria in the 2011 Chinese Expert Consensus on Surgical Treatment of Type 2 diabetes, including: (1) BMI ≥ 28 kg/m^2; (2) The patients aged ≤ 65 years; (3) The duration of diabetes ≤ 15 years; (4) Islet function above half of the normal lower limit.

2.1.2. Exclusion Criteria

(1) Type 1 diabetes disease. (2) Stress-induced hyperglycemia; hyperglycemia caused by liver disease, kidney disease or endocrine diseases; acromegaly; hyperthyroidism; drug-induced hyperglycemia. (3)

Significant organ dysfunctions resulting in disability to tolerate surgery. (4) Islet function below half of the normal lower limit.

2.2. Methods

All patients were followed up for two years. Laboratory tests and anthropometric indexes were followed up and retrospective comparisons were taken.

2.2.1. Anthropometric indexes and laboratory indexes

Body mass index (BMI) = weight/height squared (kg/m^2). Percentage of excess weight loss (EWL %) = (preoperative weight - postoperative weight)/ (preoperative weight - ideal body weight) * 100% (ideal BMI = 25 kg/m^2 for Chinese population).

Insulin was measured with radio-immuno-assay (RIA) method, HbA1c measured with chromatography, and plasma glucose level measured with hexokinase enzymatic reference method (*17*). The formula of HOMA homeostasis mode: HOMA-IR = fasting insulin (mU/mL) * fasting glucose (mmol/L) / 22.5, HOMA-β = 20 * fasting insulin (mU/mL) / (fasting plasma glucose (mmol/L) - 3.5).

The cut-off value of HOMA-IR was 1.55 for men or 2.22 for women (*18*) which means patients with HOMA-IR ≥ 1.55 for men or HOMA-IR ≥ 2.22 for women were identified as insulin resistant, with HOMA-IR < 1.55 for men or HOMA-IR < 2.22 for women as within normal limit. In regard to definitions of "complete response" and "partial response", we used the experts consensus of the American Diabetes Association (ADA) in 2013 (*16*): the partial response was defined as HbA1c < 6.5%, and fasting plasma glucose: 5.6-6.9 mmol/L for at least 1 year, under conditions of not receiving any medical and surgical treatment. The complete response was defined as HbA1c < 6.0%, and fasting plasma glucose < 5.6 mg/dL for at least 1 year, under conditions of not receiving any medical and surgical treatment. Complete response for over 5 years was defined as consistent response (*19*).

2.2.2. *Pre-surgery and follow-up examinations*

Medical history collection, physical examinations, routine laboratory tests (blood cell analysis, liver function, kidney function, blood lipids, blood glucose, blood clotting, stool, urine), endocrine assessment (thyroid function, catecholamine, growth hormone, cortisol), diabetes-related tests (hemoglobin A1c (HbA1C), oral glucose tolerance test (OGTT), insulin stimulation test, C peptide stimulation test), nutritional assessment (vitamin B_{12}, folic acid, vitamin D, serum iron), glucagon-like peptide-1 (GLP-1), Ghrelin, abdomen CT, gastrointestinal imaging, gastroscope, helicobacter pylori tests (in case of any abnormal conditions, providing treatment until normal), electrocardiogram (ECG), respiration monitoring during sleep, consultation from the related department in case of any comorbidities, and surgical risk assessment were taken before surgery.

2.2.3. *Operative procedure*

One bariatric surgeon (Nengwei Zhang) performed all the bariatric procedures at Beijing Shijitan Hospital, and their patients comprised the cohort included in this study.

For LGB surgery, all jejuno-jejunostomy anastomoses were created using a stapled technique with a 60-mm cartridge. Gastrojejunostomy was in a side-to-side anastomosis using a linear stapler and a double layer running closure with a 3-0 VICRYL suture under the ante-colic approach with closure of the mesenteric defect.

LSG surgery was performed using a Gastroscope (12.5 mm diameter) as a stent. The staple line was created using a stapled technique with a 60-mm cartridge.

2.3. *Statistical analysis*

SPSS19.0 software was used for statistical analysis of the experimental data. Normal distribution continuous variables were presented as the mean ± standard deviation; non-normal distributed variables were presented as median (range), and the categorical variables were presented as percentages. The *t* test was used for comparison of means between groups; χ^2 test or Fisher's exact test was used for comparison of categorical data between groups; $P < 0.05$ was considered statistically significant for all tests.

3. Results

67 patients completed the 2-year follow-up among the 82 patients. 15 patients were lost to follow-up (18.2%). Among them, 10 patients (66.7%) were contacted by telephone. The major reason of loss to follow-up was busy work schedule (30%), family issues (20%), and moving to other city or country (20%). The mean age of the 67 patients that finished the follow-up was 43.5 ± 7.6 years old, and the BMI pre-surgery was 36.5 ± 6.8 kg/m^2 on average. The baseline values of the patients between the two groups did not show any significant difference (Table 2).

Two years after the operation, the patients in both groups showed a successful effect of weight-loss. EWL% increased from the 1st month after surgery to the 12th month, then it reached a platform stage. EWL% was 77.8% in the LSG group, and 76.2% in the LGB group at the 2nd year after surgery. The LSG group showed a more significant effect of weight loss at the 3rd, 6th, and 9th month after surgery ($P = 0.026$, 0.039, 0.046). In the subsequent follow-up, the patients in both groups showed stable effects of weight loss, without a significant difference in EWL% (Figure1).

During the 2 years follow-up after the operation, the partial curative rate was 72.9% in the LGB group and 67.5% in the LSG group, $p = 0.355$. The complete response rates of diabetic mellitus were 62.1% in the LGB group and 60% in the LSG group, and no significant difference was found between the two groups ($p = 0.892$) (Table 3). According to the cut-off values of insulin resistance reported (*18*), all the patients had various extents of insulin resistance pre-surgery, the mean value of HOMA-IR was 4.8 (3.8-7.6). It declined from the 1st month follow-up after surgery. At the 3rd month after surgery, the insulin resistance

Table 2. The baseline values * of the patients between the LGB and LSG group

Items	LGB (*n* = 35)	LSG (*n* = 32)	*P* value
Age (Year)	39.5 ± 11.8	42.3 ± 12.8	0.453
Gender (Male, %)	47.1	41.4	0.947
Weight (Kg)	86.2 ± 13.3	89 ± 23	0.644
BMI (Kg/m²)	36.7 ± 4.6	36.5 ± 6.3	0.927
Fasting plasma glucose (mg/dL)	8.1 (6.5, 10.5)	9.8 (7.1, 11.7)	0.228
Fasting insulin (mU/mL)	11.5 (8.5, 15)	13 (9.7, 21.6)	0.311
HOMA-IR	4.3 (3.2, 5.8)	5.7 (4.5, 8.2)	0.064
HOMA-β	53.3 (28.8, 91.2)	45.6 (25.1, 81.1)	0.733
HbA1c (%)	6.9 (6.2, 7.9)	7.9 (6.9, 8.7)	0.176

*Normal distribution continuous variables were presented as the mean ± standard deviation; non-normal distributed variables were presented as median (range), and the categorical variables were presented as percentages.
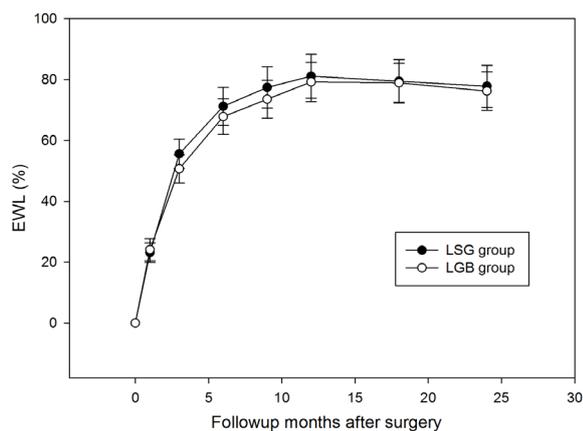
Figure 1. Decrease of EWL% after operation (results represented as mean; Student *t*-test, *p* < 0.05 for significant difference). Two years after the operation, the patients in both groups showed a successful effect of weight-loss. The LSG group showed a more significant effect of weight loss within 6 months after the operation. In the subsequent follow-up, the patients in both groups showed stable effects of weight loss, without significant differences in EWL%. In LSG group, the EWL% reduction was 55.4%, 70.3%, 80.1%, 77.4% at the 3rd, 6th, 12th, and 24th month respectively. In the LGB group, the EWL% reduction was 50.6%, 68.8%, 79.3%, 76.4% at the 3rd, 6th, 12th, and 24th month respectively. *P* values for comparison of LSG and LGB were 0.026, 0.039, 0.782, 0.798 at the 3rd month, 6th month, 12th month, and 24th month respectively.
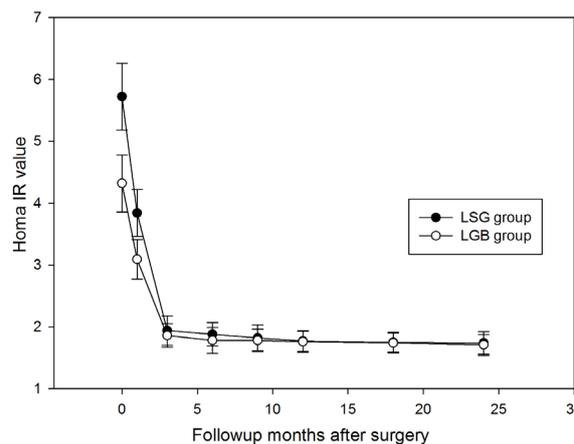
Figure 2. Change of HOMA-IR after operation (results represented as mean; Student *t*-test, *p* < 0.05 for significant difference). The HOMA-IR values of patients in both groups decreased to normal limits at the 3rd month after surgery. In the subsequent follow-up, the patients in both groups showed stable normal HOMA-IR values without significant differences. In the LSG group, the HOMA-IR value was 5.72, 1.94, 1.88, 1.51, 1.74 pre-surgery time, at the 3rd, 6th, 12th, and 24th month post-surgery respectively. In the LGB group, the HOMA-IR value was 4.32, 1.86, 1.78, 1.76, 1.71 pre-surgery, at the 3rd, 6th, 12th, and 24th month post-surgery respectively. P values for comparison of LSG and LGB were 0.064, 0.652, 0.582, 0.398, 0.638 pre-surgery, at the 3rd, 6th, 12th, and 24th month post-surgery respectively.

Table 3. HOMA-IR at the 3rd month and 2nd year and EWL at the 2nd year had statistical differences compared with the value before surgery

Items	OR	95% Conf. Interval	*P* value
Age	0.87	0.85 - 1.21	0.216
HOMA-IR at 3rd month post-surgery	1.52	1.16 - 1.9	0.039
EWL at 3rd month post-surgery	1.21	0.88 - 1.21	0.600
HOMA-IR at 2nd year post-surgery	1.63	1.35 - 2.16	0.024
EWL at 2nd year post-surgery	1.59	1.25 - 2.08	0.032

index (HOMA-IR) of both groups showed significant reduction and reached a platform stage (Figure 2). The cut-off value of HOMA-IR was 2.38 (sensitivity: 0.938, specificity: 0.75) and 2.33 (sensitivity: 0.941, specificity: 0.778) respectively for complete remission after LSG or LGB surgery. HOMA-IR below the cut-off value at the 3rd month was an important indicator for complete remission (Figure 3).

Multivariate analysis by Logistic regression also showed that the recovery of insulin resistance at the 3rd month after the operation was an independent factor for complete remission of diabetes. At the same time weight loss was not. At the 2nd year after surgery, both HOMA-IR and EWL% were independent factors for cure of diabetes (Table 4).

In the meantime we also examined GLP-1 and Ghrelin in both LGB and LSG groups (Table 5). The results showed that in the LGB group, the level of GLP-1 at the 1st month post-surgery raised significantly compared with pre-surgery (F = 18.79, *P* < 0.05), and

then, kept stable at the 3rd month and 6th month post-surgery. Ghrelin in the LGB group post-surgery was a little higher than that pre-surgery, but it didn't show any statistical significance.

In the LSG group, the level of GLP-1 didn't show any change before or after surgery. But the level of Ghrelin at the 1st month post-surgery was obviously lower than that pre-surgery, it showed statistical significance (F = 23.89, *P* < 0.05). And kept stable at the 3rd month and 6th month post-surgery.

4. Discussion

The current results of this study showed that the two bariatric surgery procedures, LGB and LSG, had similar efficacy as treatments for insulin resistance. The complete remission rates of the two types of bariatric surgeries were similar as well.

Insulin resistance was significantly relieved prior to a significant change of their body weights, at the 3rd month
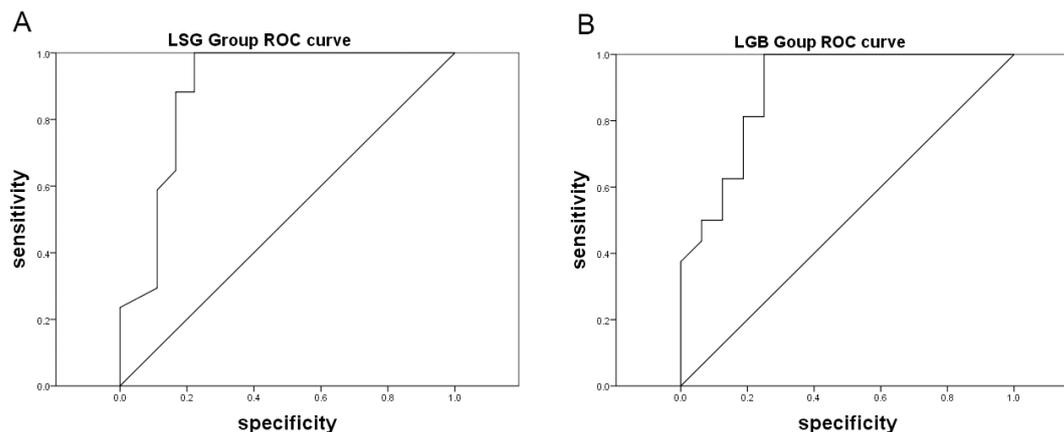
**Figure 3. ROC curves for HOMA IR to predict the curable prognosis after LSG and LGB surgery respectively. A.** The area under the ROC curve of HOMA-IR values in the LSG group was 0.891 (95% CI: 0.773 to 1.000, $P = 0.001$); the optimal cut-off value, which simultaneously maximized both the sensitivity (94.1%) and specificity (77.8%) of the HOMA-IR value smaller than 2.33. **B.** The area under the ROC curve of HOMA-IR values in the LSG group was 0.896 (95% CI: 0.786 to 1.000, $P = 0.001$); the optimal cut-off value, which simultaneously maximized both the sensitivity (93.8%) and specificity (75.0%) of the HOMA-IR value smaller than 2.38.

Table 4 Type 2 diabetes mellitus remission and glycemic control at the 2nd year follow-up after surgery

Outcomes	LSG group, $n = 35$	LGB group, $n = 32$	*P* value
Partial remission*	26 (74.3%)	26 (81.3%)	0.08
Complete remission*	17 (48.6%)	16 (50.0%)	0.19

*Partial remission means FPG ≤ 6.9 mmol/L and HbA1c < 6.5% for at least 1 year without treatment. Complete remission is defined as HbA1c < 6.0%, and fasting plasma glucose < 5.6 mmol/L for at least 1 year without any medical or surgical treatment.

Table 5 The serum hormone level of GLP-1 and Ghrelin before and after surgery (mean ± standard deviation)

Outcomes	Serum hormone	Pre-surgery (ng/L)	1 month post-surgery (ng/L)	3 month post-surgery (ng/L)	6 month post-surgery (ng/L)
LSG group	GLP-1	65 ± 13	67 ± 11	71 ± 15	74 ± 13
$n = 35$	Ghrelin	478 ± 86	285 ± 62	276 ± 56	268 ± 52
LGB group	GLP-1	66 ± 18	119 ± 31	116 ± 28	117 ± 30
$n = 32$	Ghrelin	459 ± 75	467 ± 83	486 ± 95	501 ± 92

after surgery. This suggested that weight loss was not the only cause of diabetes relief. Most of the previous studies found that bariatric surgeries resulted in poor absorption, such as LGB, had greater efficacy in the postoperative reduction of HOMA-IR than the restrictive surgeries, such as vertical gastric banding. This phenomenon can be explained by the mechanism of foregut and hindgut effects. The foregut effect meant avoiding food contact with the proximal jejunum reducing the gastrointestinal secretion of anti-incretin. A hindgut effect meant that the food, which is not completely digested quickly enters the distal intestine, and stimulates the distal intestine to secrete increnin, including glucagon like peptide 1 (GLP-1), gastric inhibitory polypeptide (GIP) and peptide tyrosine-tyrosine (PYY) (*20-22*). This study showed that LSG could also cause a similar postoperative effect for the early response of insulin resistance as that with LGB. The possible reason was that LSG, as a restrictive operation, also removed the gastric fundus, which would reduce the secretion of Ghrelin. Ghrelin secreted

at the gastric fundus promoted appetite and decreased the secretion of insulin and enhanced insulin resistance (*23,24*). Therefore, inhibition of secretion of Ghrelin could also treat the diabetes and obesity (*25*). Meanwhile, the soft and fragment diet after both LSG and LGB had the effects of restricting energy intake and shortening the intestinal transportation time which would promote the secretion of ducdenin (*26,27*).

For patients who had diabetes for a short duration, such as some patients in this study, insulin resistance, instead of dysfunction of beta-cells, was the major reason causing diabetes (*28,29*). GLP-1 and Ghrelin that changed significantly and were maintained at a stable level at the 1st month post-surgery before the change of HOMA-IR and body weight may be the reason for reduction of HOMA-IR. Enhancing insulin sensitivity was an important treatment for diabetes. In this study, the decreased HOMA-IR at the 3rd month post-surgery showed a reduction of insulin resistance, predicating good prognosis. It is consistent with the fact

that the normal value post-surgery of HOMA-IR is an independent predictor affecting the complete response rate after operations.

All patients in this study achieved partial remission, and approximately 60% of the patients achieved a complete response. At present, similar comparison studies between LGB and LSG showed postoperative response rates were above 80% for both procedures (*30,31*). In our study, the relative low remission rate may be a result of the use of the remission criteria of ADA. This remission standard also requests maintaining the indicators for up to one year.

Some studies did not use the standard criteria for diabetes response, and some studies just indicated that withdrawal of drug therapy was remission; and some defined HbA1c < 6.5%, fasting blood glucose levels of < 125 mg/dL without a remission duration requirement as the complete remission standard (*32,33*). Significant errors may occur if a different response standard had been used in the comparison of the efficacy of LGB and LSG.

The limitations of the study were that it was a non-randomized, retrospective study, in which the baseline parameters were not exactly matched between the two groups. Second, the sample size was not large which might increase sampling error. Third, the results were evaluated by HOMA-IR instead of the glucose clamp test, which was more accurate than HOMA-IR.

In summary, there were no statistical differences observed in the complete or partial remission rate of type 2 diabetes between the LSG and LGB group. In clinical practice, there was still lack of a definite and comprehensive standard for the selection of surgical styles for patients with diabetes mellitus. The metabolic surgeons chose a surgical plan according to the patient's will and interdisciplinary expertise. It is imperative to standardize the indications for surgical treatment of diabetes.

Acknowledgements

References

1. Inge TH, Courcoulas AP, Jenkins TM, Michalsky MP, Helmrath MA, Brandt ML, Harmon CM, Zeller MH, Chen MK, Xanthakos SA, Horlick M, Buncher CR, Teen LC. Weight loss and health status 3 years after bariatric surgery in adolescents. N Engl J Med. 2016; 374:113-123.
2. Behary P, Miras AD. Food preferences and underlying mechanisms after bariatric surgery. Proc Nutr Soc. 2015; 74:419-425.
3. Torres A, Rubio MA, Ramos-Levi AM, Sanchez-Pernaute A. Cardiovascular risk factors after single anastomosis duodeno-ileal bypass with sleeve gastrectomy (SADI-S): A new effective therapeutic approach? Curr Atheroscler Rep. 2017; 19:58.
4. Zhang K, Chen Y, Liu L, Lu M, Cheng J, Gao F, Wang N, Shen Z, Lu Y. The triglycerides and glucose index rather than HOMA-IR is more associated with hypogonadism in Chinese men. Sci Rep. 2017; 7:15874.
5. Hedblad B, Nilsson P, Janzon L, Berglund G. Relation between insulin resistance and carotid intima-media thickness and stenosis in non-diabetic subjects. Results from a cross-sectional study in Malmo, Sweden. Diabet Med. 2000; 17:299-307.
6. Marques-Vidal P, Mazoyer E, Bongard V, Gourdy P, Ruidavets JB, Drouet L, Ferrieres J. Prevalence of insulin resistance syndrome in southwestern France and its relationship with inflammatory and hemostatic markers. Diabetes Care. 2002; 25:1371-1377.
7. Geloneze B, Repetto EM, Geloneze SR, Tambascia MA, Ermetice MN. The threshold value for insulin resistance (HOMA-IR) in an admixtured population IR in the Brazilian metabolic syndrome study. Diabetes Res Clin Pract. 2006; 72:219-220.
8. Radikova Z, Koska J, Huckova M, Ksinantova L, Imrich R, Vigas M, Trnovec T, Langer P, Sebokova E, Klimes I. Insulin sensitivity indices: A proposal of cut-off points for simple identification of insulin-resistant subjects. Exp Clin Endocrinol Diabetes. 2006; 114:249-256.
9. Sumner AE, Cowie CC. Ethnic differences in the ability of triglyceride levels to identify insulin resistance. Atherosclerosis. 2008; 196:696-703.
10. Esteghamati A, Ashraf H, Khalilzadeh O, Zandieh A, Nakhjavani M, Rashidi A, Haghazali M, Asgari F. Optimal cut-off of homeostasis model assessment of insulin resistance (HOMA-IR) for the diagnosis of metabolic syndrome: Third national surveillance of risk factors of non-communicable diseases in Iran (SuRFNCD-2007). Nutr Metab (Lond). 2010; 7:26.
11. Zadeh-Vakili A, Tehrani FR, Hosseinpanah F. Waist circumference and insulin resistance: A community based cross sectional study on reproductive aged Iranian women. Diabetol Metab Syndr. 2011; 3:18.
12. Yamada C, Moriyama K, Takahashi E. Optimal cut-off point for homeostasis model assessment of insulin resistance to discriminate metabolic syndrome in non-diabetic Japanese subjects. J Diabetes Investig. 2012; 3:384-387.
13. Yin J, Li M, Xu L, Wang Y, Cheng H, Zhao X, Mi J. Insulin resistance determined by Homeostasis Model Assessment (HOMA) and associations with metabolic syndrome among Chinese children and teenagers. Diabetol Metab Syndr. 2013; 5:71.
14. Timoteo AT, Miranda F, Carmo MM, Ferreira RC. Optimal cut-off value for homeostasis model assessment (HOMA) index of insulin-resistance in a population of patients admitted electively in a Portuguese cardiology ward. Acta Med Port. 2014; 27:473-479.
15. Tang Q, Li X, Song P, Xu L. Optimal cut-off values for the homeostasis model assessment of insulin resistance (HOMA-IR) and pre-diabetes screening: Developments in research and prospects for the future. Drug Discov Ther. 2016; 9:380-385.
16. American Diabetes A. Standards of medical care in diabetes – 2013. Diabetes Care. 2013; 36 Suppl 1:S11-66.
17. da Fonseca-Wollheim F, Heinze KG, Liss E. Temperature-

dependent matrix effect in the direct enzymatic measurement of blood glucose.Eur J Clin Chem Clin Biochem. 1992; 30:371-375.

18. Gayoso-Diz P, Otero-Gonzalez A, Rodriguez-Alvarez MX, Gude F, Garcia F, De Francisco A, Quintela AG. Insulin resistance (HOMA-IR) cut-off values and the metabolic syndrome in a general adult population: Effect of gender and age: EPIRCE cross-sectional study. BMC Endocr Disord. 2013; 13:47.

19. Buse JB, Caprio S, Cefalu WT, Ceriello A, Del Prato S, Inzucchi SE, McLaughlin S, Phillips GL, 2nd, Robertson RP, Rubino F, Kahn R, Kirkman MS. How do we define cure of diabetes? Diabetes Care. 2009; 32:2133-2135.

20. Pendharkar SA, Drury M, Walia M, Korc M, Petrov MS. Gastrin-releasing peptide and glucose metabolism following pancreatitis. Gastroenterology Res. 2017; 10:224-234.

21. McMillan CJ, Zapata RC, Chelikani PK, Snead EC, Cosford K. Circulating concentrations of glucagon-like peptide 1, glucose-dependent insulinotropic peptide, peptide YY, and insulin in client-owned lean, overweight, and diabetic cats. Domest Anim Endocrinol. 2016; 54:85-94.

22. Belinova L, Kahleova H, Malinska H, Topolcan O, Windrichova J, Oliyarnyk O, Kazdova L, Hill M, Pelikanova T. The effect of meal frequency in a reduced-energy regimen on the gastrointestinal and appetite hormones in patients with type 2 diabetes: A randomised crossover study. PLoS One. 2017; 12:e0174820.

23. Santiago-Fernandez C, Garcia-Serrano S, Tome M, Valdes S, Ocana-Wilhelmi L, Rodriguez-Canete A, Tinahones FJ, Garcia-Fuentes E, Garrido-Sanchez L. Ghrelin levels could be involved in the improvement of insulin resistance after bariatric surgery. Endocrinol Diabetes Nutr. 2017; 64:355-362.

24. Yardimci E, Bozkurt S, Cengiz MB, Malya FU. Comparison of weight loss, ghrelin, and leptin hormones after ligation of left gastric artery and sleeve gastrectomy in a rat model. Med Sci Monit. 2017; 23:1442-1447.

25. Okumura A, Unoki-Kubota H, Matsushita Y, Shiga T, Moriyoshi Y, Yamagoe S, Kaburagi Y. Increased serum leukocyte cell-derived chemotaxin 2 (LECT2) levels in obesity and fatty liver. Biosci Trends. 2013; 7:276-283.

26. Wang L, Hu X, Bi S, Tu W, Jing Y, Song L, Lv W, Yu R. A novel polysaccharide isolated from Litchi chinensis by using a simulated gastric medium and its immunomodulatory activity. Drug Discov Ther. 2015; 9:107-115.

27. Zhu X, Lin J, Song Y, Liu H, Zhang R, Fan M, Li Y, Tian R, Fang D. A high-carbohydrate diet lowered blood pressure in healthy Chinese male adolescents. Biosci Trends. 2014; 8:132-137.

28. McEvoy CT, Cardwell CR, Woodside JV, Young IS, Hunter SJ, McKinley MC. A posteriori dietary patterns are related to risk of type 2 diabetes: Findings from a systematic review and meta-analysis. J Acad Nutr Diet. 2014; 114:1759-1775 e1754.

29. Kotani K, Imazato T, Anzai K, Kyushu Diabetes Testing Study G. Expected role of medical technologists in diabetes mellitus education teams. Biosci Trends. 2015; 9:205-206.

30. Praveen Raj P, Bhattacharya S, Saravana Kumar S, Sabnis SC, Parthasarathi R, Swamy PDK, Palanivelu C. Comparison of effects of sleeve gastrectomy and gastric bypass on lipid profile parameters in Indian obese: A case matched analysis. Obes Surg. 2017; 27:2606-2612.

31. Shea B, Boyan W, Jr., Botta J, Ali S, Fenig Y, Paulin E, Binenbaum S, Borao F. Five years, two surgeons, and over 500 bariatric procedures: What have we learned? Obes Surg. 2017; 27:2742-2749.

32. Abusnana S, Abdi S, Tagure B, Elbagir M, Maleckas A. Bariatric surgery outcomes: A single-center study in the United Arab Emirates. Diabetes Metab Syndr Obes. 2015; 8:461-471.

33. Lakdawala MA, Bhasker A, Mulchandani D, Goel S, Jain S. Comparison between the results of laparoscopic sleeve gastrectomy and laparoscopic Roux-en-Y gastric bypass in the Indian population: A retrospective 1 year study. Obes Surg. 2010; 20:1-6.

A comparative study of the blend sign and the black hole sign on CT as a predictor of hematoma expansion in spontaneous intracerebral hemorrhage

Ruili Li[1], Mingfei Yang[2],*

[1] *Graduate School, Qinghai University, Xining, Qinghai, China;*
[2] *Department of Neurosurgery, Qinghai Provincial People's Hospital, Xining, Qinghai, China.*

Summary	Hematoma expansion (HE) is a major determinant of a poor outcome in patients with a spontaneous intracerebral hemorrhage (sICH). The blend sign and the black hole sign are distinguished from non-contrast CT (NCCT) in patients with sICH, and both are independent neuroimaging predictors of HE. The purpose of the current study was to compare the value of the two signs in the prediction of HE. We retrospectively analyzed clinical and neuroimaging data from 228 patients with sICH who were treated at our hospital between August 2015 and September 2017. NCCT of the brain was performed upon admission (within 6 h of the onset of symptoms) to identify the blend sign and the black hole sign. HE was determined based on CT during a follow-up 24 h later. The sensitivity, specificity, positive predictive value (PPV), and negative predictive value (NPV) with which the blend sign and the black hole sign predicted HE were calculated. Receiver operating characteristic (ROC) curve analysis was performed in order to compare the accuracy of the two signs in predicting HE. The blend sign was identified in 46 patients (20.2%) and the black hole sign was identified in 38 (16.7%) based on NCCT of the brain upon admission. Of the 65 patients with HE, the blend sign was noted in 28 and the black hole sign was noted in 22. The blend sign had a sensitivity of predicting HE of 43.1%, a specificity of 89.0%, a PPV of 60.9%, and an NPV of 79.7%. In contrast, the black hole sign had a sensitivity of predicting HE of 33.9%, a specificity of 90.2%, a PPV of 57.9%, and an NPV of 77.4%. The area under the ROC curve was 0.660 for the blend sign and 0.620 for the black hole sign ($p = 0.516$). In conclusion, the blend sign and the black hole sign on CT are both good predictors of HE in patients with sICH, though the blend sign seems to have a higher level of accuracy.

Keywords: Intracerebral hemorrhage, hematoma expansion, CT, blend sign, black hole sign

1. Introduction

Spontaneous intracerebral hemorrhage (sICH) is a common and deadly neurological disorder with a high early mortality and poor prognosis; sICH accounts for approximately 15-30% of all strokes (*1,2*). About 30% of patients with sICH have hematoma expansion (HE), and HE is associated with a poor outcome in terms of neurological function (*3*).

Some predictors associated with HE have been identified in neuroimaging data from patients with sICH, and these predictors can help to identify patients at risk of HE and to improve clinical outcomes (*4-6*). HE occurs within the first 24 h of the onset of symptoms and is associated with fluid levels, heterogenous density, and irregular margins on computed tomography (CT) of the brain (*7*). Wada *et al*. identified a spot sign on computed tomography angiography (CTA) in patients with sICH, and they found that it was a prognostic factor related to HE (*8*). The spot sign on CTA is not only a predictor of HE in patients with sICH but also a reliable predictive factor for clinical prognosis and mortality (*9*). The spot sign

Address correspondence to:
Dr. Mingfei Yang, Department of Neurosurgery, Qinghai Provincial People's Hospital, Xining 810007, Qinghai, China.
E-mail: 18678695779@163.com

is also related to persistent bleeding during evacuation of a hematoma, rebleeding, and a larger residual hematoma after surgery (*10*). Although the spot sign is a reliable predictor of HE and a poor outcome in patients with sICH, its accuracy is affected by many factors, such as the initial hematoma volume, a history of anticoagulant therapy, and the time from onset to CTA. Potential predictors in non-contrast CT (NCCT) need to be identified in the event CTA is not possible.

Several recent studies have noted a blend sign (*4*) or a black hole sign (*5*) on NCCT when patients with sICH are admitted, and these two novel signs have both proven to be neuroimaging predictors for HE. The blend sign is blending of the hypoattenuating region and the hyperattenuated region of a hematoma with a clear margin (*4*). The black hole sign is a relatively hypodense area within a hyperdense hematoma, with an obvious boundary adjacent to brain tissue (*5*). The blend sign and the black hole sign on NCCT are associated with the spot sign on CTA, and all three are predictive factors for a poor outcome in patients with sICH (*11*). However, no studies have compared the predictive value of the blend sign and the black hole sign on NCCT in the same cohort of patients with sICH. Thus, a retrospective cohort study was conducted to compare the value of the blend sign and the black hole sign in predicting HE.

2. Materials and Methods

2.1. Patient selection

Potential subjects were patients who were admitted to this Hospital between August 2015 and September 2017 and who had sICH as verified by an imaging study. This study was approved by the biomedical ethics committee of Qinghai Provincial People's Hospital, and its design met local ethical criteria for human research. Patients were included in this study if CT upon admission was performed within 6 hours of the onset of symptoms. NCCT of the brain was performed upon admission (within 6 h of the onset of symptoms) to identify the blend sign and the black hole sign. HE was determined based on subsequent CT during a follow-up 24 h later. Demographic characteristics, smoking status, alcohol consumption, the timing of CT, a history of hypertension and diabetes mellitus, and past medical history were recorded. The above information was collected by a blinded professional neurosurgeon.

The inclusion criteria were: *i*) age over 18 years; *ii*) sICH was verified with NCCT of the brain; *iii*) NCCT was performed upon admission (within 6 hours of the onset of symptoms); and *iv*) subsequent CT was performed during a follow-up 24 h later.

Exclusion criteria were: *i*) patients with ICH secondary to a condition such as trauma, a tumor, an aneurysm, an arteriovenous malformation (AVM), or a hemorrhagic cerebral infarction, *ii*) patients who had received anticoagulant therapy, and *iii*) patients who underwent emergency evacuation of a hematoma prior to follow-up CT.

2.2. Imaging and detection of the blend sign and the black hole sign

CT scans were performed using standard clinical parameters with axial sections with a thickness of 5 mm. Two radiologists blinded to the clinical information independently reviewed CT images. In the event of a discrepancy, a consensus was reached through discussion.

The blend sign on NCCT meant that a hematoma with had well-defined components (a relatively hypoattenuated region and an adjacent hyperattenuated region). The blend sign indicated: *i*) a hematoma with a boundary between the hypoattenuated region and adjacent hyperattenuated region that was clearly visible to the naked eye; *ii*) the density of the two regions differed > 18 Hounsfield units (HU); and *iii*) the hypodense region of the hematoma was not completely encapsulated by the hyperdense region (*4*).

The black hole sign indicated: *i*) a hematoma with a hypoattenuated region and an adjacent hyperattenuated region; the relatively hypoattenuated region (black hole) had to have a distinct border; *ii*) the relatively hypoattenuated region was encapsulated within the hyperattenuating hematoma; and *iii*) the density of the two regions differed at least 28 HU (*5*).

2.3. Measurement of hematoma volume

The hematoma volume was calculated by using the ABC/2 formula. A was the largest diameter of the maximum hematoma level, B was the maximum diameter perpendicular to A, and C was the vertical depth of the hematoma. HE was defined as an increase in volume > 33% or an absolute increase of > 12.5 mL (*12*) during CT of the brain during follow-up 24 h later. Intraventricular hemorrhage is not included in the calculation of the cerebral parenchymal hematoma volume.

2.4. Statistical analysis

All statistical analysis was performed with the commercially available software SPSS version 21.0 (SPSS Inc. IBM, Armonk, NY). Continuous variables were analyzed using a *t*-test and their values are indicated as the mean ± standard deviation (SD). Categorical variables were compared using a χ^2 test, and their values are indicated as a percentage or frequency distributions Logistic regression analysis was performed to assess the association between clinical and radiological parameters and HE. Multivariate logistic

Table 1. Baseline characteristics of patients with HE and patients without HE [*n* (%)]

Items	Patients with HE (*n* = 65)	Patients without HE (*n* = 163)	χ^2/t	*p*
Mean age (yrs)	57 ± 11.5	59 ± 11.8	1.153	0.250
Sex, male	51 (78.5)	116 (71.2)	1.262	0.261
Hypertension	41 (63.1)	95 (58.3)	0.444	0.505
Diabetes mellitus	9 (13.8)	12 (9.8)	2.336	0.126
Smoking	24 (36.9)	45 (27.6)	1.911	0.167
Alcohol consumption	21 (32.3)	48 (29.4)	0.180	0.671
PLT (10^9/L)	136 ± 56	143 ± 55	0.863	0.389
Admission SBP (mmHg)	175 ± 29	168 ± 29	1.645	0.101
Admission DBP (mmHg)	107 ± 19	102 ± 20	1.728	0.085
Time to CT (h)	4.02 ± 1.36	4.52 ± 1.15	2.884	0.005
Baseline hematoma volume (mL)	31.05 ± 14.94	24.37 ± 17.14	2.751	0.006
Intraventricular hemorrhage	40 (61.5)	68 (41.7)	7.323	0.007
Blend sign	28 (43.1)	18 (11.0)	29.61	< 0.001
Black hole sign	22 (33.8)	16 (9.8)	19.32	< 0.001

Data are the mean ± SD or the number of patients. DBP, diastolic blood pressure; HE, hematoma expansion; PLT, platelet count; SBP, systolic blood pressure.

regression was used to analyze the odds ratio (OR) and 95% confidence interval (CI) of the blend sign and the black hole sign in predicting HE. The ability of the blend sign and the black hole sign to predict HE was analyzed using receiver-operator analysis. The area under the receiver operating characteristic curve (ROC) for the blend sign and the black hole sign was compared using a *Z* test. The interobserver reliability for detection of the blend sign and the black hole sign was confirmed by calculating k values. A *P* value < 0.05 was considered statistically significant.

3. Results

3.1. *Baseline characteristics*

A total of 228 patients met the inclusion criteria and all were enrolled in this study. Patients ranged in age from 26 to 79 years, and the mean age was 58.0 ± 11.7 years. A total of 61 patients (26.8%) were female, and 167 (73.2%) were male. The mean interval from the onset of ICH to CT upon admission was 4.38 ± 1.23 h, and the mean baseline volume of a hematoma was 26.27 ± 16.82 mL. A hematoma was located in the basal ganglia (140, 61.4%), cortical-subcortical areas (31, 13.6%), the thalamus (27, 11.8%), the cerebellum (16, 7%), or brain stem (14, 6.1%). Baseline characteristics for patients with HE and patients without HE are shown in Table 1.

3.2. *Patients with HE with the blend sign or the black hole sign on CT*

Of the 228 patients with sICH, 46 (20.2%) had the blend sign and 38 (16.7%) had the black hole sign on CT of the brain upon admission. Compared to patients without HE, a higher proportion of patients with HE had the blend sign or the black hole sign . Interobserver reliability was exceptional for the identification of the blend sign (k = 0.928) and the black hole sign

Table 2. Multivariate analysis of HE

Items	HE		
	OR	95% CI	*p*
Intraventricular hemorrhage	2.501	1.300-4.813	0.006
Blend sign	3.800	1.678-8.605	0.001
Black hole sign	2.726	1.097-6.777	0.031

HE, hematoma expansion.

(k = 0.915). Multivariate analysis indicated that intraventricular hemorrhage, the blend sign, and the black hole sign were associated with HE (Table 2).

Both the blend sign and the black hole sign were found in 26 patients, and 18 (69.2%) had HE. Of 20 patients with the blend sign but no black hole sign, 10 (50.0%) had HE. Of 12 patients with only the black hole sign, 4 (33.3%) had HE. A total of 170 patients had neither the blend sign nor the black hole sign, and only 34 (20.0%) had HE. The frequency of HE in patients with the blend sign and/or the black hole sign is shown in Figure 1.

3.3. *The accuracy of the blend sign and the black hole sign in predicting HE*

The blend sign had a sensitivity of predicting HE of 43.1%, a specificity of 89.0%, a positive predictive value (PPV) of 60.9%, and a negative predictive value (NPV) of 79.7%. The black hole sign had a sensitivity 33.9%, a specificity of 90.2%, a PPV of 57.9%, and an NPV of 77.4%. ROC curve analysis was used to compare the accuracy of the blend sign and the black hole sign in predicting HE, and the ROC curves for the two signs as predictors of HE in patients with sICH are shown in Figure 2. The area under the curve was 0.660 for the spot sign and 0.620 for the black hole sign. There were no significant differences in the area under ROC curves for the two signs (*p* = 0.516).
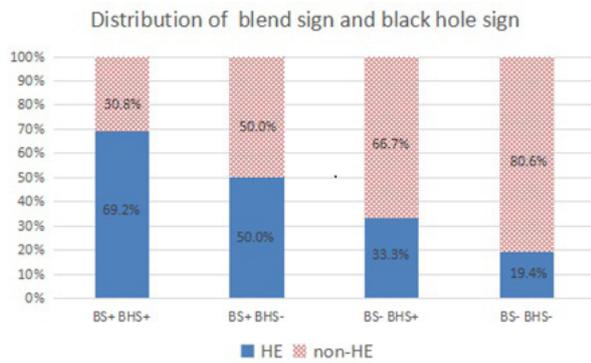
Figure 1. Frequency of a blend sign and a black hole sign in HE. BHS, black hole sign; BS, blend sign; HE, hematoma expansion. The proportion of BS+ BHS+ is 69.2%, the proportion of BS+BHS- is 50.0%, the proportion of BS-BHS+ is 33.3%, and the proportion of BS-BHS- is 19.4%.
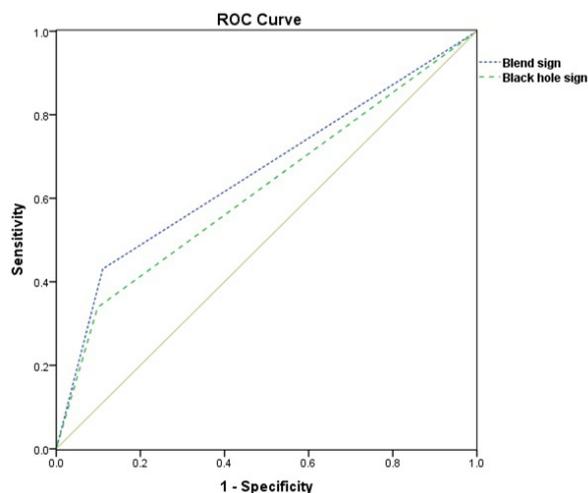

Figure 2. Receiver operating characteristic (ROC) curve as a result of classifying HE in binary terms. HE, hematoma expansion. The area under the curve was 0.660 for a blend sign and 0.620 for a black hole sign, p = 0.516.

4. Discussion

The current study is the first to compare the value of the blend sign and the black hole sign on NCCT in predicting HE in the same cohort of patients with sICH, and results indicated that the blend sign and the black hole sign are both good predictors of HE. Although the accuracy of prediction did not differ significantly, the blend sign seems to be better at predicting HE. Univariate analysis indicated that the time from the onset of symptoms to CT upon admission, baseline hematoma volume, and intraventricular hemorrhage were also associated with HE. Recent studies have indicated that the blend sign, the black hole sign, and the spot sign are all independent predictors of HE and that the spot sign has a higher level of predictive accuracy (13,14). Consistent with previous studies, the current study also found that both the blend sign and the black hole sign can effectively predict HE.

In patients with sICH, risk factors for HE include primary hypertension, cerebral amyloid angiopathy, diabetes mellitus, and abnormal coagulation function. HE is significantly associated with neurological deterioration, a poor outcome in terms of function, and a high mortality (15,16). The pathogenesis of HE may be related to the heterogeneity of a hematoma. The heterogeneity of a hematoma's density on NCCT is associated with HE within the first 24 h of the onset of symptoms (7). The main difference between the blend sign and the black hole sign is the heterogeneity of a hematoma. Compared to the black hole sign, the blend sign is easier to identify. Li *et al.* proposed this new neuroimaging predictor, and they found that the blend sign had a sensitivity of predicting HE of 39.3%, a specificity of 95.5%, a PPV of 82.7%, and an NPV of 74.1% (4). In the current study, the blend sign had a high level of sensitivity and a higher NPV but a lower level of specificity and a lower PPV. The accuracy with which the blend sign can predict HE might be influenced by many potential factors. The mean time from the onset of symptoms to CT upon admission (4.02 h in patients with HE, 4.52 h in patients without HE) was greater than that in the study by Li *et al.* (1.67 h in patients with HE, 2.76 h in patients without HE). This difference may be related to the fact that patients lived in areas at higher altitudes, that patients had to travel further before admission, or the fact that care was less accessible. In addition, the baseline hematoma volume (31.05 mL in patients with HE, 24.37 mL in patients without HE) was greater than that in the study by Li *et al.* (24.31 mL in patients with HE, 13.12 mL in patients without HE). The difference in the time from the onset of symptoms to CT upon admission and the baseline hematoma volume may have influenced the predictive value of HE. Further studies are needed to identify the exact factors that affect the accuracy with which HE is predicted. Early detection of the blend sign helps to estimate prognosis and could serve as a potential therapeutic target (17). The blend sign on an initial CT scan is closely associated with postoperative hemorrhaging in patients with sICH who undergo stereotactic minimally invasive surgery (18). The blend sign on CT may be associated with the spot sign on CTA, and both can predict secondary neurological deterioration in patients with sICH (19).

1n 2016, Boulouis *et al.* reported that the hypoattenuated region within the hematoma on NCCT could predict HE (20). However, previous studies did not provide standard imaging markers for the prediction of HE. Based on differences in the heterogeneity of a hematoma on NCCT, Li *et al.* identified the black hole sign and they confirmed that it is a novel predictor of HE in patients with sICH (5). The relationship between the black hole sign and the blend sign is still uncertain. The black hole sign was associated with the blend sign in the current study, and patients with both the blend sign and the black hole sign had a higher risk

of developing HE. The incidence of HE was higher in patients with the blend sign but not the black hole sign than in patients with only the black hole sign. The black hole sign is thought to reflect bleeding during different periods, and a recent hemorrhage appears as hypoattenuation on NCCT (*5*). After blood coagulated, serum was isolated and hyperattenuation was evident. The black hole sign seems to follow the same process as the blend sign. Li *et al*. found that the black hole sign had a sensitivity of predicting HE of 31.9%, a specificity of 94.1%, a PPV of 73.3%, and an NPV of 73.2% (*5*). In the current study, the black hole sign had a higher level of sensitivity and a higher NPV but a lower level of specificity and a lower PPV. Many factors may influence the predictive value of the black hole sign. In the current study, the mean time from the onset of symptoms to CT upon admission (4.02 h in patients with HE, 4.52 h in patients without HE) was greater than that in the study by Li *et al*. (2.3 h in patients with HE, 2.6 h in patients without HE). Furthermore, the average baseline hematoma volume also differed (31.05 mL in patients with HE, 24.37 mL in patients without HE) from that in the study by Li *et al*. (33.1 mL in patients with HE, 14.1 mL in patients without HE) (*5*). Further studies are needed to identify the exact factors affecting the predictive value of the black hole sign.

The current study had several limitations. This study was a single-center retrospective cohort study with a relatively small sample size. Only NCCT within 6 h of admission was examined, which may have led to a potential selection bias. The time from the onset of ICH to CT upon admission was relatively long, which may have affected the predictive accuracy of the blend sign and the black hole sign. In addition, this study only analyzed the blend sign and the black hole sign. A study with a larger sample size needs to be conducted in the future to compare the clinical value of comprehensive neuroimaging factors in patients with sICH.

In conclusion, the blend sign on NCCT in patients with sICH was associated with the black hole sign. Both have are accurate predictors of HE, and the blend sign appeared to have a greater predictive value. Patients with both the blend sign and the black hole sign have a higher risk of HE. Neuroimaging factors on NCCT are increasingly crucial to predicting HE when an immediate CTA is not possible. In the near future, a comprehensive scoring system should be devised to effectively predict HE and prognosis. This would benefit all patients with sICH.

Acknowledgements

References

1. Yang G, Shao GF. Elevated serum IL-11, TNF alpha, and VEGF expressions contribute to the pathophysiology of hypertensive intracerebral hemorrhage (HICH). Neurol Sci. 2016; 37:1253-1259.
2. Hemphill JC, Greenberg SM, Anderson CS, *et al*. Guidelines for the management of spontaneous intracerebral hemorrhage: A guideline for healthcare professionals from the American Heart Association/ American Stroke Association. Stroke. 2015; 46:2032-2060.
3. Guan J, Hawryluk GW. Targeting secondary hematoma expansion in spontaneous intracerebral hemorrhage-state of the art. Front Neurol. 2016; 7:187.
4. Li Q, Zhang G, Huang YJ, Dong MX, Lv FJ, Wei X, Chen JJ, Zhang LJ, Qin XY, Xie P. Blend sign on computed tomography: Novel and reliable predictor for early hematoma growth in patients with intracerebral hemorrhage. Stroke. 2015; 46:2119-2123.
5. Li Q, Zhang G, Xiong X, Wang XC, Yang WS, Li KW, Wei X, Xie P. Black hole sign: Novel imaging marker that predicts hematoma growth in patients with intracerebral hemorrhage. Stroke. 2016; 47:1777-1781.
6. Orito K, Hirohata M, Nakamura Y, Takeshige N, Aoki T, Hattori G, Sakata K, Abe T, Uchiyama Y, Sakamoto T, Morioka M. Leakage sign for primary intracerebral hemorrhage: A novel predictor of hematoma growth. Stroke. 2016; 47:958-963.
7. Blacquiere D, Demchuk AM, Al-Hazzaa M, *et al*. Intracerebral hematoma morphologic appearance on noncontrast computed tomography predicts significant hematoma expansion. Stroke. 2015; 46:3111-3116.
8. Wada R, Aviv RI, Fox AJ, Sahlas DJ, Gladstone DJ, Tomlinson G, Symons SP. CT angiography "spot sign" predicts hematoma expansion in acute intracerebral hemorrhage. Stroke. 2007; 38:1257-1262.
9. Morotti A, Jessel MJ, Brouwers HB, Falcone GJ, Schwab K, Ayres AM, Vashkevich A, Anderson CD, Viswanathan A, Greenberg SM, Gurol ME, Romero JM, Rosand J, Goldstein JN. CT angiography spot sign, hematoma expansion, and outcome in primary pontine intracerebral hemorrhage. Neurocrit Care. 2016; 25:79-85.
10. Brouwers HB, Raffeld MR, van Nieuwenhuizen KM, *et al*. CT angiography spot sign in intracerebral hemorrhage predicts active bleeding during surgery. Neurology. 2014; 83:883-889.
11. Sporns PB, Schwake M, Kemmling A, Minnerup J, Schwindt W, Niederstadt T, Schmidt R, Hanning U. Comparison of spot sign, blend sign and black hole sign for outcome prediction in patients with intracerebral hemorrhage. J Stroke. 2017; 19:333-339.
12. Davis SM, Broderick J, Hennerici M, Brun NC, Diringer MN, Mayer SA, Begtrup K, Steiner T. Hematoma growth is a determinant of mortality and poor outcome after intracerebral Hemorrhage. Neurology. 2006; 66:1175-1181.
13. Zheng J, Yu Z, Xu Z, Li M, Wang X, Lin S, Li H, You C. The accuracy of the spot sign and the blend sign for predicting hematoma expansion in patients with spontaneous intracerebral hemorrhage. Med Sci Monit. 2017; 23:2250-2257.
14. Yu Z, Zheng J, Ma L, Guo R, Li M, Wang X, Lin S, Li H, You C. The predictive accuracy of the black hole sign

and the spot sign for hematoma expansion in patients with spontaneous intracerebral hemorrhage. Neurol Sci. 2017; 38:1591-1597.

15. Dowlatshahi D, Demchuk AM, Flaherty ML, *et al*. Defining hematoma expansion in intracerebral hemorrhage: Relationship with patient outcomes. Neurology. 2011; 76:1238-1244.

16. Delcourt C, Huang Y, Arima H, Chalmers J, Davis SM, Heeley EL, Wang J, Parsons MW, Liu G, Anderson CS. Hematoma growth and outcomes in intracerebral hemorrhage: The INTERACT 1 study. Neurology. 2012; 79:314-319.

17. Li Q, Yang WS, Wang XC, Cao D, Zhu D, Lv FJ, Liu Y, Yuan L, Zhang G, Xiong X, Li R, Hu YX, Qin XY, Xie P. Blend sign predicts poor outcome in patients with intracerebral hemorrhage. PLoS One. 2017; 12:e0183082.

18. Wu GF, Shen ZK, Wang LK, Sun S, Luo J, Mao Y. Post-operative re-bleeding in patients with hypertensive ICH is closely associated with the CT blend sign. BMC Neurology. 2017; 17:131.

19. Sporns PB, Schwake M, Schmidt R, Kemmling A, Minnerup J, Schwindt W, Cnyrim C, Zoubi T, Heindel W, Niederstadt T, Hanning U. Computed tomographic blend sign is associated with computed tomographic angiography spot sign and predicts secondary neurological deterioration after intracerebral hemorrhage. Stroke. 2017; 48:131-135.

20. Boulouis G, Morotti A, Brouwers HB, Charidimou A, Jessel MJ, Auriel E, Pontes-Neto O, Ayres A, Vashkevich A, Schwab KM, Rosand J, Viswanathan A, Gurol ME, Greenberg SM, Goldstein JN. Association between hypodensities detected by computed tomography and hematoma expansion in patients with intracerebral hemorrhage. JAMA Neurology. 2016; 73:961-968.

Brief Report

Effect of electrolyzed water produced using carbon electrodes on HeLa cell proliferation

Kyoko Nakamura[1,*], Osamu Muraoka[1,2]

[1] *Pharmaceutical Research and Technology Institute, Kindai University, Osaka, Japan;*
[2] *Antiaging Center, Kindai University, Osaka, Japan.*

Summary   We developed electrolyzed water (EW) using carbon electrodes and investigated the ability of the developed EW to inhibit the proliferation of human cervical carcinoma HeLa cells. We observed that EW-containing media inhibited HeLa cell proliferation. Many very small black dots were produced in EW and these were associated with the inhibitory effect on the cell proliferation. Furthermore, the very small black dots that could inhibit cell proliferation were produced only at pH 3 to 3.5 of EW. Additional experiments showed that this inhibition of proliferation is reversible. These results suggest that the effect of EW on HeLa cells is cytostatic and not cytotoxic. Thus, our results indicate that the EW developed in this study may be used to inhibit cell proliretation.

Keywords: Electrolyzed water, carbon electrodes, cell proliferation

1. Introduction

Electrolyzed water is produced by the electrolysis of ordinary tap water or any liquid water containing dissolved electrolytes, such as sodium chloride. During the electrolysis process, a membrane partition (diaphragm) between the anode and cathode results in water being electrolyzed and the production of acidic water at the anode and alkaline water at the cathode. Various types of electrolyzed water can be produced in electrolytic cells, with or without diaphragm, using different kinds of electrolytes. Electrolyzed water is useful in various fields such as in medicine, and in agricultural and food industries (*1,2*). Electrochemically oxidized or reduced water is produced in an electrolysis chamber with a diaphragm, with electrochemically oxidized water being produced in the anode chamber. In particular, strongly acidic water (pH ≤ 3) has been used as sterile, antibacterial water for sanitizing food contact surfaces and equipment, such as cookware and glasses. Strongly acidic water (pH < 2.7) is

processed by electrolysis through a dilute sodium chloride solution and has a strong bactericidal effect on bacteria, virus and fungi (*3*). Furthermore, Nishida *et al*. reported that the gargling with this water can inhibit plaque formation (*4*). Hypochlorous acid in this water is one of the active factors responsible for the bactericidal effect (*5*). In contrast, electrochemically reduced water is produced in cathode chamber, which has an alkaline pH. Potable electrochemically reduced water (pH 8-10) is called alkali-ionic water and is popular "health water" in Japan (*2*). Electrochemically reduced water has been shown to exert anti-cancer effects. For example, electrochemically reduced water produced near the cathode during the electrolysis of ultrapure water containing sodium hydroxide at 100 V for 60 min using an electrolyzing device equipped with platinum-coated titanium electrodes suppressed tumor angiogenesis in human lung adenocarcinoma A549 cells and tumor invasion in human fibrosarcoma HT1080 cells (*6,7*). Recently, several researchers have reported the generation of electrolyzed water of neutral pH by an electrolysis chamber without a diaphragm. Neutral pH hydrogen-enriched electrolyzed water inhibited efficient colony formation of human tongue squamous cell carcinoma-derived HSC-4 cells and growth of human fibrosarcoma HT-1080 cells (*8*). Slightly acidic electrolyzed water (pH 5.0 to 6.5) produced in an electrolysis chamber without a diaphragm containing a 2% to 6% hydrogen chloride solution exhibited

antibacterial effects on oral pathogens and inhibited the proliferation of human gingival fibroblasts (*9*). Therefore slightly acidic electrolyzed water is usually used as a disinfectant.

Thus, various types of electrolyzed water are beneficial for human health. Particularly, we focused on the inhibitory effect of electrolyzed water against cancer cells. Here, we produced electrolyzed water (EW) from tap water in an electrolysis chamber without a diaphragm using special carbon electrodes. We have assessed the effect of our EW on tumor cell proliferation. Our results demonstrate that EW generated using special carbon electrodes inhibits the proliferation of human cervical carcinoma HeLa cells.

2. Materials and Methods

2.1. *Preparation of electrolyzed water (EW) using special carbon electrodes*

We used special carbon electrodes ($150 \times 30 \times 7$ mm) prepared by Toyo Tanso Co. Ltd. (Osaka, Japan) and these electrodes were graphite-resin composite electrodes. It was known that electrolysis of water using these electrodes produced amount of aqueous carbon dioxide. EW was prepared by electrolysis of tap water (W) at 10 V for 72 h in a 1,000 mL beaker equipped with special carbon electrodes. In the electrolysis process, two carbon electrodes were set in V-formations and EW was a mixture of anode-side and cathode-side electrolyzed water. Both electrodes need to be immersed to length of about 10 cm into water. Figure 1A depicts a schematic diagram of water electrolysis. We assume that carbon compounds ($C_XH_YO_Z$) were produced in the resulting EW. We confirmed that the mass of $C_XH_YO_Z$ was 2,000 and 4,000 Da by laser TOF Mass analysis (Toyo Tanso Co. Ltd.) of EW for the molecular characterization of $C_XH_YO_Z$ (data not shown). The EW turned light brown and had a pH of 3 to 3.5. On the other hand, the control (W) was colorless, transparent, and had a pH of around 7.

2.2. *Cell culture and preparation of EW-containing media*

HeLa cells were plated onto culture dishes and cultured in low glucose Dulbecco's modified Eagle medium (DMEM, Sigma, St. Louis, MO, USA) supplemented with 10% fetal bovine serum (FBS) (Nichirei Biosciences Inc., Tokyo, Japan), 100 μg/mL streptomycin, and 100 U/mL penicillin (Nacalai Tesque, Kyoto, Japan). Cells were maintained at 37°C in a humidified atmosphere containing 5% CO_2 and 95% air.

In order to investigate the effects of EW on the proliferation of HeLa cells, media were prepared using EW or W (control) instead of ultra-pure water. The
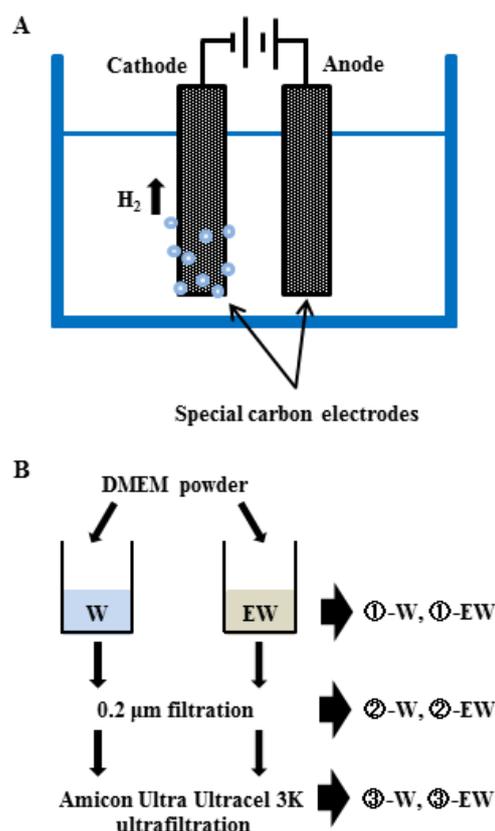
Figure 1. Schematic view of EW generation system and preparation of culture media. A. Principle of EW preparation. The chemical reaction is follows:

Anode side
$$H_2O \rightarrow 2H^+ + O^\bullet + 2e^-$$
$$C + 2 O^\bullet \rightarrow CO_2 \text{ (aq)}$$
$$C + O^\bullet + H_2O \rightarrow C_XH_YO_Z \quad C_XH_YO_Z: \text{ the expected molecular weight of 2,000~4,000}$$
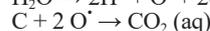
Cathode side
$$2H^+ + 2e^- \rightarrow H_2$$
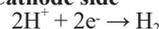
B. Schematic flow diagram representing the preparation of various media. Add DMEM powder to W or EW with gentle stirring (①-W or ①-EW). Filtration through 0.2-μm filter of ①-W or ①-EW (②-W or ②-EW). Furthermore, ②-W or ②-EW is filtered using Amicon Ultra-15 3K centrifugal filter units (③-W or ③-EW).

preparation of various media used in this experiment are shown in Figure 1B. First, DMEM powder (Nissui Pharmaceutical Co., Ltd., Tokyo, Japan) was dissolved in W or EW (①-W or ①-EW) according to manufacturer's instruction. Then, these media were filtered through a 0.2-μm filter (cellulose acetate membrane) (②-W, ②-EW). Furthermore, ②-W and ②-EW were each filtrated using Amicon Ultra-15 3K centrifugal filter units (low-binding regenerated cellulose membrane) (Uitracel-3K, Millipore Co. Ltd., Billerica, MA, USA) (③-W, ③-EW). The ①-EW turned brownish-yellow and was somewhat turbid, which many differently sized black dots were visible. The ②-EW turned weakly brownish-yellow and was a little turbid, which very small black dots had precipitated to the bottom after being left standing for a few days. The ③-EW turned yellow and exhibited relatively low turbidity, which very small black dots did not observed

under the microscope.This process generated 6 types of media (①-W, ①-EW, ②-W, ②-EW, ③-W and ③-EW) that were each sterilized by autoclaving at 121°C for 15 min and then supplemented with 10% FBS, 0.584 g/L glutamine, 100 μg/mL streptomycin, 100 U/mL penicillin, and 10% sodium hydrogen carbonate. The final average pH values were as follows: ①-W, 8.41; ①-EW, 8.21; ②-W, 8.24; and ②-EW, 8.05. EW media had a slightly lower pH than that of W media, but all media were still alkaline. Filtration of media using Amicon Ultra-15 3K centrifugal filter units had no effect on pH (data not shown).

2.3. Cell proliferation and EW washout assay

After removing the culture media, the HeLa cells grown in culture dishes were washed with sterile PBS (phosphate buffered saline) (137 mM sodium chloride, 8.1 mM sodium phosphate dibasic, 2.7 mM potassium chloride, and 1.47 mM potassium phosphate monobasic) and detached with 0.25% trypsin-EDTA. HeLa cells were collected by centrifugation at 800×g for 5 min and resuspended in each type of culture media (①-W, ①-EW, ②-W, ②-EW, ③-W and ③-EW). HeLa cells were seeded onto culture flasks at a density of 8 × 10⁴ cells/flask and incubated for 3 days at 37°C in a humidified atmosphere containing 5% CO_2 and 95% air. The effect of EW on cell proliferation was then assessed by counting the number of viable cells. HeLa cells were trypsinized, stained with trypan blue, and counted in a hemocytometer every day for 3 days.

The reversibility of the inhibition of cell proliferation after EW washout was assessed in an additional study by replacing EW media with W control media after 2 days. HeLa cells cultured in ②-EW medium for 2 days were washed twice with PBS and resuspended in ②-W control or ②-EW medium. HeLa cells were trypsinized, stained with trypan blue, and counted in a hemocytometer every day for additional 3 days.

3. Results and Discussion

To investigate the effects of EW-containing media on tumor cell proliferation in human cervical carcinoma HeLa cells, HeLa cells were first cultured in ①-W (control) or ①-EW media for 3 days. Figure 2A and 2B are photographs of HeLa cells after a day of culture in ①-W (control) (Figure 2A) or ①-EW (Figure 2B) media. We observed differently sized black dots in the ①-EW medium under the microscope (Figure 2B). We speculate that these black dots were broken pieces of carbon (Figure 2B) from the carbon electrode used in water electrolysis. These black dots were not observed in the ①-W (control) medium (Figure 2A). Interestingly, HeLa cell proliferation was markedly inhibited by incubation in cell culture media containing
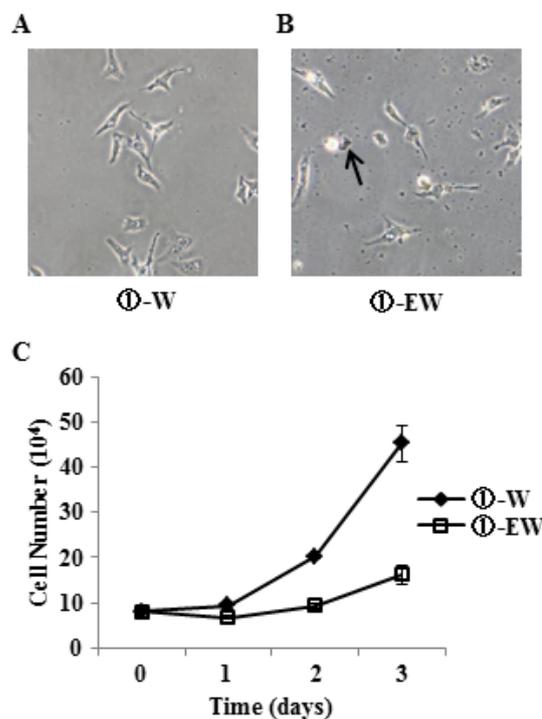
Figure 2. The effect of ①-W and ①-EW media on proliferation of HeLa cells. Cells were seeded at a density of 8 × 10⁴ cells in flasks containing each culture medium. After 1 day of incubation, cells were photographed at ×10 **(A, B)** and then counted daily for 3 days **(C)**. The arrow indicates a conceivable broken piece of carbon electrode. Data are expressed as the mean ± SD of three independent experiments.

EW compared to those containing W (control) (Figure 2C). These results demonstrate that EW-containing medium has the potential to inhibit the proliferation of HeLa cells.

In this study, EW was prepared by electrolysis of ordinary tap water. Although it was conceivable that hypochlorous acid might be produced by electrolysis of chlorine ions in tap water, EW generated in this study weakly contained hypochlorous acid at very low chlorine level (0.00325 ppm) and culture media for HeLa cells prepared using EW were sterilized by autoclaving at 121°C for 15 min. Since hypochlorous acid was removed by boiling in culture media, we focused on black dots in cell culture media as an inhibitor of cell proliferation. To test whether these black dots in ①-EW medium are involved in cell proliferation, we attempted to remove the dots from the medium using a 0.2-μm filter. As shown in Figure 3B, the relatively large black dots in ②-EW medium could be removed using a 0.2-μm filter. However, very small black dots were still observed in ②-EW medium (Figure 3B), indicating that there did not adsorbed onto 0.2-μm filter membrane. ②-EW medium still retained the ability to inhibit cell proliferation to the same extent as ①-EW (Figure 2C and 3C). ①-W (control) medium was also filtered in the same way as that for ②-W medium (Figure 3A); this filtration had no effect
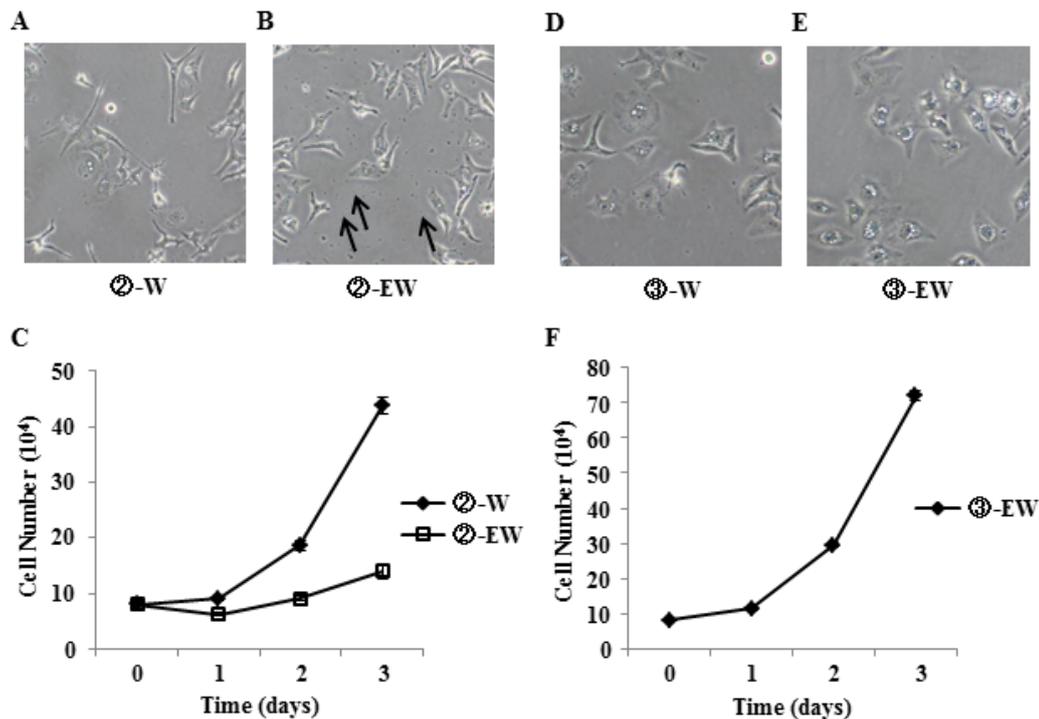
Figure 3. The effect of ②-W or ②-EW and ○3-EW media on proliferation of HeLa cells. Each ②-W and ②-EW was prepared by filtration (0.2 μm) of ①-W and ①-EW, respectively. Cells were seeded at a density of 8 × 10⁴ cells in flasks containing each culture medium. After 1 day of incubation, cells were photographed at ×10 **(A, B)** and counted every day for 3 days **(C)**. The arrows indicate very small black dots. Each ③-W and ③-EW was prepared by centrifugation of ②-W and ②-EW in Amicon Ultra-15 3K centrifugal filter units. Cells were seeded at a density of 8×10⁴ cells in flasks containing each culture medium. After 1 day of incubation, cells were photographed at ×10 (D, E) and then counted for 3 days (F). Filtration of Amicon Ultra-15 3K centrifugal filter units had no effect on cell proliferation (data not shown). Data are expressed as the mean ± SD of three independent experiments.

on cell proliferation (Figure 2C and 3C). Thus, these results indicate that the very small black dots that passed through the 0.2-μm filter were associated with significant reduction of cell proliferation. Sometimes, EW with a pH greater than 3.5 was generated. Many very small black dots were observed in EW with a pH greater than 3.5 by microscopy. Surprisingly, cell culture medium containing EW with at a PH greater than 3.5 was unable to inhibit HeLa cell proliferation (data not shown). We found that the very small black dots that could inhibit cell proliferation were produced only at pH of 3 to 3.5. Therefore, the pH of EW is very important for the inhibition of cellular proliferation.

Next, to remove these black dots involved in inhibiting tumor cell proliferation from ②-EW medium, we used ultrafiltration membranes with much smaller pore sizes, between 0.001 and 0.1 μm. Ultrafiltration membranes are typically classified by the nominal molecular weight limit (NMWL). Since the predicted molecular weights of carbon compounds ($C_xH_yO_z$) produced in EW were between 2,000 and 4,000 Da, the ②-EW was centrifuged using Amicon Ultra-15 3K centrifugal filter units (3 kDa cutoff) (Millipore) and this solution was designated as ③-EW. A similar treatment was performed for ②-W control to produce ③-W, and the very small black dots were efficiently removed in ③-EW medium as clear as ③-W medium (Figure 3D and 3E). Surprisingly, removing these black
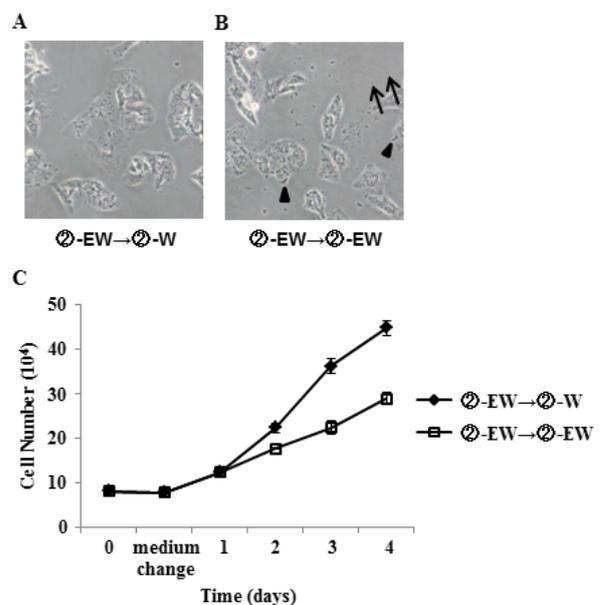

Figure 4. Reversibility of the inhibitory effect of ②-EW on the proliferation of HeLa cells. Cells were seeded at a density of 8 × 10⁴ cells in flasks containing ②-EW medium and counted for 2 days. After 2 days of incubation, cells were washed with PBS and reincubated with ②-W control or ②-EW medium for more 3 days. Cells were photographed a day after medium replacement at ×10 **(A, B)** and then counted for more 3 days **(C)**. The arrows indicate very small black dots and the arrowheads indicate many very small black dots bind to cell surface. Data are expressed as the mean ± SD of three independent experiments.

dots from EW recovered the ability of HeLa cells to proliferate in the media (Figure 3F). Cell proliferation rates showed no change in the ③-W medium (data not shown), indicating that centrifugation using Amicon Ultra-15 3K centrifugal filter units (3 kDa cutoff) had no influence on cell proliferation in HeLa cells. Thus, these results indicate that black dots in EW can inhibit proliferation of HeLa cells and can be removed using Amicon Ultra-15 3K centrifugal filter units. Therefore, we suggest that the very small black dots produced in EW have the ability to inhibit tumor cell proliferation and exhibit molecular weights ranging from about 3,000 Da to a molecular weight small enough to enable the dots to pass through a 0.2-μm filter.

To determine whether inhibition of HeLa cell proliferation by EW-containing media was a reversible phenomenon, we assessed whether HeLa cells cultured in ②-EW medium would regain the capacity to proliferate when the medium is replaced with ②-W control medium. HeLa cells cultured in ②-EW medium for 2 days were washed twice with PBS to remove black dots, followed by replacement of the medium with ②-W control medium or ②-EW medium. As shown in Figure 4A, PBS washes were able to decrease the number of black dots in the flasks containing the replacement ②-W medium. In contrast, a number of black dots were observed in the flasks containing the replacement ②-EW medium and some of them were binding to cell surface (Figure 4B). Since the cell surface of many lipid bilayers had negative charges, small black dots might be electrostatically bounded to cell surface. Removal of ②-EW medium (black dots) by PBS washing resulted in acceleration of the growth rate of HeLa cells (Figure 4C). These results suggest that the inhibitory effect on cell proliferation by EW is reversible, and the black dots expected to be associated with the inhibition of cell proliferation reversibly stuck on the cell surface. These results further indicate that the anti-proliferative effect of EW is not due to a cytotoxic effect and can be stopped by washing twice with PBS.

Growth factors are important for regulating cell proliferation. Growth factors bind to cell surface receptors to initiate signaling pathways that result in the cell proliferation. Insulin-like growth factor 1 (IGF-1) is one of the major regulators of cell proliferation (*10*). Upon IGF-1 binding, the tyrosine kinase activity of IGF-1 receptor (IGF-1R) leads to downstream signal activation of the mitogen-activated protein kinase and phosphoinositide 3-kinase-Akt pathways, which promote cell proliferation (*11*). Furthermore, IGF-1R plays a central role in the development of many types of tumors (*12,13*). In our study, we investigated the proliferation of HeLa cells in presence of FBS. Introduction of the monoclonal antibody alpha-IR3 against human IGF-1R reduces proliferation of human non-autocrine neuroblastoma cells SK-N-SH and LF in the presence of FBS (*14*). Thus, we hypothesize that

carbon compounds produced in EW may inhibit cell proliferation by suppressing the signaling pathway for IGF-1R cell proliferation. Future studies are needed to test our hypothesis and to elucidate the mechanism of the anti-proliferation effect of EW in HeLa cells. Furthermore, the electrostatic potential of IGF-1R is overwhelmingly negative (*15*). The C domain of IGF-1 is electropositive and important for its receptor binding activity (*16*). Therefore, it is possibility that carbon compounds electrostatically inhibit the IGF-1 binding to IGF-1R and we hope elucidate this possibility in further studies.

In conclusion, we developed EW from tap water using special carbon electrodes and this EW was containing carbon compounds observed very small black dots with molecular weights 2,000 and 4,000 Da. We found that the developed EW inhibited HeLa cell proliferation and that carbon compounds were associated with this significant inhibition of tumor cell proliferation. We also found that washing the cells with PBS could inactivate the inhibitory effect of EW, indicating that there was reversible association between HeLa cells and certain carbon compounds produced in EW and the inhibitory effect of EW was not due to a cytotoxic effect. These findings suggest a novel mechanism for EW in the inhibition of tumor cell proliferation.

Acknowledgements

References

1. Al-Haq MI, Sugiyama J, Isobe S. Applications of electrolyzed water in agriculture and food industries. Food Sci Technol Res. 2005; 11:135-150.
2. Shirahata S, Hamasaki T, Teruya K. Advanced research on the health benefit of reduced water. Trends food sci technol. 2012; 23:124-131.
3. Okuda R, Sasazaki H, Kanehira M, Okabe T, Abe S, Tagami A, Iwamatsu Y, Miya Y, Shimizu Y. Bactericidal effect of high oxidation potential water viewed from a morphological change. Japanese Journal of Conservative Dentistry. 1994; 37:755-765. (in Japanese)
4. Nishida T, Eda M, Shimada K, Yamada K, Ito K, Murai S. Effects of Acid Electrolysis Water on Plaque Formation. Nihon Shishubyo Gakkai Kaishi. 1993; 35:692-697. (in Japanese)
5. Shiba A, Murai S, Amagasa T. Electrolyzed acidic water in the dental clinic. Tokyo: Quintessence. 1997:35-38.
6. Ye J, Li Y, Hamasaki T, et al. Inhibitory effects of electrolyzed reduced water on tumor angiogenesis. Biol Pharm Bull. 2008; 31:19-26.
7. Kinjo T, Ye J, Yan H, Hamasaki T, Nakanishi H, Toh K, Nakamichi N, Kabayama S, Teruya K, Shirahata S. Suppressive effects of electrochemically reduced water on matrix metalloproteinase-2 activities and *in*

vitro invasion of human fibrosarcoma HT1080 cells. Cytotechnology. 2012; 64:357-371.

8. Saitoh Y, Okayasu H, Xiao L, Harata Y, Niwa N. Neutral pH hydrogen-enriched electrolyzed water achieves tumor-preferential clonal growth inhibition over normal cells and tumor invasion inhibition concurrently with intracellular oxidant repression. Oncol Res. 2008; 17:247-255.

9. Nakamura T, Oda H, Sato S. Effects of slightly acidic electrolyzed water on oral pathogens and human gingival fibroblasts. Jpn J Conserv Dent. 2010; 53:570-578.

10. Valentinis B, Baserga R. IGF-1 receptor signaling in transformation and differentiation. Mol Pathol. 2001; 54:133-137.

11. Adams TE, Epa VC, Garrett TP, Ward CW. Structure and function of the type 1 insulin-like growth factor receptor. Cell Mol Life Sci. 2000; 57:1050-1093.

12. Macaulay VM. Insulin-like growth factors and cancer. Br J Cancer. 1992; 65:311-320.

13. Baserga R. The insulin-like growth factor I receptor: A key to tumor growth? Cancer Res. 1995; 55:249-252.

14. Burke TW, Vuk-Pavlović S. Insulin-like growth factor-I is a serum component stimulating growth of human neuroblastoma. In Vitro Cell Dev Biol Anim. 1993; 29A:391-394.

15. Lou M, Garrett TP, McKern NM, Hoyne PA, Epa VC, Bentley JD, Lovrecz GO, Cosgrove LJ, Frenkel MJ, Ward CW. The first three domains of the insulin receptor differ structurally from the insulin-like growth factor 1 receptor in regions governing ligand specificity. Proc Natl Acad Sci U S A. 2006; 103:12429-12434.

16. Gill R, Wallach B, Verma C, Ursø B, De Wolf E, Grötzinger J, Murray-Rust J, Pitts J, Wollmer A, De Meyts P, Wood S. Engineering the C-region of human insulin-like growth factor-1: Implication for receptor binding. Protein Eng. 1996; 9:1011-1019.

Individual nursing care for the elderly among China's aging population

Jiangbo Bao[1,2], Qi Tang[3,4,*], Yingyao Chen[2]

[1] *School of Nursing, Fudan University, Shanghai, China;*
[2] *School of Public Health, Fudan University, Shanghai, China;*
[3] *Scientific Research Center, Shanghai Public Health Clinical Center, Fudan University, Shanghai, China;*
[4] *Department of Infectious Diseases, Shanghai Public Health Clinical Center, Fudan University, Shanghai, China.*

Summary　　By the end of 2014, China had an elderly population age 60 or over totaling 212 million; this group accounted for 15.5% of the country's total population of 1.37 billion, which means that China has passed the threshold for an aging population. As China's population ages and the disease spectrum changes, nursing services for the elderly must be expanded. Given differences in the health status, financial situation, and family composition of each elderly person, modern society is tending towards individual nursing care for the elderly. Adapting to the changing composition of society by age will present new challenges.

Keywords: Aging of the population, nursing care, healthcare, long-term care

Aging of the population means that a population consists of more individuals of an older age, which is typically defined using the age 65 as a cutoff. A country is considered to have an aging population when the proportion of the population age 60 over exceeds 10% of the total population or age 65 over exceeds 7% (*1*). Population aging has many important socio-economic and health consequences, including an increase in the old-age dependency ratio, which presents challenges for the fields of nursing, public health, and economic development (*2*).

1. Aging of the Chinese population

By the end of 2014, China had an elderly population age 60 or over numbering 212 million; this population accounted for 15.5% of the country's total population of 1.37 billion, which means that China has passed the threshold for an aging population (*3*). According to data from the United Nations, the world's elderly population grew at an average rate of 2.5% from 1990-2010, while China's elderly population grew at an average rate of 3.3% (*4*). According to the World Health Organization, 35% of China's total population will be over the age of 60, making China the world's most elderly society in 2050 (*5*).

2. Nursing needs of the elderly

The elderly have greater nursing needs because they are primarily a population with common chronic conditions and geriatric diseases, such as diabetes, dementia, cardiopathy, cerebrovascular disease, and respiratory disease (Figure 1) (*1,6,7*). The prevalence of chronic conditions in the elderly is 4.2 times that in the population as a whole, and each elderly person usually has 2-3 different conditions (*8*).

According to data from the China Health and Family Planning Statistical Yearbook 2016, the prevalence of hypertension among the elderly age 60 or over was six times that of citizens ages 18-44 and twice that of citizens ages 45-59 (Figure 2). In addition, the elderly had a high mortality from different tumors, and lung cancer in particular (Figure 3).

An increasing number of elderly patients have common chronic conditions and geriatric diseases. In contrast, patients with intractable and rare diseases such as HIV, fragile X syndrome, and Allan-Herndon-Dudley syndrome are gradually aging (*9,10*).

As China's population ages and the disease
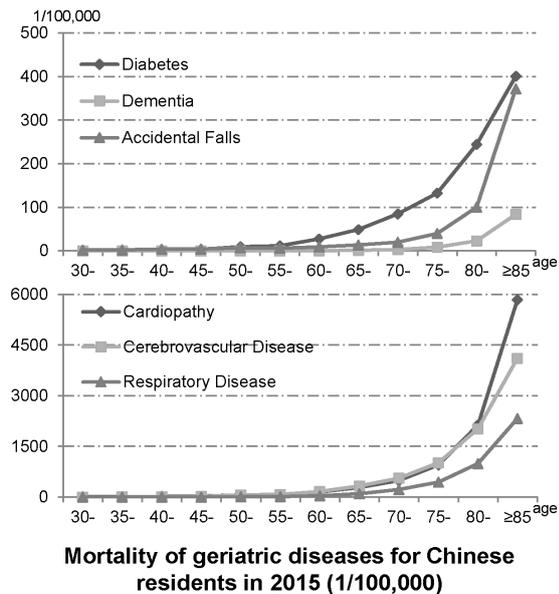
Figure 1. Mortality from geriatric diseases for Chinese citizens in 2015. The elderly had a high mortality from geriatric diseases, and particularly from cardiopathy, cerebrovascular disease, and respiratory disease.
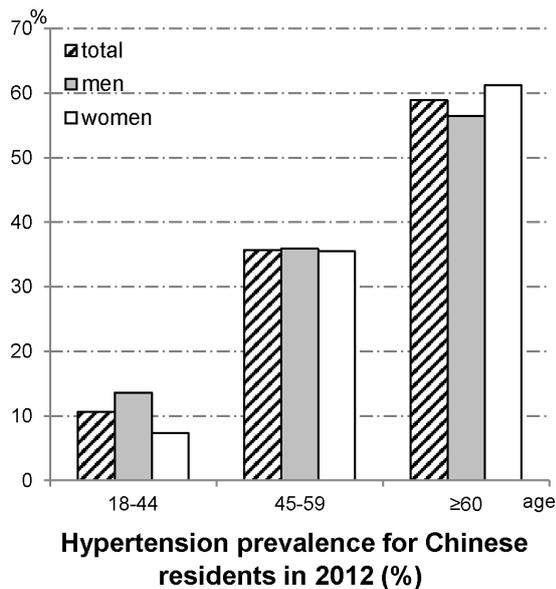
Figure 2. Prevalence of hypertension among Chinese citizens in 2012. The prevalence of hypertension among the elderly age 60 or over was 6 times that of citizens ages 18-44 and twice that of citizens ages 45-59.

Figure 3. Mortality from different malignancies for Chinese citizens in 2015. The elderly have a high mortality from tumors, and lung cancer in particular.

spectrum changes, nursing services for the elderly must be expanded. How should geriatric nursing adeptly respond to these challenges is a significant concern.

3. Individual nursing care for the elderly

When birthrate and mortality trends have been fairly regular over time, population growth is positively correlated with age, which implies that if the population

age 65 or over is increasing, then the proportion age 80 or over is also increasing (*11*). The health status, financial situation, and family composition of 65-year-olds and 80-year-olds vary greatly, so healthcare and nursing care should also vary from person to person. Modern society is tending towards individual nursing care for the elderly. Adapting to the changing composition of society by age will present new challenges.

Health status. The first challenge concerns expanded nursing services for individual elderly with a different health status; tailored services are not easily provided by social support systems (*12*). Elderly individuals with a different health status need a corresponding level of nursing. Elderly who are relatively healthy may need little help, elderly with some health problems may need some care, and elderly with severe health problems may be unable to care for themselves. However, individual nursing care for the elderly has not been implemented in China because of faults in disease prevention among healthy elderly and a lack of nursing care for elderly who are unable to care for themselves. At present, care is still focused on individuals who are ill.

Financial situation. As the prevalence of disability, frailty, and chronic diseases increases dramatically, the burden of disease will become a key issue for the elderly and their families (*13*). Given the need for regular insurance when healthy and medical insurance in the event of illness, China needs to have long-term care insurance for individuals who are unable of caring for themselves.

Family composition. The families of elderly individuals in China differ and vary in terms of their composition; this is mainly evident from where the elderly live (*14*). Compared to the elderly who live with

their children, the elderly who live alone have more complicated and more difficult issues of healthcare and nursing care. As the population ages, nursing care for the elderly who live alone will pose an enormous social burden in the future.

On the positive side, the health status of older people of a given age is improving over time thanks to societal and medical advances. Over time, better health will significantly reduce the effort needed to provide individual nursing care for the elderly as China's population ages.

References

1. Deeg DJ. Handbook of Aging and the Social Sciences. Int J Epidemiol. 2016; 45:1302-1303.
2. Song P, Chen Y. Public policy response, aging in place, and big data platforms: Creating an effective collaborative system to cope with aging of the population. Biosci Trends. 2015; 9:1-6.
3. National Health and Family Planning Commission of PRC. China Health and Family Planning Statistical Yearbook. 2016.
4. United Nations. 2015 Revision of World Population Prospects. 2015. *https://esa.un.org/unpd/wpp/Publications/Files/WPP2015_Methodology.pdf* (accessed October 24, 2017).
5. World Health Organization. Global Health and Aging. 2011. *https://www.nia.nih.gov/sites/default/files/global_health_and_aging.pdf* (accessed October 19, 2017).
6. Tang Q, Song P, Xu L. The Government's role in regulating, coordinating, and standardizing the response to Alzheimer's disease: Anticipated international cooperation in the area of intractable and rare diseases. Intractable Rare Dis Res. 2016; 5:238-243.
7. Ipek E, Demirelli S, Ermis E, Inci S. Sarcoidosis and the heart: A review of the literature. Intractable Rare Dis Res. 2015; 4:170-180.
8. Liu JF, Chen Z, Yang FK, He XP, Chen W, Deng S. The current situation and coping strategies of chronic diseases for the elderly in China. China & Foreign Medical Treatment. 2014; 23:194-198. (in Chinese)
9. Jin X, Chen L. Fragile X syndrome as a rare disease in China – Therapeutic challenges and opportunities. Intractable Rare Dis Res. 2015; 4:39-48.
10. Shimojima K, Maruyama K2, Kikuchi M, Imai A, Inoue K, Yamamoto T. Novel SLC16A2 mutations in patients with Allan-Herndon-Dudley syndrome. Intractable Rare Dis Res. 2016; 5:214-217.
11. Gavrilov LA, Heuveline P. Aging of population. In The Encyclopedia of Population ed. by Paul Demeny and Geoffrey McNicoll. 2003; 1:32-37.
12. Zeng Y, Feng Q, Hesketh T, Christensen K, Vaupel JW. Survival, disabilities in activities of daily living, and physical and cognitive functioning among the oldest-old in China: A cohort study. Lancet. 2017; 389:1619-1629.
13. Kim J, Lee E, Kim S, Lee TJ. Economic burden of osteoporotic fracture of the elderly in South Korea: A national survey. Value Health Reg Issues. 2016; 9:36-41.
14. Zeng Y, Hesketh T. The effects of China's universal two-child policy. Lancet. 2016; 388:1930-1938.

Communication

The effects of health education and promotion with regard to severe fever with thrombocytopenia syndrome (SFTS) in rural residents: A pilot study in China

Yuyan Wu[1], Guiming Fu[1], Song Guo[1], Ling Ye[2], Juan Hou[1], Jinna Wang[1], Zhenyu Gong[1,*]

[1] *Zhejiang Provincial Center for Disease Control and Prevention, Hangzhou, Zhejiang, China;*
[2] *Daishan County Center for Disease Control and Prevention, Daishan, Zhoushan, Zhejiang, China.*

Summary	Severe fever with thrombocytopenia syndrome (SFTS) has spread throughout Asia, including China, South Korea, and Japan. In China, the main victims of SFTS were farmers. Measures to protect farmers were urgently needed but limited, and health education and promotion was proposed as an option. A pilot community trial was conducted to provide health education about SFTS in 2013 in Daishan County, Zhejiang Province, China, and results indicated that health education had promise. An educational campaign was conducted for three years. The incidence of SFTS decreased 0.3 per 1,000 person-years, and rural residents' awareness of SFTS increased substantially. Numerous habits or work practices that increased the likelihood of tick bites have also been changed. In the future, education could emphasize adopting healthy habits or work practices to reduce tick bites and thus reduce the incidence of SFTS, like regularly weeding around a house surrounded by shrubs, not sitting or lying on the ground when resting, and protecting one's self when doing farm work.

Keywords: Severe fever with thrombocytopenia syndrome, health education, China

1. Introduction

Severe fever with thrombocytopenia syndrome (SFTS) is an emerging infectious disease caused by a novel bunyavirus; SFTS was first reported in central China in 2009, and the virus that causes it was first discovered in 2011 (*1,2*). Since then, SFTS cases have been reported in many countries, like South Korea, Japan, and the US (*3-5*). Prior to 2013, there were as many as 10,000 SFTS cases worldwide (*6*). In China, SFTS was mainly found in Henan, Hubei, Shandong, Jiangsu, Zhejiang, and Liaoning, with an average case fatality rate of 12% that rose to 30% in some areas (*7,8*). In Zhejiang Province, SFTS was first discovered in 2011, and dozens of SFTS cases have been reported every year since (data not published). Without vaccines or specific drugs to prevent

or treat SFTS, the condition has become an increasingly concerning global health threat (*1*).

The risk factors for infection with SFTS are varied (*9*). SFTS is believed to be transmitted by ticks, and most SFTS cases have involved tick bites (*2,10-13*). Moreover, most cases involved farmers living in villages or working in the fields (*1*). In Zhejiang Province, farmers were reported to account for 92% of all SFTS cases between 2011 and 2013 (*14*). Most patients with SFTS had fed or come in contact with livestock like cows and sheep or animals like dogs (*15-17*). In other words, traditional farming practices in China are likely to involve contact with ticks, and some habits or work practices might lead Chinese farmers to be victims of SFTS. However, farmers in China usually have a low level of education, a limited range of activity, and limited ways to learn about protecting themselves from against SFTS. Thus, measures need to be taken to inform farmers know SFTS, how to protect themselves from tick bites, and how to prevent SFTS. Nonetheless, systematic health education and promotion for primary prevention of SFTS is rare in China, and the same holds true for evaluation of the effects of that health education.

Since 2013, a pilot health education and promotion

program has been conducted to teach about SFTS in select towns west and south of Daishan County since SFTS cases were reported in that area. Health education and promotion was provided in Daishan every year and it mainly included specialized lectures, educational information (illustrated brochures) on SFTS, public notices on SFTS, posters, and messages in WeChat (a very popular social media app in China). Three years have passed, and the effects of that health education have not been determined. Thus, the current study randomly chose one village where the program was conducted and another village with comparable characteristics like geography, environment, and incidence of SFTS where the program has not been conducted. One aim of this study was to evaluate changes in knowledge of and attitudes towards SFTS and practices with regard to SFTS after 3 years of education. A second aim was to examine habits or work practices that could help to reduce tick bites and thus reduce the incidence of SFTS.

2. Study sites and survey methodology

This study was conducted in November 2016 (about two months after the last educational session) in Daishan county, Zhejiang Province, China. The Village of Gaoting Zhakouere (denoted here simply as Gaoting) where the educational program was conducted served as the study group, and the Village of Daidong Longtou (denoted here simply as Daidong) served as the control group. Gaoting is south of the City of Daishan and has a total population of 1,560, while Daidong is northeast of the city and has a population of 2,610. Both places are close to the hills. From January 2012 to December 2013, there were 3 SFTS cases in Gaoting and 3 in Daidong. Gaoting is at a latitude of 30°17'26.24", a longitude of 122°11'59.57", and an altitude of 2 meters; Daidong is at a latitude of 30°14'55.86", a longitude of 122°11'28.20", and an altitude of 3 meters. The density of ticks in Gaoting and Daidong was comparable from 2013 to 2016 (data not published). Since 2013, a total of 5,000 pieces of educational information were sent to residents, 10 lectures were conducted, 2 specials aired on TV, and 8 public notices and 12 posters were posted in Gaoting. Ten physicians were trained to provide professional advice when they were consulted. These physicians were stationed in three general hospitals in the City of Daishan and one community health service center in Gaoting.

A unified questionnaire was used in both Gaoting and Daidong and stratified random sampling was used. Both villages (Gaoting and Daidong) were quartered (east, south, west, and north). Forty families were randomly chosen from each quarter according to their address, and one family member (above the age of 12) in each chosen family was asked to consent to participate in this study. Thus, respondents were 320 families in total.

SFTS cases reported in the two villages between January 2014 and November 2016 were tallied.

Data were compiled and analyzed using the statistical software IBM SPSS 16.0 and MS Excel. Selected variables like sex, frequency of farming, location of the house, and occupation were compared between Gaotiong and Daidong using chi-square tests of independence. Odds ratios were calculated to determine association, and 95% confidence intervals were calculated for these odds ratios. P values less than 0.05 were considered significant.

This study was approved by the Zhejiang Provincial Center for Disease Control and Prevention, China.

3. The effects of health education about SFTS

Differences in knowledge, attitudes, and practices (KAP) were analyzed using 306 questionnaires, representing a total response rate of 95.63% (306/320). In Gaoting, 150 families responded to the questionnaire, for a response rate of 93.75% (150/160), while the response rate was 97.50% (156/160) in Daidong. There were no significant differences in sex, age, or occupation of respondents in Gaoting and Daidong ($x^2 = 0.04$, $p = 0.84$, $t = 3.08$, $p = 0.20$, and Fisher's $p = 0.16$, respectively).

Results indicated that the educational campaign since 2013 had substantially increased the public's awareness of SFTS and it had changed many habits that increased susceptibility to tick bites. In Gaoting, 83.33% (125/150) of respondents knew about SFTS; 129 respondents thought ticks could transmit diseases, and 107 of those respondents were aware that SFTS could be transmitted by tick bites. In Daidong, 32.05% (50/156) of respondents knew about SFTS. Only 6 people were aware that SFTS could be transmitted by tick bites (Table 1).

Based on the current results, people in Gaoting were more likely to go to the hospital to receive routine treatment when they were bitten by a tick (57/150) than people in Daidong (25/156) ($x^2 = 18.82$, $p < 0.001$) (Table 1). In Gaoting, 14 families raised animals (including dogs, cats, livestock, and poultry), and 9 (64.29%) of those families raised them in pens. In Daidong, 60.34% (35/58) of families raised animals in pens. Of the families that raised animals, 34.72% (25/72) had seen ticks on animals. However, 78.57% (11/14) of families in Gaoting and 24.14% (14/58) in Daidong regularly killed ticks. Eighty-five-point-nine percent (97/114) of responding farmers in Gaoting and 17.56% (23/131) in Daidong responded that they take measures to protect themselves while farming ($x^2 = 111.2$, $p < 0.001$) (Table 1).

From January 2014 to November 2016, a total of 3 SFTS cases were confirmed, with an incidence density of 0.66 per 1,000 person-years. The incidence density before health education was 0.96 per 1,000 person-years, and the attributable risk (AR) was 0.30 per 1,000 person-years. Based on these findings, health education about SFTS reduced the incidence of SFTS 0.30 per 1,000 person-years.

4. Risk factors related to tick bites

SFTS is mainly transmitted by ticks. Tick bites are the intermediate link in SFTS transmission. Thus, blocking the route of transmission (avoiding being bitten by ticks) would effectively reduce the incidence of SFTS.

There were few SFTS cases in one small village, so tick bites were chosen as an outcome variable. The aim was to analyze which habits or work practices might be risk factors for tick bites that could lead to SFTS. Results indicated that 35.90% (56/156) of people in Daidong had been bitten by ticks. One hundred and fifty-one

Table 1. Comparison of knowledge about SFTS in Gaoting and Daidong

Items	n	Awareness rate (%)	n	Awareness rate (%)	p value
Knowledge					
Will people get ill if bitten by a tick?: yes	127	84.67	27	17.31	< 0.001
Can ticks transmit disease?: yes	129	86.00	18	11.54	< 0.001
Have you heard of SFTS?: yes	125	83.33	50	32.05	< 0.001
Which of these vectors can transmit SFTS? Ticks, fluids from patients (true)	107	71.33	6	3.85	< 0.001
Attitudes & practices					
What would you do if bitten by a tick? Go to the hospital for routine treatment and then be followed by medical personnel for two weeks (true)	57	38	25	16.03	< 0.001
Avoid contact with wild animals	23	15.33	21	13.46	0.64
Percentage of respondents who regularly weed around the house	–	85.92	–	62.07	0.014
Percentage of respondents who raise animals in pens	–	64.29	–	60.34	0.79
Percentage of respondents who regularly kill ticks on animals	–	78.57	–	24.14	< 0.001
Percentage of respondents who refrain from sitting or lying on the ground when resting	–	78.95	–	15.27	< 0.001
Percentage of respondents who use protection before doing farm work	–	85.09	–	17.56	< 0.001

Table 2. Risk factors related to tick bites

Items	Items	History of tick bites		OR	95% CI
		Ever been bitten	Never been bitten		
Occupation	farmer	49	78	1.53	0.59-3.95
	non-farmer	7	17		
Location of fields[a,*]	hillsides	7	6	2.00	0.63-6.35
	low lands	42	72		
Frequency of farm work[a,*]	≥ once a day	4	5	1.87	0.41-8.61
	< once a month	9	21		
	≥ once a week	27	40	1.58	0.63-3.96
	< once a month	9	21		
	≥ once a month	40	57	1.64	0.68-3.95
	< once a month	9	21		
Will people get ill if bitten by a tick?[*,#]	yes	5	22	0.17	0.04-0.72
	no	8	6		
Can ticks transmit diseases?[*,#]	yes	4	13	0.41	0.09-1.92
	no	6	8		
Location of your house[*]	in the middle of the village	37	84	0.26	0.11-0.59
	on a hillside	19	11		
Are there any shrubs around your house?[*]	yes	12	17	1.23	0.53-2.79
	no	44	76		
Do you regularly weed the shrubs around your house?[b,*]	yes	3	15	0.04	0.01-0.32
	no	9	2		
Do you raise animals?	yes	25	32	1.59	0.81-3.13
	no	31	63		
Do you regularly kill ticks?[c,*]	yes	4	9	0.44	0.12-1.70
	no	19	19		
What would you do if you saw a wild animal?	Stay away from it	4	17	0.35	0.11-1.11
	Catch or kill it	52	78		
What posture do you adopt when taking breaks from farm work?[a,*]	Stand	3	17	0.24	0.07-0.88
	Sit/lie on the ground	43	59		
Did you take measures to protect yourself before doing farm work?[a,*]	yes	4	19	0.28	0.09-0.87
	no	45	59		

[*]: Missing responses to this question were excluded. [#]: Respondents who answered "I don't remember/have no idea" to this question were excluded from analysis. [a]: The odds ratio was calculated based on 127 farmers. [b]: The odds ratio was calculated based on families whose houses were surrounded by shrubs. [c]: The odds ratio was calculated based on families who raised animals.

of the respondents in Daidong were divided into two groups depending on whether they had or had not been bitten by a tick during their lifetime. The remaining 5 respondents were excluded because of missing responses or because they were unable to recall if they had ever been bitten. As shown in Table 2, the risk factors related to tick bites were not knowing whether people would get sick if bitten by a tick, not regularly weeding around the house, resting on the ground while farming, and not taking measures to one's self while doing farm work. Knowing that people will get sick if bitten by a tick, regularly weeding around a house surrounded by shrubs, not sitting or lying on the ground when resting, and protecting one's self before doing farm work could significantly reduce the incidence of tick bites (Table 2).

5. Health education of rural residents as an effective way to help reduce the risk of SFTS

SFTS is a zoonotic disease transmitted by ticks. Elimination of its vectors (ticks) and changes in people's habits or work practices to avoid contact with ticks or patients are believed to be effective ways to prevent SFTS. Tick control has been a topic for almost half a century, and numerous problems with safety and resistance have occurred because of the use of chemical insecticides (*18-22*). Killing every tick is not feasible, but bad habits can be changed to avoid contact with ticks while controlling the density of ticks to an acceptable level. The current authors are devoted to discovering new environmentally friendly insecticides to control ticks, but before those discoveries are made the only effective way to help prevent SFTS is through health education.

Based on recent studies, health education about SFTS has promise as a way to improve rural residents' awareness of SFTS and to change habits or work practices to reduce the risk of SFTS. Health education has reduced the incidence of SFTS 0.3 per 1,000 person-years in Gaoting in the City of Daishan, China. The current study involved a case control study to examine habits or work practices that might be risk factors for tick bites. In this study, knowing that people will get sick if bitten by a tick, regularly weeding around a house surrounded by shrubs, not sitting or lying on the ground when resting, and protecting one's self before doing farm work were effective at reducing tick bites and thus to reducing the incidence of SFTS. However, this was a pilot study, and its sample size was limited. Further studies need to be conducted to confirm the value of these habits or work practices, which could then be stressed in future educational campaigns. In the future, improved forms of health education could be provided, like widespread health education in school that in turn results in "children teaching adults" about diseases like rabies or AIDS.

References

1. Li D. A highly pathogenic new bunyavirus emerged in China. Emerg Microbes Infect. 2013; 2:e1.
2. Yu XJ, Liang MF, Zhang SY, *et al*. Fever with thrombocytopenia associated with a novel bunya virus in China. N Engl J of Med. 2011; 364:1523-1532.
3. Kim KH, Yi J, Kim G, Choi SJ, Jun KI, Kim NH, Choe PG, Kim NJ, Lee JK, Oh MD. Severe fever with thrombocytopenia syndrome, South Korea, 2012. Emerg Infect Dis. 2013; 19:1892-1894.
4. Takahashi T, Maeda K, Suzuki T, *et al*. The first identification and retrospective study of Severe Fever with Thrombocytopenia Syndrome in Japan. J Infect Dis. 2014; 209:816-827.
5. Yoshikawa T, Fukushi S, Tani H, *et al*. Sensitive and specific PCR systems for detection of both Chinese and Japanese severe fever with thrombocytopenia syndrome virus strains and prediction of patient survival based on viral load. J Clin Microbiol. 2014; 52:3325-3333.
6. Xing Z, Schefers J, Schwabenlander M, Jiao Y, Liang M, Qi X, Li C, Goyal S, Cardona CJ, Wu X, Zhang Z, Li D, Collins J, Murtaugh MP. Novel bunya virus in domestic and captive farmed animals, Minnesota, USA. Emerg Infect Dis. 2013; 19:1487-1489.
7. Ding F, Zhang W, Wang L, Hu W, Soares Magalhaes RJ, Sun H, Zhou H, Sha S, Li S, Liu Q, Li Q, Yang W, Huang L, Li C, Yin W. Epidemiologic features of severe fever with thrombocytopenia syndrome in China, 2011-2012. Clin Infect Dis. 2013; 56:1682-1683.
8. Liu Y, Li Q, Hu W, Wu J, Wang Y, Mei L, Walker DH, Ren J, Wang Y, Yu XJ. Person-to-person transmission of severe fever with thrombocytopenia syndrome virus. Vector Borne Zoonotic Dis. 2012; 12:156-160.
9. Xing X, Guan X, Liu L, *et al*. A case-control study of risk sources for severe fever with thrombocytopenia syndrome in Hubei Province, China. Int J Infect Dis. 2017; 55:86-91.
10. Jiang XL, Wang XJ, Li JD. Severe fever with thrombocytopenia syndrome bunya virus isolation and identification of domestic animals. Chinese Journal of Virology. 2012; 28:252-257. (in Chinese)
11. Liu Y, Huang XY, Du YH. Survey on ticks and detection of new bunyavirus in the endemic areas of fever thrombocytopenia and leukopenia syndrome in Henan Province. Chinese Journal of Preventive Medicine. 2012; 46:500-504. (in Chinese)
12. Zhang WH, Zeng XY, Zhou MH. Seroepidemiology of severe fever with thrombocytopenia syndrome bunyavirus in Jiangsu Province. Disease Surveillance. 2011; 26:676-678. (in Chinese)
13. Song LH, Qi S, Pang W. Analysis of the epidemiology of severe fever with thrombocytopenia syndrome in the City of Dalian. Journal of Medical Pest Control. 2012;

28:1325-1327. (in Chinese)

14. Sun J, Chai C, Lv H, Lin J, Wang C, Chen E, Zhang Y, Chen Z, Liu S, Gong Z, Jiang J. Epidemiological characteristics of severe fever with thrombocytopenia syndrome in Zhejiang Province, China. Int J Infect Dis. 2014; 25:180-185.

15. Chai CL, Sun JM, Lin JF, Shi XG. Analysis on clinical and epidemiological characteristics of severe fever with thrombocytopenia syndrome in Zhejiang Province. Chinese Journal of Preventive Medicine. 2012; 13:904-907. (in Chinese)

16. Hu BS, Hu HP. Analysis of the epidemiological features of severe fever with thrombocytopenia syndrome in 77 cases. Chinese Journal of Preventive Medicine . 2014; 15:601-603. (in Chinese)

17. Ma T, Sun JM, Shi XG. Research advances on epidemiology of severe fever with thrombocytopenia syndrome. Chinese Journal of Vector Biology & Control. 2015; 26:327-329. (in Chinese)

18. Alavanja MC, Hoppin JA, Kamel F. Health effects of chronic pesticide exposure: Cancer and neurotoxicity. Annu Rev Publ Health. 2004; 25:155-197.

19. Daniels JL, Olshan AF, Savitz DA. Pesticides and childhood cancers. Environ Health Persp. 1997; 105:1068-1077.

20. Rosas LG, Eskenazi B. Pesticides and child neurodevelopment. Curr Opin Pediatr. 2008; 20:191-197.

21. Castro-Janer E, Martins JR, Mendes MC, Namindome A, Klafke GM, Schumaker TT. Diagnoses of fipronil resistance in Brazilian cattle ticks (Rhipicephalus (Boophilus) microplus) using in vitro larval bioassays. Vet Parasitol. 2010; 173:300-306.

22. Freitas Ede P, Zapata MT, Fernandes Fde F. Monitoring of resistance or susceptibility of adults and larvae of Amblyomma cajennense (Acari: Ixodidae) to synthetic acaricides in Goiás, Brazil. Exp Appl Acarol. 2011; 53:189-202.

Communication

Competency and challenges in malaria microscopy in China

Jianhai Yin, He Yan, Mei Li, Yao Ruan, Xueqiang Zhang, Liying Wang, Cunli Cao, Zhigui Xia, Shuisen Zhou[*]

National Institute of Parasitic Diseases, Chinese Center for Disease Control and Prevention, WHO Collaborating Centre for Tropical Diseases, National Center for International Research on Tropical Diseases, Ministry of Sciences and Technology, Key Laboratory of Parasite and Vector Biology, Ministry of Health, Shanghai, China.

Summary	Precise diagnosis is a key measure for malaria control and elimination, and malaria microscopy is still the gold standard method recommended by the World Health Organization (WHO) for malaria diagnosis. Analysis of the competency in malaria microscopy in China will benefit to identify the challenges in this skill and provide some suggestions for improvement in order to reach the requirement of WHO procedures for certification of malaria elimination, and finally contribute to malaria elimination by 2020 in China. According to a series of external assessment activities about malaria microscopy, malaria microscopists from both the national and provincial level but not the levels below provincial level performed quite well in *Plasmodium spp* identification, but their competency in differentiation of *P. ovale* and *P. vivax* and parasite counting by microscopy were not good enough at all levels. Therefore, it is necessary to strengthen the competency in species identification and parasite counting especially at the lower levels in the first line through training and practice as well as regular quality assurance with enough policy support.

Keywords: Malaria microscopy, species identification, parasite counting, quality assurance

1. Introduction

The annual incidence rate of indigenous malaria in China is decreasing, but malaria is still a very significant health problem, especially the importation of malaria has been an important challenge against malaria elimination in this country (*1,2*). Precise and prompt laboratory diagnosis and appropriate treatment is a key strategy to control and eliminate malaria. There are many limitations such as low sensitivity within the detection limit, poor specificity due to morphological changes that are enhanced by staining and similarities between several parasites, and operator dependence because even highly qualified microscopists can make an incorrect or incomplete assessment of the *Plasmodium spp*. A variety of diagnostic methods are used for *Plasmodium* parasites identification and speciation. However, malaria microscopy on Giemsa-stained thick and thin blood smears with species identification and parasite counting is still the gold standard method recommended by the World Health Organization (WHO) for malaria diagnosis, clinical trials efficacy evaluation and epidemiological surveys. Moreover, qualified microscopy competency is a major indicator of WHO procedures for certification of malaria elimination (*3*).

However, it is difficult to maintain competency in malaria microscopy with the rapid decline of indigenous malaria cases, especially in first line clinics, due to its complexity and time-consuming and inconsistency of results compared with other diagnostic assays such as rapid diagnostic tests (RDT) and polymerase chain reactions (PCR) (*4-6*). It is also potentially due to the lack of fiscal and personnel investments in malaria microscopy (*7*).

Therefore, the China malaria diagnosis reference laboratory network (*8*) based on centres for disease control and prevention or institutes of parasitic diseases at different levels covering all 24 historical malaria-endemic provinces has been set up. It performs

*Address correspondence to:
Dr. Shuisen Zhou, National Institute of Parasitic Diseases, Chinese Center for Disease Control and Prevention, WHO Collaborating Centre for Tropical Diseases, National Center for International Research on Tropical Diseases, Ministry of Sciences and Technology, Key Laboratory of Parasite and Vector Biology, Ministry of Health, Shanghai 200025, China.
E-mail: shuisenzhou@126.com

Table 1. Results of malaria microscopy in EQAs, 2013-2015

Scoring	Identification of species						Quantification of parasite counts					
	2013-1	2013-2	2014-1	2014-2	2015-1	2015-2	2013-1	2013-2	2014-1	2014-2	2015-1	2015-2
Win	39	43	42	42	42	42	11	9	15	16	16	14
Lose	6	2	3	3	3	0	4	9	0	2	2	4
Total	45	45	45	45	45	42	15	18	15	18	18	18

EQA, External Quality Assessment.

quality assurance to guarantee and maintain the performance of diagnostic assays including malaria microscopy in clinics and in the field. Meanwhile, China participates in different external assessment activities about malaria microscopy organized by WHO. In addition, competency in malaria microscopy at different administrative levels was expected to improve through systematic training before technique competitions for malaria parasite detection (*9*). Above all, a comprehensive analysis of the competency in malaria microscopy in China can help us identify the challenges in this skill and provide some suggestions for improvement, and contribute to the achievement of malaria elimination by 2020 in China.

2. Competency in malaria microscopy

First of all, three rounds of External Competency Assessment (ECA) of malaria microscopists were held in China organized by WHO by 2015. Microscopists (35 person-times) from the malaria endemic provinces including Anhui, Yunnan, Henan, Hubei, Hainan, Jiangsu, Sichuan, Shanghai, Guangxi, Fujian and National Institute of Parasitic Diseases (NIPD) in the year 2010; Yunnan, Anhui, Jiangsu, Henan, Hainan, Shanghai, Shandong, Guizhou, Guangxi and NIPD in the year 2012; and Yunnan, Jiangsu, Sichuan, Henan, Guangxi, Shanghai, Fujian, Guizhou, Shandong, Anhui, Tengchong of Yunnan and NIPD in the year 2015, were assessed through a scheduled examination of *Plasmodium spp* identification and parasite counting respectively. Overall, their performance was generally good ($\chi^2 = 2.520$, $p = 0.112$). In detail, there was one microscopist ranked in Level 1, seven Level 2 and four Level 3 in 2010; five Level 1, four Level 2 and two Level 3 in 2012; and eight Level 1, two Level 2 and two Level 4 in 2015. And five microscopists were assessed repeatedly, and two of them raised their competency from level 2 to level 1 and the other three remained the same (two remained level 1, one remained level 2).

Moreover, two rounds of External Quality Assessment (EQA) Programme for malaria microscopy (*10*) in NIPD each year were also organized by WHO during 2013 and 2015, 15 slides were included per round, totally covering 34 slides of *P. falciparum*, 23 slides of *P. vivax*, 3 slides each of P. malariae and *P. knowlesi*, 2 slides of *P. ovale* and 25 negative slides.

As a result, all the *P. falciparum*-positive slides and negative slides were identified correctly, while 3 slides of *P. vivax*-positve were misdiagnosed as *P. ovale*, one slide of *P. malariae*-positive was misdiagnosed as *P. knowlesi*, one *P. knowlesi*-positive was misdiagnosed as *P. ovale*, one *P. knowlesi*-positive and one *P. ovale*-positive as *P. vivax* (Table 1). As a result, no significance was found in the identification of species ($\chi^2 = 2.217$, $p = 0.330$), while parasite counting was statistically different among these three years ($\chi^2 = 13.665$, $p = 0.001$): 2014 was better than 2013 ($\chi^2 = 8.627$, $p = 0.003$), no difference in 2015 *vs.* 2013 ($\chi^2 = 3.391$, $p = 0.066$) and 2015 *vs.* 2014 ($\chi^2 = 0.996$, $p = 0.318$).

Since then, a national competency assessment programme concerning *Plasmodium spp* identification only has been organized by national laboratory (*8*). Briefly, nineteen microscopists from 19 provincial malaria diagnosis laboratories took part in the activity. Only two participants correctly identified all 20 slides, seven failed in one slide, six incorrectly identified two slides, two individuals failed in three slides, and one each incorrectly identified four and six slides, respectively. Particularly, twelve participants identified the *P. vivax*-positive slide as *P. ovale*. There existed a *P. ovale* positive slide that was the most difficult one for participants with nine failing to identify it with most of them (6/9) incorrectly identifying it as *P. vivax*.

Last but not least, malaria microscopy including blood slide preparation and *Plasmodium spp* identification and parasite counting is a very important part of National technique competition for diagnosis of parasitic diseases carried out in China, four representatives working for disease control and prevention at different levels were selected as contestants (age < 45 and at least two contestants from county-level) per province every year with no duplicates in the entries between years. Although a quite good performance was found in every year, the competency in malaria microscopy was not good enough (Table 2). There was significance of performance in blood film preparation (F = 17.3, $p < 0.01$) and malaria microscopy on the whole (F = 4.5, $p < 0.01$) from 2011 to 2015 (Table 2). Moreover, malaria parasite identification of *P. falciparum* (F = 14.2, $p < 0.01$) and *P. vivax* (F = 3.4, $p < 0.01$) were also different among these five competitions (Table 2). Additionally, *P. ovale*-positive slides were added into the competition from the

Table 2. Comparison of malaria microscopy in the national competitions, 2011-2015

Content	2011	2012	2013	2014	2015	*F* value	*p* value
Blood film preparation							
(mean ± SD)	86.9 ± 10.4	87.3 ± 9.2	90.8 ± 9.7	94.4 ± 4.0	91.0 ± 6.2	17.3	< 0.01
Malaria microscopy							
(mean ± SD)	44.3 ± 22.0	53.4 ± 25.4	56.8 ± 24.7	52.9 ± 23.1	54.1 ± 26.1	4.5	< 0.01
Parasite identification							
(detection rate, %)							
P. falciparum	55.3	67.8	62.1	64.5	61.1	14.2	< 0.01
P. vivax	73.9	62.6	68.8	79.0	65.3	3.4	< 0.01

year 2014, and there was no difference in performance between 2014 (36.3%) and 2015 (47.6%).

3. Challenges and prospects

Various assessment activities and competitions not only implement the quality assurance for malaria microscopy, but also are good models to be used as training courses to improve the competency of microscopists.

Although the competency for *Plasmodium spp* identification was quite good at both national and provincial levels according to the results of WHO ECA, EQA Programme and National Competency Assessment Programme referred to above, it was still difficult to differentiate *P. ovale* from *P. vivax*. This may be attributed to the morphologic similarity between them (*11*) or because of only sporadic ovale malaria cases in China (*12,13*). However, ovale malaria cases have increased in China due to travellers returning from endemic areas (*1,2*). In addition, it was also not good enough in parasite counting at these two levels, but malaria parasite density is critical for patient management especially when parasite resistance to available therapy is increasing and particularly in clinical trials and drug efficacy studies.

Meanwhile, the competency in *Plasmodium spp* identification and parasite counting by microscopy at levels below the provincial level was lower nationally. To some extent, differences in competency between endemic and non-endemic provinces had an impact on the overall level (*9,14*). It also may be attributed to less opportunity to detect malaria cases with the reduction in local cases, or because several much simpler and rapid diagnostic assays were used instead of malaria microscopy (*4*). While microscopists at county level are the main health workers for malaria control and prevention as the first line, their deficiency in malaria diagnosis will be a big challenge for malaria elimination.

Therefore, certified microscopists should receive more training courses as well as be invited as teachers in training malaria microscopy as a first line with strong policy supports, but it must pay much more attention to the identification of rare malaria parasites in China. Moreover, other diagnostic tools such as nucleic acid amplification with high sensitivity and specificity should

be considered in routine malaria diagnosis, especially because of its advantages in detecting asymptomatic infections. In addition, quality assurance of malaria diagnosis must be carried out regularly.

Acknowledgements

References

1. Feng J, Xiao H, Xia Z, Zhang L, Xiao N. Analysis of malaria epidemiological characteristics in the People's Republic of China, 2004-2013. Am J Trop Med Hyg. 2015; 93:293-299.
2. Yin JH, Yang MN, Zhou SS, Wang Y, Feng J, Xia ZG. Changing malaria transmission and implications in China towards National Malaria Elimination Programme between 2010 and 2012. PloS One. 2013; 8:e74228.
3. World Health Organization. WHO procedures for certification of malaria elimination. Wkly Epidemiol Rec. 2014; 89:321-325.
4. Hawkes M, Kain KC. Advances in malaria diagnosis. Expert Rev Anti Infect Ther. 2007; 5:485-495.
5. Proux S, Suwanarusk R, Barends M, Zwang J, Price RN, Leimanis M, Kiricharoen L, Laochan N, Russell B, Nosten F, Snounou G. Considerations on the use of nucleic acid-based amplification for malaria parasite detection. Malaria J. 2011; 10:323.
6. Snounou G, Viriyakosol S, Zhu XP, Jarra W, Pinheiro L, do Rosario VE, Thaithong S, Brown KN. High sensitivity of detection of human malaria parasites by the use of nested polymerase chain reaction. Mol Biochem Parasitol. 1993; 61:315-320.
7. Johnston SP, Pieniazek NJ, Xayavong MV, Slemenda SB, Wilkins PP, da Silva AJ. PCR as a confirmatory technique for laboratory diagnosis of malaria. J Clin Microbiol. 2006; 44:1087-1089.
8. Yin JH, Yan H, Huang F, Li M, Xiao HH, Zhou SS, Xia ZG. Establishing a China malaria diagnosis reference laboratory network for malaria elimination. Malaria J. 2015; 14:40.
9. Fu Q, Li SZ, Wang Q, Zhang L, Liu W, Zheng X, Zhang SS, Xia ZG, Zhou SS, Chen Z, Wang LY, Zhou XN. Report of analysis of National Technique Competition

for Diagnosis of Parasitic Diseases in 2011--II Analysis of capabilities of *Plasmodium* detection. Zhongguo Xue Xi Chong Bing Fang Zhi Za Zhi. 2012; 24:274-278. (in Chinese)

10. Ashraf S, Kao A, Hugo C, Christophel EM, Fatunmbi B, Luchavez J, Lilley K, Bell D. Developing standards for malaria microscopy: External competency assessment for malaria microscopists in the Asia-Pacific. Malaria J. 2012; 11:352.

11. Collins WE, Jeffery GM. *Plasmodium ovale*: Parasite and disease. Clin Microbiol Rev. 2005; 18:570-581.

12. Yao LN, Zhang LL, Ruan W, Chen HL, Lu QY, Yang TT. Species identification in 5 imported cases previously diagnosed as Vivax malaria by parasitological and nested PCR techniques. Zhongguo Ji Sheng Chong Xue Yu Ji Sheng Chong Bing Za Zhi. 2013; 31:221-223, 234. (in Chinese)

13. Zhou RM, Zhang HW, Deng Y, Qian D, Liu Y, Chen WQ, Yan QY, Su YP, Zhao XD, Xu BL. Laboratory detection on two cases with imported *Plasmodium ovale* infection. Zhongguo Ji Sheng Chong Xue Yu Ji Sheng Chong Bing Za Zhi. 2013; 31:127-130. (in Chinese)

14. Zhang SS, Xia ZG, Yin JH, Yan H, Zhou SS, Li SZ, Zheng X, Huang F, Li M, Chen HT, Wang Q, Zhang L, Liu W, Xiao N, Zhou XN. Analysis report of the national technique competition for diagnosis of parasitic diseases in 2012: I. Capability analysis of *Plasmodium* detection. Zhongguo Ji Sheng Chong Xue Yu Ji Sheng Chong Bing Za Zhi. 2013; 31:131-134. (in Chinese)

Researchers of chronic obstructive pulmonary disease gathered at the 2017 Japan-China Joint Medical Workshop on Aging and Health

Tatsuo Sawakami[1], Jufeng Xia[1], Peipei Song[2,3,*]

[1] *Graduate School of Medicine, the University of Tokyo, Tokyo, Japan;*
[2] *Graduate School of Frontier Sciences, The University of Tokyo, Tokyo, Japan;*
[3] *Shanghai Health Development Research Center, Shanghai Medical Information Center, Shanghai, China.*

Summary	As the number of elderly and the size of the total population increase, population aging will become a major problem because of an increase in diseases associated with aging, such as chronic obstructive pulmonary disease (COPD). The 2017 Japan-China Joint Medical Workshop on Aging and Health was held at The University of Tokyo on December 2, 2017 with a focus on management of COPD. More than 50 experts in the fields of respiratory medicine, emergency medicine, traditional Chinese medicine, and Kampo (traditional Japanese medicine) from Japan and China presented the results of their research and shared their experiences treating COPD from different perspectives. Guidelines for diagnosis and management of COPD in different countries were described at the workshop, and advances in recent research into the treatment of COPD with Kampo and traditional Chinese medicine were fully discussed. The results of the workshop should help to improve GOLD guidelines and they should greatly help to optimize COPD treatment.

Keywords: Chronic obstructive pulmonary disease, traditional Chinese medicine, Kampo, ShuFengJieDu Capsules

The 2017 Japan-China Joint Medical Workshop on Aging and Health was held at The University of Tokyo on December 2, 2017. The workshop started with introductory remarks by the workshop chairs, Drs. Kazuhisa Sekimizu (Teikyo University, Japan) and Wei Zhang (Shandong University of Traditional Chinese Medicine, China). Next were a series of speeches by 11 experts from Japan and China. Closing remarks were given by Dr. Wei Tang (The University of Tokyo, Japan). The theme of this workshop was the management of chronic obstructive pulmonary disease (COPD). More than 50 experts in the fields of respiratory medicine, emergency medicine, traditional Chinese medicine, and Kampo (traditional Japanese medicine) from Japan and China discussed related topics in depth and they shared their experiences

treating COPD.

COPD is a progressive disease that causes chronic bronchitis and emphysema in older people. As of 2016, 251 million people worldwide had COPD, and COPD is currently the fourth leading cause of death. The World Health Organization (WHO) has predicted that the COPD will become the third leading cause of death by 2030 (*1-4*). In order to facilitate COPD management, more than 50 experts from China and Japan discussed the treatment of COPD from different perspectives at the workshop. The guidelines for diagnosis and management of COPD in different countries were described. In addition, advances in recent research into treatment of COPD with Kampo and traditional Chinese medicine were discussed in depth.

Dr. Yasuhiro Yamauchi from Respiratory Medicine, The University of Tokyo Hospital described clinical guidelines for COPD diagnosis and care in Japan. According to annual reports from the Ministry of Health, Labor, and Welfare, the mortality of patients with COPD in Japan has decreases since 2010. Over 16,000 patients died from COPD in 2011. Deaths

Address correspondence to:
Dr. Peipei Song, Shanghai Health Development Research Center, No. 1477 West Beijing Road, 200041, Shanghai, China.
E-mail: songpeipei@shdrc.org

decreased to 15,000 (*5,6*) prior to 2016. According to Dr. Yamauchi, "This is due to the increased use and improvement of COPD guidelines in Japan; the dissemination of clinical guidelines on COPD has greatly helped to decrease the mortality of COPD".

Dr. Wei Zhang of the Shandong University of Traditional Chinese Medicine Hospital described treatment of COPD with traditional Chinese medicine in China. COPD can be graded based on the extent of air flow limitation and the severity of the symptoms. Patients are divided in four groups: A, B, C, and D (*7*). Group A have low-risk COPD and few symptoms. Group B has low-risk COPD but more symptoms. Groups C has high-risk COPD but few symptoms. Group D has high-risk COPD and more symptoms. As Dr. Zhang explained, "In traditional Chinese medicine, the ABCD assessment can be described as a righteous qi or an evil qi". Group A, for example, has an abundance of righteous qi but a slight amount of evil qi, so broad-spectrum antivirals such as ShuFengJieDu Capsule (SFJDC) are recommended. A clinical study on COPD has indicated that a combination of SFJDC and conventional therapy can improve lung function and reduce the duration of hospitalization (*8*).

Dr. Masayuki Hojo of the NTT Medical Center, Tokyo described the prevalence and features of eosinophilic COPD in Japan. According to guidelines from the Global Initiative for Chronic Obstructive Lung Disease (GOLD), an inhaled corticosteroid (ICS) is recommended for severe to very severe COPD when frequent exacerbations are not adequately controlled by optimized long-acting bronchodilation (*9*). According to Dr. Hojo, fewer patients in Japan receive a regimen including an ICS than in Western countries. Post hoc analysis of the FLAME trial indicated that an ICS is just one of many options and that an ICS is not always the most appropriate treatment for a patient who had more than two exacerbations a year (*10*).

Dr. Xiaolan Cui of the Institute of Chinese Materia Medica, China Academy of Chinese Medical Sciences described the substances in and the efficacy of SFJDC. SFJDC contain rhizoma Polygoni cuspidati, fructus Forsythiae, radix Bupleuri, herba Patriniae, herba Verbenae, rhizoma Phragmitis, and radix Glycyrrhizae. An *in vitro* study by Dr. Cui and his colleagues indicated that SFJDC have broad-spectrum antiviral activity against viruses such as respiratory syncytial viruses, the Sendai virus, the Coxsackie virus, the H1N1 influenza virus, and the H3N2 influenza virus as well as antibacterial activity against bacteria such as Staphylococcus aureus, Staphylococcus epidermidis, Staphylococcus albus, Escherichia coli, Pseudomonas aeruginosa, beta hemolytic Streptococcus, Candida albicans, Proteus spp., and Neisseria gonorrhoeae (*11*). The study by Dr. Cui and his colleagues indicated that SFJDC can reduce the incidence of respiratory infections leading to lung damage.

Dr. Jing Yu of the Faculty of Pharmacy, Yokohama University explained how Kampo medicine is used to treat COPD. He also described the general concept of Kampo, its history, and Kampo medicines used in Japan. As Dr. Yu explained, Kampo originated from traditional Chinese medicine and developed in Japan after the 7th century (*12,13*). Japanese practitioners of Kampo developed their own unique formulations and treatments. In Japan, Kampo is strictly managed and assessed. Crude drugs must be identified and assessed to produce Kampo medicines. Crude drugs must undergo many processes such as morphological evaluation, chemical evaluation, molecular biological evaluation, serum pharmacological evaluation, biological evaluation, and 3D-HPLC (*14*). Hochuekkito is prescribed to treat COPD in Japan. Hochuekkito contains radix Astragali, rhizoma Atractylodis lanceae, radix Panacis ginseng, radix Angelicae, radix Bupleuri, fructus Zizyphi, pericarpium Aurantii nobilis, radix Glycyrrhizae, rhizoma Cimicifugae, and rhizoma Zingiberis. Studies on Hochuekkito have indicated that it has anti-inflammatory and anti-viral action and that it aids the digestive system and immune system, alleviating a patient's symptoms (*15,16*).

Dr. Wei Zhang of the Shuguang Hospital affiliated with the Shanghai University of Traditional Chinese Medicine described the clinical use of traditional Chinese medical in pulmonary rehabilitation for patients with COPD. In China, traditional Chinese medicine is used to prevent and relieve pulmonary symptoms of patients with COPD. In a study by Dr. Zhang and his colleagues, the respiratory function of patients with COPD improved after 4 months of traditional Chinese breathing training (*17*).

Dr. Zhijun Jie of Respiratory Medicine, the Fifth People's Hospital of Shanghai described the mechanism, treatment of viral infection, and management of acute deterioration of COPD (AECOPD) in China. AECOPD is a phenomenon whereby patients with COPD have an aggressive airway obstruction, difficulty breathing, and increased sputum in a short amount of time. Patients with AECOPD have a higher rate of infection with respiratory viruses and atypical clinical manifestations; this is especially true for patients over the age of 65 (*18,19*). Studies by Dr. Jie and his colleagues have examined the pharmacological action of Chinese medicine against influenza. SFJDC markedly reduced the inflammation caused by influenza viruses through the ERK-NK-kB pathway (*20,21*). Although research on antiviral therapy for AECOPD is still underway, traditional Chinese medicine may benefit patients with AECOPD.

Dr. Tiejun Zhang of the Tianjin Institute of Pharmaceutical Research, State Key Laboratory of Drug Delivery Technology and Pharmacokinetics, Tianjin Engineering Laboratory of Quality Control Technology of Traditional Chinese Medicine described mechanisms of action of SFJDC as a treatment for pulmonary

inflammation. In a study on SFJDC by Dr. Zhang and his colleagues, HPLX-Q/TOF-MS identified 94 chemical components of SFJDC. Forty-six compounds were identified as potential bioactive constituents (8 flavonoids, 4 anthraquinones, 4 stilbenes, 2 iridoids, 2 lignans, 2 naphthalenes, 1 phenylglycoside, 1 triterpenoid saponin, 3 other compounds, and 19 metabolites). Moreover, 28 compounds in SFJDC acted on 22 pathways through 41 related targets and 10 active components acted on 3-phosphoinositide dependent protein kinase-1 (PDPK1), mitogen-activated protein kinase 10 (MAPK10), and inflammatory response pathways including mitogen-activated protein kinase (MAPK), extracellular regulated protein kinases (ERK), and arachidonic acid metabolism. *In vivo* studies using a rat and mouse model of pneumonia, a rat model of pharyngitis, a mouse model of peritonitis, and a rat model of fever have indicated that SFJDC have anti-inflammatory and antipyretic action.

Dr. Jufeng Xia of the Graduate School of Medicine, The University of Tokyo described how the anti-tumor, anti-inflammatory, and anti-viral action of SFJDC can be used. In a study by Dr. Xia and his colleagues, SFJDC markedly inhibited the proliferation of HepG2.2.15 cells, which are derived from a hepatoma cell line and transfected with the HBV genome, and they inhibited the Akt/mTOR, and Ikba/NF-kB pathways. These results indicate that SFJDC may serve as a potential component of anti-tumor therapy. In addition, Drs. Atmika Paudel and Suresh Panthee of the Graduate School of Pharmaceutical Sciences, The University of Tokyo described the pharmacokinetic analysis of therapeutically effective antimicrobials using a silkworm model of infection and use of *in vivo* transcriptomic analysis to identify virulence factors in Staphylococcus (*22*). Studies have indicated that this new antimicrobial has promise as a novel approach for COPD management.

As has been indicated by the topics mentioned here, more than 50 experts from China and Japan discussed the management of COPD in depth at the Japan-China Joint Medical Workshop. Information shared at the workshop will help to further refine the clinical guidelines on COPD in both countries and it should help to improve treatment for patients with COPD.

References

1. Berry CE, Wise RA. Mortality in COPD: Causes, risk factors, and prevention. COPD. 2010; 7:375-382.
2. Soydan S, Ignak S, Unay Demirel O, Karadag G, Aykent A, Aslan S. Chryseobacterium indologenes infection in a patient with chronic obstructive pulmonary disease. Drug Discov Ther. 2017;11:165-7.
3. Masuda S, Omori H, Onoue A, Lu X, Kubota K, Higashi N, Ogata Y, Katoh T. Comorbidities according to airflow limitation severity: Data from comprehensive health examination in Japan. Environ Health Prev Med. 2017; 22:13.
4. GBD 2016 Causes of Death Collaborators. Global, regional, and national age-sex specific mortality for 264 causes of death, 1980-2016: A systematic analysis for the Global Burden of Disease Study 2016. Lancet. 2017; 390:1151-1210.
5. Ukawa S, Tamakoshi A, Yatsuya H, Yamagishi K, Ando M, Iso H, JACC Study Group. Passive smoking and chronic obstructive pulmonary disease mortality: Findings from the Japan collaborative cohort study. Int J Public Health. 2017; 62:489-494.
6. Ukawa S, Tamakoshi A, Yatsuya H, Yamagishi K, Ando M, Iso H. Association between average daily television viewing time and chronic obstructive pulmonary disease-related mortality: Findings from the Japan collaborative cohort study. J Epidemiol. 2015; 25:431-436.
7. Vogelmeier CF, Vestbo J, Hurd SS, Decramer M. Changes in GOLD: Today and tomorrow. Lancet Respir Med. 2015; 3:424-426.
8. Tao Z, Yang Y, Shi W, Xue M, Yang W, Song Z, Yao C, Yin J, Shi D, Zhang Y, Cai Y, Tong C, Yuan Y. Complementary and alternative medicine is expected to make greater contribution in controlling the prevalence of influenza. Biosci Trends. 2013; 7:253-256.
9. Marcoa R, Rodrigues DM, Dias M, Ladeira I, Vaz AP, Lima R, Guimarães M. Classification of Chronic Obstructive Pulmonary Disease (COPD) according to the new Global Initiative for Chronic Obstructive Lung Disease (GOLD) 2017: Comparison with GOLD 2011. COPD. 2017:1-6. doi: 10.1080/15412555.2017.1394285.
10. Takahashi S, Betsuyaku T. The chronic obstructive pulmonary disease comorbidity spectrum in Japan differs from that in western countries. Respir Investig. 2015; 53:259-270.
11. Bao Y, Gao Y, Cui X. Effect of Shufeng Jiedu capsules as a broad-spectrum antibacterial. Biosci Trends. 2016; 10:74-78.
12. Motoo Y, Seki T, Tsutani K. Traditional Japanese medicine, Kampo: Its history and current status. Chin J Integr Med. 2011;17:85-87.
13. Yakubo S, Ito M, Ueda Y, Okamoto H, Kimura Y, Amano Y, Togo T, Adachi H, Mitsuma T, Watanabe K. Pattern classification in kampo medicine. Evid Based Complement Alternat Med. 2014; 2014:535146.
14. Sakakibara I. 3D-HPLC fingerprints of Kampo medicine and botanical raw materials. Nihon Yakurigaku Zasshi. 2008; 132:265-269. (in Japanese)
15. Dan K, Takanashi K, Akiyoshi H, Munakata K, Hasegawa H, Ogawa K, Watanabe K. Mechanism of action of the anti-influenza virus active kampo (traditional Japanese herbal) medicine, hochuekkito. Pharmacology. 2017; 101:148-155.
16. Tatsumi K, Shinozuka N, Nakayama K, Sekiya N, Kuriyama T, Fukuchi Y. Hochuekkito improves systemic inflammation and nutritional status in elderly patients with chronic obstructive pulmonary disease. J Am Geriatr Soc. 2009; 57:169-170.
17. Yu XQ, Li JS, Li SY, Xie Y, Wang MH, Zhang HL, Wang HF, Wang ZW. Functional and psychosocial effects of pulmonary Daoyin on patients with COPD in China: Study protocol of a multicenter randomized controlled trial. J Integr Med. 2013;11:140-146.
18. Jing X, Zhang G, Zhang B, Dai L, Wang X, Jia L, Wang H, An L, Yang Y, Cheng Z. Efficacy and safety of low-dose urokinase for the treatment of hemodynamically stable AECOPD patients with acute pulmonary

thromboembolism. Clin Respir J. 2017. doi: 10.1111/crj.12751.

19. Baddini-Martinez J, de Padua AI. Chronic obstructive pulmonary disease: Time to discuss new concepts. Lancet. 2016; 388:2740-2741.

20. Li Y, Chang N, Han Y, Zhou M, Gao J, Hou Y, Jiang M, Zhang T, Bai G. Anti-inflammatory effects of Shufengjiedu capsule for upper respiratory infection via the ERK pathway. Biomed Pharmacother. 2017; 94:758-766.

21. Tao Z, Gao J, Zhang G, Xue M, Yang W, Tong C, Yuan Y. Shufeng Jiedu Capsule protect against acute lung injury by suppressing the MAPK/NF-kappaB pathway. Biosci Trends. 2014; 8:45-51.

22. Paudel A, Hamamoto H, Panthee S, Kaneko K, Matsunaga S, Kanai M, Suzuki Y, Sekimizu K. A novel spiro-heterocyclic compound identified by the silkworm infection model inhibits transcription in Staphylococcus aureus. Front Microbiol. 2017; 8:712.

BST
BioScience Trends

Guide for Authors

1. Scope of Articles

BioScience Trends is an international peer-reviewed journal. BioScience Trends devotes to publishing the latest and most exciting advances in scientific research. Articles cover fields of life science such as biochemistry, molecular biology, clinical research, public health, medical care system, and social science in order to encourage cooperation and exchange among scientists and clinical researchers.

2. Submission Types

Original Articles should be well-documented, novel, and significant to the field as a whole. An Original Article should be arranged into the following sections: Title page, Abstract, Introduction, Materials and Methods, Results, Discussion, Acknowledgments, and References. Original articles should not exceed 5,000 words in length (excluding references) and should be limited to a maximum of 50 references. Articles may contain a maximum of 10 figures and/or tables.

Brief Reports definitively documenting either experimental results or informative clinical observations will be considered for publication in this category. Brief Reports are not intended for publication of incomplete or preliminary findings. Brief Reports should not exceed 3,000 words in length (excluding references) and should be limited to a maximum of 4 figures and/or tables and 30 references. A Brief Report contains the same sections as an Original Article, but the Results and Discussion sections should be combined.

Reviews should present a full and up-to-date account of recent developments within an area of research. Normally, reviews should not exceed 8,000 words in length (excluding references) and should be limited to a maximum of 100 references. Mini reviews are also accepted.

Policy Forum articles discuss research and policy issues in areas related to life science such as public health, the medical care system, and social science and may address governmental issues at district, national, and international levels of discourse. Policy Forum articles should not exceed 2,000 words in length (excluding references).

Case Reports should be detailed reports of the symptoms, signs, diagnosis, treatment, and follow-up of an individual patient. Case reports may contain a demographic profile of the patient but usually describe an unusual or novel occurrence. Unreported or unusual side effects or adverse interactions involving medications will also be considered. Case Reports should not exceed 3,000 words in length (excluding references).

News articles should report the latest events in health sciences and medical research from around the world. News should not exceed 500 words in length.

Letters should present considered opinions in response to articles published in BioScience Trends in the last 6 months or issues of general interest. Letters should not exceed 800 words in length and may contain a maximum of 10 references.

3. Editorial Policies

Ethics: BioScience Trends requires that authors of reports of investigations in humans or animals indicate that those studies were formally approved by a relevant ethics committee or review board.

Conflict of Interest: All authors are required to disclose any actual or potential conflict of interest including financial interests or relationships with other people or organizations that might raise questions of bias in the work reported. If no conflict of interest exists for each author, please state "There is no conflict of interest to disclose".

Submission Declaration: When a manuscript is considered for submission to BioScience Trends, the authors should confirm that 1) no part of this manuscript is currently under consideration for publication elsewhere; 2) this manuscript does not contain the same information in whole or in part as manuscripts that have been published, accepted, or are under review elsewhere, except in the form of an abstract, a letter to the editor, or part of a published lecture or academic thesis; 3) authorization for publication has been obtained from the authors' employer or institution; and 4) all contributing authors have agreed to submit this manuscript.

Cover Letter: The manuscript must be accompanied by a cover letter signed by the corresponding author on behalf of all authors. The letter should indicate the basic findings of the work and their significance. The letter should also include a statement affirming that all authors concur with the submission and that the material submitted for publication has not been published previously or is not under consideration for publication elsewhere. The cover letter should be submitted in PDF format. For example of Cover Letter, please visit http://www.biosciencetrends.com/downcentre.php (Download Centre).

Copyright: A signed JOURNAL PUBLISHING AGREEMENT (JPA) form must be provided by post, fax, or as a scanned file before acceptance of the article. Only forms with a hand-written signature are accepted. This copyright will ensure the widest possible dissemination of information. A form facilitating transfer of copyright can be downloaded by clicking the appropriate link and can be returned to the e-mail address or fax number noted on the form (Please visit Download Centre). Please note that your manuscript will not proceed to the next step in publication until the JPA Form is received. In addition, if excerpts from other copyrighted works are included, the author(s) must obtain written permission from the copyright owners and credit the source(s) in the article.

Suggested Reviewers: A list of up to 3 reviewers who are qualified to assess the scientific merit of the study is welcomed. Reviewer information including names, affiliations, addresses, and e-mail should be provided at the same time the manuscript is submitted online. Please do not suggest reviewers with known conflicts of interest, including participants or anyone with a stake in the proposed research; anyone from the same institution; former students, advisors, or research collaborators (within the last three years); or close personal contacts. Please note that the Editor-in-Chief may accept one or more of the proposed reviewers or may request a review by other qualified persons.

Language Editing: Manuscripts prepared by authors whose native language is not English should have their work proofread by a native English speaker before submission. If not, this might delay the publication of your manuscript in BioScience Trends.

The Editing Support Organization can provide English proofreading, Japanese-English translation, and Chinese-English translation services to authors who want to publish in BioScience Trends and need assistance before submitting a manuscript. Authors can visit this organization directly at http://www.iacmhr.com/iac-eso/support.php?lang=en. IAC-ESO was established to facilitate manuscript preparation by researchers whose native language is not English and to help edit works intended for international academic journals.

4. Manuscript Preparation

Manuscripts should be written in clear, grammatically correct English and submitted as a Microsoft Word file in a single-column format. Manuscripts must be paginated and typed in 12-point Times New Roman font with 24-point line spacing. Please do not embed figures in the text. Abbreviations should be used as little as possible and should be explained at first mention unless the term is a well-known abbreviation (*e.g.* DNA). Single words should not be abbreviated.

Title Page: The title page must include 1) the title of the paper (Please note the title should be short, informative, and contain the major key words); 2) full name(s) and affiliation(s) of the author(s), 3) abbreviated names of the author(s), 4) full name, mailing address, telephone/fax numbers, and e-mail address of the corresponding author; and 5) conflicts of interest (if you have an actual or potential conflict of interest to disclose, it must be included as a footnote on the title page of the manuscript; if no conflict of

interest exists for each author, please state "There is no conflict of interest to disclose"). Please visit Download Centre and refer to the title page of the manuscript sample.

Abstract: The abstract should briefly state the purpose of the study, methods, main findings, and conclusions. For article types including Original Article, Brief Report, Review, Policy Forum, and Case Report, a one-paragraph abstract consisting of no more than 250 words must be included in the manuscript. For News and Letters, a brief summary of main content in 150 words or fewer should be included in the manuscript. Abbreviations must be kept to a minimum and non-standard abbreviations explained in brackets at first mention. References should be avoided in the abstract. Key words or phrases that do not occur in the title should be included in the Abstract page.

Introduction: The introduction should be a concise statement of the basis for the study and its scientific context.

Materials and Methods: The description should be brief but with sufficient detail to enable others to reproduce the experiments. Procedures that have been published previously should not be described in detail but appropriate references should simply be cited. Only new and significant modifications of previously published procedures require complete description. Names of products and manufacturers with their locations (city and state/country) should be given and sources of animals and cell lines should always be indicated. All clinical investigations must have been conducted in accordance with Declaration of Helsinki principles. All human and animal studies must have been approved by the appropriate institutional review board(s) and a specific declaration of approval must be made within this section.

Results: The description of the experimental results should be succinct but in sufficient detail to allow the experiments to be analyzed and interpreted by an independent reader. If necessary, subheadings may be used for an orderly presentation. All figures and tables must be referred to in the text.

Discussion: The data should be interpreted concisely without repeating material already presented in the Results section. Speculation is permissible, but it must be well-founded, and discussion of the wider implications of the findings is encouraged. Conclusions derived from the study should be included in this section.

Acknowledgments: All funding sources should be credited in the Acknowledgments section. In addition, people who contributed to the work but who do not meet the criteria for authors should be listed along with their contributions.

References: References should be numbered in the order in which they appear in the text. Citing of unpublished results, personal communications, conference abstracts, and theses in the reference list is not recommended but these sources may be mentioned in the text. In the reference list,

cite the names of all authors when there are fifteen or fewer authors; if there are sixteen or more authors, list the first three followed by *et al.* Names of journals should be abbreviated in the style used in PubMed. Authors are responsible for the accuracy of the references. Examples are given below:

Example 1 (Sample journal reference):
Inagaki Y, Tang W, Zhang L, Du GH, Xu WF, Kokudo N. Novel aminopeptidase N (APN/CD13) inhibitor 24F can suppress invasion of hepatocellular carcinoma cells as well as angiogenesis. Biosci Trends. 2010; 4:56-60.

Example 2 (Sample journal reference with more than 15 authors):
Darby S, Hill D, Auvinen A, *et al.* Radon in homes and risk of lung cancer: Collaborative analysis of individual data from 13 European case-control studies. BMJ. 2005; 330:223.

Example 3 (Sample book reference):
Shalev AY. Post-traumatic stress disorder: diagnosis, history and life course. In: Post-traumatic Stress Disorder, Diagnosis, Management and Treatment (Nutt DJ, Davidson JR, Zohar J, eds.). Martin Dunitz, London, UK, 2000; pp. 1-15.

Example 4 (Sample web page reference):
Ministry of Health, Labour and Welfare of Japan. Dietary reference intakes for Japanese. *http://www.mhlw.go.jp/houdou/2004/11/h1122-2a.html* (accessed June 14, 2010).

Tables: All tables should be prepared in Microsoft Word or Excel and should be arranged at the end of the manuscript after the References section. Please note that tables should not in image format. All tables should have a concise title and should be numbered consecutively with Arabic numerals. If necessary, additional information should be given below the table.

Figure Legend: The figure legend should be typed on a separate page of the main manuscript and should include a short title and explanation. The legend should be concise but comprehensive and should be understood without referring to the text. Symbols used in figures must be explained.

Figure Preparation: All figures should be clear and cited in numerical order in the text. Figures must fit a one- or two-column format on the journal page: 8.3 cm (3.3 in.) wide for a single column, 17.3 cm (6.8 in.) wide for a double column; maximum height: 24.0 cm (9.5 in.). Please make sure that the symbols and numbers appeared in the figures should be clear. Please make sure that artwork files are in an acceptable format (TIFF or JPEG) at minimum resolution (600 dpi for illustrations, graphs, and annotated artwork, and 300 dpi for micrographs and photographs). Please provide all figures as separate files. Please note that low-resolution images are one of the leading causes of article resubmission and schedule delays. All color figures will be reproduced in full color in the online edition of the journal at no cost to authors.

Units and Symbols: Units and symbols

conforming to the International System of Units (SI) should be used for physicochemical quantities. Solidus notation (*e.g.* mg/kg, mg/mL, mol/mm^2/min) should be used. Please refer to the SI Guide www.bipm.org/en/si/ for standard units.

Supplemental data: Supplemental data might be useful for supporting and enhancing your scientific research and BioScience Trends accepts the submission of these materials which will be only published online alongside the electronic version of your article. Supplemental files (figures, tables, and other text materials) should be prepared according to the above guidelines, numbered in Arabic numerals (*e.g.*, Figure S1, Figure S2, and Table S1, Table S2) and referred in the text. All figures and tables should have titles and legends. All figure legends, tables and supplemental text materials should be placed at the end of the paper. Please note all of these supplemental data should be provided at the time of initial submission and note that the editors reserve the right to limit the size and length of Supplemental Data.

5. Submission Checklist

The Submission Checklist will be useful during the final checking of a manuscript prior to sending it to BioScience Trends for review. Please visit Download Centre and download the Submission Checklist file.

6. Online Submission

Manuscripts should be submitted to BioScience Trends online at http://www.biosciencetrends.com. The manuscript file should be smaller than 5 MB in size. If for any reason you are unable to submit a file online, please contact the Editorial Office by e-mail at office@biosciencetrends.com.

7. Accepted Manuscripts

Proofs: Galley proofs in PDF format will be sent to the corresponding author via e-mail. Corrections must be returned to the editor (proof-editing@biosciencetrends.com) within 3 working days.

Offprints: Authors will be provided with electronic offprints of their article. Paper offprints can be ordered at prices quoted on the order form that accompanies the proofs.

Page Charge: Page charges will be levied on all manuscripts accepted for publication in BioScience Trends ($140 per page for black white pages; $340 per page for color pages). Under exceptional circumstances, the author(s) may apply to the editorial office for a waiver of the publication charges at the time of submission.

(*Revised February 2013*)

JOURNAL PUBLISHING AGREEMENT (JPA)

Manuscript No.:

Title:

Corresponding Author:

The International Advancement Center for Medicine & Health Research Co., Ltd. (IACMHR Co., Ltd.) is pleased to accept the above article for publication in BioScience Trends. The International Research and Cooperation Association for Bio & Socio-Sciences Advancement (IRCA-BSSA) reserves all rights to the published article. Your written acceptance of this JOURNAL PUBLISHING AGREEMENT is required before the article can be published. Please read this form carefully and sign it if you agree to its terms. The signed JOURNAL PUBLISHING AGREEMENT should be sent to the BioScience Trends office (Pearl City Koishikawa 603, 2-4-5 Kasuga, Bunkyo-ku, Tokyo 112-0003, Japan; E-mail: **office@biosciencetrends.com**; Tel: **+81-3-5840-8764**; Fax: **+81-3-5840-8765**).

1. Authorship Criteria

As the corresponding author, I certify on behalf of all of the authors that:

1) The article is an original work and does not involve fraud, fabrication, or plagiarism.

2) The article has not been published previously and is not currently under consideration for publication elsewhere. If accepted by BioScience Trends, the article will not be submitted for publication to any other journal.

3) The article contains no libelous or other unlawful statements and does not contain any materials that infringes upon individual privacy or proprietary rights or any statutory copyright.

4) I have obtained written permission from copyright owners for any excerpts from copyrighted works that are included and have credited the sources in my article.

5) All authors have made significant contributions to the study including the conception and design of this work, the analysis of the data, and the writing of the manuscript.

6) All authors have reviewed this manuscript and take responsibility for its content and approve its publication.

7) I have informed all of the authors of the terms of this publishing agreement and I am signing on their behalf as their agent.

2. Copyright Transfer Agreement

I hereby assign and transfer to IACMHR Co., Ltd. all exclusive rights of copyright ownership to the above work in the journal BioScience Trends, including but not limited to the right 1) to publish, republish, derivate, distribute, transmit, sell, and otherwise use the work and other related material worldwide, in whole or in part, in all languages, in electronic, printed, or any other forms of media now known or hereafter developed and the right 2) to authorize or license third parties to do any of the above.

I understand that these exclusive rights will become the property of IACMHR Co., Ltd., from the date the article is accepted for publication in the journal BioScience Trends. I also understand that IACMHR Co., Ltd. as a copyright owner has sole authority to license and permit reproductions of the article.

I understand that except for copyright, other proprietary rights related to the Work (*e.g.* patent or other rights to any process or procedure) shall be retained by the authors. To reproduce any text, figures, tables, or illustrations from this Work in future works of their own, the authors must obtain written permission from IACMHR Co., Ltd.; such permission cannot be unreasonably withheld by IACMHR Co., Ltd.

3. Conflict of Interest Disclosure

I confirm that all funding sources supporting the work and all institutions or people who contributed to the work but who do not meet the criteria for authors are acknowledged. I also confirm that all commercial affiliations, stock ownership, equity interests, or patent-licensing arrangements that could be considered to pose a financial conflict of interest in connection with the article have been disclosed.

Corresponding Author's Name (Signature):

Date:

BioScience Trends (www.biosciencetrends.com)

Pearl City Koishikawa 603, 2-4-5 Kasuga, Bunkyo-ku, Tokyo 112-0003, Japan; E-mail: office@biosciencetrends; Tel: +81-3-5840-8764; Fax: +81-3-5840-8765